Glycerol etherification with isobutene for the production of fuel additives

by

Özge Deniz Bozkurt

A Dissertation Submitted to the

Graduate School of Sciences and Engineering

in Partial Fulfillment of the Requirements for

the Degree of

Doctor of Philosophy

in

Chemical and Biological Engineering

March 2019

To the scientific world with equal women contribution

Glycerol etherification with isobutene for the production of fuel additives

Koç University

Graduate School of Sciences and Engineering

This is to certify that I have examined this copy of a doctoral dissertation by

Özge Deniz Bozkurt

and have found that it is complete and satisfactory in all respects,

and that any and all revisions required by the final

examining committee have been made.

Committee Members:

……

Assoc. Prof. Alper Uzun

……

Prof. Özlem Keskin

……

Assoc. Prof. Uğur Ünal

……

Prof. Ahmet Sirkecioğlu

……

Prof. Ramazan Yıldırım

Date: ……

Abstract

Etherification of glycerol with isobutene is an industrially promising reaction to produce glycerol *tert*-butyl ethers (GTBE) as renewable fuel additives. The desired ethers are the di-GTBE (DTBGE) and tri-GTBE (TTBGE) with better solubility in hydrocarbon fuels. In this thesis study, we have studied glycerol etherification with isobutene on solid acid catalysts in batch and flow reactor systems for the enhanced production of the desired ethers. Our literature review pointed out to the usability of the cost effective and commercial solid acid catalysts in this reaction. A thorough catalysts screening study was conducted, for the first time in literature, with over 70 solid acid catalysts including ion exchange resins, zeolites, mesoporous silica and heteropolyacids under identical conditions in a multiple batch reactor system. The commercial Amberlyst™ ion exchange resins and zeolite H-Beta yielded more than 80 wt% selectivity to DTBGE and TTBGE. Desired ether selectivity was observed to increase with increasing acid strength for zeolites and mesoporous silica supported heteropolyacids, ascertained by ammonia temperature programmed desorption (NH_3-TPD) experiments. We modified Amberlyst 15™ ion exchange resin by partially exchanging the H^+'s of its sulfonic acid sites with Na^+. Acid strength of the remaining sulfonic acid sites increased with increasing Na^+-exchange, determined by our Fourier Transform Infrared Spectroscopy (FTIR) based method, and was further validated by the density functional theory (DFT) calculations. Batch reactor measurements at high glycerol conversion illustrated the enhancement in the desired ether selectivity together with the suppression of isobutene dimerization with an increase in acid strength. Furthermore, a laboratory scale once-through fixed-bed tubular flow reactor was exploited for the first time in literature. The minimum eligible Amberlyst 15™ catalyst particle size without pressure drop was ascertained to be 250 microns. The estimated Mears and Weisz-Prater parameters indicated that the 250-425 micron particle size fraction had negligible external and internal mass transfer resistance throughout the whole glycerol conversion range.

Flow reactor tests at differential glycerol conversion revealed the formation of DTBGE and TTBGE as primary products at high acid strength. Moreover these desired products were obtained at significantly faster rates in the flow reactor compared to the batch reactor. For instance, the corresponding rates of desired ether production in volume basis were 7400 $g_{DTBGE + TTBGE} \times (L_{cat} \times h)^{-1}$ and 66 $g_{DTBGE + TTBGE} \times (L_{reactor} \times h)^{-1}$, in the flow and batch systems, respectively. Data also demonstrated that the catalyst activity remained the same for an extended time-on-stream of at least two days. We then prepared fuel additive mixtures with different concentrations of GTBE. The density, water solubility and viscosity of the GTBE mixtures decreased with increasing TTBGE content, corresponding to a decrease in the number of hydroxyl groups. Blending 3.45 vol% TTBGE-rich (34 wt% TTBGE) GTBE in gasoline enhanced the octane number and reduced the vapor pressure. Power and emission tests in a gasoline engine dynamometer, performed for the first time in literature, indicated the commercial potential of GTBE as a replacement of the conventional gasoline oxygenate methyl *tert*-butyl ether (MTBE), due to the fact that their blends provided similar torque values, specific fuel consumption and mean emissions of CO_2, CO, NO_x and total hydrocarbon emissions (THC).

Özetçe

Gliserolün izobüten ile eterleşmesi, alternatif yakıt katkısı olarak kullanılabilecek gliserol tersiyer bütil eterlerinin (GTBE) üretildiği bir reaksiyon olup endüstriyel potansiyele sahiptir. İstenilen reaksiyon ürünleri, hidrokarbon yakıtlarda daha iyi çözünebilen di-GTBE (DTBGE) ve tri-GTBE (TTBGE)'dir. Bu tez çalışmasında, gliserolün izobüten ile eterifikasyonu ile kesikli ve sürekli reaktör sistemlerinde katı asit katalizörler varlığında yüksek seçicilikte istenilen GTBE üretimi incelenmiştir. Literatür taramamız, ticari ve ucuz katı asit katalizörlerin bu reaksiyonda kullanılabileceğini ifade etmiştir. Detaylı katalizör tarama çalışmamızda, iyon değişim reçineleri, zeolitler, mezopor silika ve heteropoliasitleri içeren 70'ten fazla katı asit katalizör literatürde ilk defa aynı reaksiyon şartlarında çoklu kesikli reaktör sisteminde test edilmiştir. Ticari katalizörlerden Amberlyst 15 iyon değişim reçineleri ve zeolit H-Beta, istenilen eterlere kütlece %80'in üzerinde seçiciliğe sahip olmuştur. Zeolit ve mezopor silika destekli heteropoliasitlerde istenilen eter seçiciliğindeki artış, amonyak sıcaklık programlı desorpsiyon (NH_3-TPD) sonuçlarına göre asidik kuvvetin artışı ile paralellik göstermektedir. Amberlyst 15™ iyon değişim reçinesinin sülfonik asit bölgelerindeki H^+'lar kısmi olarak Na^+ ile değiştirildiğinde geri kalan sülfonik asit bölgelerinin asidik kuvvetinin arttığı Fourier Dönüşümlü Kızılötesi Spektroskopisi (FTIR) temelli yöntemimiz ile gösterilmiş ve yoğunluk fonksiyoneli teorisi hesaplamaları ile desteklenmiştir. Kesikli reaktör sisteminde yüksek gliserol dönüşümünde gerçekleştirilen katalitik performans testlerine göre asidik bölgeler kuvvetlendikçe istenilen eter seçiciliği artmakta, bunun tam tersi olarak izobüten dimerleşmesi baskılanmaktadır. Sürekli reaktör sistemi olarak literatürde ilk defa tek geçişli sabit yataklı tüp akış reaktörü detaylı çalışılmıştır. Amberlyst 15™ katalizörünün 250 mikrondan büyük tanecik boyutu kullanıldığında reaktörde basınç düşüşü problemi ortadan kalkmaktadır. Hesaplanan Mears ve Weisz-Prater değişkenlerine göre 250-425 mikron tanecik boyutu için tüm gliserol dönüşümlerinde dış ve iç kütle aktarımı sınırlamaları göz ardı edilebilir düzeydedir. Sürekli

reaktör sisteminde çok düşük gliserol dönüşümünde gerçekleştirilen deneyler yüksek asit kuvvette DTBGE ve TTBGE'nin birincil ürünler olarak oluştuğunu göstermiştir. Ayrıca istenilen eterler sürekli reaktör sisteminde kesikli sisteme göre daha hızlı elde edilebilmektedir. Şöyle ki, sürekli ve kesikli reaktör sistemlerinde hacim tabanlı üretim hızı sırasıyla 7400 $g_{DTBGE + TTBGE} \times (L_{katalizör} \times h)^{-1}$ ve 66 $g_{DTBGE + TTBGE} \times (L_{reaktör} \times h)^{-1}$ olmuştur. Ayrıca sürekli sistemde katalizör aktivitesi en az iki gün sabit seyretmektedir. Farklı GTBE derişimi içeren yakıt katkısı karışımları hazırlanmıştır. GTBE karışımında TTBGE miktarı arttıkça ve hidroksil grubu sayısı azaldıkça yoğunluk, sudaki çözünürlük ve viskozitenin azaldığı gözlenmiştir. TTBGE derişimi yüksek olan (34 wt% TTBGE) GTBE karışımı benzine hacimce %3.45 oranında katıldığında oktan sayısının arttığı, buhar basıncının düştüğü tespit edilmiştir. Benzin motor dinamometresinde yapılan güç ve emisyon testleri sonucunda GTBE'nin ticari ölçekte kullanılabileceği ve geleneksel benzin katkısı metil tersiyer bütil etere (MTBE) alternatif olabileceği gösterilmiştir, çünkü iki katkının da motorda ürettiği tork değerleri, özgül yakıt sarfiyatı ve CO_2, CO, NO_x ile toplam hidrokarbon (THC) emisyonları benzer bulunmuştur.

Acknowledgments

This thesis work was financed by the Scientific and Technological Research Council of Turkey (**TUBITAK**) through Industrial R&D Projects Support Program (1501) with project number 3130673. I kindly acknowledge the financial support from Turkish Accelerator & Radiation Laboratory (**TARLA**).

The main research was conducted at Koç University Tüpraş Energy Center (**KUTEM**) and **TÜPRAŞ R&D Center**. Several catalyst characterizations were done at Koç University Surface Science and Technology Center (**KUYTAM**). I am thankful to the investors and staff of these world class research centers. I am sending my special thanks to **Asst. Prof. Cem Albayrak**, **Dr. Rıza Kızılel**, **Prof. Can Erkey**, **Dr. Barış Yağcı** and **Prof. Alphan Sennaroğlu.**

I admire my supervisor **Assoc. Prof. Alper Uzun** as he has been the longest term idol in my life. I appreciate my PhD thesis committee members **Assoc. Prof. Uğur Ünal** and **Prof. Özlem Keskin** for their valuable time and guidance. I am thankful to **Prof. Ahmet Sirkecioğlu** and **Prof. Ramazan Yıldırım** for their contribution to the finalization of my thesis.

I have special thanks to **Dr. Serdar Çelebi** from TÜPRAŞ R&D for his long-term agility and enthusiasm towards increasing the value of our project as well as his support to my professional career. I respectfully greet **Nur Bağlar**, **Dr. Doğan Günbaş** and **Meliz Tunç** for their qualified contribution to our project. The FTIR-ATR studies were conducted by **Cüneyt Karakaya**, while the Matlab codes for the density calculations were generated by **Mehmet Yağcı** from TÜPRAŞ R&D. I appreciate **Fatih Yılmaz** from FORD OTOSAN for the valuable discussions on gasoline performance testing.

I am grateful to the current and former UZUN LAB members **Samira Kurtoğlu**, **Dr. Azam Khodadadi**, **Fulya Erdem, Ahsan Jalal**, **Kaan Yalçın**, **Tolga Koçer**, **Betül Şeker, Dr. Melike Babucci**, **Özge Akarçay** and **Elif Kocaman** for creating a friendly and enthusiastic working environment, as well as to my dear work-study students **Seda Sarp**, **Ayça Kazaz**, **Begüm Artuner** and **Özge Özaltay** for their young energy. I am sending my best regards to the NEMO members **Zeeshan Shah**, **Vahid Nozari**, **Ayda Nemati**, **Harun Kulak**, **Mert Polat** and **Saffiye Kavak**. I greet the KAYA LAB members **Navid Solati**, **Dr. Mohammad Panahi**, **Abdullah Kahraman** and **Amir Rahimi** whom we share the same office and have had nice conversations. I appreciate ÜNAL LAB members **Dr. Eylül Saraç** and **Tuğçe Beyazay** for their kind fellowship. I have special appreciation to **Kardelen Kaya** for her warm friendship. I am grateful to **Dr. Ehsan Sarayloo** and **Dr. Fatih Rahim** for enjoying the PhD evenings together.

I have admiration to my valuable friends **Ezgi Taşköy**, **Dilara Karadeniz** and **Dr. Kübra Yıldız** for being in my life since high school years. I appreciate my chemical engineer ladies **Duygu Rodop**, **Bahar Ayhopa** and **Müge Asena** for their lovely friendship. I send my special greetings to the "Delft Kuzuları" **Seval Güneş** and **Sena Alikşioğlu** as they have colored my life with various activities since our TU Delft times. I am thankful to **Dr. Onursal Yakaboylu** for the useful philosophical discussions.

I am greeting my sister **Müge Bozkurt**, my mother **Ümit Bozkurt** and my father **Bülent Bozkurt** with love and gratitude for their unlimited support.

I appreciate myself, **Dr. Özge Deniz Bozkurt**, for the intense curiosity and enthusiasm on learning the life. I respect and praise all people, all decisions, all sorrow and all joy leading me to this point.

Table of Contents

List of Tables

List of Figures

Nomenclature

GTBE	=	glycerol tertiary butyl ether
tert	=	tertiary
G	=	glycerol
IB	=	isobutene
MTBGE	=	mono-*tert*-butyl glycerol ether (also mono-GTBE)
DTBGE	=	di-*tert*-butyl glycerol ether (also di-GTBE)
TTBGE	=	tri-*tert*-butyl glycerol ether (also tri-GTBE)
DIB	=	di-isobutene
TIB	=	tri-isobutene
TetraIB	=	tetra-isobutene
TBA	=	*tert*-butyl alcohol
MTBE	=	methyl-*tert*-butyl ether
C4	=	hydrocarbons with four carbon atoms
H-Beta	=	zeolite Beta in hydrogen form
H-Y	=	zeolite Y in hydrogen form
TSA	=	tungstosilicic acid hydrate
TPA	=	tungstophosphoric acid hydrate
HPA	=	heteropolyacid
MCM-41	=	Mobil Composition of Matter No. 41 mesoporous silica
SBA-15	=	Santa Barbara Amorphous-15 mesoporous silica
XRF	=	X-ray fluorescence
XRD	=	X-ray diffraction
SEM	=	scanning electron microscopy
EDX	=	energy dispersive X-ray
NH_3-TPD	=	ammonia temperature programmed desorption
TCD	=	thermal conductivity detector
BET	=	Brunauer-Emmett-Teller
GC	=	gas chromatography
FID	=	flame ionization detector
MS	=	mass spectrometer
TGA	=	thermogravimetric analysis
FTIR	=	Fourier transform infrared spectroscopy
DFT	=	density functional theory
MR	=	Mears criteria for external diffusion
CWP	=	Weisz Prater criteria for internal diffusion
cat	=	catalyst
r_{Gly}	=	rate of glycerol conversion (mol glycerol/g cat.sec)
ρ	=	density (kg/m^3)
R	=	catalyst particle radius (m)
n	=	reaction order
k_c	=	mass transfer coefficient (m/s)
C		concentration (mol/l)
D	=	mass diffusivity of glycerol in isobutene (m^2/s)
ø	=	association parameter for diffusivity calculation
M	=	molecular weight (g/mol)
T	=	temperature (K)

μ	=	dynamic viscosity (Pa.s or N.s/m^2 or kg/m.s)
υ	=	kinematic viscosity (m^2/s)
V	=	Molar volume (m^3/mol)
Sh	=	Sherwood's number
d_p	=	diameter of the catalyst pellet (m)
Re	=	Reynolds number
Sc	=	Schmidts number
U	=	superficial fluid velocity (m/s)
D_e	=	effective diffusivity (m^2/s)
ϕ_p	=	catalyst pellet porosity
τ	=	tortuosity
σ_c	=	constriction factor
NEDC	=	New European Driving Cycle
ASTM	=	American standard testing method

Chapter 1

Introduction

1.1.Introduction

Light olefins are C2-C4 hydrocarbons following as ethylene, propylene, butene, and butadiene, obtained as side products in crude oil refineries, mainly from steam cracking and catalytic cracking units. Light olefins are used as petrochemical building blocks for example in the production of polyethylene, polypropylene and methyl tertiary butyl ether (MTBE) [1,2]. In addition, light olefins can be converted into gasoline (C5-C10) and diesel (C10-C20) range products by oligomerization [3,4]. The global light olefins market is governed by the companies Royal Dutch Shell of the Netherlands; Petrochina and China Petro & Chemical Corp of China; Reliance Industries Limited of India; Dow, DuPont, Exxon Mobil Corporation and Honeywell International Inc. of U.S.; Gazprom of Russian Federation; Saudi Arabian Oil Co. of Saudi Arabia, and BASF SE of Germany. The market size is expected to reach $475 billion in 2023 [5].

Isobutene (IB) is one of the butenes formed in the catalytic cracking units in crude oil refineries. One of the major uses of IB is the production of an octane booster fuel oxygenate, MTBE, synthesized by reacting the C4 olefin mixture with methanol under mild acidic conditions. Established commercial MTBE production employs sulfonic ion exchange resins, such as Amberlyst 15™ and Amberlyst 35™ in liquid phase under moderate temperature (30–100 °C) and pressure (20 bar) conditions [6-8]. MTBE is now regarded as an environmentally unfriendly chemical and banned in the US because of contaminating the groundwater reservoirs by its high water miscibility. Turkey still uses MTBE up to 12 vol% blend in gasoline, and pays annually over $50 million for the import of over 100000 tones MTBE.

Glycerol etherification with IB produces di- and tri-*tert*-butyl ethers of glycerol (DTBGE and TTBGE) (**Figure 1-1**), generally referred as the “desired ethers” with very slight water miscibility. These desired ethers have been claimed as MTBE alternatives, with their

potential in improving the fuel performance of gasoline, and also of diesel [9-14]. However, the applicability of DTBGE and TTBGE instead of MTBE has not yet been experimentally demonstrated in an engine.

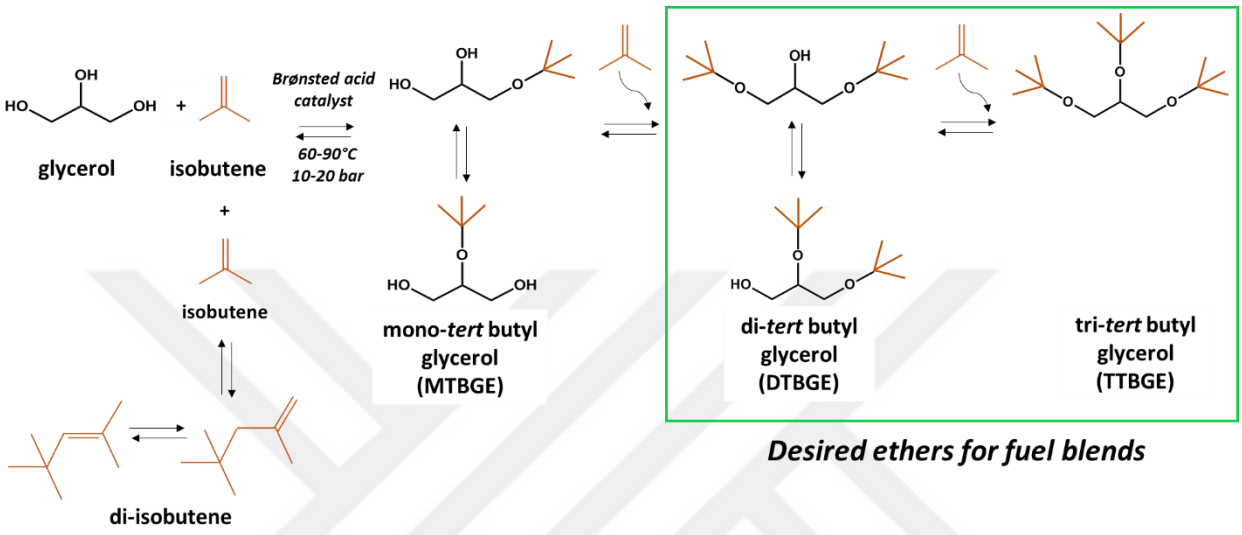

Figure 1-1. Reaction scheme of glycerol etherification with isobutene with the desired products.

The experimental research has focused on the batch-wise catalytic production of GTBE. So far in literature, macroreticular acidic ion exchange resins, zeolites, mesoporous silica, heteropolyacids and Brønsted acid functionalized novel catalysts have been tested for their yields of desired ethers in batch reactor systems and at different reaction conditions (temperature ranging from 60 to 90 °C, catalyst amount from 1 to 7.5 wt% of initial glycerol, initial isobutene:glycerol ratio of 2:1 to 4:1 mol:mol, reaction time from 1 to 50 h) [15]. Alteration of the reaction conditions influenced on the yields of the desired ethers. In addition to reaction conditions, catalyst structural properties have been shown to alter the yields. For instance, catalyst modifications decreasing the Brønsted acid capacity in ion exchange resins

and catalyst modifications increasing the Brønsted acid strength and pore size in zeolites and mesoporous silica improved the yields of desired ethers.

1.2.Motivation

It was apparent that the selectivity to DTBGE and TTBGE as the desired products to be exploited as alternative fuel additives depends not only on reaction conditions but also on the type of catalysts. Drawing structure-condition-performance relationships was infeasible regarding that different reaction conditions and catalyst types were utilized in previous literature studies. Thus, the performance of many different catalysts should be tested under identical conditions. Besides, only high conversion data from batch reactors were available in literature as controlling the conversion is not simple in batch systems. There was a need to investigate the product selectivity at very low glycerol conversion to identify the primary and secondary products of the reaction network. Apart from that, the productivity of batch and flow reactors should be compared to assess which type of system would be used in the commercial scale production. Fuel compatibility, engine power, and engine emission data of glycerol ethers in gasoline blends were not available in literature, although these ethers have been mentioned in literature as alternatives of the conventional gasoline oxygenate MTBE. Reporting the fuel additive performance of glycerol ethers in a real gasoline engine would be a significant contribution to the literature.

1.3.Objective

Our aim is to reveal the most significant structural properties of heterogeneous Brønsted acid catalysts for obtaining high yields of the desired DTBGE and TTBGE in batch and flow reactor systems, as well as examining the fuel additive performance of these ethers.

1.4.Approach to reach the Objective

Approach 1: Catalyst screening in the batch reactor system under identical conditions,

Approach 2: Studying the acid strength and product selectivity relationship of ion exchange resins as the promising commercial catalysts,

Approach 3: Exploiting the flow reactor system to understand the reaction network and production rate over ion exchange resins,

Approach 4: Determining the physical fuel properties of glycerol ethers and testing the ethers in an internal combustion gasoline engine to provide engine performance data in terms of power and emissions.

1.5.Thesis Structure

This thesis consists of six chapters with the first chapter presenting the research proposal, followed by five chapters exposing our systematic work prepared as one review and four research papers. As each paper accommodates an individual Material and Methods section, a separate methods chapter is not included in the thesis. All chapters contain individual conclusion sections, however a separate Conclusion and Outlook section is accommodated to discuss the main outcomes of the thesis study as well as the future research directions. A distinct References section embodies the literature cited in different chapters. Appendices contain supplementary information related to each research paper presented in chapters 3-6.

In the second chapter of this thesis, an extensive literature review investigates the open literature covering the journal articles and patents published in years between 1990's and 2018 mainly on glycerol etherification with isobutene. The review also contains information on different glycerol valorization routes wherein similar acid catalysts were used, with the aim of

brainstorming on which catalyst modification and what type of reactor configuration could enable high yields of the desired GTBEs. This work was published in ***Fuel Processing Technology*** in 2015, with the title "**Alternative fuel additives from glycerol by etherification with isobutene: Structure–performance relationships in solid catalysts**".

In the third chapter of this thesis, using Approach 1, we tested over 80 Brønsted acid catalysts consisting of ion exchange resins, zeolites, mesoporous silica, heteropolyacids and supported heteropolyacids in batch reactor under identical conditions (temperature of 75 °C, catalyst amount 7.5 wt% of initial glycerol, isobutene:glycerol ratio of 3:1 mol:mol, reactor pressure 10-15 bar, reaction time of 6 h). This extensive study disclosed the ion exchange resins to be the most promising catalysts resulted in highest yields of desired ethers (86 wt% di- + tri-GTBE for Amberlyst 15™). This work was submitted to ***Catalysis Today***, with the title "**Screening of solid acid catalysts for etherification of glycerol with isobutene under identical conditions**". We have also made a patent application about the precise dosing of liquid phase isobutene to the multiple batch reactor system, titled "**Kesikli reaktörler için sıvılaştırılmış gaz yakıt dolum metodu ve sistemi-A system and method for feeding liquified gas fuel to batch reactors"**.

The fourth chapter focuses on the Amberlyst 15™ ion exchange resin, based on the Approach 2. The desired di- and tri-GTBE yield was further increased upon cation exchange modification with Na^+. We developed a Fourier Transfer Infrared Spectroscopy (FTIR) based method to determine the acid strength of Amberlyst 15™ and its Na^+-exchanged counterparts. Using this method, acid strength of the remaining acid sites increased with partially exchanging some portion of the protonic sites with sodium cations, resulting in higher selectivity to desired ethers and lower selectivity to isobutene oligomers. Using our Approach 3, we conducted glycerol etherification in a flow reactor at differential glycerol conversion (< 3 wt%) with Amberlyst 15™ counterparts of low and high acid strength. **The tubular flow reactor system**

was for the first time exploited in literature for the etherification of glycerol with isobutene. At infinitesimal glycerol conversion, the desired di- and tri-GTBE formed as the primary reaction products on Brønsted acid sites of high strength. Combination of Approach 2 and 3 helped us to understand the enhanced selectivity to the desired ethers at high acid strength. This work is published in ***Molecular Catalysis*** with the title "**Assessment of acid strength in sodium-exchanged acid resins: consequences on glycerol etherification with isobutene in batch and flow reactors**". We also made a patent application to Turkish Patent Institute, named "**Gliserinin eterifikasyonu için bir sistem ve yöntem-A system and method for glycerine etherification**".

In the fifth chapter, based on the Approach 3, we tested our most promising commercial catalyst, Amberlyst 15™, in our flow reactor system to determine the minimum catalyst particle size without pressure drop and with negligible mass transfer resistance. Mears and Weisz-Prater parameters were calculated to evaluate the external and internal mass transfer limitations, respectively, for the first time in literature for glycerol etherification with isobutene. **The superior productivity of the flow reactor compared to a batch reactor has been realized by this study, as a novel contribution to literature**. We have prepared a manuscript titled "**Etherification of glycerol with isobutene in a once-through fixed bed tubular flow reactor**" to be submitted to ***Applied Catalysis B: Environmental***.

In the sixth chapter, to realize Approach 4, six GTBE mixtures with changing individual ether concentrations were prepared to test **their fuel compatibility with gasoline**. With improved octane number and reduced vapor pressure, the GTBE blend of the **highest tri-GTBE content** was selected as the most compatible fuel additive formulation. An **internal combustion engine dynamometer** was used to test the power output and emissions from this GTBE blend and also from the 3.45 vol% MTBE blend. At urban driving conditions of 2400 rpm engine speed, the power output of the GTBE blend was similar to that of the MTBE blend.

The GTBE blend emitted **lower CO_2 and CO** compared to gasoline. Our results confirmed that GTBE is an alternative gasoline additive to MTBE as their blends provide similar torque values, specific fuel consumption and mean emissions. **With this study, the engine test results with GTBE were for the first time reported in literature.** This work has been submitted to the ***Fuel*** journal with the title "**Compatibility of di- and tri-*tert*-butyl glycerol ethers with gasoline**".

Chapter 2

Alternative Fuel Additives from Glycerol by Etherification with Isobutene: Structure-Performance Relationships in Solid Catalysts

This chapter has been published in Fuel Processing Technology 138 (2015) 780-804, by authors Ö.D. Bozkurt, F.M. Tunç, N. Bağlar, S. Çelebi, İ.D. Günbaş and A. Uzun. The original manuscript has been rearranged and reformatted to conform the format requirements of the dissertation.

2.1.Introduction

For the last decade, transesterification of triglycerides has gained importance in the production of biodiesel, which is a renewable and biodegradable alternative to fossil fuel resources with its excellent fuel blending properties, such as lubricity, high flash point, viscosity, limited exhaust emissions and high cetane number [16-19]. In the presence of an alkali compound, such as NaOH, KOH, and alkoxides or an acid, such as sulfuric, phosphoric, hydrochloric, and organic sulfonic acid catalysts, the triglycerides of fats and oils are transesterified homogenously by short-chain alcohols, such as methanol and ethanol [20,21].

Heterogeneous catalysts, such as zeolites [22], heteropolyacids impregnated on different solid supports [23], $CaMnO_3$ [24], and KNO_3/Al_2O_3 [25], have also been developed for transesterification of triglycerides. However, more studies are required for heterogeneous catalysts to be used in the production of biodiesel commercially because of their stability problems. The most important process in the large scale production of biodiesel is the transesterification of triglycerides using alkali catalysts which are approximately 4000 times more active than their acid counterparts [26]. One of the side effects of this process is that approximately 10 wt% glycerol by-product is generated. A current market study announced that in 2013, 63% of global glycerol production was sourced from the biodiesel industry, with over 1.4 million tons of biodiesel associated glycerol [27]. The estimated biodiesel production in the upcoming years is shown in **Figure 2-1**. According to **Figure 2-1**, it can be approximated that over 3 million tons of crude glycerol will be produced when the biodiesel production reaches to 41 billion liters (36 million tons) by 2020 [28].

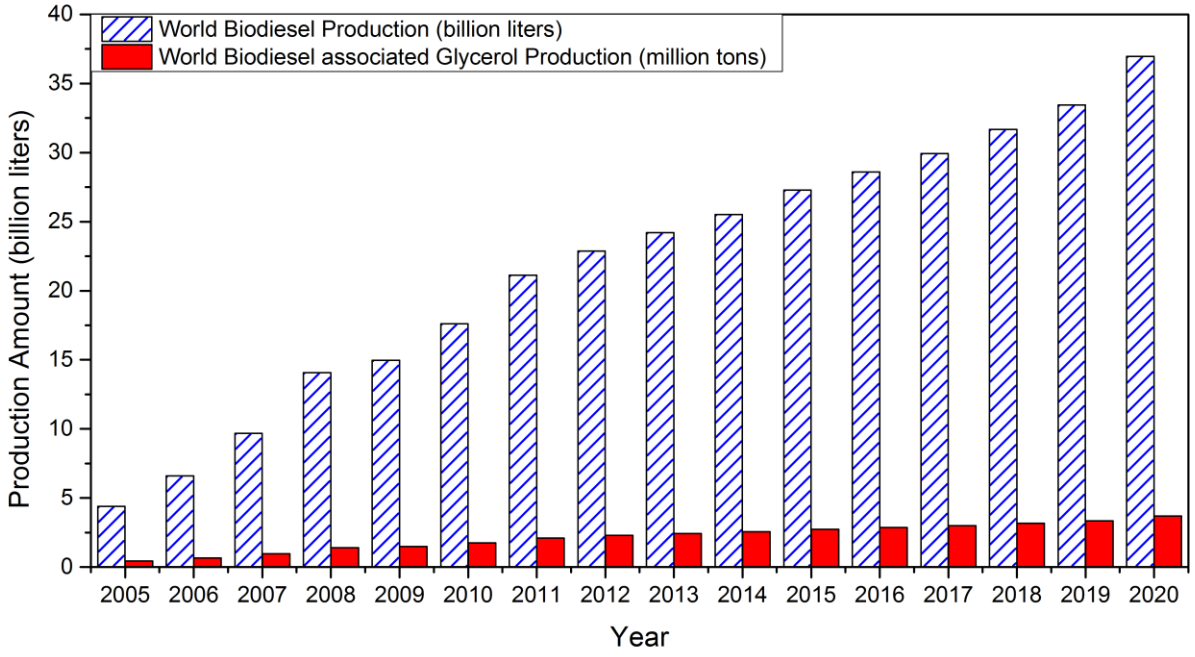

Figure 2-1. Development of the world biodiesel market; world biodiesel production in billion liters and associated glycerol production in million tons in years 2005–2010 (data) and 2010–2020 (projection). Redrawn from Ref. [28].

Such tremendous increase in glycerol production will directly affect the overall economy of the biodiesel production. Direct combustion of glycerol is not feasible in engines because glycerol is associated with high viscosity, low heating value, high auto-ignition temperature and corrosive salt content (for crude glycerol), moreover its incomplete combustion results in carcinogenic acrolein production [29-31]. Therefore, new processes should be proposed to transform by-product glycerol to value-added chemicals. Some of the different strategies and approaches for this purpose are summarized in **Figure 2-2**. Among these transformation strategies, the route including the production of fuel additives from glycerol by etherification has received special attention since such glycerol ethers can be blended with gasoline, diesel and jet fuel [14]. Recently, European Commission Directive 2009/28/EC has set a target mandating 10% of the energy share in transportation to be supplied by renewable

sources by 2020 [32]. The "Biofuels Transport Roadmap" of International Energy Agency claims that 27% of transport fuel in 2050 will consist of biofuels [33]. Fuel additives produced with the alternative etherification route and containing high amount of renewable glycerol would meet future renewable targets [34], enhance the total biofuel output in biodiesel production [35], reduce dependency on depleting sources, alleviate petroleum price uncertainties and support the growing biodiesel industry [36].

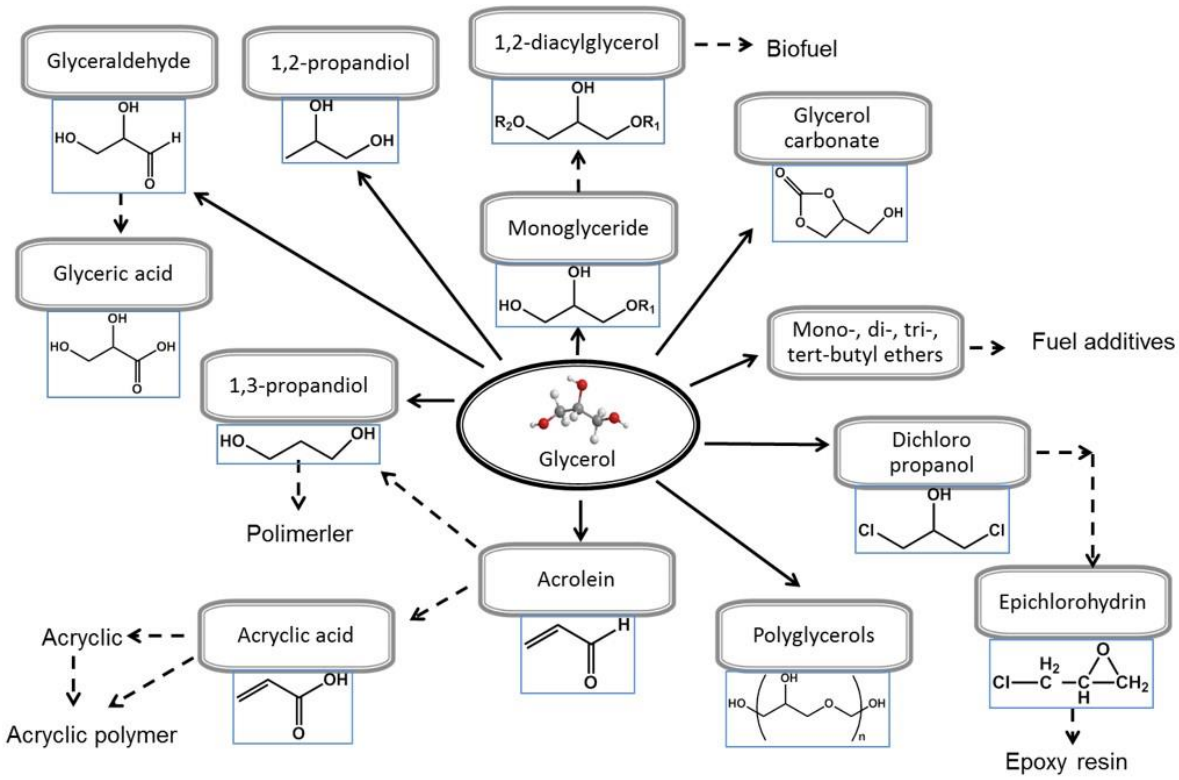

Figure 2-2. Glycerol-based chemicals production routes.

Transformation of glycerol into glycerol ethers have been studied through several chemical routes namely, acetylation, esterification and etherification processes. Isobutene (IB) [37-62], tertiary butyl alcohol [39,63-79], glycerol [80-83], and refinery fractions [10,54] were used for the etherification reaction as alkylation agents. Among these routes, the etherification of glycerol with IB and butanol is important as the reaction products can be directly blended with fuels. Among these two alkylation agents IB has an advantage of being readily available in petroleum refineries.

IB is one of the butenes formed in the catalytic cracking units of crude oil refineries. The $C4^{=}$ mixture is an isomeric combination of 1-butene, cis/trans-2-butene and IB. One of the major uses of IB is the production of octane booster fuel oxygenate, methyl tertiary butyl ether (MTBE), done by reacting the C4 olefin mixture with methanol under mild acidic conditions, wherein solely IB is reactive while the other components in the C4 mixture act as inert. Established commercial MTBE production employs sulfonic ion exchange resins such as Amberlyst 15™ and Amberlyst 35™ in liquid phase under moderate temperature (30-100 °C) and pressure (20 bar) conditions, while other catalysts such as zeolites and heteropolyacids have been proposed for the process [8,84,85]. MTBE is now regarded as an environmentally unfriendly chemical because of contaminating the groundwater reservoirs by its high water miscibility. Therefore, the projected decline in MTBE production is likely to influence on the future IB consumption [86]. Glycerol etherification with IB produces di- and tri-tertiary butyl ethers of glycerol (DTBGE and TTBGE), generally referred to ‘higher ethers’ with very slight water miscibility, which are fuel oxygenate alternatives of MTBE. These higher ethers can also be blended with diesel. When blended, they can reduce carbon monoxide, particulate matter, nitrogen oxide, hydrocarbon and aldehyde emissions, which result from incomplete combustion [87,88], as well as improving the cold flow properties [89,90]. Production of the higher ethers can be realized commercially by using the catalysts of the well-established MTBE process, as

both reactions are etherification in which IB is used as the alkylation agent. Biodiesel production can be coupled with glycerol etherification [35,44,90], for example desired ethers can be extracted by the FAME feed in an extraction unit. Integrated biodiesel and petroleum refineries may be developed in which glycerol from biodiesel production and IB from petroleum refining (*e.g.* catalytic cracking) are fed to an etherification unit to obtain the diesel and bio-diesel additives directly. Fuel additives produced with these ways would reduce the transportation costs and improve the economy of the overall process.

Fuel additives production from glycerol has been elaborated in several review articles [29,30,34,36,91-99], with the driving force of benefiting from this biodiesel industry by-product in the energy field. Behr et al. [34] remarked that the production of the DTBGE and TTBGE from biodiesel industry derived glycerol would help achieving the renewable targets of European Union. Demirbas [91] pointed out to the feasibility of glycerol alkyl ethers produced by using IB, because of their cloud point and viscosity reducing potential in diesel fuel. Guerrero-Pérez et al. [92] highlighted glycerol as a platform chemical in future bio-refineries and remarked the success of using strong acid macroreticular ion-exchange resins and sulfonic mesostructured silica as acid catalysts in experimental glycerol etherification studies with IB, which yield in complete glycerol conversion and over 90% selectivity towards desired ethers. Rahmat et al. [36] mentioned the cloud point depressant/pour point improver properties of glycerol ethers in diesel blends and octane boosting properties in gasoline blends and then elucidated how glycerol conversion and selectivity to desired ethers are influenced by solid catalyst properties, such as acidity, basicity, porosity, surface area, pore volume, catalyst loading and operating conditions such as reactant feed, temperature and reaction time. Gupta et al. [29] evaluated the usage of surplus glycerol as an energy source in various pathways, also discussing the potency of glycerol tertiary ethers as diesel additives by means of their good blending properties, high cetane number and high oxygen content which could prevent

incomplete fuel combustion. Ayoub et al. [93] took a look at the world glycerol market and reported that surplus glycerol has been increasing in parallel with biodiesel industry in European Union, US and Southeast Asia (projected to be 5.8 billion pounds in 2020). Therefore, the use of that much glycerol to value-added products would be significant in solving the excess glycerol problem and reducing biodiesel manufacturing costs. Leoneti et al. [94] addressed a fuel additives production from glycerol as one alternative way for sustaining the biofuel market. It was stated the potential of utilizing tertiary butyl alcohol, IB or FCC (fluidized catalytic cracking) gasoline for producing the branched oxygen containing glycerol ethers. Izquerido et al. [95] addressed some issues in glycerol etherification with IB, including the importance of reaction conditions, reaction phases, viscosity of reaction mixture, stirring rate, solvent effect and catalyst improvement such as creating strong acid centers by sulfonic acid functionalization, increasing the surface area, pore size and pore volume by acid treatment or avoiding secondary reactions by H^+ exchange with metal cations. Zhou et al. [96] indicated the main disadvantage of biodiesel derived crude glycerol to be its impurity. Therefore, usability of crude glycerol in new applications and availability of cheaper refining processes were shown to be among the challenges for its commercialization. The value-added products, *i.e.* tertiary butyl ethers of glycerol, which are most likely to be produced by using strong acid ion exchange resins in commercial scale, have high potential to be used in diesel and gasoline as alternative fuel oxygenates to conventional ones such as MTBE and ethyl *tert*-butyl ether (ETBE), with an increasing demand for these new alternatives in the market in a few years. In their thorough review Zhou et al. [97], evaluated the research conducted between 2008 and 2012 on catalytic conversion of glycerol to fuels and value-added products, in which they connected the success in etherification of glycerol to tertiary butyl glycerol to the catalyst types. Quispe at al. [30] adverted the volatility of the glycerol market with price fluctuations because of biodiesel derived glycerol; however, exploring new applications for this abundant crude glycerol would

help its price stabilization. They addressed the importance of glycerol tertiary butyl ethers produced by selective etherification, as fuel additives in gasoline or petroleum engines without changing the existing designs. Bagheri et al. reviewed the catalytic conversion pathways of glycerol into a variety of chemicals including etherification. They pointed out the favorability of using IB as an alkylation agent since 100% glycerol conversion at various temperature ranges over using macroreticular ion exchange or sulfonic mesostructured silica catalysts is achievable [98]. Ardi et al. [99] compiled the advantages and disadvantages of glycerol refining methods of vacuum distillation, ion exchange, activated carbon and membrane separation, stating the potential of membrane separation technology for the crude glycerol purification process more economical when compared to the widespread vacuum distillation technology, as well as providing a sustainable biodiesel industry.

As can be deduced from the review papers mentioned above, glycerol is a noteworthy raw material for fuel additives production. Utilization of crude glycerol from biodiesel industry as a raw material in fuel additives production, following proper refining steps, would help sustaining the growing biodiesel industry. Crucial reaction parameters and catalyst types for obtaining high glycerol conversion and desired ether yields in glycerol etherification have been presented in detail. However, these reviews mostly focus on the reaction conditions but not on the type of catalysts and their structure-performance relationships for this reaction. Moreover, the modifications of catalyst structures to improve the catalytic properties were not elaborated much. Therefore, to complement these reviews, here we present an extended review on glycerol etherification with IB on heterogeneous catalysts, preliminary focusing on the type of catalysts and their structure-performance relationships based on worldwide research conducted from 1990 to the end of 2014.

2.2.Etherification of glycerol with isobutene

2.2.1. Reaction mechanisms, thermodynamics and kinetics

The general mechanism between glycerol and IB to produce glycerol ethers is introduced in Reactions 1 to 3 and in **Figure 2-3**. The reaction of glycerol (G) with IB produces isomers of MTBGE: 3-*tert*-butoxy-1,2-propanediol (MTBGE1) and 2-*tert*-butoxy-1,3-propanediol (MTBGE2), isomers of DTBGE: 2,3-di-*tert*-butoxy-1-propanol (DTBGE1) and 1,3-di-*tert*-butoxy-2-propanol (DTBGE2) and TTBGE (1,2,3-tri-*tert*-butoxypropane).

G + IB ↔ MTBGE (1)

MTBGE + IB ↔ DTBGE (2)

DTBGE + IB ↔ TTBGE (3)

Primary hydroxyl groups of glycerol are preferred over secondary hydroxyl groups in the reaction, thus more abundant mono- and di-ethers are 3-*tert*-butoxy-1,2-propanediol and 1,3-di-*tert*-butoxy-2-propanol, respectively [39,40]. Without mentioning a catalyst type or a reaction condition, generally, protonation of glycerol molecule by heat or catalyst effect turns glycerol to an electron acceptor, which then accepts electrons from the electron donor isobutene [36].

As secondary reactions, disproportionation of glycerol ethers (Reactions 4 and 5), oligomerization of IB to C8, C12 and C16 olefins, such as di-isobutene (DIB) as a C8-product (Reaction 6) and tri-isobutene (TIB) as a C12-product (Reaction 7) and, the formation of *tert*-butyl alcohol (TBA) in the presence of water, (Reaction 8) may occur [41,45].

2 DTBGE ↔ TTBGE + MTBGE (4)

2 MTBGE ↔ DTBGE + G (5)

IB + IB ↔ DIB (6)

DIB + IB → TIB (7)

IB + H_2O ↔ TBA (8)

Among the ether products, DTBGE and TTBGE are preferred for diesel/biodiesel blends as they have less polar structure and better solubility in diesel fuel compared to MTBGE; for instance, MTBGE was reported to be insoluble for over 3% v/v diesel blends [100]. As MTBGE enhances the water solubility of fuels, having low MTBGE concentrations is suggested for diesel, biodiesel and gasoline blends [101].

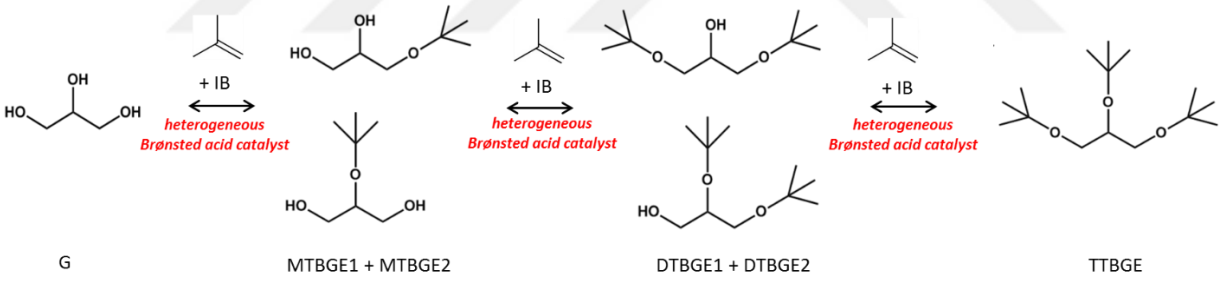

Figure 2-3. The reaction mechanism of glycerol etherification with isobutene, tertiary butylation.

Behr and Obendorf introduced the first liquid-liquid equilibrium (LLE) diagrams of the species in the glycerol etherification reaction [38]. In the quaternary system of G, IB (denoted as I), MTBGE (denoted as M) and higher ethers DTBGE + TTBGE (denoted as H) at 20 bar to ensure liquid IB, there are two miscibility gaps, for instance glycerol is immiscible with IB as

well as with higher ethers (**Figure 2-4**). IB phase keeps most of the high ethers as the nonpolar phase, while glycerol keeps the MTBGE as the polar phase. Two distinct phases at the beginning of the reaction, isobutene in the upper phase and glycerol in the lower phase, was found to merge after a specific glycerol conversion, because the solubilization of glycerol in the upper phase increases with increasing MTBGE and DTBGE concentrations. This phenomena is also visible from the phase diagram that two-phase system can pass into a one-phase system in the case of decreasing glycerol and increasing MTBGE/higher-ether concentrations (MGH triangle) or decreasing glycerol, decreasing IB and increasing MTBGE concentrations (MGI triangle) [38]. For instance, after 40 minutes of the reaction, the two-phase period ended, in which both lower and upper phase consisted of similar concentrations of components, following approximately as 40 wt% DTBGE, 30 wt% MTBGE and 5 wt% glycerol (IB and TTBGE concentrations not provided).

Liu et al. have recently developed a liquid-liquid-solid mass transfer model in the heterogeneous etherification of glycerol with isobutene (**Figure 2-6**) [102]. The liquid-liquid-solid notation represented the isobutene rich phase-glycerol rich phase-catalyst surface. They assumed the catalyst particles to disperse in the glycerol rich phase, with the isobutene rich phase interacting with the glycerol rich phase. Isobutene is always transferred to the glycerol rich phase and its flux maximizes when MTBGE formation rate in the glycerol rich phase was the highest (at 2nd hour). DTBGE and TTBGE are trasferred from the glycerol rich phase to the isobutene rich phase until the reaction equilibrium is achieved (at 5th hour). Later on, as glycerol is consumed, the ether products occure in the isobutene rich phase.

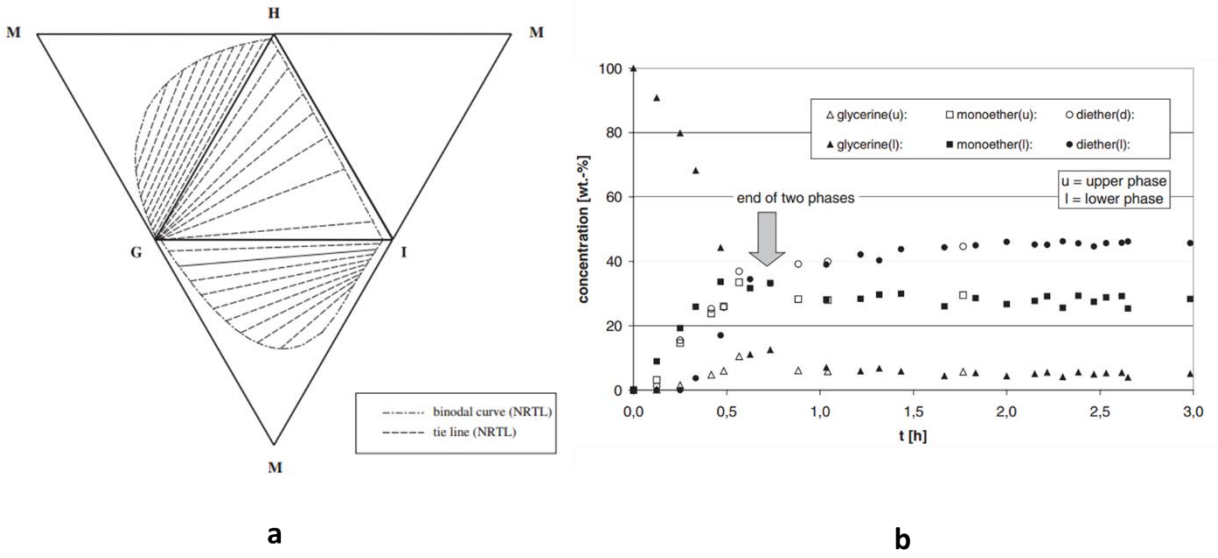

Figure 2-4. a: Phase diagram of the quaternary system for glycerol (G), mono-ether (M), higher-ethers (H) and isobutene (I), NRTL model, T=90 °C, P=20 bar; **b:** Concentration-time graph for glycerol, mono-ether and di-ether showing the point where two phases merge into one phase. Reprinted from Ref. [38] with permission from John Wiley and Sons, Copyright 2002.

Liu et al. performed extensive study to undersrand the phase behaviour in glycerol etherification with isobutene. The LLE model of Behr and Obendorf was later improved by them (**Figure 2-5**) [103] by taking the lumped DTBGE and TTBGE as separate compounds since their solubilities were different. The experimental LLE data, which consists of glycerol and tertiary butyl ethers, were fit to NRTL, UNIFAC, UNIFAC-LLE and UNIFAC-Dortmund models for temperatures 70, 80, 90, and 100 °C at 101.3 kPa and respective model parameters were obtained for this system. The phase diagram by Liu et al., as shown in **Figure 2-5**, demonstrates that there is only one phase for a mixture of high glycerol and high MTBGE concentration at around 30 wt%. However, when DTBGE concentration increases and MTBGE concentration decreases, immisciblity begins and two phases were observed (**Figure 2-5 a**). When there is TTBGE in the medium, two phases are more likely to occur even at low

concentrations of TTBGE; whereas one phase can occur at very low glycerol and high MTBGE concentrations (**Figure 2-5 b**). When there are DTBGE and TTBGE in the medium together with glycerol, the system is almost immiscible and can only become a single phase at very low glycerol and very high DTBGE concentrations (**Figure 2-5 c**). This result can explain why "the end of two phases" was observed by Behr and Obendorf under elevated MTBGE concentration over 30 wt% and dropped glycerol concentration under 10 wt% in the etherification medium.

Liu and coworkers also developed a kinetic model for the etherification of glycerol with IB over a heterogeneous catalyst, NKC-9, which is a commercial macroporous strong acidic ion exchange resin [104]. Catalyst particles smaller than 0.6 mm were employed to eliminate internal diffusion limitations; while the stirring rate in the batch reactor were fixed above 1200 rpm to eliminate external diffusion limitations. A modified Eley-Rideal mechanism correlated well with the experimental data, in which acceleration of the reaction rates with increasing MTBGE concentration was considered. In the model, glycerol and IB were the species adsorbing into nearby active sites, while the adsorption of MTBGE, DTBGE, TTBGE and DIB were negligible. Adsorption of glycerol and IB was followed by the formation of MTBGE in the first surface reaction. Surface reactions for the formation of DTBGE and TTBGE preceeded with the interaction of bulk phase MTBGE and DTBGE, respectively, with absorbed IB; whereas the DIB formation occurred with the interaction of two nearby absorbed IB species. These surface reactions were claimed to be the rate limiting step. After complete glycerol conversion, IB conversion was observed to slow down, which was also the case observed by Karinen and Krause, using Amberlyst 35^{TM} macroreticular ion exchange resin as a catalyst [40]. In addition, Klepacova et al., using Amberlyst 15™ macroreticular ion exchange resin, pointed out the influence of glycerol on the dissociation of proton from sulfonic acid functional groups to activate IB to form tertiary butyl cation [41].

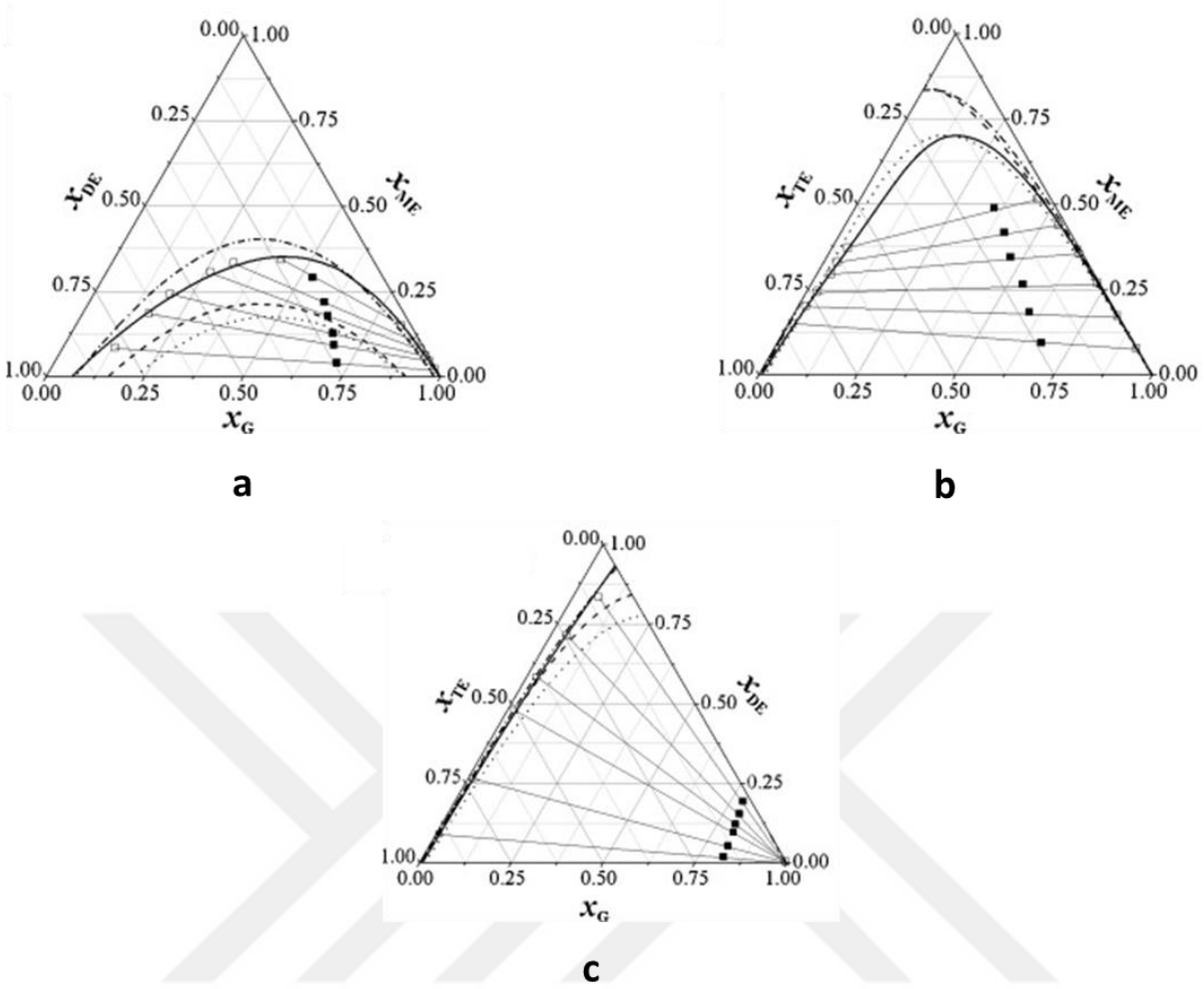

Figure 2-5. The experimental and modeled phase diagrams of the ternary system for glycerol (G) with its tertiary butyl ethers mono-*tert*-butyl glycerol (ME), di-*tert*-butyl glycerol (DE) and tri-*tert*-butyl glycerol (TE), Model predictions with NRTL, UNIFAC, UNIFAC-LLE and UNIFAC-Dortmund models, T=90 °C, P=1.013 bar. **a:** G-ME-DE; **b:** G-ME-TE; **c:** G-DE-TE. ▪ Overall composition; ▫ Experimental tie line data; ― Phase diagram calculated by NRTL model; ○ Tie lines calculated by NRTL model. Reprinted from Ref. [103] with permission from Elsevier, Copyright 2013.

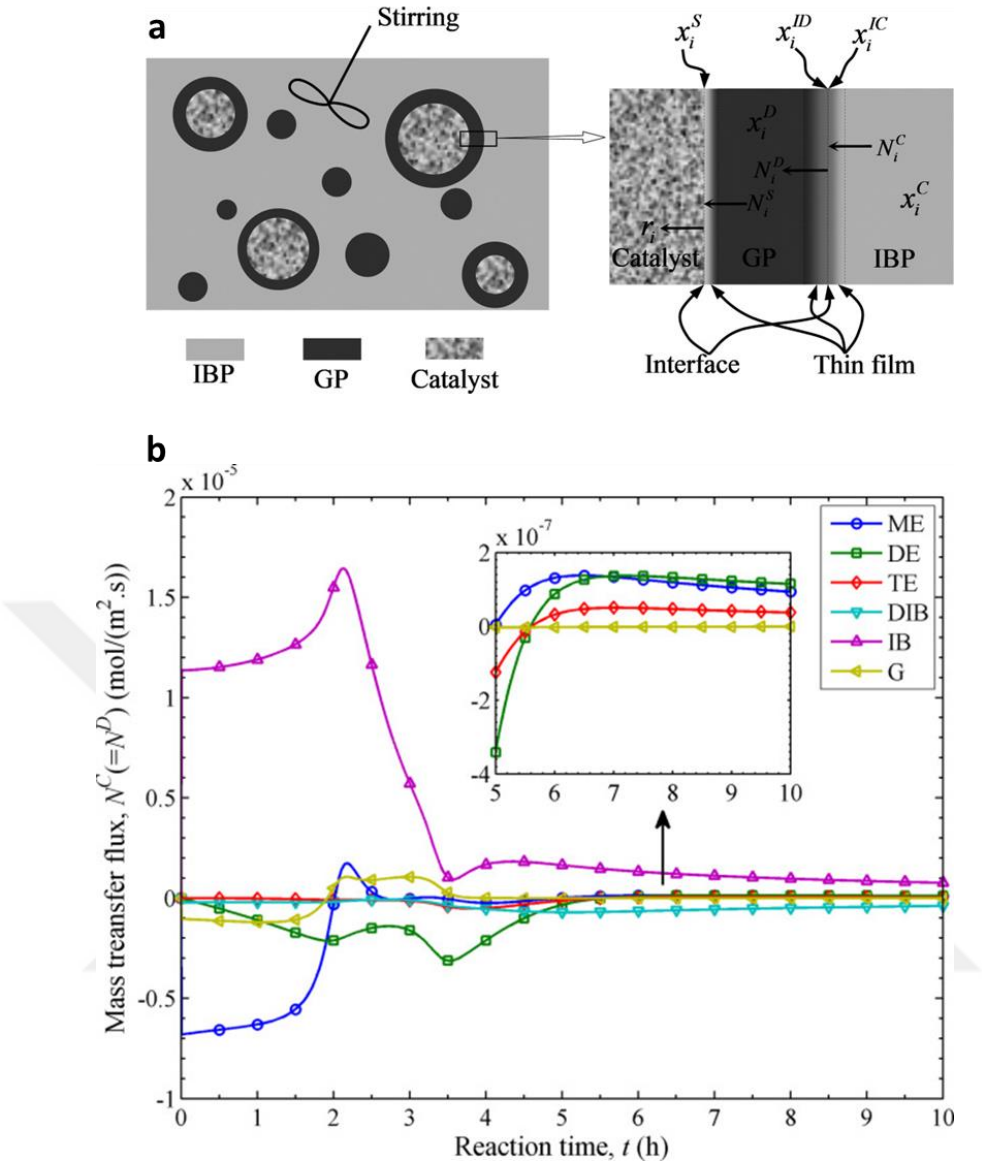

Figure 2-6. a: Mass transfer model by Liu et al. for the stirred batch reactor; **b:** change in the molar mass transfer fluxes between the isobutene rich and glycerol rich phases with reaction time [102]. Positive flux represents transfer from isobutene rich to the glycerol rich phase, and vice versa. Reaction conditions are 90 °C, 5.7 wt% glycerol catalyst loading, 4:1 isobutene:glycerol molar ratio. Composition of the reaction mixture was retrieved from a previous study [104]. Reaction components are glycerol (G), isobutene (IB), mono-*tert*-butyl glycerol (ME), di-*tert*-butyl glycerol (DE), tri-*tert*-butyl glycerol (TE) and di-isobutene (DIB). Reprinted from Ref. [102] with permission from Elsevier, Copyright 2013.

2.2.2. Process designs and experimental settings

ARCO Process [105] and the BEHR Process [38] have been proposed for continuous glycerol ether production by employing homogenous acid catalyst *p*-toluenesulfonic acid (p-TSA) (**Figure 2-7 a and b**).

In ARCO Process, etherification is carried out in a two-phase CSTR; the lower (polar) phase consisting of unreacted glycerol, catalyst and MTBGE is recycled back to the reactor; while the IB and higher ether containing upper phase is first sent to a flash unit to remove excess IB and then the rest of the upper phase is washed with water to get rid of glycerol, catalyst and MTBGE traces and finally form the product phase. In BEHR process, continuous acid catalyzed reaction is performed in three consecutive stirred vessels. Pure glycerol is fed to the extractor instead of the reactors to extract catalyst and MTBGE from the reaction product. Raffinate phase from the extractor, which consists of unreacted IB and higher ethers, is sent to a flash unit to remove unreacted IB, while the lower phase of the flash is directed to a vacuum rectification column to obtain pure higher ethers. Finally, the upper phase of the rectification column becomes the high purity desired ether products and the lower phase containing catalyst is sent back to the reactor. Using the kinetic and LLE data from Behr and Obendorf's study [38] as basis, the BEHR process has latter been improved in several conceptual designs [106-108], including the integration into FAME production process [35].

Process configurations for continuous glycerol ether production using heterogeneous catalysts have also been introduced in a patent by Noureddini [90] and in a conceptual design by Di Serio and coworkers [44]. The process idea by Noureddini [90] couples FAME production with glycerol etherification so that the final product is biodiesel blend with the tertiary butyl ethers of glycerol with a cloud point below 0 °C (**Figure 2-7 c**). Crude glycerol is refined through removal of anions (*e.g.* Na^+, K^+) and methanol before being fed to the

etherification reactor, in which Amberlyst 15™ ion exchange resin is used as a catalyst. The final biodiesel blend consists of 88 wt% FAME and 12 wt% ethers (*e.g.* > 80 wt% of ethers is DTBGE and the rest mainly TTBGE), while the production of IB oligomers is ignored by stating that the careful selection of the catalyst and reaction conditions may minimize oligomer production.

The conceptual design by Di Serio et al. [44] simulated in Chemcad™, pure glycerol instead of crude glycerol is considered (**Figure 2-7 d**). FAME is used as the extracting agent of glycerol tertiary butyl ethers from the reaction mixture and this mixture was washed with water to remove excess glycerol, followed by the removal of C8-C12 hydrocarbons in series of flash units. The final product was a biodiesel blend with 92.5 wt% FAME, 2.2 wt% MTBGE, 4.7 wt% DTBGE, 0.5 wt% TTBGE and trace amounts of G and DIB, which was claimed to be suitable as a fuel with additive according to biodiesel standard EN 14214.

There has been no flow reactor study on glycerol etherification with isobutene. Besides, pure glycerol and pure IB in liquid form have been used in most of the studies to understand the basic facts of the etherification reaction. However, there are also a few studies revealing the conversion and yield outcomes in the case of crude glycerol from biodiesel production [37,54], IB from petrochemical C4 fraction [54], and FCC gasoline itself [10]. Almost all studies have employed laboratory scale batch reactor settings.

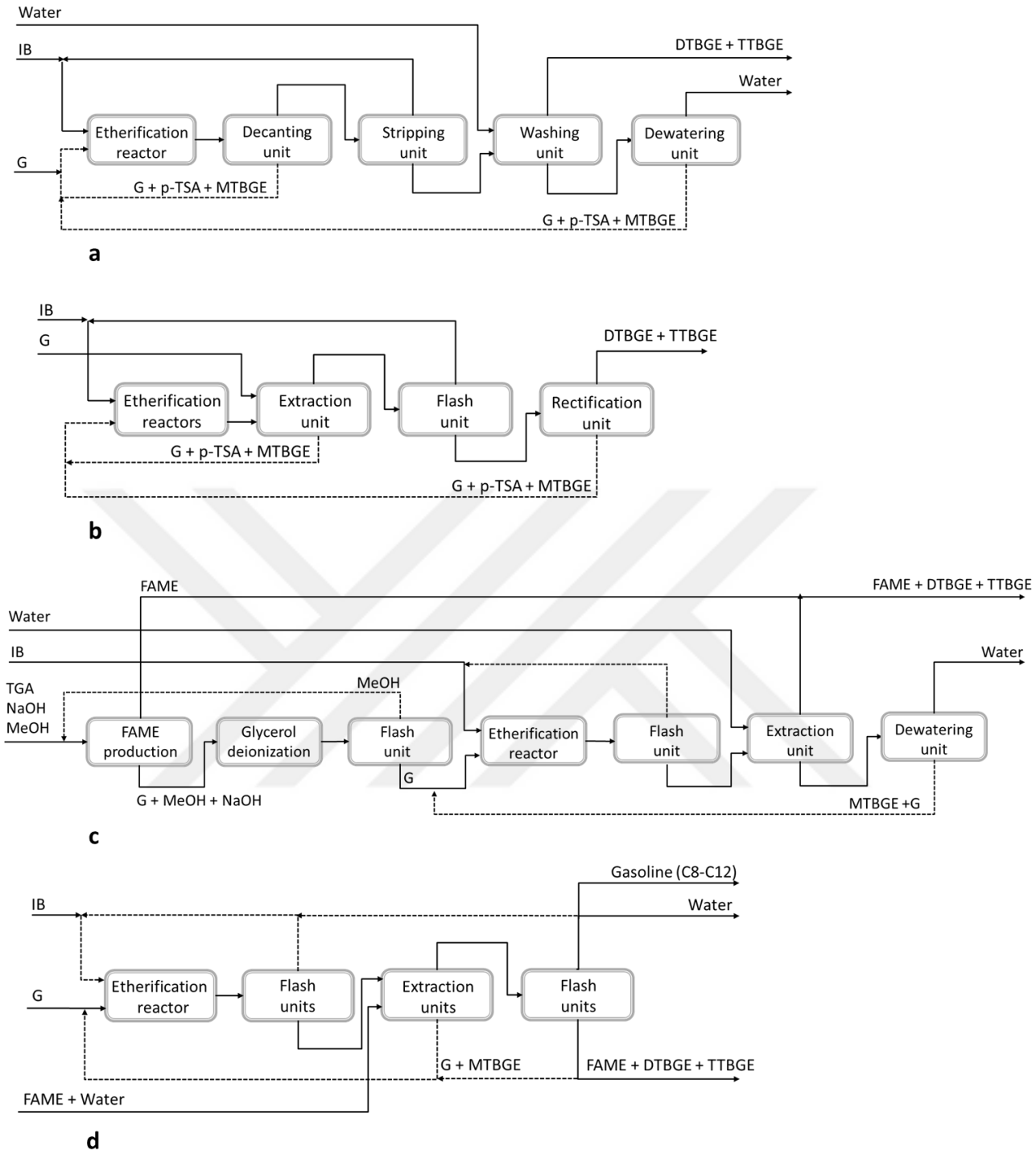

Figure 2-7. Flow charts for continuous production of glycerol tertiary butyl ethers. Redrawn from original process flow diagrams; **a:** ARCO Process [105]; **b:** BEHR Process [38]; **c:** Process design from H. Noureddini [90]; **d:** Process design from Di Serio et al [44].

Flow reactor systems have been studied in glycerol etherification with tertiary butyl alcohol [64,67,71,72,109], ethanol etherification with C5 olefins [110], glycerol etherification with ethanol [111] and glycerol ketalization with acetone [112]. Simasatitkul et al. investigated a reactive distillation column for glycerol etherification with TBA in which reaction and separation occurs in a single unit to reduce the capital cost. Simulation of the column in Aspen Plus demonstrated that the total annual cost of the column can be minimized by optimizing the number of reactive, rectifying and stripping stages to give 99 mol% glycerol conversion and 99 mol% yield of the desired di- and tri-ethers [109]. Lemos et al. used a pressurized tubular flow reactor system for glycerol etherification with ethanol. Amberlyst 15™ ion exchange resin and zeolite Beta were tested at 150-250 °C temperature, 10:1 ethanol:glycerol molar ratio, 400 mg catalyst and 85 bar pressure conditions. Glycerol conversion and ether yield were higher in the case of Amberlyst 15™, wherein ether yield was strongly dependent on temperature and catalyst loading [111].

2.2.3. Catalyst types

The etherification of glycerol with isobutene was performed using either homogeneous or heterogeneous catalysts with acidic properties. In the early studies (1970's to 2000's), homogenous catalysts, such as *p*-toluenesulfonic acid and heterogeneous catalysts, such as acidic ion exchange resins, which were already used in commercial ether production (*e.g.* MTBE), were applied [37-39] in glycerol etherification with isobutene. Although high glycerol conversion, high desired ether selectivity and low DIB selectivity were obtained with homogenous catalysts, difficulties in catalyst-product separation, corrosion and environmental issues reduced the interest on the commercialization of glycerol ether production. Subsequently, as well as improving the catalytic environment of ion exchange resins [41,43,45,48], different heterogeneous catalysts covering pure or modified wide pore zeolites

[39,41,45,48,49,52,54,55,58], functionalized mesostructured materials [42,46,50,60] and other heterogeneous acid catalysts such as montmorillonite K-10, amorphous microporous mixed oxide [38] , sulfonated peanut shell [47], solid heteropolyacids [38,45,53], spherical silica supported Hyflon [51], sulfonated graphene [61], sulfonic acid functionalized aerogels [57], triflic acid supported on gamma alumina [60,62] were elaborated by comparing their performance with acidic ion exchange resins and attempting to understand effects of catalyst structures, such as porosity, surface area, pore size, pore volume, acid capacity, acid strength on catalytic activity, expressed by glycerol conversion, ether selectivity and side product formation.

Here, we focus on heterogeneous catalysts used for glycerol etherification with isobutene and petrochemical C4 fractions, by grouping them into four main groups: i) ion exchange resins (**Figure 2-8 a**); ii) zeolites (**Figure 2-8 b**); iii) mesoporous silica (**Figure 2-8 c**); and iv) other heterogeneous catalysts with functional groups (**Figure 2-8 d-f**). Studies are reviewed in chronological order, so as to help the reader grasp the accumulation and advancement in time. Employed heterogeneous catalysts, their structural properties, and their catalytic performances in the test reactions are presented in **Table 2-1** to **Table 2-6**.

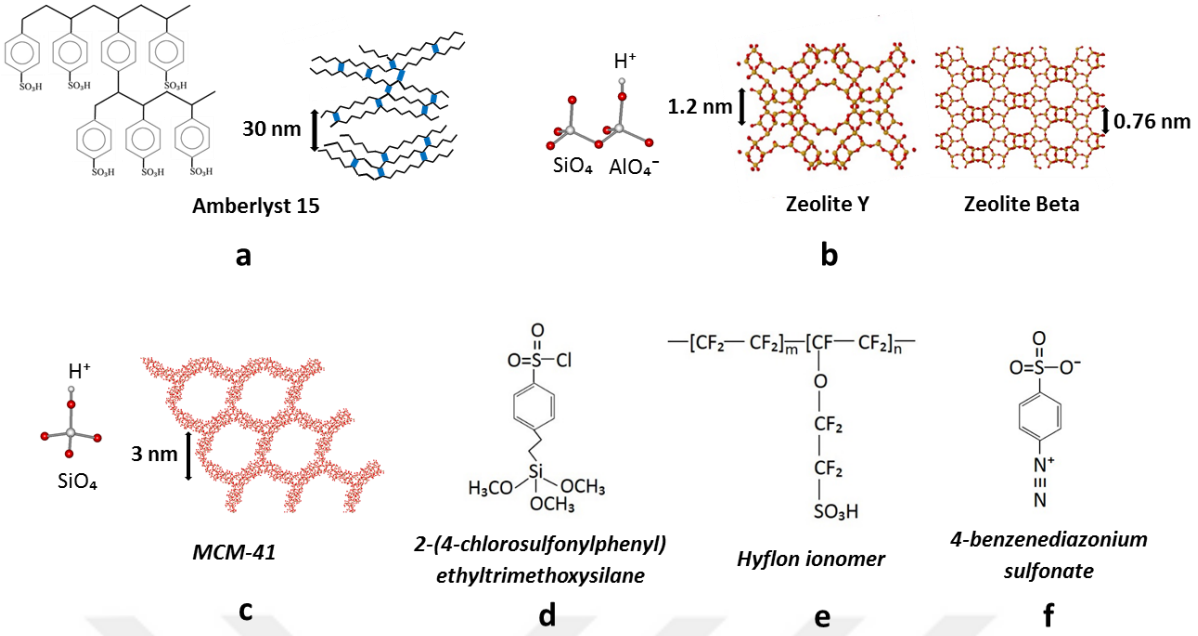

Figure 2-8. Structures of some heterogeneous catalysts. **a:** Amberlyst 15™ macroreticular ion exchange sulfonic acid functional groups and pore structure; **b:** Zeolite H-Y and H-Beta unit structure and cage structure; **c:** Mesoporous silica MCM-41 unit structure and cage structure. Structures of some functional groups; **d:** 2-(4-Chlorosulfonylphenyl) ethyltrimethoxysilane (CSPTMS) used for sulfonation of zeolites and mesoporous silica; **e:** Hyflon ionomer used for functionalization of spherical silica; **f:** 4-benzenediazoniumsulfonate used for sulfonation of reduced graphene oxide.

2.2.3.1. Ion exchange resins

Ion exchange resins are insoluble solid matrices with specific ions attached. These ions can be interchanged with similarly charged ions in a liquid media reversibly with no overall change in the resin's structure. The reactive functional groups in an ion exchange resin can exchange acids, alkalis or metal ions during a reaction, thus may act as catalysts [113]. These macroreticular resins may possess a wide range of pore sizes in their structure. According to

the IUPAC classification porous materials, they can be i) microporous with a pore diameter smaller than 2 nm, ii) mesoporous with a pore diameter between 2-50 nm) and iii) macroporous with a pore diameter larger than 50 nm. Larger macropores correspond to smaller surface areas while smaller micropores point out larger surface areas. Micropore and macropore formation for the ion exchange resins depend on the type of phase separating chemicals called porogenic solvents and the concentration of divinyl crosslinking copolymer used together with the vinyl polymer during resin synthesis [114]. Amberlyst ion exchange resins from Rohm and Haas Company, especially the strong acidic macroreticular catalysts, Amberlyst 15™ and 35™, have been widely used in industry for the production of fuel ether oxygenates (MTBE, ETBE, etc.) via etherification of alcohol with iso-olefins. The catalytic property of Amberlyst resins originates from the sulfonic groups attached to cross-linked styrene divinylbenzene copolymer matrix (**Figure 2-8**) [115]. Although Amberlyst acidic resins are the most popular, SAC-13 ion exchange resins, which consist of carbon fluorine backbone with sulfonic acid carrying side chains [116], were also used as heterogeneous catalysts in some etherification studies [42]. Physical properties and catalytic performance results of tested ion exchange resin catalysts are presented in **Table 2-1** and **Table 2-2**, respectively.

Noureddini et al. [37] conducted one of the first studies on glycerol etherification with IB by using Amberlyst 15™ ion exchange resin as a catalyst. Different reaction conditions, such as temperature, isobutene:glycerol ratio (IB:G, 1:1, 2:1, and 3:1), reaction time, and catalyst amount with respect to the glycerol amount converted were investigated, upon which the optimum reaction conditions yielded in 95 mol% glycerol conversion and high concentrations of desired ethers in the final product mixture. Desired ether formation decreased at higher temperatures both for 2:1 and 3:1 IB:G molar ratios. In contrast, it was found that DIB formation is dependent on both temperature and IB:G molar ratio. For instance, lower concentrations of DIB were obtained at higher temperatures for 3:1 IB:G molar ratio, and at

lower temperatures for 2:1 IB:G molar ratio. In addition, DTBGE and TTBGE concentrations decreased and DIB concentrations increased with progressing reaction time. After two hours of the reaction, the concentrations were almost fixed, which indicates an apparent equilibrium, with glycerol conversion up to 99 mol% for 3:1 IB:G feed. In this case, at first free IB and then the higher ethers became the source of IB in the oligomerization reaction, drawing a gradually increasing trend for MTBGE+DIB and a decreasing one for DTBGE + TTBGE. Afterwards, the desired ether production was positively affected by using over 5 wt% catalyst of glycerol. The catalyst Amberlyst 15™ was also shown to retain its catalytic activity during five consecutive runs each taking four hours reaction time. In the same study, some impurities, such as methanol, water, methyl esters and sodium hydroxide were added to the reactions to mimic crude glycerol etherification with IB. Methanol and water caused partial depletion of IB via formation of MTBE and tertiary butanol, there was no negative effects of methyl esters. However, the existence of sodium hydroxide disturbed the catalyst and reduced the ether yields.

Table 2-1. Physical characteristics of regular and modified ion exchange resin catalysts.

Ion exchange resin	Structure[b]	Cross-linked structure[c]	Form	Acid capacity (meq H^+/g cat)	Average pore diameter (nm)	BET area (m^2/g)	Particle size (mm)	Moisture capacity (wt%)	T_{max}[h] (°C)	Pore volume (cm^3/g)	V_{sp}[i] Water (cm^3/g)	V_{sp}[i] Glycerol (cm^3/g)
Amberlyst 15™ (Dry)[a]	MR	V	H^+	4.7	30	53		≤1.6	120	0.4	1.02	1.13
Amberlyst 15™ (Wet)[a]	MR	V	H^+	4.7	30	53	0.6-0.85	52-57	120	0.4		
Amberlyst 35™ (Dry)[a]	MR	V	H^+	5.2	30	50		≤3	150	0.35	1.01	1.27
Amberlyst 35™ (Wet)[a]	MR	V	H^+	5.2	30	50	0.7-0.95	51-57	150	0.35		
Amberlyst 36™ (Dry)[a]	MR	M	H^+	5.4	24	33		≤1.65	150	0.2	1.50	1.82
Amberlyst 36™ (Wet)[a]	MR	M	H^+	5.4	24	33	0.6-0.85	53-59	150	0.2		
Amberlyst 39 (Wet)[a]	MR	L	H^+	5.0	23	32		60-65	130	0.2	2.23	2.51
Amberlyst 31™ (Wet)[a]	G	L	H^+	4.8				63-67	130		3.02	2.84
Amberlyst 119™ (Wet)[a]	G	M	H^+	4.9				49-55	130		1.32	1.49
CT-275[a]	MR	V	H^+	≥5.20	40-70	20-40	0.42-1.2	51-59	145	0.4-0.6		
SAC-13[a]				0.12	>10	>200			200	>0.6		
Amberlyst 15™				4.9[d]								
25Na-Amberlyst 15™				3.7[d]								
51Na-Amberlyst 15™				2.4[d]								
77Na-Amberlyst 15™				1.2[d]								
Amberlyst 35™ (Dry)				3.47[e]		36.3						
Amberlyst 35™ (Dry)				3.45[f]		35.1						
Amberlyst 35™ (Dry)				0.47[g]		n/a						

[a]Commercial catalyst properties provided by the companies, data taken from [39,42]; [b]MR: macroreticular structure, G: gel type polymer; [c]V:very, M:medium, L:low; [d]Acidity determined by potentiometric titration for both regular and sodium exchanged Amberlyst 15™; nNa Amberlyst 15™ means n% of acidic protons exchanged with Na^+ ions [48]; [e]After the 1st run (8 h) with petrochemical C4 fraction with 41.7 wt% isobutene and p.a. grade pure glycerol [54]; [f]After the 3rd run (24 h) with petrochemical C4 fraction with 41.7 wt% isobutene and p.a. grade pure glycerol [54]; [g]After the 3rd run (24 h) with petrochemical C4 fraction with 41.7 wt% isobutene and refined glycerol [54]; [h]Maximum operating temperature limit; [i]V_{sp} is the volume of swollen polymer, determined in closed calibrated ampoules [39,41].

Behr and Obendorf [38] observed that glycerol forms a mixture of ethers with no glycerol oligomerization or decomposition as side reactions when reacting pure glycerol with pure IB under defined conditions over different acid catalysts including homogenous (p-toluenesulfonic acid and heteropolyacid) and heterogeneous types (Amberlyst 15™, montmorillonite K-10 and amorphous microporous mixed oxide-AMM), while IB was consumed for the reactions with the amounts following as etherification > dimerization >> hydration to TBA, therefore hydration was neglected. Very low glycerol conversion and DTBGE selectivity was obtained with the heterogeneous catalysts, which was interpreted as a result of poor solubility of these catalysts in glycerol, while with the homogeneous catalysts mass transfer limitation was eliminated by solubilization of the active sites in glycerol. However, Noureddini et al. [37] had achieved higher glycerol conversion and higher desired ether selectivity by employing 2.5 fold of catalyst weight under similar temperature, molar feed and reaction time conditions with Amberlyst 15™. Therefore, the reason for low glycerol conversion and selectivity could be inadequate amount of catalyst [51].

Table 2-2. List of studies on glycerol etherification with isobutene using acidic ion exchange resins as heterogeneous catalysts.

Temperature (°C)	Pressure[a] (bar)	Catalyst loading (wt% of G)	Reaction time (h)	IB:G ratio (mol:mol)	Type of ion exchange resin	Glycerol conversion (mol% otherwise stated)	Desired ether selectivity[e] (mol% otherwise stated)	DIB formation	Reference
80	17	5	2	2	Amberlyst 15™	95	87 wt%	3[f]	[37]
80	17	5	2	3	Amberlyst 15™	99	84 wt%	11[f]	[37]
93	17	5	2	3	Amberlyst 15™	99	80 wt%	3[f]	[37]
93	17	5	4	3	Amberlyst 15™	99	72 wt%	10[f]	[37]
90	14	2.17	5	2	Amberlyst 15™	45	34 (DTBGE)	2[f]	[38]
90	auto	7.5	8	4	Amberlyst 15™ (dry)	96	79	13[f]	[39]
60	auto	7.5	8	4	Amberlyst 15™ (dry)	100	87	11[f]	[39]
60	auto	7.5	8	4	Amberlyst 15™ (wet)	100	80	3[f]	[39]
60	auto	7.5	8	4	Amberlyst 35™ (dry)	100	89	3[f]	[39]
60	auto	7.5	8	4	Amberlyst 35™[,b]	97	95	n/a	[39]
60	auto	7.5	8	4	Amberlyst 35™ (wet)	100	88	8[f]	[39]
60	auto	7.5	8	4	Amberlyst 36™ (dry)	100	91	6[f]	[39]
60	auto	7.5	8	4	Amberlyst 36™ (wet)	10	4	0[f]	[39]
60	auto	7.5	8	4	Amberlyst 39™ (wet)[c]	100	93	5[f]	[39]
60	auto	7.5	8	4	Amberlyst 39™ (wet)	28	13	1[f]	[39]
60	auto	7.5	8	4	Amberlyst 31™ (wet)[c]	14	31	4[f]	[39]
60	auto	7.5	8	4	Amberlyst 31™ (wet)	11	17	7[f]	[39]
60	auto	7.5	8	4	Amberlyst 119™ (wet)[c]	6	16	1[f]	[39]
60	auto	7.5	8	4	Amberlyst 119™ (wet)	11	4	0[f]	[39]
80	15	1 g	7	2	Amberlyst 35™ (wet)[c]	>74	55	8[g]	[40]
80	15	1 g	7	3	Amberlyst 35™ (wet)[c]	>95	74	11[g]	[40]
80	15	1 g	7	4	Amberlyst 35™ (wet)[c]	>95	97	19[g]	[40]
60	auto	7.5	8	4	Amberlyst 15™[,b], in dioxane	79	47	n/a	[41]
60	auto	7.5	8	4	Amberlyst 35™[,b], in dioxane	61	53	n/a	[41]
90	auto	7.5	8	4	Amberlyst 35™[,b], in dioxane	33	20	69[g]	[41]
75	8 + VLE	5	1	4	Amberlyst 15™	95	94	6[f]	[42]
75	8 + VLE	5	1	4	Amberlyst 36™	98	88	4[f]	[42]
75	8 + VLE	5	1	4	CT275	89	95	3[f]	[42]
75	8 + VLE	5	4	4	Amberlyst 15™	99	90	15[f]	[42]
75	8 + VLE	5	4	4	Amberlyst 36™	96	89	11[f]	[42]
75	8 + VLE	5	4	4	CT275	100	87	7[f]	[42]

75	8 + VLE	5	4	4	SAC-13[d]	-	-	-	[42]
80	n/a	5	5	1.5	Amberlyst 35™	85	46	27[g]	[43]
80	n/a	5	5	1.5	Amberlyst 35™, in cationic emulsifier	79	61	57[g]	[43]
80	n/a	5	5	2	Amberlyst 35™, in cationic emulsifier	82	69	57[g]	[43]
80	n/a	5	5	2.5	Amberlyst 35™, in cationic emulsifier	93	85	55[g]	[43]
92	15	1.1	8	2	Amberlyst 15™[,c]	93	53	5[f]	[44]
70	15	6	2	4	Amberlyst 15™	91	85	n/a	[47]
60	20	0.75	20	4	Amberlyst 15™[,c], powder	>90	74	11[g]	[45]
60	20	7.5	20	4	Amberlyst 15™[,c], powder	>90	69	39[g]	[45]
60	20	7.5	20	4	Ag(62)Amberlyst 15™[,c], powder	>90	92	11[g]	[45]
60	20	7.5	20	4	Al(57)Amberlyst 15™[,c], powder	>90	87	9[g]	[45]
60	20	7.5	20	4	Na(45)Amberlyst 15™[,c], powder	>90	69	3[g]	[45]
60	20	7.5	20	4	Amberlyst 15™[,c]	98	76	20[g]	[48]
60	20	7.5	20	4	Na(25)Amberlyst 15™[,c]	98	80	4[g]	[48]
60	20	7.5	20	4	Na(51)Amberlyst 15™[,c]	99	90	2[g]	[48]
60	20	7.5	20	4	Na(77)Amberlyst 15™[,c]	100	72	0[g]	[48]
70	5 + VLE	7.5	6	2.5	Amberlyst 15™ (dry)	97	72	5[f]	[51]
70	5 + VLE	7.5	6	3	Amberlyst 15™ (dry)	99	84	7[f]	[51]
70	5 + VLE	7.5	6	4	Amberlyst 15™ (dry)	100	92	7[f]	[51]
70	5 + VLE	7.5	6	5	Amberlyst 15™ (dry)	100	95	12[f]	[51]
70	5 + VLE	3	6	2.5	Amberlyst 15™ (dry)	30	18	n/a	[51]
75	10 + VLE	0.5 g	4	4	Amberlyst 15™	73	35	33[f]	[52]
75	10 + VLE	0.5 g	24	4	Amberlyst 15™	99	77	36[f]	[52]
90	auto	10	8	3[h]	Amberlyst 35™ (dry)	59	64	5[f]	[54]
90	auto	10	8	4[h]	Amberlyst 35™ (dry)	81	71	5[f]	[54]
90	auto	10	8	3	Amberlyst 35™ (dry)	87	67	21[f]	[54]
90	auto	10	8	4	Amberlyst 35™ (dry)	80	80	35[f]	[54]
90	auto	10	8	3[i]	Amberlyst 35™ (dry)	59	67	1[f]	[54]
90	auto	10	8	3[h]	Amberlyst 35™ (dry), 3rd cycle	43	59	2[f]	[54]
90	auto	10	8	3[i]	Amberlyst 35 (dry), 3rd cycle	9	17	2[f]	[54]

[a]Auto: autogenous pressure, VLE: vapor liquid equilibrium after pressurizing the reactor; [b]Catalyst swollen in glycerol for 15 h before the reaction; [c]Catalyst washed with methanol and dried prior to reaction; [d]SAC-13 ion exchange resin yielded in two-phase system with low glycerol conversion thus fractions could not be determined; [e]Selectivity for di- and tri-tertiary butyl ethers of glycerol based on glycerol. Values are mol% unless otherwise stated; [f] wt% DIB in the product mixture; [g]mol% selectivity of isobutene to DIB; [h]Petrochemical C4 fraction with 41.7 wt% isobutene was used with p.a. grade pure glycerol; [i]Refined glycerol from FAME production instead of p.a. grade pure glycerol was used together with the 41.7 wt% isobutene containing C4 fraction.

Extending the work by Noureddini et al. [37], Klepáčová et al. [39] performed an extensive study on glycerol etherification with IB by employing different types of Amberlyst ion exchange resins (*e.g.* A 15, A 31, A 35, A 36, A 39, and A 119) both in dry and wet forms with the aim of testing their performance for glycerol conversion and selectivity to DTBGE and TTBGE. Temperature of 60 °C, catalyst loading of 7.5 wt%/glycerol and IB:G molar ratio of 4:1 were kept constant in all set of experiments, since these reaction conditions have yielded successful results previously [117]. The stirring rate in all experiments was fixed to be 1200 rpm as it eliminates external mass transfer effects. Glycerol conversion and the corresponding desired ether yields were influenced by the properties of catalysts, such as water content (dry or wet), structure (gellular or macro-reticular), pore size, degree of crosslinking, and swelling of catalysts in glycerol. Dry catalyst showed better performance, because the water form of wet catalyst reacts with produced ethers to disproportionate ethers back to glycerol. In addition, water molecules can block the diffusion of glycerol molecules into the pores of small pore sized resins to interact with the active sites and hamper the formation of large ethers. Thus, glycerol etherification can only occur at the surfaces of the catalysts. Among dry catalysts, complete conversion of glycerol and highest yields of desired ethers were achieved with macroporous Amberlyst 15™, 35™, 36™, and 39™. However, only Amberlyst 15™ and 35™ showed complete glycerol conversion and high desired ether selectivity (*e.g.* > 80 mol%) among the wet catalysts since they have larger pores compared to other Amberlyst catalysts, thus, water molecules cannot block the diffusion of glycerol into the pores. In addition, lower DIB but higher TTBGE concentrations in the case of dry Amberlyst 35™ could be related to its larger swollen volume by glycerol which might be associated with larger pore size, when compared to dry Amberlyst 15™. Gellular type resin catalysts showed inferior performance compared to macro-reticular resins, because of their gel phase structure with micro openings. It is known that macro-reticular resins dominate the conventional gellular resins in terms of efficiency,

conversion, chemical-physical resistance and lifetime [115]. While a gel type resin is not porous in dry state, a macroreticular resin, which is produced by simultaneous precipitation and polymerization (copolymerization technique) possesses a macropore phase accompanied by a micro spherical gel phase [118]. Macroreticular resins with high degree of cross-linking are found to be very active both in wet and dry forms. In addition, a reaction catalyzed by macroreticular resins swollen in glycerol gave better desired ether yields when compared to their dry forms (non-swollen). For instance treating the dry catalyst at 60 °C in glycerol (4 cm^3 glycerol/g catalyst) prior to reaction brought about an increase in desired ether yield from 88.7 to 91.7 mol%, although glycerol conversion dropped from 100 to 96.8 mol% [39]. Swelling of polymeric resins is an important phenomena occurring when a dry polymer is contacted with a liquid phase wherein different components of the liquid phase are adsorbed selectively at different extents. The selective swelling of a polymeric resin is known to effect its catalytic activity, as the conversion and reaction rate are dependent on the concentrations in the polymer phase [119]. Therefore, the variation of polymer phase glycerol concentrations for dry and glycerol swollen Amberlyst 15™ catalysts might have influenced on glycerol conversion and ether selectivity in the case of Klepáčová's measurements [39].

Following the work by Klepáčová et al. [39], Karinen and Krause [40] examined ether selectivity at different reaction temperatures and different IB:G molar ratios over Amberlyst 35™ catalyst by explaining the effect of viscosity on mass transfer between polar glycerol phase, non-polar IB phase and the catalyst. The stirring rate of the batch reactor was set to 1300 rpm, as the reaction rate and product distribution were observed to depend on stirring speeds up to 1000 rpm such that more oligomerization products were obtained when stirring rate was below 1000 rpm. At 1300 rpm stirring, 80 °C and a low IB:G molar feed (*e.g.* 1.5:1), the high viscosity of the reaction mixture caused the reactants to move slower. This mass transfer limitation was observed to enhance IB dimerization, cause resulting in incomplete glycerol

conversion and brought about a higher fraction of TTBGE in the product mixture when compared to 2:1 molar ratio case, because the high viscosity condition slowed down the desorption of MTBGE and DTBGE from the catalyst surface. Therefore, some of these lower ethers were etherified up to TTBGE, but still the concentration of MTBGE was higher than DTBGE and much higher than TTBGE. Additionally, IB conversion could not be completed even though complete glycerol conversions were achievable at low viscosity conditions, possibility because of thermodynamic limitations. It was proposed that the reaction mechanism to occur in a way that i) glycerol and IB reactants adsorb on the catalyst, ii) glycerol is etherified to a specific ether product, iii) ether products desorb from the catalyst, iv) after all glycerol is consumed, both oligomerization of IB and further etherification of existing MTBGE/DTBGE ethers ceases. The mixture of G and IB consists of two phases at 90 °C if the concentration of IB or G by weight is less than 95 wt% according to the L-L diagram of Behr and Obendorf [38] (**Figure 2-4**). There is no L-L data for lower temperatures, the feed can be said to be a two-phase mixture at 60-80 °C for the IB:G molar ratio range 1.5:1 to 4:1. Karinen and Krause [40] explained the catalytic behavior with viscosity effects at different IB:G feed ratios. At 80 °C, when IB:G molar feed was changed from 1.5:1 to 2:1, the corresponding decrease in viscosity resulted in an efficient use of IB (*e.g.* 92 mol% IB reacted to form ethers and 8 mol% IB to form DIB). However, above 2:1 molar ratio, oligomerization was triggered again because of IB abundance. Therefore, more IB dimers were formed (*e.g.* 89 mol% IB reacted to form ethers while 11 mol% IB to form DIB at 3:1 molar ratio), and the amount of desired ethers also increased. Increasing IB:G ratios favored the formation of desired ethers in the final ether mixture with much less MTBGE formation. At low temperatures *i.e.* < 70 °C, DTBGE and TTBGE selectivity were low because of high viscosity, whereas at high temperatures *i.e.* > 80 °C, the oligomerization rate exceeded the etherification rates, overwhelming the viscosity effect. Thus, operation at higher temperature resulted in elevated DIB formation and lower

DTBGE and TTBGE selectivity. These results correlate well with similar studies, in which desired ether production decreased when optimum temperatures were exceeded [37,39] and DIB formation increased when IB:G molar ratio increased [37,51].

The etherification of glycerol over ion exchange resins was also studied in a reaction medium with solvents, as the polarity of solvents can influence the solubility of compounds and the activation of the catalysts. Klepáčová et al. studied the influence of catalysts and temperatures by focusing on Amberlyst types 15 and 35 in the presence of solvents [41]. The reactor setting was similar to that of their previous study [39], but the catalysts were swollen in a mixture of solvent and glycerol for 15 hours before injecting the IB to the reaction medium. Out of three solvents, namely dioxane, sulfolane and dimethyl sulfoxide, the least polar solvent dioxane demonstrated the highest performance because of several reasons including good solubilization of IB, absence of chemisorption on sulfonic groups of the resin catalyst and the easy transport of non-polar ether products from the resin into the non-polar solvent. However, comparing the glycerol conversion and desired ether selectivity with the previous study of Klepáčová et al. with glycerol swollen catalyst [39] using dioxane seemed to bring lower performance, at around 40 mol% lower glycerol conversion and desired ether selectivity. It was stated that swelling the catalyst in glycerol provided dissociation of the proton from the $–SO_3H$ group and, thus, the resin was polarized. IB solubilized in the solvent moved from the solution into the polarized resin, with a diffusion limited transport rate. IB then interacted with the free proton from dissociated $–SO_3H$ group with a very high rate, formed *tert*-butyl cation ($C_4H_9^+$). Increased polarity inside the resin was claimed to stabilize the *tert*-butyl cation. Etherification proceeded as the reactants came into contact. Besides, some of the tertiary butyl cations may have reacted with IB, but with slower rates, resulting in IB dimerization. Using solvent can help for solubilizing IB better, however, it failed to enhance the contact of IB with glycerol inside the resin, because the conversion of glycerol to ethers was low in the solvent added case. This

lower conversion of glycerol to ethers might be because of the phase separation of the non-polar IB and polar glycerol. Similar points were discussed by Karinen and Krause [40] and Behr and Obendorf [38] (in a solvent free reaction medium) who showed that initially two separate phases existed, and after a glycerol conversion of over 60 mol%, the phases dissolved in each other, resulting in highly favored etherification reaction. Klepáčová et al. [41] observed the highest TTBGE yield in the case of Amberlyst 35™, possibly because of the higher acidity of this catalyst compared to Amberlyst 15™. TTBGE concentration for Amberlyst 35™ was more than 50 mol% for that of Amberlyst 15™ at the end of the eight hour experiment. Increasing the reaction temperature improved not only the etherification rates, but also the secondary reactions, such as dealkylation of higher ethers into lower ethers or glycerol and side reactions such as IB oligomerization into DIB. Therefore, in overall, glycerol conversion and higher ether production decreased, which was also shown in other studies [37,39,40,45,54]. Another outcome of that study [41] was the set of kinetic parameters for 11 equilibrium reactions in glycerol etherification by IB over Amberlyst 35™ catalyst, estimated by least squares method for a pseudo-homogenous kinetic model; low values of activation energies pointed out to the diffusion control on the reactions.

Mangourilos and co-workers [43] used a cationic emulsifier to improve the mass transfer between the highly polar, hydrophilic glycerol phase and the non-polar, hydrophobic IB phase during glycerol etherification in the presence of Amberlyst 35™ ion exchange resin as a catalyst. The alkyl imidazoline cationic emulsifier called ROT1 was added to the reaction medium with a final concentration of 0.1 wt%. The experiments with and without emulsifier were run in a batch reactor by using pre-glycerol swollen Amberlyst 35™ and by applying 1.5:1 IB:G molar feed ratios at pH 1.5 (adjusted by phosphoric acid). Employing cationic emulsifier not only resulted in lower glycerol conversion (*i.e.* from 85% to 79 mol%), but also in a lower yield of MTBGE, whereas the yield of DTBGE remained constant. However, the yield of

TTBGE increased from 3 to 12 mol%, meaning that more glycerol was converted into TTBGE and the selectivity to higher ethers increased. Nevertheless, the conversion of IB to ethers decreased, pointing out to the higher yield of IB dimers in the cationic emulsifier case. Thus, although cationic emulsifier helped the desired ether yield to increase, the ratio of DIB over desired ethers became higher. The group interpreted the high reactivity of IB as a result of enhanced mass transfer between the glycerol phase on the swollen catalyst and the IB phase in the bulk media, whose interface area was widened via emulsion formation between the two phases. Additional experiments performed at lower viscosity conditions, at higher IB:G molar feeds, pointed out to decreased IB consumption rate that was deduced from IB:G versus half pressure time data. For instance, a longer half pressure time observed by applying a high IB:G ratio meant slower consumption of IB. However, a better contact between the glycerol and IB phase was obtained, resulting in improved glycerol conversion and IB conversion to ethers. Therefore, less DIB produced per mole of corresponding desired ethers *i.e.* DTBGE and TTBGE than the case with lower IB:G ratio. This positive effect of low viscosity was also observed previously [40].

The next improvement in Amberlyst studies was the modification of Amberlyst 15™ by exchanging some of its acidic protons with silver, magnesium, aluminum or sodium cations, with the aim of restricting the oligomer formation and increasing higher ether selectivity [45]. Lee et al. preferred to use the fine grinded powder form of Amberlyst instead of the bead form to overcome the internal mass transfer limitations and achieve glycerol conversion in much shorter reaction times. The final product mixture was found to be dependent on the density of (modified) acidic sites and the nature of the cation, in addition to already reported temperature, IB:G molar ratio and reaction time conditions. The exchange with cations resulted in reduced acid capacity, and thus, lower catalytic performance because of partial neutralization. Moreover, the rates of both glycerol etherification and IB oligomerization decreased. As IB

oligomerization was more strongly suppressed, the final product mixture consisted of lower amounts of DIB. Interaction of catalysts with IB was analyzed by pulse chemisorption analysis technique detected by a thermal conductivity detector (TCD). There were no TCD peaks in the case of untreated Amberlyst 15™ catalyst, as well as the other tested heterogeneous catalyst - cesium salt of heteropolyacid-, indicating that all of the analysis gas IB was chemisorbed on those catalysts, and the consumption of IB during chemisorption was linked to oligomerization. Cation exchanged catalysts acquired lower affinity to IB, with different strength for each cation, *e.g.* H-Amberlyst > Ag(62)Amberlyst > Al(57)Amberlyst > Mg(52)Amberlyst > Na(45)Amberlyst. Here, numbers in parenthesis mean percentage of cation replacement, for instance, Ag(62) meaning 62 mol% replacement of acidic protons with silver cations in the Amberlyst resin. 50 mol% reduction in acidic site density resulted in 90% reduction in ether production rate, which meant that catalyst loading should be 10 times more for the modified ones to achieve the same conversion rates as unmodified regular powdered Amberlyst (7.5 wt% for modified powdered Amberlyst and 0.75 wt% for unmodified powdered Amberlyst) at prolonged reaction times. Regarding IB affinity, the lowest DIB formation, but at the same time, the lowest TTBGE formation was observed at the sodium modified catalyst. The highest TTBGE concentration was observed for aluminum and silver modified Amberlysts, possibly because of the enhanced interaction with the IB molecules, thus, an elevated possibility of etherification, which was thought to help formation of TTBGE by double etherification of MTBGE in one step. In addition, both modifications resulted in increased higher ether selectivity when compared to the regular catalyst. About catalyst deactivation, regular Amberlyst 15™ was claimed to retain its performance after several cycles without significant loss in activity, but reusability tests were not done for the cation exchanged Amberlyst 15™. However, a long run of 24 h indicated that the yields of MTBGE, DTBGE, and TTBGE were almost constant between hours 10 to 24. Subsequently, Lee et al. [48] focused on sodium

modification of Amberlyst 15™ by introducing Na(25), Na(51), and Na(77) forms, as in a previous study their data illustrated that the sodium modification of Amberlyst 15™ reduces the selectivity to DIB [45]. Applying their previous reaction conditions, but this time using Amberlyst 15™ in bead form (1 mm diameter) instead of powder form, lower DIB concentrations were obtained at higher sodium concentrations, because of reduced acidity and activity of the catalyst. For instance, sodium exchange of 0, 25, 51, and 77 mol% with Amberlyst H^+'s resulted in DIB selectivity of 17, 4, 0.3, and 0.2 mol%, respectively in the final product mixture consisting of unconverted glycerol (at a glycerol conversion of ≥95%), MTBGE, DTBGE, and DIB. The highest yield for DTBGE and TTBGE was observed for Na(51) Amberlyst 15™; while the yields were 30 mol% lower for no sodium treated case. Partial neutralization of acidic resin with sodium cation caused IB affinity to decrease, so that IB oligomerization was suppressed in the 2 IB ↔ DIB equilibrium reaction. As a result, the decomposition of ether products via equilibrium shift in TTBGE ↔ MTBGE + 2 IB reaction slowed down. The decomposition of TTBGE over unmodified Amberlyst was faster than the decomposition over modified one, resulting in a higher amount of TTBGE production over the sodium modified catalyst.

Besides these studies focusing on pure IB feed, petrochemical C4 fraction as an IB source has been recently considered by Turan and coworkers [54] in heterogeneous etherification studies using Amberlyst type catalysts. Refinery C4 fractions having IB contents from 20.7 to 41.7 wt%, in addition to i-butane, n-butane, trans-2-butene, cis-2-butene and 1-butene were used as an alkylation agent. C4 fraction with 41.7 wt% IB content for 4:1 IB:G molar feed yielded the best performance following as 81 mol% glycerol conversion and 71 mol% selectivity to desired ethers using Amberlyst 35^{TM} as a catalyst. For a more dilute feed in IB concentration, namely the 3:1 IB:G molar feed, lower conversion and selectivity were obtained, continuing to decrease in the 2nd and 3rd catalytic cycles, which was accompanied by

the decrease in acidity and surface area, however the reason of deactivation was not specified. Relatively lower conversion of glycerol when compared to the pure IB case could be sourced by the lower IB concentration in the C4 fraction. For instance, glycerol could be converted by 59 mol% with the IB in 41.7 wt% dilute IB stream, while 87 mol% conversion was achieved using pure IB although the IB:G molar ratios were the same. Increasing the reaction temperature from 80 °C to 120 °C on Amberlyst 35^{TM} catalyst whose thermal stability limit is 150 °C caused an increase in i) dealkylation (*e.g.* IB removal from unstable DTBGE), ii) oligomerization and iii) etherification of glycerol by other butenes (as the carbocations of these butenes are less stable/more reactive than of IB). Therefore reaction temperature over 100 °C was not recommended. When pure IB instead of this C4 fraction was used with 4:1 IB:G feed, several folds of DIB was produced. The existence of other hydrocarbons in the C4 fraction was claimed to create a diluted medium for IB which turned out to produce less TTBGE and DIB, but more DTBGE. According to Turan et al. [54], using C4 fractions instead of pure IB is reasonable from economical point of view as IB can be utilized in this way to produce higher amounts of DTBGE, which is still desired ether. As well as using pure glycerol, the group also attempted to refine crude glycerol from FAME production up to 95 wt% purity and used as a feed together with the C4 fraction. Refined glycerol yielded in higher DTBGE and lower TTBGE-DIB concentrations when compared to pure glycerol, with decreasing catalytic activity of Amberlyst 35^{TM} substantially following the 3rd catalytic cycle. It was commented that dilution of the IB feed with the impure glycerol feed slowed down the etherification reaction, which favored DTBGE production at the beginning, but the impurities, such as methanol, inorganic salts, FAME, acids, mono-glycerides remaining in the refined glycerol deactivated the catalyst.

Amberlyst 15™ ion exchange resin has recently been used by Saengarun et al. in the etherification of glycerol with propylene and 1-butene for the production of propyl- and butyl-glycerol ethers, respectively, in a batch reactor system at 20 bar and 100 °C. Fuel tests

demonstrated that 10 vol% fuel blends of these alkyl glycerol ethers reduce the cloud point of biodiesel and improve the octane number of gasoline [120].

2.2.3.2. Zeolites

Zeolites are crystalline solid structures formed by a regular framework of aluminum and silicon atoms connected together with oxygen atoms. The pores may host water, cations or some other molecules. The application of zeolites as catalysts originates from their shape selectivity, ion-exchange properties, acidity and/or possibility to act as supports for metal ions. With their acidic properties, zeolites, such as zeolite A, Beta, Y, Mordenite and ZSM-5, are commercially applied in petroleum industry [121]. The catalytic activity of a zeolite originates from Brønsted and Lewis acid sites. The –OH bridging between framework Al and Si atoms creates the proton donor Brønsted acid sites; while there exist different ideas about the origin of electron acceptor Lewis acid sites. For instance, Uytterhoeven claimed that dehydration of the bridging –OH gave rise to tri-coordinated framework Al, which acts as a Lewis acid site [122]. However, according to Jacobs and Beyer, Lewis acid sites are not related to framework Al but to non-framework Al species, which are formed by dealumination of the zeolite and leaching of the framework aluminum [123]. The second model is widely accepted. Especially the penta-coordinated non-framework Al species is thought to be responsible for Lewis acidity. Moreover these species were observed to coordinate with the oxygen atoms nearest to the framework Al and create a polarizing effect on the bridging –OH groups in the zeolite framework, thus enhancing the acid strength via synergism [124-126].

Zeolites generally belong to microporous and mesoporous materials, usually showing mesoporosity in the range of 5% to 20%, with significant mesoporosity observed for zeolite Beta and ZSM-5 especially after dealumination [127] . Zeolites can also be classified based on the number of Si or Al atoms connected to O atoms in the ring structure; small pore zeolites

with 8 ring structure, medium pore zeolites with 10 ring structure (*e.g.* ZSM-5) and large pore zeolites with 12 ring structure (*e.g.* Mordenite, Beta, Y) [57,127].

From late 1980's, zeolites have been investigated as catalysts in petrochemical and organic synthesis, because of their favorable acidity, thermal stability and shape-selectivity features. Zeolites can catalyze electrophilic/nucleophilic substitutions, hydrogenation and isomerization reactions [128]. Petrochemical MTBE synthesis from IB and methanol has been widely studied with acidic zeolites; for instance H-Beta zeolite with optimum Si/Al ratio was observed to have high activity when compared to some other zeolites such as H-Y and H-ZSM-5. Moreover, when MTBE selectivity of zeolites is compared to that of Amberlyst ion exchange resins, by-product formation from IB dimerization/oligomerization was found to be very low since zeolites could adsorb methanol reactant more efficiently but IB reactant less efficiently [129].

The former idea of using zeolites for catalyzing the etherification between an olefin and glycerol was introduced in a patent by Dewattines and Hinnekens [130], claiming that if an acidic large pore zeolite with three dimensional crossed channels and a Si/Al ratio higher than 5 is used as an etherification catalyst at pressures from 3 to 70 bar, temperature from 50 to 200 °C, molar ratio olefin/glycerol from 1:1 to 6:1 and weight of catalyst from 0.01 to 10 wt% of glycerol; then the tertiary alkyl ethers could be produced effectively. Out of different heterogeneous acid catalysts with high glycerol conversion covering zeolite H-Beta, zeolite H-Y, Amberlyst 15™ and cesium salt of silicotungstic acid, the lowest amount of DIB was produced over zeolite H-Y. Using zeolite H-Y resulted in a high selectivity of TTBGE (24.6 mol% MTBGE, 60.4 mol% DTBGE, 6.4 mol% TTBGE); while using H-Beta yielded MTBGE+DTBGE with high selectivity (32.4 mol% MTBGE, 54.6 mol% DTBGE, 0.22 mol% TTBGE). In addition, these zeolites yielded less TTBGE, but more DTBGE when compared to

Amberlyst 15™ ion exchange resin. Therefore, this invention of 1990's pointed out the feasibility of employing zeolites for producing glycerol ethers. The physical properties and catalytic performance summaries of the zeolites used in glycerol etherification with isobutene is given in **Table 2-3** and **Table 2-4**.

.

Table 2-3. Physical characteristics of regular and modified zeolite catalysts.

Type of zeolite[*]	SiO_2/Al_2O_3 ratio	Acid capacity (meq H^+/g cat)	Crystallinity[f] (%)	BET area (m^2/g)	Pore volume (cm^3/g)	Pore area[j] (m^2/g)	External surface area (m^2/g)	Sulfur content[k]	Reference
H-Y	30	0.56[d]		697	0.29[g]	169			[39]
H-Beta	25	1.03[d]		681	0.20[g]	309			[39]
H-Y	12.3[a]	3.76(2.01)[d]		754	0.48(0.24)[h]				[49]
H-Y + 1 M citric acid	56.1[a]	1.35(0.91)[d]		817	0.56(0.34)[h]				[49]
H-Y + 2 M citric acid	67.8[a]	0.99(0.77)[d]		811	0.57(0.35)[h]				[49]
H-Y + 0.5 M nitric acid	32.8[a]	1.40(1.01)[d]		860	0.55(0.29)[h]				[49]
H-Y + 1 M nitric acid	101.6[a]	0.48(0.46)[d]		844	0.57(0.34)[h]				[49]
H-Beta	20[b]		100	584	0.23	462	122		[52]
H-Beta-CS	110[b]	0.75[e]	27	330	0.14	243	87	0.74	[52]
H-Beta-MwS	142[b]	0.72[e]	45	505	0.18	394	111	0.70	[52]
H-Beta	20[b]		100	573	0.23		203		[55]
H-Beta-MwS(0.7)		0.30[e]	50	502	0.20		152	0.31	[55]
H-Beta-MwS(1.0)		0.42[e]	49	501	0.21		165	0.40	[55]
H-Beta-MwS(1.4)	142[b]	0.72[e]	45	505	0.24		183	0.70	[55]
H-Beta-MwS(1.8)		0.74[e]	37	249	0.16		87	0.74	[55]
H-Beta-MwS(2.2)		0.76[e]	30	88	0.04		36	0.77	[55]
H-ZSM-5	40[b]		100	300	0.06		87		[55]
H-ZSM-5-MwS(0.7)		0.17[e]	50	355	0.07		112	0.14	[55]
H-ZSM-5-MwS(1.4)		0.26[e]	54	345	0.05		111	0.16	[55]
H-ZSM-5-MwS(1.8)	56[b]	0.52[e]	53	213	0.02		79	0.68	[55]
H-ZSM-5-MwS(2.2)		0.54[e]	44	92	0.01		48	0.70	[55]
H-Mordenite	13[b]		100	413	0.10		42		[55]
H-Mordenite-MwS(1.4)		0.62[e]	31	529	0.15		67	0.14	[55]
H-Mordenite-MwS(1.6)	52[b]	0.82[e]	29	426	0.07		58	0.60	[55]
H-Mordenite-MwS(1.8)		0.77[e]	32	500	0.12		60	0.72	[55]
H-Mordenite-MwS(2.2)		0.62[e]	30	489	0.11		55	0.70	[55]
H-Beta	23.9[c]	(0.57)[d]		480					[56]
H-Beta + La^{+3}	25.2[c]	(0.67)[d]		415					[56]
H-Beta + Ce^{+3}	25.6[c]	(0.64)[d]		421					[56]
H-Beta + Nd^{+3}	24.3[c]	(0.73)[d]		433					[56]
H-Beta + Eu^{+3}	25.2[c]	(0.66)[d]		421					[56]
H-Beta	42.8[b]	0.55[e], 0.45[d]	100	568	0.31[i]				[58]

H-Beta, hierarchical	55[b]	0.53[e], 0.25[d]	100	750	0.24[i]	[58]
H-Beta, fluorinated	53.6[b]	0.44[e], 0.43[d]	86	477	0.15[i]	[58]
H-Beta, hierarchical + fluorinated	55.4[b]	0.52[e], 0.3[d]	68	499	0.18[i]	[58]

[*]CS: sulfonation by conventional heating, MwS: sulfonation by microwave heating, Numbers in parenthesis indicate grams of CSPTMS sulfonation agent is used per 2 grams of zeolite, *e.g.* Beta-MwS(0.7) means 0.7 grams of CSPTMS used per 2 grams of zeolite sample, 0.1 mol rare earth metal is introduced per 10 gram of H-Beta zeolite sample. [a] Determined from ICP analysis; [b]Bulk ratio, determined from XRF; [c]Determined from EDS; [d]Determined from NH_3-TPD; numbers in parenthesis refer to strong acidity; [e]Determined from potentiometric titration; [f]Determined from XRD patterns; [g]Micropore volume, calculated from N_2 adsorption; [h]Determined with BJH method; pore volume values in parenthesis are from the pores with 1.7-300 nm size; [i]Micropore volume, calculated from Ar physisorption; [j] Determined from N_2 adsorption-desorption; [k]mmol organic sulfonic acid group/g sample determined from TGA.

Table 2-4. The list of studies on glycerol etherification with isobutene using zeolites as heterogeneous catalysts.

Temperature (°C)	**Pressure[a] (bar)**	**Catalyst loading (wt% of G)**	**Reaction time (h)**	**IB:G ratio (mol:mol)**	**Type of zeolite[c]**	**Glycerol conversion (mol%)**	**Desired ether selectivity[d] (mol%)**	**DIB formation[e] (wt%)**	**Reference**
60	auto	7.5	8	4	H-Y	95	69	3	[39]
60	auto	7.5	8	4	H-Beta	100	81	15	[39]
90	auto	7.5	8	4	Y	100	75	12	[39]
90	auto	7.5	8	4	H-Beta	18.0	63	51	[39]
60	auto	7.5	8	4	H-Y, in dioxane	89	58	n/a	[41]
60	auto	7.5	8	4	H-Beta, in dioxane	66	50	n/a	[41]
80	auto	1	5	4	H-Y, in dioxane	35	27	0	[49]
80	auto	1	5	4	H-Y + 0.5 M citric acid, in dioxane	79	50	0	[49]
80	auto	1	5	4	H-Y + 1.0 M citric acid, in dioxane	82	57	0	[49]
80	auto	1	5	4	H-Y + 1.0 M nitric acid, in dioxane	75	46	0	[49]
75	10 + VLE	0.5 g	4	4	H-Beta	44	68	5	[52]
75	10 + VLE	0.5 g	4	4	H-Beta -CS	93	51	2	[52]
75	10 + VLE	0.5 g	4	4	H-Beta -MwS	100	83	2	[52]
75	10 + VLE	0.5 g	24	4	H-Beta	49	61	6	[52]
75	10 + VLE	0.5 g	24	4	H-Beta -CS	100	88	10	[52]

75	10 + VLE	0.5 g	24	4	H-Beta -MwS	100	91	9	[52]
75	10 + VLE	0.5 g	48	4	H-Beta	49	61	6	[55]
75	10 + VLE	0.5 g	24	4	H-ZSM-5	25	17	0	[55]
75	10 + VLE	0.5 g	48	4	H-Mordenite	37	16	0	[55]
75	10 + VLE	0.5 g	48	4	H-Beta -MwS(1.4)	100	90	9	[55]
75	10 + VLE	0.5 g	48	4	H-ZSM-5-MwS(1.8)	98	83	5	[55]
75	10 + VLE	0.5 g	48	4	H-Mordenite-MwS(1.6)	99	79	2	[55]
70	15	6	2	3	H-Beta	79	61	2	[56]
70	15	6	2	3	H-Beta + La^{+3}	89	74	2	[56]
70	15	6	2	3	H-Beta + Ce^{+3}	82	68	2	[56]
70	15	6	2	3	H-Beta + Nd^{+3}	93	75	3	[56]
70	15	6	2	3	H-Beta + Eu^{+3}	87	70	2	[56]
90	auto	10	8	3[b]	H-Beta	73	76	34	[54]
90	auto	10	8	4[b]	H-Beta	71	73	40	[54]
75	8 + VLE	0.5 g	24	4	H-Beta	50	70	1 to 3	[58]
75	8 + VLE	0.5 g	24	4	H-Beta, hierarchical	97	57	6 to 9	[58]
75	8 + VLE	0.5 g	24	4	H-Beta, fluorinated	48	74	n/a	[58]
75	8 + VLE	0.5 g	24	4	H-Beta, hierarchical, fluorinated	96	63	n/a	[58]

[a]Auto: autogenous pressure, VLE: vapor liquid equilibrium after pressurizing the reactor; [b]Petrochemical C4 fraction with 41.7 wt% isobutene was used as alkylation agent; [c]CS: sulfonation by conventional heating, MwS: sulfonation by microwave heating, Numbers in parenthesis indicate grams of CSPTMS sulfonation agent is used per 2 grams of zeolite, *e.g.* Beta-MwS(1.4) means 1.4 grams of CSPTMS used per 2 grams of zeolite sample; [d]Selectivity for di- and tri-tertiary butyl ethers of glycerol based on glycerol; [e]wt% DIB in the product mixture.

Klepáčová et al. extensively focused on two large pore zeolites, zeolite H-Y (SiO_2/Al_2O_3=30) and Beta (SiO_2/Al_2O_3=25), in parallel with Amberlyst ion exchange resins, to compare their selectivity for IB:G ratio of 4 at 60 °C and 90 °C in a batch system [39]. The selectivity for TTBGE was much lower for zeolites when compared to Amberlyst catalysts, consistent with the results of Dewattines and Hinnekens [130]. For instance, no TTBGE production was observed for zeolite H-Beta; maximum TTBGE concentration was 14.3 wt% at 90 °C (12 mol% selectivity) and 7.1 wt% (5 mol% selectivity) at 60 °C for zeolite H-Y. Zeolite H-Beta demonstrated no TTBGE production because of steric hindrance, but higher DIB and higher DTBGE production at 60 °C were obtained, so that desired ether selectivity in terms of DTBGE was higher for H-Beta at that temperature (69.4 % for Y, 80.6 % for Beta). Additionally, increasing the temperature from 60 to 90 °C resulted in better desired ether yields for zeolite H-Y (+10%), but much lower yields for H-Beta (-80%), since H-Beta was strongly deactivated by the elevated DIB production. Deactivation of zeolites by coking with oligomers has been proposed in the literature, with narrower zeolites being subject to oligomerization of IB easily [131].

In a latter study by Klepáčová and coworkers [41], the comparison of reaction rates for zeolite H-Y and zeolite H-Beta in solvent dioxane indicated that reactions on H-Beta took place faster than on the H-Y so that the equilibrium of etherification was achieved earlier. Here the equilibrium is defined as the maximum glycerol conversion after which the splitting of ethers result in re-formation of glycerol. However, once the equilibrium was reached, oligomerization of IB was favored, resulting in C8 olefins. This reaction triggered the decomposition of already produced ethers. Therefore, both glycerol conversion and DTBGE production decreased after the reaction reached equilibrium, earlier for H-Beta when compared to H-Y. Better performance was obtained with H-Y in terms of higher ether selectivity (56%), when compared to H-Beta (50%) and also to Amberlyst 15™ (48%) and Amberlyst 35™ (49%) resins; however, the

highest TTBGE concentration in the final product mixture was observed over Amberlyst 35^{TM}. When compared to the no solvent case, both the glycerol conversion and desired ether selectivity were lower in dioxane under identical experimental conditions (*i.e.* 60 °C, 8 hours, IB:G=4:1). It was concluded that, although the performances of different zeolites are acceptable, using zeolites in the etherification reaction of glycerol is not technically as favorable as ion exchange resins, because of their easy deactivation (*e.g.* by DIB) and high price [41].

Once the limitations of zeolites were clarified, the studies were directed to modify these heterogeneous catalysts with the aim of enhancing the selectivity for desired ethers. Xiao et al. [49] treated NH_4^+ form of zeolite H-Y with citric acid or nitric acid (0-1 M citric acid or 0-2 M nitric acid) and calcined in air at 500 °C to prepare the H-Y form to investigate the change in zeolite properties such as Si/Al ratio, the number of acid sites, acid strength etc. and to assess the corresponding catalytic activity. Acid treatment is in general performed to remove some aluminum from the framework causing an increase in Si/Al ratio [132]. Zeolite dealumination has been observed to improve the catalytic activity in various reactions, such as cracking, acylation, etherification and oligomerization, mainly by controlled formation, removal of extra framework aluminum species, and enhancement in framework acid sites [133,134]. In the study performed by Xiao and coworkers [49], acid treatment of H-Y with 1.0 M citric acid resulted in increased total DTBGE and TTBGE selectivity, from 27 to 57 mol% and no IB oligomers were observed. It should be noted that the catalyst loading applied by Xiao et al. was 40.4 mg zeolite for 4.04 g glycerol (1 wt%), which is one fifth of that from Klepáčová et al [39]. Under similar reaction conditions applied by Klepáčová et al. and Xiao et al. (*e.g.* 90 and 80 °C, 8 and 7 h run, IB:G=4:1), the desired ether yields were 75 and 12 mol%, respectively, therefore the catalyst loading is a crucial parameter. The comparison of citric acid treated zeolite with commercial ion exchange resin SAC-13 revealed the superior performance of the modified zeolite, with 12 mol% higher selectivity to DTBGE and TTBGE. NH_3-TPD profile pointed out

to the reduction of total amount of acid sides in acid treated H-Y, while the FTIR-pyridine spectra indicated the dominance of strong Brønsted acid site concentration over Lewis acid sites after acid treatment. Therefore, the strength of the acid sites increases with a corresponding decrease in their numbers. N_2 adsorption analysis revealed the increase in surface areas and pore volumes, especially the volume contributed by larger pores in acid treated H-Y. In addition, citric acid treatment increased the number of pores whose sizes were larger than 30 Å, whereas nitric acid treatment seemed to form more pores with lower size. Thus, nitric acid treatment is not as effective as citric acid treatment in creating large pores. Zeolite treated with nitric acid results in a lower conversion and DTBGE + TTBGE selectivity than zeolite after citric acid treatment, possibly because of severe dealumination and formation of smaller pores. For instance, 1 M nitric acid treatment brought about 46 mol% DTBGE + TTBGE selectivity, while this number was 57 mol% for 1 M citric acid treatment. In conclusion, the catalytic improvement via acid treatment was interpreted to be influenced by enhanced Brønsted acidity and by facilitated mass transfer into the pores. The concept of Brønsted/Lewis acid synergy in dealuminated zeolites is significant since this can influence the Brønsted acid strength. For instance, as found by NMR studies, if the extra framework aluminum species (EFAL) formed by dealumination which act as Lewis sites are in close proximity to the oxygen atoms nearby the framework aluminum species, then the Brønsted acidity is improved [125,135].

Gonzalez et al. modified zeolite H-Beta by post synthesis sulfonic acid addition via conventional heating and microwave heating [52], and then tested microwave assisted sulfonation on a wider range of zeolites, covering H-Beta, H-ZSM-5 and H-Mordenite [55]. The sulfonic acid source was 2-(4-chlorosulfonylphenyl) ethyltrimethoxysilane (CSPTMS) (**Figure 2-8 d**). Acidic conditions during sulfonation resulted in partial dealumination of the zeolite framework, followed by the formation of silanol groups (Si–OH). The silanol groups then reacted with CSPTMS, leading the formation of sulfonic acid groups. According to XRF

and XPS results, the elevated Si/Al ratio indicated dealumination during sulfonation, which was interpreted to provide addition of new sulfonic acid groups to the zeolites (**Figure 2-9**). Sulfonation by heating improved the glycerol conversion and TTBGE selectivity, especially for the microwave sulfonated H-Beta (called B-MwS) with the desired higher ether selectivity of 91 mol% after 24 h of reaction time, while the desired ether selectivity remained as 88, 60 and 77 mol% for conventional heat sulfonated H-Beta (called B-CS), non-modified zeolite and reference catalyst Amberlyst 15™, respectively. Reported turnover frequencies (TOF) were 0.63, 0.60 and 0.17 h^{-1} for B-MwS, B-CS and Amberlyst 15™, meaning that sulfonated zeolites had at least 3 times more glycerol converted per mole of active protonic sites per hour than Amberlyst 15™. Nitrogen adsorption-desorption and XRD results demonstrated that B-CS had a higher decrease in external surface area, micropore area, BET surface area, pore volume and higher loss in crystallinity with respect to B-MwS. Superiority of B-MwS to B-CS by means of catalytic activity, while their acid capacities were similar (similar amounts of Brønsted acid sites), was related to the wider surface area, pore volume, mesoporosity; thus easier access to its acidic sides. Applying microwave sulfonation on several zeolite types, it was found that each type of zeolites showed different changes in surface area because of their i) different degree of dealumination, ii) loss of crystal structure and iii) fractional plugging of the pores by the sulfonic groups. Dealumination by sulfonation increased the surface area of ZSM-5 and Mordenite, except for Beta, possibly because of the loss of crystallinity for the flexible zeolite Beta. Moreover, zeolite H-Beta encountered great reduction in BET surface area, from 573 m^2/g to 88 m^2/g under 2.2 g CSPTMS treatment, at high degree of sulfonation, because of the blockage of the pores by sulfonic acid groups. Dealumination was easiest for Na-Beta, but most difficult for ZSM-5 because of its less flexible framework (ZSM-5 has three-dimensional 10-ring pore system with channels able to include 6.36 Å). Therefore, lower CSPTMS concentrations could be applied for H-Beta to obtain the same degree of sulfonation, checked

by S/Si atomic ratio from XPS spectra. For each catalyst, sulfonation at the optimum extent, corresponding to 1.4 g CSPTMS/2 g Na-Beta, 1.6 g CSPTMS/2 g Mordenite, 1.8 g CSPTMS/2 g ZSM-5, brought an increase in glycerol conversion and desired ether selectivity. Although the acid capacity of the catalysts would increase by applying higher amounts of the sulfonation agent, the concomitant decrease in BET area and pore volume could have resulted in diminished catalytic activity. Glycerol conversions which were lower than 50 mol% at non-sulfonated case increased over 98 mol% upon optimum sulfonation by using the same amount of catalyst, while the desired ether selectivity increased from 61 to 90 mol% for Beta (in 48 h); from 17 to 84 mol% for ZSM-5 (in 24 h) and from 16 to 79 mol% for Mordenite (in 48 h). Introduction of strong Brønsted acid sites via sulfonation was claimed to have improved the catalytic activity. Further sulfonation beyond the optimum points caused a decrease in TTBGE selectivity, from 36 to 18 mol% for Beta; from 28 to 6 mol% for ZSM-5 and from 21 to 7 mol% for Mordenite, probably because of steric hindrance of excess sulfonic acid groups in the pores. Other factors improving the catalytic activity were presented as pore size distribution (*e.g.* 3-D pore system of Beta compared to 1-D pore system of Mordenite) and external surface area (*e.g.* larger surface area of sulfonated Beta than Mordenite). Additionally, sulfonated Mordenite and ZSM-5 samples showed DIB formation of 1.6 and 4.5 wt% in among all products, corresponding to 3 mol% DIB + 93 mol% ethers and 9 mol% DIB + 91 mol% ethers in the product mixture, which was not observed over unmodified zeolites of the same type.

Recently, Gonzalez and coworkers investigated the effects of hierarchical porosity on zeolite H-Beta for glycerol etherification with IB [58]. By definition, hierarchical zeolites possess at least two levels of porosity in their structures, namely mesoporosity or macroporosity in addition to the regular microporosity. Therefore, they can handle reactions with larger molecules [136]. Gonzalez et al. synthesized one regular Beta zeolite and one with additional porosity by using phenylaminopropyltrimethoxysilane (PHAPTMS) as a silanization agent.

The silanization agent, PHAPTMS, blocks the formation of zeolite crystals via organo-functionalization of protozeolitic units. Argon adsorption-desorption isotherms showed that silanization attributed mesoporous regions to the Beta zeolite; for instance, the number of 2-7 nm sized pores increased while < 1 nm sized pores decreased. Hierarchical Beta (called h-Beta) resulted in better glycerol conversion because of easier access of the reactants to the acid sites in the enlarged pores, however only a slight increase in TTBGE selectivity was observed. Hierarchical Beta seemed to have 97 mol% glycerol conversion, 57 mol% desired ether selectivity (with 2 mol% TTBGE selectivity) and forms 6 to 9 wt% DIB, while the non-modified one was associated with 50 mol% glycerol conversion, 70 mol% desired ether selectivity (with 1 mol% TTBGE selectivity) and forms averagely 1 to 3 wt% DIB in the final product mixture. In the same study, H-Beta modification by fluorination (by 0.3 wt% NH_4F) was also performed for glycerol etherification with IB, since this modification was successful on glycerol etherification with t-butanol [70] in enhancing the strong acid sites and selectivity to higher ethers. Based on previous IR/XPS/NMR/catalytic studies, fluorine was claimed to form complexes with Al and Si atoms in the zeolite framework; increasing the Brønsted acidity in the former case and decreasing the Brønsted/Lewis acidity ratio in the latter case, thus an optimum fluorine concentration was required for the best catalytic activity [137]. This optimum condition might be related to the Brønsted/Lewis synergy. Fluorination of hierarchical zeolite Beta (called h-Beta-F) attributed to the performance improvement in terms of conversion and selectivity to higher ethers, although it has lower acid capacity than regular Beta or h-Beta. While additional porosity meant easier access to the active sites of the catalyst, fluorination meant increased strength of the Brønsted acid sites. Their combined effect yielded in elevated TTBGE selectivity in h-Beta-F when compared to h-Beta (from 2% of 8%), with similar conversion of glycerol and selectivity for the desired DTBGE + TTBGE (97% conversion and 57% selectivity for h-Beta, while 96% conversion and 63% selectivity for h-Beta-F at 75 °C).

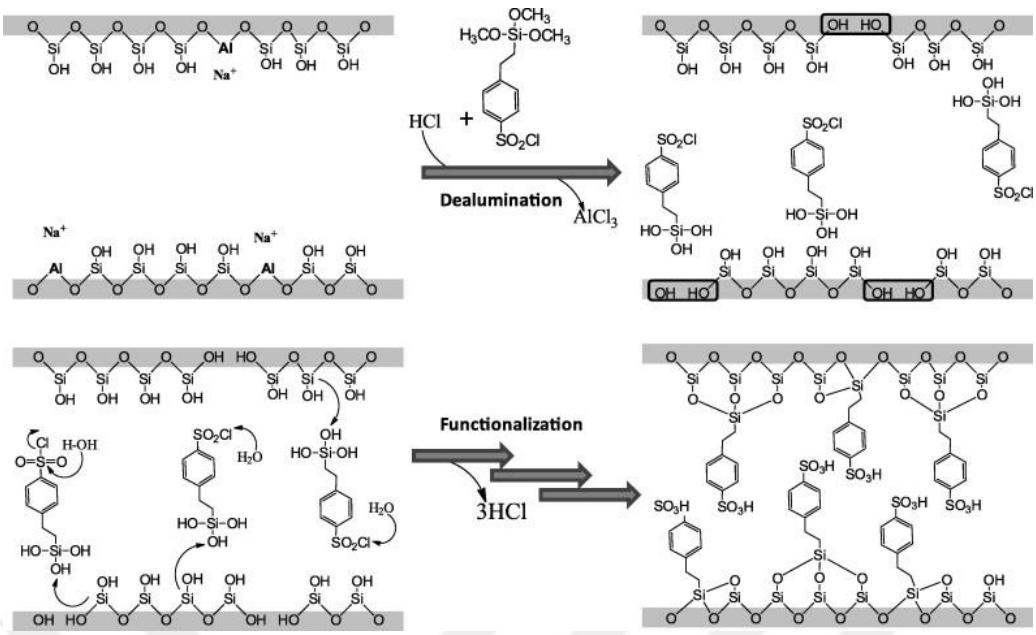

Figure 2-9. Sulfonic acid functionalization in zeolite H-Beta. Formation of new silanol (Si-OH) groups by zeolite dealumination in acidic medium and reaction of sulfonation agent CSPTMS with silanol groups to form the sulfonated zeolite. Reprinted from Ref. [52] with permission from Elsevier, Copyright 2012.

Concurrently with the studies of Gonzalez et al., Zhao and coworkers performed ion exchange with rare earth cations (La^{+3}, Ce^{+3}, Nd^{+3} and Eu^{+3}) in zeolite H-Beta, increasing the number of acid sites, to improve the selectivity for desired DTBGE + TTBGE [56]. Rare earth metals, the metals from lanthanide series, are known to enhance the catalytic activity of hydrogen transfer reactions and the thermal stability of catalysts [138]. Rare earth cations are found to be in $RE(H_2O)_n^{+3}$ form with a strong electrical potential which ionizes to give protons to the medium: $RE(H_2O)_n^{+3} \rightarrow RE(OH)(H_2O)^{+2}_{n-1} + H^+$. These protons then interact with the oxygen atoms of the zeolite framework, creating new Brønsted acid sites. According to N_2 adsorption–desorption analysis by Zhao et al., the introduction of rare earth cations was observed to reduce the surface area and pore diameter of H-Beta zeolite (*e.g.* pore diameter

dropped few angstroms from 7.7 Å), while there was an increase in strong acidity in all cases, caused by the exchange of rare earth cations with aluminum atoms in the zeolite structure. The best results were obtained for Nd^{+3} modified H-Beta, which improved the desired ether selectivity from 61 to 75 mol%. Moreover, the modified zeolite was determined to be reusable since it retained its activity even after three cycles. The improved activity was interpreted to be the result of increased number of Brønsted acid sites.

The etherification of glycerol with olefins from FCC gasoline and petrochemical C4 fractions have also been studied over zeolites. Kiatkittipong et al. [10] used the FCC gasoline of C4 to C12 hydrocarbons including 25 v/v% olefins (1.2 v/v% C4 and 6.7 v/v% C5 olefins) as well as 5 v/v% n-paraffins, 40 v/v% i-paraffins, 10 v/v% naphthenes and 20 v/v% aromatics with ~5:1 volume ratio in a reaction with glycerol corresponding to IB:G ratio of approximately 0.05 and catalyst loading of 50 wt% of glycerol by using zeolite H-Beta and Amberlyst 15™, Amberlyst 16 as catalysts, with the aim of improving the gasoline quality. Comparing the iso-olefinic C4, C5, C6 and C7 concentrations before and after the reaction, it was observed that C4-C5 concentrations, such as IB, 2-methylbutene-1 and 2 methylbutene-2 in FCC gasoline decreased, with the best result obtained with Amberlyst 16 (100% glycerol conversion). The activity of H-Beta was the lowest in terms of catalytic activity and no TTBGE was produced. Turan et al. investigated the etherification of a petrochemical fraction of only C4 hydrocarbons, consisting of 41.7 wt% IB, 23.7 wt% i-butane, 10.7 wt% trans-2-butene, 7.4 wt% cis-2-butene and 5.4 wt% n-butane as the main components, by using H-Beta as a catalyst, as well as Amberlyst 35™ [54]. Significant amount of DIB was produced by using H-Beta, which was attributed to i) a number of Lewis acid sites formed during calcination of the zeolite that support dimerization reaction and ii) slow diffusion of glycerol and ethers into narrow zeolite pores. The desired ether selectivity of H-Beta were 76 mol% for 3:1 IB:G and 73% for 4:1 IB:G ratio, which are higher than Amberlyst 35™ (64 and 72 mol%, respectively), even though more

TTBGE was observed for Amberlyst, since MTBGE concentrations in the product mixture was minor in the case of the zeolite (12 wt% MTBGE for zeolite and > 16 wt% MTBGE for ion exchange resin). TTBGE formation for zeolite H-Beta could not exceed that of Amberlyst 35^{TM} because of its small pore size and poorer Brønsted acidity when compared to Amberlyst 35^{TM}. For instance, TTBGE concentration was more than fourfold of that obtained by H-Beta when the catalyst was Amberlyst 35^{TM}. It should be noted that the group worked at 90 °C at which zeolite Beta could be deactivated because of triggered oligomerization of IB [39].

Zeolites can be used at high reaction temperatures because of their high thermal stability. Mravec and coworkers tested zeolite H-Beta of different Si/Al ratios for glycerol etherification with ethanol in a batch reactor system at 200 °C for 8 h by using ethanol to glycerol molar ratio of 15:1 and catalyst amount of 10 wt% of glycerol. Turnover number of glycerol (moles of glycerol converted during 8 h over mol H^+) increased with BET surface area and Si/Al ratio of the zeolite. H-Beta had a higher catalytic performance compared to Amberlyst 35^{TM} tested at 140 °C [139]. Similarly, glycerol etherification with isobutene can be studied at higher temperatures using zeolites. However, elevated reaction pressures (> 20 bar) will be required to keep isobutene at liquid phase.

Zeolites can catalyze the etherification of biobased materials other than glycerol [140,141], or other reactions of glycerol [142]. For instance, Lanzafame et al. recently used zeolite Beta, ZSM-5 and Mordenite for the etherification of HMF (5-hydroxymethylfurfural) with ethanol in a batch reactor system at 140 °C. Fresh catalysts were characterized by *in-situ* FTIR spectroscopy with pyridine adsorption. The number of Lewis and Brønsted strong acidic sites were calculated by integrating the areas under 1450 and 1545 cm^{-1} bands, respectively. Lewis acid sites were shown to be responsible for the direct etherification of HMF to 5-(ethoxymethyl) furan-2-carbaldehyde (EMF), as the rate constant for EMF formation had linear

correlation with the number of Lewis acid sites [140]. The group also tested the effect of having Fe or B heteroatoms instead of Al, thus lower Lewis acidity in ZSM-5 framework. Having less number of Lewis acid sites altered the reaction network in such a way that EMF is produced via acetalization of HMF on Brønsted acid sites [141]. Jamil et al., studied glycerol condensation with acetone over H-Beta for the production of a green fuel additive solketal. The zeolite was partially dealuminated by acid treatment to improve the solketal yield, up to 94 wt% [142]. These studies emphasize on the influence of small catalyst modifications on product yields. In parallel, Serrano et al. in a recent literature review have declared that the development in zeolite preparations such as controlling the number of Brønsted and Lewis active sites, hierarchical synthesis with larger pore dimensions and incorporation of metal species seems promising for the utilization of zeolites in biomass valorization for the production of biofuels and bio-based molecules [143].

2.2.3.3. Mesoporous silica

Mesoporous silica with larger pore sizes of 2 to 50 nm have been developed as better alternatives to microporous crystalline materials including zeolites to overcome the drawbacks of limited mass transfer of reactants and products onto or out of the active sites [144]. These materials can be synthesized by using inorganic precursors, such as silica and organic templates, which are mainly surfactants. Once the organic templates form micelles in solution, inorganic precursors are added, upon which electrostatic, van der Waals and hydrogen bonding interactions define the textural properties of the mesoporous material. When the organic template is removed by solvent refluxing or by calcination at high temperature, pore size of the final structure is determined by the size of surfactant micelles. MCM-41 is an earlier form of mesoporous materials with parallel tubes of 2 to 5 nm pore size in hexagonal arrangement, resulting in a 2-D structure with mesopores (**Figure 2-8 c**). MCM-41 can be synthesized by

condensing silica gel or tetraethyl orthosilicate (TEOS) around cetyltrimethylammonium (CTMA or CTAB) surfactant micelles, in which the negatively charged silica groups interact with the positively charged groups of the surfactant molecules, followed by the combustion of the organic surfactant fraction in the final calcination step, resulting in hollow hexagonal silica tubing [144,145]. SBA-15 is another version of mesoporous silica, with larger pore sizes than MCM-41, such as 6 to 15 nm and with a thicker wall. SBA-15 is synthesized by using block copolymers such as the triblock copolymer Pluronic P-123 instead of surfactants along with a silica source. Once the block copolymer is removed; amorphous silicate structure is obtained [145]. HMS is also a common type of mesoporous silica, with 3 to 4 nm pore size with a wormhole-like framework, prepared by employing electrically neutral amines, such as dodecylamine (dda), as a template and then removing the amines to reach final mesoporous structure [146].

Use of mesostructured materials as catalysts for the etherification reaction started slightly later than that of ion exchange resins and zeolites. Mesostructured silica functionalized with organo-sulfonic groups have already been used as successful alternatives to conventional solid acid catalysts in fatty acid esterification [147,148] and sugar hydrolysis [149,150]. The properties of sulfonic acid mesoporous silica, such as high surface area, larger pores, narrower pore size distribution, easy access to Brønsted acid sites and strong acidity, favored its applicability also for the etherification [42,50,52,55,59,60] of glycerol. **Table 2-5** and **Table 2-6** present physical characteristics and catalytic performance results of mesoporous silica.

Table 2-5. Physical characteristics of regular and modified mesoporous silica catalysts.

Type of mesoporous silica[a]	BET area (m^2/g)	Pore volume (cm^3/g)	Pore size[b] (nm)	S/Si surface ratio[c]	Sulfur content[d]	Organic incorp.[e] (%)	Acid capacity[f] (meq H^+/g cat)	Reference
Pr-SBA-15	666	1.19	8.2			91	1.21	[42]
Ar-SBA-15	720	1.03	8.0			99	1.24	[42]
MCM-41	1717	1.88	2.8					[50]
MCM-41-TFESA	807	1.48	2.6					[50]
SBA-15	274	1.14	3.9					[50]
SBA-15-TFESA	124	0.59	3.8					[50]
SBA-15	1082	1.68						[52]
SBA-15-CS	640	0.81		0.03	0.83		0.35	[52]
SBA-15-MwS	575	0.74		0.07	1.01		0.75	[52]
MCM-41	989	1.04	3.93					[59]
SBA-15	1212	1.30	7.31					[59]
HMS(dda)	612	1.96	4.03					[59]
Al-MCM-41	808	0.86	3.63				0.81	[59]
Al-SBA-15	488	0.65	6.92				0.55	[59]
MCM-41-P	696	0.63	3.80					[59]
SBA-15-P	704	0.82	7.57					[59]
MCM-41-S	807	1.29	3.37		0.20		0.24	[59]
HMS(dda)-S	497	1.65	4.01		0.64		0.63	[59]
MCM-41	1252	1.74	2.7					[60]
MCM-41-TFA	960	1.75	2.6 and 30					[60]

[a]Pr: propylsulfonic acid, Ar: arenesulfonic acid, TFESA: tetrafluoroethanesulfonic acid, CS: sulfonation by conventional heating, MwS: sulfonation by microwave heating, dda: dodecylamine, TFA: triflic acid; [b]Determined from nitrogen adsorption desorption applying BJH model; [c]Determined from XPS; [d]mmol organic sulfonic acid group/g sample, determined from TGA; [e]Estimated from HNCS elemental analysis from actual sulfur content and max theoretical content; [f]Determined from potentiometric titration for sulfonated samples and by thermal desorption of cyclohexylamine for Al containing samples.

Table 2-6. List of studies on glycerol etherification with isobutene using mesoporous silica as heterogeneous catalysts.

Temperature (°C)	Pressure[a] (bar)	Catalyst loading (wt% of G)	Reaction time (h)	IB:G ratio (mol:mol)	Type of mesoporous silica[b]	Glycerol conversion (mol%)	Desired ether selectivity[c] (mol%)	DIB formation[d] (wt%)	Reference
75	8 + VLE	5	4	4	Ar-SBA-15, sulfonated	100	92	0	[42]
75	8 + VLE	5	4	4	Ar-SBA-15, sulfonated, 3rd cycle	97	93	n/a	[42]
75	8 + VLE	5	4	4	Ar-SBA-15, sulfonated, 4th cycle	93	90	n/a	[42]
75	8 + VLE	5	4	4	Pr-SBA-15, sulfonated	90	86	0	[42]
80	n/a	4	5	3	MCM-41-TFESA, in emulsifier	95	77	n/a	[50]
80	n/a	4	5	3	SBA-15-TFESA, in emulsifier	94	80	n/a	[50]
75	10 + VLE	0.5 g	4	4	SBA-15	41	13	3.3	[52]
75	10 + VLE	0.5 g	4	4	SBA-15-CS, sulfonated	98	61	0.7	[52]
75	10 + VLE	0.5 g	4	4	SBA-15-MwS, sulfonated	99	91	1.7	[52]
75	10 + VLE	0.5 g	24	4	SBA-15	62	14	10.0	[52]
75	10 + VLE	0.5 g	24	4	SBA-15-CS, sulfonated	99	85	2.2	[52]
75	10 + VLE	0.5 g	24	4	SBA-15-MwS, sulfonated	100	91	6.8	[52]
75	10 + VLE	0.5 g	24	4	MCM-41	20	13	very low	[59]
75	10 + VLE	0.5 g	24	4	SBA-15	23	11	very low	[59]
75	10 + VLE	0.5 g	24	4	HMS(dda)	30	12	very low	[59]
75	10 + VLE	0.5 g	24	4	Al-MCM-41, aluminated	47	20	very low	[59]
75	10 + VLE	0.5 g	24	4	Al-SBA-15, aluminated	41	22	very low	[59]
75	10 + VLE	0.5 g	24	4	MCM-41-P, phosphorylated	45	30	very low	[59]
75	10 + VLE	0.5 g	24	4	SBA-15-P, phosphorylated	40	43	very low	[59]
75	10 + VLE	0.5 g	24	4	MCM-41-S, sulfonated	60	55	very low	[59]
75	10 + VLE	0.5 g	24	4	HMS(dda)-S, sulfonated	100	84	very low	[59]
80	n/a	5	5	1.5	MCM-41-TFA	88	48	n/a	[60]

[a]VLE: vapor liquid equilibrium after pressurizing the reactor; [b]Pr: propylsulfonic acid, Ar: arenesulfonic acid, TFESA: tetrafluoroethanesulfonic acid, CS: sulfonation by conventional heating, MwS: sulfonation by microwave heating, dda: dodecylamine, TFA: triflic acid; [c]Selectivity for di- and tri-tertiary butyl ethers of glycerol based on glycerol; [d]wt% DIB in the product mixture.

One of the keystone studies with sulfonated mesostructured silica for the etherification of glycerol with IB was performed by Melero et al. [42]. In this study, propylsulfonic-acid-functionalized mesostructured silica (Pr-SBA-15) and arenesulfonic-acid-functionalized mesostructured silica (Ar-SBA-15) (*e.g.* in **Figure 2-10**) were used to optimize the reaction conditions (temperature and IB to glycerol molar ratio) for highest glycerol conversion and DTBGE + TTBGE selectivity. The sulfonic acid functionalized mesoporous silica was synthesized by one-step method in which tetrahydroxysilane (TEOS) and thiol precursor trimetoxysilanes were co-condensed on the Pluronic 123 template polymer species in acidic medium with hydrogen peroxide [151,152]. 3-mercaptopropyltrimethoxysilan (MPTMS) and 2-(4-chlorosulfonylphenyl)ethyltrimethoxysilane (CSPTMS) were used as thiol precursors to synthesize Pr-SBA-15 and Ar-SBA-15, respectively. According to XRD and nitrogen adsorption data, the functionalized catalysts still had large surface area and pore size in the mesoporous region so that the steric hindrance for large glycerol ethers could be avoided. After 4 h of reaction, the highest glycerol conversion and desired ether selectivity were obtained in the case of Ar-SBA-15 (100% conversion of glycerol and 92 mol% higher ether selectivity), followed by Amberlyst type resins (96-99 mol% conversion of glycerol and 89-90 mol% higher ether selectivity), CT-275 (100 mol% conversion of glycerol and 87 mol% higher ether selectivity), Pr-SBA-15 (90 mol% conversion of glycerol and 96 mol% higher ether selectivity) and SAC-13 (< 50 mol% conversion of glycerol, not properly determined selectivity because of two-phase system). Although Ar-SBA-15 had lower pore size, pore volume and wall thickness than Pr-SBA-15, its superior performance can be attributed to the higher BET surface area (720 m^2/g for Ar-SBA-1 compared to 666 m^2/g Pr-SBA-15) and the higher acid capacity of arene-SO_3H moieties, which is 1.24 meq H^+/g when compared to propyl-SO_3H following as 1.21 meq H^+/g. Besides, both type of mesoporous catalysts prevented the formation of IB oligomers; that was interpreted to be the oligomerization inhibiting effect of silica matrices of

these materials. For the $–SO_3H$ sites, polystyrene-type environment in ion exchange resins seems to favor the dimerization of IB in a greater extent than the silica environment of SBA-15. In contrast, sulfonic acid resins, Amberlyst 15™, Amberlyst 36™, and CT-275, favored the formation of IB dimers, which was also the case in previous glycerol *tert*-butylation studies [37-41,44,45,48,51,52,54]. Arenesulfonic acid functionalized mesoporous silica SBA-15 was shown to be a good alternative to commercial ion exchange resins. Even though it has lower acid capacity (less sulfonic acid sites) per gram of catalyst compared to Amberlyst 15™ and 36™, and the oligomerization reaction of IB to DIB is not supported by its silica matrix. Thus, it can provide opportunities to avoid extra cost of product purification. Ar-SBA-15 was also proved to preserve its catalytic activity in four consecutive cycles each 4 h long without any significant deactivation.

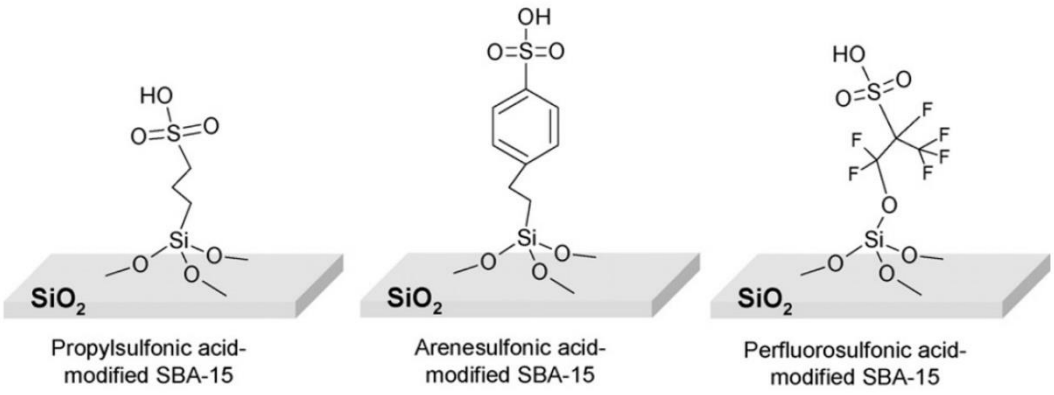

Figure 2-10. Mesoporous silica SBA-15 with attached sulfonic acid functional groups; propylsulfonic acid, arenesulfonic acid and perfluorosulfonic acid. Reprinted from Ref. [153] with permission from Elsevier, Copyright 2009.

Voicu et al. tested the catalytic activity of tetrafluoroethanesulfonic acid (TFESA) supported on two types of mesoporous silica, namely MCM-41 and SBA-15 [50]. Mesoporous MCM-41 and SBA-15 were first synthesized with known methods [154,155] and then

impregnated with 10 wt% solutions of the acid, resulting in modified MCM-41 with 8.36 wt% TFESA and SBA-15 with 8.83 wt% TFESA. Working in a batch autoclave at 80 °C, 3:1 IB:G molar ratio, 1200 rpm mixing, 4 wt% catalyst, and 0.1 wt% ammonium quaternary salt emulsifier per weight of glycerol, with the latter one to enhance the mass transfer between glycerol and IB phase per weight of glycerol, high glycerol conversion (96 mol%) and selectivity (77 mol%) was obtained for modified MCM-41 (with 15 mol% TTBGE yield) and 95 mol% conversion and 80 mol% selectivity for modified SBA-15 (with 20 mol% TTBGE yield) was obtained. Relatively higher yields of desired ethers for SBA-15-TFESA was related to its larger pore size (38 Å, compared to 26 Å), although its surface area and pore volume was lower than that of MCM-41, determined by nitrogen adsorption-desorption. The acidity of the catalysts was not determined directly, but higher TFESA loading on SBA-15 might have resulted in higher acidity. Stronger acidity and easier access to the active sites through larger pores, as well as the enhanced mass transfer between glycerol and IB reactants in the presence of an emulsifier could have resulted in higher yields of desired ethers.

Gonzalez et al. [52], performed studies with regular and functionalized forms of mesoporous silica, with the aim of comparing the catalytic activities in glycerol etherification with IB. Sulfonic acid functionalized SBA-15 was synthesized as proposed by Zhao et al., by direct co-condensation in an acidic medium by using SiO_2, CSPTMS, HCl, and H_2O with a ratio of 1.2:0.2:6.5:180 [156], in which the sulfonation step employed refluxing with conventional or microwave heating (SBA-15-CS and SBA-15-MwS). Both SBA-15-CS and SBA-15-MwS were observed to show better glycerol conversion and selectivity towards DTBGE and TTBGE when compared to pure SBA-15, mainly because of increasing the amount of Brønsted acid sites, although there were reductions in surface area and pore volume for modified catalysts. For instance in 4 h, 98 mol% conversion with 61 mol% desired ether selectivity and 99 mol% conversion with 91 mol% desired ether selectivity were obtained on

SBA-15-CS and SBA-15-MwS, respectively, while regular SBA-15 yielded in 41 mol% glycerol conversion and 13 mol% desired ether selectivity. Moreover, sulfonated mesoporous silica had better performance compared to Amberlyst 15™ and comparable performance over sulfonated zeolite Beta, with reduced IB dimerization.

Gonzalez et al. later extended the scope of mesoporous silica [59], using MCM-41 and HMS, as well as SBA-15, with some modifications, such as post-synthesis aluminum incorporation to MCM-41, post-synthesis phosphorus incorporation to MCM-41 and SBA-15, sulfonation of MCM-41 during its synthesis and post-synthesis sulfonation of HMS. Without any modification, all types of mesoporous silica were observed to show low glycerol conversion (< 30%) and desired ether selectivity (< 15%), because of low number of acidic sites. Conversions from 40 to 100 mol% and selectivity from 14 to 84 mol% were obtained depending on the type of silica and aluminum, phosphoric acid or sulfonic acid functional groups. Mesoporous structure was maintained during modifications, with minor changes in average pore diameter, *i.e.* less than half nanometer, showing usually decreasing trend of pore diameter mainly because of the retaining of un-incorporated aluminum or the introduction of phosphoric or sulfonic groups in the pores. Alumination done by aluminum isopropoxide increased the acidity and the number of Brønsted acid sites, thus yielded in higher glycerol conversions. However, as the acidic strength was not sufficient, the final DTBGE + TTBGE amounts were low. Phosphoric acid modification resulted in improved selectivity towards higher ethers because of the higher acid strength of phosphoric groups. The best performance was obtained by sulfonic acid modification, related to the higher Brønsted acidity of sulfonic acid over phosphoric acid. The sulfonated HMS catalyst with the amine template dodecylamine, namely HMS(dda) with high acid capacity and sulfonic acid incorporation, demonstrated the highest conversion (100 mol% glycerol conversion) and selectivity towards DTBGE and TTBGE (84 mol%) in four hours among all other modified catalysts. Even though the surface area, pore size

and pore volume of HMS(dda) decreased considerably, its catalytic activity was interpreted to be enhanced by its textural mesopores that helped i) incorporation of more sulfonic acid groups and ii) transport of the molecules into the framework mesopores. Therefore, the acid strength which is related to the nature of the introduced acidic groups (*e.g.* highest for sulfonic acid groups) seems to be more important than the acid capacity (or acidity), originating from the amount of protonic sides per gram of catalyst, together with the textural mesoporosity which eliminates diffusion limitations and eases the accessibility to the functional groups.

Parallel to these studies, Mangourilos et al. [60] utilized triflic acid (TFA) functionalized mesoporous silica MCM-41 in glycerol etherification. MCM-41 was first synthesized and then pore volume impregnation method was employed with 10 wt% TFA aqueous solution [50]. The pore size distributions obtained from the adsorption branch of the nitrogen adsorption-desorption isotherms using the Barett-Joyner-Halenda method (BJH) indicated that triflic acid impregnation caused a new mesoporosity around 30 nm pore size, in addition to the regular porosity of MCM-41 of 2.6 nm pore size. The etherification reaction over MCM-41-TFA yielded in 88 mol% conversion of glycerol with 48 mol% desired ether selectivity. The low selectivity could be a reason of the low IB:G molar ratio (1.5:1), for instance some previous studies (with ion exchange resins as catalyst) encountered relatively high MTBGE concentrations at low molar feeds [37,40,51].

Sadjadi and Heravi have mentioned in their recent literature review that mesoporous silica can be functionalized with metal complexes, nanoparticles and heteropolyacids. Reusable heterogeneous catalysts can be constructed by the incorporation of heteropolyacids on SBA. Moreover, heteropolyacids can be immobilized on amine or ionic liquid modified mesoporous silica can successfully be used in alkylation, desulfurization, epoxidation, and oxidation

reactions [157]. Heteropolyacid impregnated mesoporous silica have not been tested in glycerol etherification with isobutene, but will take place in our study.

2.2.3.4. Other heterogeneous catalysts

In addition to ion exchange resins, zeolites and mesoporous silica, some other heterogeneous acid catalysts have been screened for their catalytic efficiency to produce desired ethers of glycerol in the etherification reaction with IB. We convey the important physical properties and the corresponding catalytic performance of some novel catalysts in **Table 2-7** and **Table 2-8**, respectively.

Behr and Obendorf [38] tested the performance of three different heterogeneous catalyst following as Montmorillonite K-10, a commercial clay produced via calcination of natural montmorillonite silicate, 20 wt% heteropolyacid phosphotungstic acid (PTA) on montmorillonite K-10 and amorphous microporous mixed oxide (AMM) in glycerol conversion, DTBGE selectivity and DIB yields. The best performance was achieved by Montmorillonite K-10 supported PTA, 31 mol% glycerol conversion and 25 mol% DTBGE selectivity, which were closer to 45 mol% glycerol conversion and 34 mol% DTBGE selectivity with Amberlyst 15™. In addition, oligomerization of IB was not observed over these heterogeneous catalysts except for Amberlyst 15™. The reasons for low catalytic activities could be the relatively small pore size (average of 3.8 nm for Montmorillonite K-10 and > 1 nm for AMM) and the weak Brønsted acidity [158,159]. In addition, deposition of PTA on Montmorillonite K-10 has been proved to result in enhancement in density and strength of Brønsted acid sites [158].

Table 2-7. Physical characteristics of some novel catalysts.

Catalyst type[a]	BET area (m^2/g)	Pore volume (cm^3/g)	Pore size[b] (nm)	S/Si surface ratio[c]	Sulfur content (mmol/g)	Active phase loading (wt%)	Acid capacity (meq H^+/ g cat)	Reference
Peanut shell, sulfonated	10.45		41.95		1.93[d]		2.07[h]	[47]
H1170/LM50	12	0.48	27.2			15.80[g]	0.16[i]	[51]
H850/LM50	24	0.51	26.0			14.50[g]	0.17[i]	[51]
H730/LM50	29	0.47	28.2			15.76[g]	0.23[i]	[51]
H730/MS3030	177	0.33	7.7			18.12[g]	0.14[i]	[51]
H730/ES70Y	204	0.33	11.8			19.14[g]	0.17[i]	[51]
SC-AG(1.4)	547	4.50	59	0.003	0.05[e]		0.07[i]	[57]
SMw-AG(1.4)	353	0.62	35	0.031	0.22[e]		0.24[i]	[57]
SMw-AG(0.7)	537	3.20	48		0.04[e]		0.05[i]	[57]
SMw-AG(2.8)	211	0.48	22		0.27[e]		0.30[i]	[57]
SC-LG(1.4)	702	1.47	30	0.002	0.02[e]		0.02[i]	[57]
SMw-LG(1.4)	669	1.2	30	0.006	0.04[e]		0.04[i]	[57]
Sulfonated graphene (SG)	427 (RGO)				1.9[f]			[61]
20 wt% TFA/ γ-Al_2O_3	267	1.43	3.9					[62]
30 wt% TFA/ γ-Al_2O_3	286	2.16	4.4					[62]
10 wt% TFA/ γ-Al_2O_3	243	2.39	5.1					[60]

[a]H1170-H850-H730: Hyflon Ion S4X perfluorosulfonic ionomers, LM50-MS3030-ES70Y: silica supports, AG: Aerogel, LG: Lyogel, SC: Sulfonated by conventional heating, SMw: Sulfonated by microwave heating, Numbers in parenthesis indicate the amount (g) of CSPTMS used per 2 grams of AG or LG, RGO: reduced graphene oxide, TFA: triflic acid. Determined from [b]N_2 adsorption-desorption BJH method, [c]XP spectra, [d]EDS, [e]TGA, [f]CHNSO elemental analysis, [g]Thermo-gravimetric and differential calorimetric analysis (TG-DSC), [h]NH_3-TPD, [i]Potentiometric titration.

Zhao et al. [47] introduced the idea of using peanut shell, which is a biomass waste, as a green catalyst for etherification of glycerol with isobutylene. At first, the peanut shell was partially carbonized under nitrogen flow at 450 °C and then sulfonated in concentrated sulfuric acid at 210 °C. The resulting catalyst showed higher thermal stability (300 °C), larger pore size (41.95 nm) and smaller particle size when compared to Amberlyst 15™ ion exchange resin, but with lower surface area and acid capacity. FTIR bands at 1040 and 1181 cm^{-1} that of SO_2 stretching indicated the covalently bound sulfonic acid groups on the modified peanut shell. The influence of reaction time (0.3 to 4 h), temperature (50-90 °C), IB:G mole ratio (2:1 to 5:1) and catalyst loading (1 to 8 wt% of glycerol) on glycerol conversion and desired ether selectivity, as well as the reusability of catalyst (one to five cycles) were assessed. The highest performance was achieved at 70 °C, 4:1 molar ratio, 6 wt% catalyst loading in two hours

reaction time, at 99 mol% glycerol conversion and 92 mol% DTBGE + TTBGE selectivity, therefore showing superior performance over Amberlyst 15™. The co-existence of hydrophobic carbonized shell and hydrophilic −COOH and $-SO_3H$ groups on the catalyst was claimed to adsorb both IB and glycerol successfully onto active sites, which would be sustaining the superior performance of this novel catalyst.

Table 2-8. The list of studies on glycerol etherification with isobutene using some novel heterogeneous catalysts.

Temperature (°C)	Pressure (bar)	Catalyst loading (wt% of G)	Reaction time (h)	IB:G ratio (mol:mol)	Catalyst type[b]	Glycerol conversion (%)	Desired ether selectivity[c] (mol%)	DIB formation	Reference
90	14	2.2	5	2	Montmorillonite K-10	4	0	0	[38]
90	14	2.2	5	2	PTA on montmorillonite K-10	31	25	0	[38]
90	14	2.2	5	2	Amorphous microporous mixed oxide	<12	<9	0	[38]
70	15	6	2	4	Peanut shell, sulfonated	99	92	3[d]	[47]
70	15	2	2	4	Peanut shell, sulfonated	65	n/a	n/a	[47]
70	15	6	4	4	Peanut shell, sulfonated	100	94	6[d]	[47]
80	15	6	2	4	Peanut shell, sulfonated	98	88	5[d]	[47]
70	15	6	4	3	Peanut shell, sulfonated	95	73	n/a	[47]
70	15	6	2	4	Peanut shell, sulfonated, 3rd cycle	99	92	n/a	[47]
70	15	6	2	4	Peanut shell, sulfonated, 5th cycle	99	92	n/a	[47]
60	20	17	2	4	$Cs_{2.5}SiW$	n/a	n/a	34[e]	[45]
60	20	17	20	4	$Cs_{2.5}SiW$	50	90	45[e]	[45]
70	5+ VLE	3	6	2.5	H1170/LM50	14	13	n/a	[51]
70	5+ VLE	3	6	2.5	H850/LM50	14	7	n/a	[51]
70	5+ VLE	3	6	2.5	H730/LM50	16	21	n/a	[51]
70	5+ VLE	3	6	2.5	H730/MS3030	49	38	n/a	[51]
70	5+ VLE	3	6	2.5	H730/ES70Y	41	34	n/a	[51]
70	5+ VLE	7.5	6	4	H730/ES70Y	100	97	4[d]	[51]
70	5+ VLE	7.5	17	3	H730/ES70Y, 1st cycle	98	86	2[d]	[51]
70	5+ VLE	7.5	17	3	H730/ES70Y, 2nd cycle	99	88	2.3[d]	[51]
70	5+ VLE	7.5	17	3	H730/ES70Y, 3rd cycle	99	86	1.5[d]	[51]
80	auto	5	5	3	$HSiW.20H_20$, without emulsifier	94	59	68[e]	[53]
80	auto	5	5	3	$HSiW.20H_20$, in 0.7 wt% C_{19}	99	90	45[e]	[53]
80	auto	5	5	3	$HSiW.20H_20$, in 0.1 wt% Dinoram S	92	85	44[e]	[53]
80	auto	5	5	3	$HSiW.20H_20$, in 0.7 wt% C_{12}-C_{14}	98	82	47[e]	[53]
75	10 + VLE	0.5 g	24	4	SC-AG(1.4)	96	44	<1[d]	[57]
75	10 + VLE	0.5 g	4	4	SC-AG(1.4)	71	18	<1[d]	[57]
75	10 + VLE	0.5 g	24	4	SMw-AG(1.4)	99	75	<1[d]	[57]
75	10 + VLE	0.5 g	4	4	SMw-AG(1.4)	79	28	<1[d]	[57]

75	10 + VLE	0.5 g	24	4	SMw-AG(0.7)	72	22	<1[d]	[57]
75	10 + VLE	0.5 g	24	4	SMw-AG(2.8)	87	59	<1[d]	[57]
75	10 + VLE	0.5 g	24	4	SC-LG(1.4)	37	0	n/a	[57]
75	10 + VLE	0.5 g	24	4	SMw-LG(1.4)	57	13	n/a	[57]
70	10	4	7	3	Sulfonated graphene (SG)	99.6	86	0.1[d]	[61]
70	10	4	7	4	Sulfonated graphene (SG)	99.7	92	0.3[d]	[61]
70	10	4	7	5	Sulfonated graphene (SG)	99.8	96	0.5[d]	[61]
70	10	4	7	6	Sulfonated graphene (SG)	99.5	97	0.6[d]	[61]

[a]VLE: vapor liquid equilibrium after pressurizing the reactor; [b]PTA: phosphotungstic acid, $Cs_{2.5}SiW$: cesium salt of silicotungstic acid, $HSiW.20H_20$: silicotungstic acid hydrate, H1170-H850-H730: Hyflon Ion S4X perfluorosulfonic ionomers, LM50-MS3030-ES70Y: silica supports, C_{19}, Dinoram S and C_{12-14} are amphoteric, cationic and non-ionic emulsifiers, respectively, SC: Sulfonated by conventional heating, SMw: Sulfonated by microwave heating, AG: Aerogel, LG: Lyogel. Numbers in parenthesis indicate the amount (g) of CSPTMS used per 2 grams of AG or LG, TFA: triflic acid; [c]Selectivity for di- and tri-tertiary butyl ethers of glycerol based on glycerol; [d]wt% DIB in the product mixture; [e]mol% selectivity of isobutene to DIB.

Lee et al. [45] tested heteropolyacid catalysts; silicotungstic acid (HSiW) as the homogeneous one and cesium salt of the heteropolyacid silicotungstic acid ($Cs_{2.5}SiW$) as the heterogeneous one, in glycerol etherification with IB. $Cs_{2.5}SiW$ yielded in low glycerol conversion and high IB oligomerization, *i.e.* 50 mol% glycerol conversion and 37 mol% DIB selectivity, which was interpreted to result from deactivation of the catalyst by the formation of basic sites via Cs^+ cation integration, followed by the condensation of glycerol molecules. Moreover, as the nature of the Keggin anion of the heteropolyacid molecule tends to keep protonated IB (carbenium cation) bound in alkoxy state, formation of oligomeric IB species by coupling with nearby IBs is highly favored.

Voicu et al. [53] tested the catalytic activity of silicotungstic acid hydrate, which is a solid heteropolyacid with the molecular formula of $H_4SiW_{12}O_{40}.30H_2O$, in glycerol etherification with IB, by using three different types of emulsifiers in the reaction medium, namely cationic emulsifier N-tallow propylene diamine (Dinoram S), non-ionic emulsifier ethoxylated alcohol (C_{12}-C_{14}) and amphoteric emulsifier ammonium quaternary salt (C_{19}), in addition to a non-emulsifier case as a reference. As used previously [43,50], emulsifiers are anticipated to increase both glycerol (polar phase) and IB (non-polar phase) concentrations at the catalyst surface with enlarging the surface area between these two phases by the formation of "IB droplets in glycerol" emulsion. This strategy indicated enhancements on desired ether selectivity and reduction in IB oligomer selectivity, with the best performance obtained in the case of C_{19}. This amphoteric emulsifier, when used as 0.8 wt% of glycerol, was observed to improve glycerol conversion, and DTBGE + TTBGE selectivity, as well as reducing IB oligomers.

Spherical silica supported Hyflon catalysts (SSHC), which consist of sulfonic acid ionomers supported on silica carrier, were elaborated by Frusteri et al. [51]. Out of three

different Hyflon Ion S4X perfluorosulfonic ionomers with varying sulfonic group concentrations, the one called H730 with highest acid capacity (1.23 meq H^+/g ion for pure ionomer) was integrated into three different silica supports, spherical silica MS3030, ES70Y, and fumed silica LM50, while the other two ionomers with lower acid capacity were integrated into only LM50, all with incipient wetness method. Using spherical silica supported H730 ionomers yielded in improved desired ether selectivity and diminished IB oligomerization. In addition, the TOF_{Gly} (mol of glycerol converted per acid site per time) values of spherical silica supported catalysts, which are 30-40 times that of Amberlyst 15™ ion exchange resin pointed out to their superiority, although Amberlyst 15™ had higher acid capacity (*i.e.* 4.5 meq H^+/g cat compared to ~0.2 meq H^+/g cat for ionomer supported catalyst). The superior activity of SSHC were connected to their higher surface area, lower surface acidity, better active site accessibility and electron repulsing fluorine atoms nearby the $-SO_3H$ groups (**Figure 2-8 e**). Successful catalytic performance was achieved with H730 ionomer on ES70Y type spherical silica, yielding in complete glycerol conversion and over 97 mol% selectivity to desired ethers of glycerol. Furthermore, this novel catalyst retained its activity during three cycles of 17 h-long runs. It is important to note that the performance of Amberlyst ion exchange resin under identical conditions was lower than that of H730/ES70Y even in the first catalytic cycle.

Gonzalez et al. [57] introduced sulfonated silica aerogel and lyogel for two novel glycerol etherification catalysts. Gels were synthesized with sol-gel method based on hydrolysis and condensation of tetrametoxysilane (TMOS), dried by lyophilization or supercritical methods to produce lyogel (LG, with 10 nm pore size) and aerogel (AG, with 65 nm pore size), respectively, and finally sulfonated post-synthetically under conventional or microwave heating in 2-(4-chlorosulfonylphenyl) ethyltrimethoxysilane (CSPTMS) solution. Sulfonic acid incorporation was highly effective under microwave heating, especially for AG, because of its larger pores. Because of the higher amount of sulfonic acid groups and corresponding Brønsted

acidity, as well as the retainage of larger pores, although surface area dropped, sulfonated AG demonstrated superior performance over sulfonated LG, with the best catalytic performance achieved with microwave sulfonated AG following as 99% glycerol conversion and 75% selectivity to desired ethers in mol basis, which was comparable to the reference catalyst Amberlyst 15™, moreover TOF_{Gly} for AG was more than 10 times that of Amberlyst 15™. In addition, sulfonated AG demonstrated no DIB production and thus it was resistant to catalyst deactivation in consecutive runs. Lastly, increasing the sulfonic acid incorporation to AG by applying higher CSPTMS concentration was found to reduce both glycerol conversion and selectivity to higher ethers, which was interpreted to source from pore blocking and thus hindered accessibility to active sites.

As another novel catalysts, sulfonated graphene was employed by Zhou et al. [61] and it was compared with other sulfonated catalysts such as peanut shell, aerogel, zeolite H-Beta, zeolite H-ZSM-5 and Hyflon supported on spherical silica. The reduced graphene oxide (RGO) was produced from graphite, and then treated RGO with ethanol, hypophosporus acid and 4-benzenediazoniumsulfonate (**Figure 2-8 f**) to obtain sulfonated graphene (SG) with benzenesulfonic acid functional groups. Employing SG as a heterogeneous catalyst for glycerol etherification with IB under varying IB:G feed conditions from 3:1 to 6:1 mol/mol, almost complete glycerol conversion and 86-97 mol% desired ether selectivity were achieved, with very low DIB production < 0.1 wt% in the final product mixture. This high catalytic activity for the desired reaction was connected to the amphiphilicity of SG with hydrophobic graphene parts and hydrophilic benzenesulfonic acid groups that would keep both polar glycerol and non-polar IB phases on its surface therefore these reactants could interact easily. Additionally, the open structure consisting of graphene layers, instead of a porous structure allows the products to leave the active sites in a shorter time, preventing IB oligomerization and catalyst deactivation resulting from the blockage by oligomers.

2.2.4. Compatibility of glycerol ethers with fuel blends

In order to test the applicability of glycerol ethers in biodiesel blends, Noureddini et al. [37] assessed the physical properties of biodiesel fuel blended with 20 wt% glycerol ether mixture, having 4.8 wt% MTBGE, 12.4 wt% DTBGE and 2.8 wt% TTBGE in the final blend, decreasing cloud point (from 0 to -5 °C), pour point (from -3 to -6 °C) and viscosity (*i.e.* from 4.3 to 4.0 mm^2/s at 40 °C) when compared to non-blended pure methyl esters. These results are consistent with the ones claimed in the invention [90], in which a blend of 12 wt% glycerol ethers (final blend including 3.5 wt% MTBGE, 5.6 wt% DTBGE and 1.8 wt% TTBGE) and 88 wt% biodiesel was claimed to reduce the kinematic viscosity from 5.9 to 5.4 mm^2/s, and the cloud point from 0 to -5°C.

Melero et al. [46] performed another study to investigate the properties of biodiesel formulation blended with some glycerol-derived oxygenated compounds. E100 biodiesel blended with 10 wt% of tertiary butyl glycerol products originating from glycerol etherification with IB over Ar-SBA-15 arenesulfonic acid functionalized mesoporous silica catalyst resulted in improved cold flow properties, such as reduced pour point (from -4 to -6 °C), cold filter plugging point (from 1 to 0 °C) and viscosity (from 4.12 to 4.05).

Moreover, Kiatkittipong et al. determined the fuel properties of FCC gasoline following the conversion of its C4-C5 fractions into glycerol ethers by glycerol etherification. The etherified FCC gasoline indicated higher research octane number (RON) and lower Reid vapor pressure (RVP) properties, 90.1 RON and 4.5 psia blending Reid vapor pressure (bRvp) in comparison with the non-etherified one with 88 RON and 6.5 psia bRvp. Therefore the group concluded the favorability of etherifying the FCC gasoline with glycerol for fuel extending.

Beatrice et al. [76,160] studied the engine performance of diesel blended 10 vol% with glycerol ethers consisting of 58 wt% TTBGE, 39 wt% DTBGE and 2 wt% MTBGE. They found out that the ignition delay of blended diesel was alike, while the soot and NO_x particulate emissions were lower than unblended diesel.

Sidhu et al. have recently tested pure glycerol as a fuel additive in diesel and biodiesel emulsions [161]. In the emulsification method, glycerol is stabilized in small droplets in diesel by the help of surfactants and take role as fuel oxygenates. 5 and 10 vol% emulsions of glycerol in biodiesel and diesel fuels decreased the emissions of NO_x and smoke, however hydrocarbon and carbon monoxide emissions were elevated, as well as the emulsion viscosity, density, and fuel consumption. Therefore investigation of the engine emissions of glycerol derivatives in diesel/biodiesel formulations are recommended in future studies.

2.3.Economic aspects and possible bottlenecks of the process

The growing biodiesel industry would provide crude and refined glycerol as an abundant, sustainable, non-toxic and inexpensive raw material for the value-added products from glycerol [82,92,162]. Utilization of biodiesel derived glycerol is expected to reduce biodiesel prices and to stabilize glycerol prices at low values [16,17,29,34,36,96,163-166]. Purification of crude glycerol is significant but costly by means of eliminating methanol, fatty acid and catalyst residues (*e.g.* NaOH) sourcing from biodiesel process [29,36,164,167], however the required extent of purification for etherification is not stated well. Current average prices of 95.5-99.5% purity refined glycerol and 80% purity crude glycerol follow as $800/ton and $300/ton, respectively [164,168], therefore the prices of purified glycerol would be between those values depending on the extent of purification, the size of the biodiesel production facility, as the

purification cost increases with decreasing facility size and the type of catalysts used in biodiesel production, as heterogeneous transesterification catalysts result in less impurities in the final crude glycerol [30,96,97,99]. The minimum cost for 98 wt% purification is approximated to be $0.15 per kg of crude glycerol [169].

Considering the widely used glycerol to IB molar ratio of 3, approximately 2 kg of IB reacts with 1 kg glycerol, therefore IB concentration in the petrochemical feed will be significant in determining the reactor size and final product concentration. The cost and lifetime of the heterogeneous catalyst with proper activity selected for large scale production are also influential in process design and economy. Neither laboratory scale continuous reactor study nor pilot scale batch or continuous reactor study exist for glycerol etherification with IB, so that not much is known about process scale-up and costs. Conceptual designs for cost estimation is also missing in the case of heterogeneous catalysts. Martin et al. [35] performed a conceptual design and optimization of an integrated process in which liquid biofuels, ethanol via fermentation, biodiesel via transesterification and glycerol ethers via etherification with pure IB over homogeneous catalyst, are produced from algae. The mathematical optimization assigning the value of $1/kg for liquid biofuel and $2.2/kg for IB pointed out that the price of IB should be reduced to half, otherwise over 60% of the biofuel production cost stems from the cost of IB. That result emphasizes the importance of exploiting available petrochemical IB sources instead of pure IB for the reduction of fuel additive production costs. New studies with plug flow reactors in which cheaper glycerol and IB feedstocks can help to designate the sizing and costs of a process with tunable capacity for the large scale realization of desired glycerol tertiary butyl ethers.

2.4.Outlook and Future Research

Table 2-9 presents the effect of catalyst modifications performed over Amberlysts, zeolites and mesoporous silica on the structural catalyst properties and the catalytic activity in glycerol etherification reaction with IB. **Table 2-10** shows the best performing catalysts selected from the above-mentioned heterogeneous catalyst groups with over 90 mol% glycerol conversion and desired ether selectivity. Although the catalytic activity of several type of catalyst on glycerol etherification with IB have been well presented, there are also several points to be investigated to realize the heterogeneous catalyst systems for future's sustainable large scale fuel additives production.

Detailed kinetic studies should be performed on heterogeneous catalysts to understand their catalytic activation and deactivation mechanisms. Reaction mechanisms and corresponding catalyst lifetimes are still unknown for the majority of catalysts mentioned above. Apart from batch reactor settings, flow reactors could be exploited to work under differential conversions so as to identify primary and secondary products under varying reaction conditions. Data to be collected on turnover frequency and catalyst recycling will also be valuable in comparing the performance of different type of catalysts. Moreover, detailed characterization of the catalysts under working conditions is required to reveal the structure-performance relationships at the atomic scale. Such measurements would also help to identify the active sites responsible for the production of individual products and to elucidate the structural changes occurring on these sites as they are acting for the reaction [170].

Table 2-9. Effect of modifications on the structure and performance of the heterogeneous catalysts, compared to the unmodified forms.

Catalyst group	Catalyst	Modification	Modification result	Glycerol conversion	Desired ether selectivity	DIB formation	Reference
Ion exchange resins	Amberlyst 15™	Partial neutralization with Ag^{+}, Mg^{+2}, Al^{+3}, Na^{+} cations	Decrease in the number of acid sites per g catalyst	Increased (slightly)	Increased	Decreased	[45,48]
Zeolites	Zeolite H-Y	Dealumination with citric/nitric acid treatment	Increase in surface area, pore volume, Si/Al ratio and strong/weak Brønsted acidity	Increased	Increased	n/a	[49]
Zeolites	Zeolite H-Beta, H-ZSM-5, Mordenite	Dealumination & sulfonation under conventional and microwave heating	Decrease in surface area, but increase in Si/Al ratio and Brønsted acid capacity	Increased	Increased	Increased	[52,55]
Zeolites	Zeolite H-Beta	Ion exchange with rare earth cations La^{+3}, Ce^{+3}, Nd^{+3} and Eu^{+3}	Decrease in surface area and pore volume, but increase in Si/Al ratio and strong Brønsted acidity	Increased	Increased	Increased (slightly, except Ce^{+3})	[56]
Zeolites	Zeolite H-Beta	Hierarchical porosity	Increase in surface area and Si/Al ratio, some micropores transform into mesopores, slight decrease in Brønsted acidity	Increased	Decreased	Increased	[58]
Zeolites	Zeolite H-Beta	Fluorination	Decrease in surface area and Brønsted acidity, but increase in Si/Al ratio and Brønsted acidity strength	Decreased (slightly)	Increased	n/a	[58]
Mesoporous silica	SBA-15	Sulfonation under conventional and microwave heating	Decrease in surface area and pore volume, but increase in Brønsted acid capacity	Increased	Increased	Decreased	[52]
Mesoporous silica	SBA-15, MCM-41	Post synthesis alumination	Decrease in surface area, pore size and pore volume, but increase in Brønsted acid capacity	Increased	Increased	n/a	[59]
Mesoporous silica	SBA-15, MCM-41	Phosphoric acid functionalization	Decrease in surface area and pore volume, but increase in Brønsted acid strength (less than sulfonic acid)	Increased	Increased	n/a	[59]
Mesoporous silica	HMS	Post synthesis sulfonation	Decrease in surface area, pore size (slightly) and pore volume, but increase in Brønsted acid capacity	Increased	Increased	n/a	[59]

Table 2-10. High performance catalysts as promising the candidates for future fuel oxygenate production from glycerol by using isobutene.

Type of catalyst	Glycerol conversion (mol%)	Desired ether selectivity[a] (mol%)	DIB formation[b] (wt%)	Pore size (nm)	Surface area (m^2/g)	Acid capacity (meq H^+/ g cat)	Reference
Amberlyst 15™, regular	100	92 (32)	7	30	53	4.7	[51]
Zeolite H-Beta, sulfonated	100	91 (36)	9	1 to 9	505	0.72	[52]
SBA-15, sulfonated	100	91 (39)	7	n/a	575	0.75	[52]
SBA-15, sulfonated	100	92 (34)	0	8	720	1.24	[42]
Peanut shell, carbonized and sulfonated	100	94 (40)	6	41.95	10.45	2.07	[47]
Hyflon, spherical silica supported	100	97 (51)	5	11.8	204	0.17	[51]
Graphene, sulfonated	~100	97 (59)	0.6	n/a	n/a	n/a	[61]

[a]Numbers in parenthesis are mol% selectivity to TTBGE; [b]wt% DIB in the product mixture.

Moreover, the promising catalysts shall be tested with refinery fractions of different C4 olefin concentrations and refined glycerol derived from biodiesel industry to study their catalytic performances in real feeds. The activity of these promising catalysts at different glycerol purities should be investigated in order to identify the extent of crude glycerol purification and the corresponding catalyst lifetime. Conceptual process designs can help to define the optimum feed concentrations and recognize the major costs associated with refined glycerol, fuel additives production process, and if necessary, purification of desired ethers DTBGE + TTBGE from the product mixture including also glycerol, MTBGE and DIB. For example promising results have been published on raw feeds of IB, such as petrochemical C4 fraction or FCC gasoline and with refined glycerol from biodiesel production. However, the low concentration of IB in the feed would definitely require larger reactors and increase the operating costs such as heating, but at the same time lower amounts of DIB formed would decrease the purification costs, therefore an optimum petrochemical feed composition for minimum cost could be figured out by well-established process designs.

Lastly, it is significant to note that the renewability of fuel additives production from glycerol and IB is dependent on the sustainability and availability of these raw materials. Futuristic process designs may consider bio-based glycerol and IB as the renewable raw materials. IB has been shown to be produced from sugars via fermentative route [171-175] or from ethanol via heterogeneous catalysis with $Zn_xZr_yO_z$ mixed oxides [176]. Therefore, future's renewable fuel additives production could be performed in an integrated biorefinery along with the bio-based fuels.

2.5.Conclusion

This review has elaborated the heterogeneous catalysts employed in glycerol etherification studies with isobutene, specifically focusing on prominent catalyst properties and reaction conditions which yield in highest glycerol conversion and selectivities to its desired di- and tri-tertiary butyl ethers, which would be utilized as fuel additives. Macroreticular acidic ion exchange resins (Amberlyst 15™ and 35™), zeolites (H-Beta and H-Y) and mesoporous silica (SBA-15 and MCM-41) also with their modification, as well as the novel catalysts with porous supports and Brønsted acid functional groups have been shown to be active catalysts yielding in complete glycerol conversion and over 90 mol% selectivity to desired ethers. Modifications, in general, seem to enhance glycerol conversion and selectivity to desired ethers, especially for zeolites and mesoporous silica because of the increase in Brønsted acidity. For novel-type catalysts, the existence of mesopores or macropores that allow easier transport of reactants-products, large surface areas and Brønsted acid functional groups in general are the key points of high catalytic activity. Further research for benefiting from heterogeneous acid catalyst for sustainable fuel additives production from glycerol should focus on the studies about reaction mechanisms and kinetics to understand the conditions for high catalytic activity and the usability of biodiesel derived glycerol together with petrochemical C4 fractions as raw materials for large scale applications.

Chapter 3

Screening of Solid Acid Catalysts for Etherification of Glycerol with Isobutene under Identical Conditions

3.1.Introduction

Methyl *tert*-butyl ether (MTBE) is the globally used gasoline additive. However, it is considered as a contaminant for the ground water resources because of the leaks from the underground petroleum storage tanks [177,178]. Therefore, the usage of MTBE has been banned or limited in many states in the US [179]. Hence, there is an ongoing research for finding green alternatives.

Biodiesel industry is associated with glycerol surplus which needs to be valorized in alternative pathways. One of these routes is the production of glycerol-based fuel additives, via etherification of glycerol [71,180] to produce glycerol tertiary butyl ethers (GTBE) that can potentially replace MTBE [34,36]. This industrially promising reaction has been studied for almost 20 years. The performance of different heterogeneous catalysts including ion exchange resins [38-41,54,181,182], zeolites [10,39,41,49,52,54,56,58,183], mesoporous silica [42,50,52,59,60], and supported heteropolyacids [15,38,184] have so far been reported for glycerol etherification with isobutene to produce GTBE [15].

When glycerol and excess isobutene are in contact on a Brønsted acid site, glycerol etherification, isobutene oligomerization, and isobutene hydrolysis reactions occur simultaneously (**Scheme 3-1**). Glycerol etherification proceeds in three steps with one, two, and three levels of butylation of glycerol with isobutene (IB), forming mono-*tert*-butyl glycerol (MTBGE), di-*tert*-butyl glycerol (DTBGE), and tri-*tert*-butyl glycerol (TTBGE), respectively [39]. The reaction medium is initially a two-phase mixture at low glycerol conversions. These two phases dissolve in each other with decreasing glycerol concentration and increasing ether concentration as the reaction proceeds. The mono-*tert*-butyl ether formed at the beginning of the reaction acts as a good solvent enhancing the mass transfer between glycerol and isobutene phases. Merging of these two phases was observed at a glycerol conversion of 60-70% [40,104].

Oligomerization of IB takes place as a side reaction, forming mainly di-isobutene (DIB). Less number of remaining hydroxyl groups in DTBGE and TTBGE products, namely the desired ethers, provides them a less polar character, thus they can be dissolved in non-polar hydrocarbon fuels and utilized as fuel additives [34].

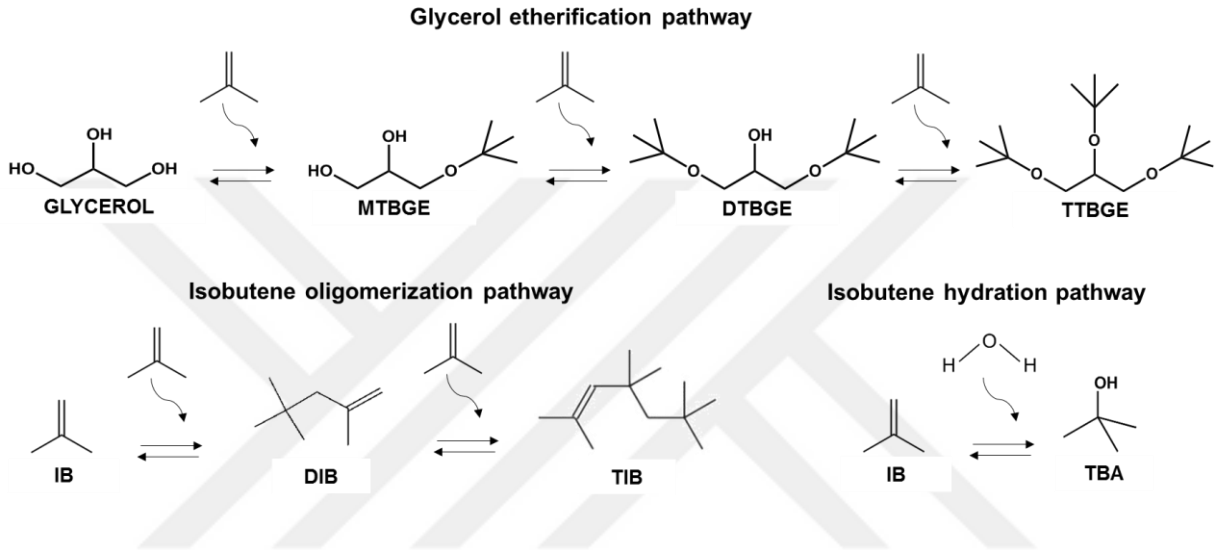

Scheme 3-1. Reaction of glycerol and isobutene over Brønsted acid catalysts.

Selectivity to the desired products depends on the catalyst structure at fixed reaction conditions. The highest yield for di- and tri-ethers were achieved in macroreticular type ion exchange resins (*e.g.* Amberlyst 15^{TM} and 35^{TM}) with large pore diameter, while no TTBGE was produced over zeolite Beta because of the steric hindrance [39]. Initial etherification rate over ion exchange resins and zeolite type catalysts increased with the catalyst acidity [41]. Accessibility of the reactants to the active sites is controlled by internal diffusion [54]. Moreover, acid site density is another factor controlling the selectivity. For instance, in a study focusing on comparing the performance of resin catalysts with zeolites, it was inferred that differences in product selectivities over Amberlyst 35^{TM} and zeolite Beta was because of the

much lower concentration of acid sites in zeolite Beta. This difference led to a higher DTBGE selectivity, but because of the presence of Lewis acidity in zeolite Beta, DIB selectivity was also high [54].

There are also several studies examining the effect of modifications on a certain type of catalyst. When Amberlyst 15^{TM} protonic sites were partially exchanged with different cations, isobutene affinity of the catalyst was altered at different degrees. Moreover, changing the extent of cation exchange influenced the product selectivity as well [15]. Selectivity to the desired ethers (DTBGE and TTBGE) increased with the modifications on zeolites, such as acid wash [49], sulfonic acid functionalization [52], hierarchical synthesis and/or fluorination [58], and rare earth cation exchange [56] because of the strengthened Brønsted acidity, improved textural properties (increased surface area, pore size, pore volume, and additional mesoporosity), and higher accessibility of the Brønsted acid sites. Similarly, the presence of functional groups with higher acid strength were revealed to enhance the selectivity towards desired ethers in the functionalized mesoporous silica samples [42].

However, other than the catalyst structure, the reaction conditions, such as temperature, IB:G mole ratio, catalyst loading, and reaction time, can also induce an influence on the higher ether selectivities. For instance, a higher temperature is associated with more di-isobutene production [39] as isobutene dimerization rate is more temperature sensitive [41]. Moreover, the selectivity of isobutene to form glycerol ethers is optimum at an IB:G mole ratio of 3:1 and at 80 °C, while exceeding this stoichiometric ratio results in excessive DIB production [40]. Furthermore, a longer reaction time was also shown to increase the DIB and TTBGE selectivity [42,52]. Hence, the selectivity to di- and tri- ethers as the desired products depends not only on the type of catalysts but also on the reaction conditions. However, because the studies reported previously for glycerol etherification using catalysts from different families were performed mostly under incomparable conditions, drawing a definitive structure-performance relationship

is not possible. Thus, there is a strong need for comparing the catalytic performance of different types of catalysts under identical conditions. Hereby, we present the results of our comprehensive catalyst screening study considering more than 70 different solid acid catalysts including ion exchange resins, zeolites, and heteropolyacids, and their counterparts modified by simple treatments. Some of these catalysts were used in the literature under various, and most of the time incomparable, conditions. However, more than half of the catalysts considered here are reported for the first time in the literature for the etherification of glycerol with isobutene. The results presented here offer a guideline for the rational design of solid acid catalysts for producing green alternatives to MTBE from glycerol.

3.2.Material and Methods

3.2.1. Catalyst preparation

3.2.1.1. Cation exchange resins

Amberlyst 15^{TM}, Amberlyst 35^{TM} (dry), and Amberlyst 36^{TM} (Dow Chemical Co.), were used as-received. The water content for these as-received resin catalysts were less than 3 wt% (as noted by the vendor). Additionally, Amberlyst 15^{TM} was subjected to cation exchange treatment to partially exchange the protons on the [$–SO_3^-H^+$] groups with different cations. Aqueous cation exchange solutions of 0.2-1.0 M were prepared using metal nitrates or chlorides: $NaNO_3$ (Aldrich, 99.995%), NaCl (Merck, 99.5%), $LiNO_3$ (Aldrich, 99.99%), KNO_3 (Aldrich, 99.999%), $Ca(NO_3)_2.xH_2O$ (Aldrich, 99.997%), $Ni(NO_3)_3.6H_2O$ (Aldrich, 99.999%), $CsNO_3$ (Aldrich, 99.999%), $La(NO_3)_3$ (Aldrich, 99.99%) and $Ce(NO_3)_3.6H_2O$ (Aldrich, 99.999%). Approximately 2.5 g of as-received Amberlyst 15^{TM} (dry) beads was treated in 15 ml metal solution for 12 h at 50 or 310 rpm at room temperature. After treatment, the excess solution over the intact ~0.5 mm beads of averagely half mm size was removed using a Pasteur pipette, the beads were washed two times with 15 ml deionized water in each wash cycle, water was

removed again by a Pasteur pipette, and finally the beads were dried under vacuum at 70 °C for 12 h. Water content after the cation exchange modification determined by TGA was 7.3±2 wt%.

3.2.1.2. Zeolites

Zeolite H-Y (CBV780, Si/Al=40 and CBV400, Si/Al=2.55), H-Beta (CP811C-300 , Si/Al=150 and CP814E, Si/Al=12.5), NH_4^+-Mordenite (CBV21A, Si/Al=10), and NH_4^+-ZSM-5 (CBV2314, Si/Al=12.5 and CBV8014, Si/Al=40) (Zeolyst International) were used after calcination in static air at 500 °C for 5 h. Additionally, zeolite Y (CBV780) and Beta (CP811C-300) were subjected to different modifications including steam treatment, acid treatment, and metal exchange. These zeolites were calcined at 500 °C for 5 h in static air before and after the modifications.

Steam treatment: A system similar to that proposed by Agudelo et al. [185] was used to treat the zeolites in steam flow. Two grams of calcined zeolite was placed into a quartz reactor and supported on quartz wool. The reactor was heated up to 500 °C at a heating rate of 5 °C/min. A 100 ml three-neck flask filled with 75 ml distilled water was heated by a round bottom heater to 120 °C. The first neck was closed with a lid, the second neck was attached to N_2 gas inlet (20 ml/min) and the third neck was connected to the top inlet of the reactor using a 1/8-inch stainless steel line, wherein the line was heated to 100 °C with an external heating wire to prevent water condensation. The steam flowed through the catalyst for 1 h or 3 h at 500 °C using 20 ml/min N_2 as the carrier gas.

Acid treatment: Aqueous HCl and citric acid solutions were prepared using hydrochloric acid (Merck, 37 vol%) and citric acid monohydrate (Merck, > 99.5 vol%). Zeolites were treated with 0.25 M HCl solution (20 ml solution/g zeolite) at 60 °C under 500 rpm for 3 h or with 1.0 M citric acid solution (20 ml solution/g zeolite) at 80 °C under 500 rpm for 3 h. The mixture was centrifuged at 5000 rpm for 5 min. The pellet was washed with distilled water until the pH

became neutral, centrifuged again at 5000 rpm for 5 min, and then dried under vacuum at 110 °C for 12 h.

Metal exchange: Aqueous solutions of metal nitrates were prepared using $La(NO_3)_3.6H_2O$ (Aldrich, 99.999%) and $Ce(NO_3)_3.6H_2O$ (Aldrich, 99.999%). Zeolites were treated with 0.4 M lanthanum or cerium nitrate solutions (25 ml solution/g zeolite) at 90 °C under 500 rpm for 1 h. Centrifugation and drying were the same as in the case of the acid treatment.

3.2.1.3. Heteropolyacids

Tungstosilicic acid hydrate (TSA), tungstophosphoric acid hydrate (TPA), and molybdatophosphoric acid hydrate (MPA) were purchased from Merck and used after drying at 100°C for 12 h to remove any water content.

Preparation of cesium salt of heteropolyacids: 0.1 M aqueous heteropolyacid solutions were prepared for each of the three heteropolyacids. Cesium nitrate solution of 0.1 M was prepared from $CsNO_3$ (Aldrich, 99.999%). 15.6 ml of 0.1 M $CsNO_3$ solution was added dropwise in 6.2 ml 0.1 M heteropolyacid solution (to form 2 g of $Cs_{2.5}H_{0.5}PW_{12}O_{40}$). White precipitates were dried at 110 °C under vacuum for 12 h and then calcined at 300 °C for 3 h.

Wet impregnation on supports: SiO_2 (Sigma Aldrich), MCM-41 (ACS Material), and SBA-15 (ACS Material) were used as the silica-based supports. 0.5 g dried heteropolyacid was dissolved in 10 ml water and the solution was added dropwise on 0.5 g support to form 50 wt% heteropolyacid loading. The mixtures were stirred at room temperature under 100 rpm for 24 h. The white precipitates were dried at 110 °C under vacuum for 12 h and then calcined at 300 °C for 3 h.

3.2.2. Catalyst characterization

3.2.2.1. Acid-base titration

The catalyst sample (55±5 mg) was placed into 10 ml of 2.0 M sodium chloride (≥ 99.5 wt%, Merck) solution and stirred at 100 rpm for 24 h. Later, the liquid part was transferred into a beaker and titrated with 0.01 M sodium hydroxide (diluted from 1.0 M NaOH, Merck) solution using a syringe pump (Aladdin, World Precision Instruments) and monitoring the pH with a pH-meter (WTW Inolab, pH electrode WTW Sentix 41) under stirring. When the pH increased to neutral 7.0±0.1, titration was stopped and the volume of NaOH solution was recorded. Brønsted acid capacity per gram of catalyst in mmol H^+/g_{cat} unit was calculated using **Equation 3-1**.

$$\text{acid capacity} = \frac{molarity\ of\ NaOH\ solution\left(\frac{mmol}{mL}\right) x\ volume\ of\ NaOH\ solution\ used\ (ml)}{catalyst\ amount\ (g)} \quad \textbf{(Equation 3-1)}$$

3.2.2.2. X-ray fluorescence

Zeolites H-Y (CBV780) and H-Beta (CP811C-300) were analyzed for their Si/Al ratios by XRF. A Bruker S8 Tiger XRF spectrometer in standardless mode under helium atmosphere with an 18 mm mask was used. The samples were loaded into an XRF sample cup (Chemplex Industries Inc., Cat. No: 1430) with a thin-film support (Prolene film with 4µm thickness, Chemplex Industries, Inc., Cat. No: 426). The loose powder method was selected for the measurement together with "Best analysis" assuming oxide matrix. SpectraPlus Eval2 V2.2.454 software was used for data interpretation. Concentrations of SiO_2 and Al_2O_3 were calculated in wt% using KA1 lines for Si and Al, then converted into moles. Lanthanum amount in La^{+3}-exchanged H-Beta was calculated using La LA1 lines.

3.2.2.3. X-ray diffraction (XRD)

XRD measurements were performed using a Bruker D8 Discover X-Ray Diffraction system with a Cu Kα1 radiation source with the wavelength of 1.5418Å. A Vantec-1 detector with a 11 mm slit was used. The power rating of X-ray generator was 40 kV and 40mA. The 2θ range of the measurements was 10–90° with a step size of 0.01263°. 10 mg sample was fixed on a glass slide and attached on the sample holder. Phase identification was done using the ICDD PDF-4 2014 database.

3.2.2.4. Scanning electron microscopy (SEM)

SEM images were retrieved by using a Zeiss Ultra Plus field emission scanning electron microscope. Pristine and Na^+-exchanged Amberlyst 15™ samples were analyzed under ultra-high vacuum with 10 kV accelerating voltage and at 5.0 mm working distance. A secondary electron detector was used for imaging.

3.2.2.5. Ammonia temperature programmed desorption (NH_3-TPD)

Zeolite and heteropolyacid catalysts having a considerably high reaction performance were analyzed by NH_3-TPD measurements to compare the acid strength. A Micrometrics AutoChem II 2920 instrument with a TCD detector connected to an MKS Cirrus II mass spectrometer was used for these measurements. Approximately 100±5 mg catalyst was loaded into the sample holder of the instrument. The catalysts were first flushed with He for 1 h at 500 °C for zeolites and 250 °C for heteropolyacids, then treated with 10 vol% NH_3-He for 1 h at room temperature, flushed again in He flow at 110 °C to remove any physisorbed ammonia, and then, the TCD signals were recorded during a temperature ramp in He flow at a heating rate of 10 °C/min up to 800 °C for zeolites and at a heating rate of 3 °C/min up to 700°C for heteropolyacids. TCD signals obtained as a function of temperature (°C) were deconvoluted using Fityk (0.9.8) using Voigt function [186]. For zeolites, obtained peaks at low temperature region (< 400 °C) region

were assigned to weak Brønsted acid sites; while those at high temperature region (> 400 °C) were assigned to strong Brønsted and Lewis acid sites [187]. Amount of the acid sites were determined by the calibrated desorbed ammonia peak areas.

3.2.2.6. Brunauer-Emmett-Teller (BET) pore volume and surface area analysis

BET analyses were done by using a Micrometrics ASAP 2020 Physisorption Analyzer. Prior to each analysis, 100 mg of the catalyst sample was dried at 110 °C under vacuum for 1 h. Degassing was performed at 300 °C for 5 h using helium. Volumetric N_2 adsorption/desorption isotherms were measured between P/P_0 =0.01–0.95 at liquid nitrogen temperature. BET surface areas were calculated between P/P_0 =0.05−0.3 using liquid nitrogen (10 data points). Pore distribution was obtained by the Barrett, Joyner, and Halenda (BJH) method using Harkins and Jura *t*-curve.

3.2.3. Catalytic performance measurements

3.2.3.1. Batch reactor measurements

Catalytic performance tests were performed using a Parr Series 5000 Multiple Reactor System with six stainless steel autoclave reactors of 75 ml each. 6.0 g glycerol (≥ 99.5%, Sigma Aldrich) and 0.45 g catalyst, corresponding to a catalyst loading of 7.5 wt% of glycerol, were loaded into the reactor and the reactors were sealed. Then the reactors were pressurized in nitrogen to 8 bar from the gas inlet port, followed by the dosing of 18 ml (11 g) isobutene (99.9%, Messer) using a system enabling the transfer of a desired volume of liquid isobutene with the help of nitrogen. When the transfer of isobutene was finished, the reactor was heated to 75 °C. Initial gas pressure in the reactor at the beginning of the reaction at 75 °C was measured as 10.5±1 bar. The reaction was run at autogenous pressure (the gas pressure varied depending on the alterations in the liquid volume as the reaction proceeds). Stirring was performed at 1200 rpm using magnetic stirring bars. The reaction was carried out for 6 h on

each catalyst. The final pressure for each run was approximately 5 bar. At the end of each run, the reaction mixture was transferred into a glass tube and examined in terms of liquid volume compared with the initial liquid volume of glycerol to determine whether glycerol conversion was high or not. High glycerol conversion was associated with an increase in the liquid volume. To refresh the used catalyst, solid catalyst particles were first filtered and mixed with ethanol, the liquid portion was removed, and the solid part was washed twice with methanol and dried at 70 °C under vacuum overnight.

3.2.3.2. Product analysis

Liquid products (approximately 15 g for each run) having high glycerol conversions were separated from the catalyst by filtration using a syringe filter, and then the liquid part was homogenized by vortexing, prior to the gas chromatographic analysis. Liquid products with very low glycerol conversions associated with low liquid levels (less than 65 wt% glycerol conversion) were not analyzed. In a standard GC procedure, 510±1 mg homogenized product sample was added to 165.0±0.5 mg octanol (≥ 99.0 %, Merck) in a volumetric flask of 10 ml and diluted to 10 ml with ethanol (≥ 99.8%, Sigma Aldrich) for reaching a homogenous mixture. The liquid part was homogenized by vortexing prior to the GC analysis. In a standard GC analysis, 510±1 mg was taken from the homogenized product and added to 165.0±0.5 mg octanol (≥ 99.0%, Merck) in a volumetric flask and diluted to 10 ml with ethanol (≥ 99.8%, Sigma Aldrich). After vortexing, a part of the homogenized solution was moved into a 2 ml-GC-vial and placed in the autosampler. Composition analysis was done in a gas chromatograph-mass spectrometer system (Agilent 7890B GC equipped with a 5977A Series GC/MSD) equipped with an HP Innowax column (30 m x 0.25 mm x 0.25 µm). Octanol was used as the internal standard for quantification. Split mode was run for the injection (1 µl sample, split ratio of carrier gas:sample was 100:1). The oven temperature increased from 40 to 240 °C at a ramp rate of 10 °C/min. Peak assignments of all products were confirmed by GC-MS. Calibrations

for glycerol, mono-*tert*-butyl glycerol ((±)-3-*tert*-butoxy-1,2-propanediol, ≥97.0 vol%, Aldrich), and di-isobutene (2,4,4-trimethylpentene, ≥90.0 vol%, Merck) were done using commercially available compounds. Quantifications of di-*tert*-butyl glycerol, tri-*tert*-butyl glycerol, tri-isobutene, tetra-isobutene, and tertiary butyl alcohol were done by using a GC-FID response factor method [188]. The glycerol conversion was determined once the mole based amounts of glycerol, MTBGE, DTBGE, and TTBGE in the GC sample were calculated (see **Table A-1** and **A-2** in **Appendix A**).

3.3.Results and Discussion

3.3.1. Brønsted acid capacity

All prepared regular and modified catalysts were subjected to acid-base titration to determine the number of Brønsted acid sites (the acid capacity). Acid capacities of these catalysts are given in **Table 3-1**. Here, we note that the catalysts which do not provide a high glycerol conversion were not characterized in detail.

Table 3-1. Brønsted acid capacities of tested catalysts determined by acid-base titration

Catalyst	**Acid capacity (mmol H^+/g_{cat})**
Ion exchange resins	
Amberlyst 15™	4.50
Amberlyst 15™ 0.4 M Na^+-exchange (powder)	2.27
Amberlyst 15™ 0.6 M Na^+-exchange (powder)	1.75
Amberlyst 15™ 0.2 M Na^+-exchange (bead)	3.33
Amberlyst 15™ 0.4 M Na^+-exchange (bead)	2.22
Amberlyst 15™ 0.4 M Na^+-exchange (with NaCl*) (bead)	2.54
Amberlyst 15™ 0.6 M Na^+-exchange (bead)	1.76
Amberlyst 15™ 0.8 M Na^+-exchange (bead) †	1.59
Amberlyst 15™ 0.8 M Na^+-exchange (with NaCl*) (bead) †	1.74
Amberlyst 15™ 1.0 M Na^+-exchange (bead) †	1.31
Amberlyst 15™ 1.0 M Na^+-exchange (with NaCl*) (bead) †	1.47
Amberlyst 15™ 0.4 M Li^+-exchange (bead)	2.78
Amberlyst 15™ 0.4 M K^+-exchange (bead)	2.77
Amberlyst 15™ 0.4 M Cs^+-exchange (bead)	1.86
Amberlyst 15™ 0.4 M Ca^{+2}-exchange (bead) †	0.93
Amberlyst 15™ 0.4 M Ni^{+3}-exchange (bead) †	1.37
Amberlyst 15™ 0.4 M La^{+3}-exchange (bead) †	0.36
Amberlyst 15™ 0.4 M Ce^{+3}-exchange (bead) †	0.54
Amberlyst 35™	4.80

Amberlyst 36™	5.00
Amberlyst 36 0.1 M Na^+-exchange (bead)	4.60
Amberlyst 36 0.3 M Na^+-exchange (bead)	3.80
Zeolites	
Zeolite Y (CBV 780) (SiO_2/Al_2O_3=80)	0.13
Zeolite Y (CBV 780) 1 h steam	0.13
Zeolite Y (CBV 780) 3 h steam	0.14
Zeolite Y (CBV 780) 3 h steam + HCl	0.12
Zeolite Y (CBV 780) HCl	0.14
Zeolite Y (CBV 780) Citric acid	0.26
Zeolite Y (CBV 780) 0.4 M La^+-exchange	0.04
Zeolite Y (CBV 780) 0.4 M Ce^+-exchange	0.10
Zeolite Y (CBV 400) (SiO_2/Al_2O_3=5.1)	0.25
Zeolite Beta (CP811C-300) (SiO_2/Al_2O_3=300)	0.22
Zeolite Beta (CP811C-300) 1 h steam	0.21
Zeolite Beta (CP811C-300) 3 h steam	0.15
Zeolite Beta (CP811C-300) 3 h steam + HCl	0.15
Zeolite Beta (CP811C-300) HCl	0.13
Zeolite Beta (CP811C-300) Citric acid	0.18
Zeolite Beta (CP811C-300) 0.4 M La^+-exchange	0.13
Zeolite Beta (CP811C-300) 0.4 M Ce^+-exchange	0.23
Zeolite Beta (CP814E) (SiO_2/Al_2O_3=25)	0.82
CBV21A Zeolit Mordenite (SiO_2/Al_2O_3=20) †	2.44
CBV2314 Zeolit ZSM-5 (SiO_2/Al_2O_3=23) †	0.58
CBV8014 Zeolit ZSM-5 (SiO_2/Al_2O_3=80) †	0.40
Heteropolyacids	
TSA	1.95
CsTSA	0.43
TPA	4.04
CsTPA	0.14
MPA†	12.90
CsMPA†	0.33
Supported Heteropolyacids	
TSA/SiO_2 (50:50)	0.53
TSA/MCM-41(5:95) †	0.05
TSA/MCM-41(50:50)	0.72
TSA/SBA-15(5:95) †	0.08
TSA/SBA-15 (50:50)	0.81
CsTSA/MCM41(50:50) †	0.32
CsTSA/SBA-15 (50:50)	0.35
TPA/SiO_2 (50:50)	1.96
TPA/MCM41(5:95) †	0.16
TPA/MCM41(50:50)	0.57
TPA/SBA-15 (5:95) †	0.29
TPA/SBA-15 (50:50)	0.75
CsTPA/MCM41(50:50) †	1.02
CsTPA/SBA-15 (50:50) †	0.35
MPA/SiO_2 (50:50) †	4.30
MPA/MCM41(50:50) †	4.26
MPA/SBA-15 (50:50) †	4.12
CsMPA/MCM41(50:50) †	0.20
CsMPA/SBA-15 (50:50) †	0.26
Supports	
SiO_2 †	0.03
SBA-15 †	0.08
MCM-41 †	0.09

†Gas chromatographic analysis of the products obtained using these catalysts were not performed. These catalysts yielded in low glycerol conversion (< 65 wt%) as observed from the visible glycerol phase after the reaction, and not elaborated further; *Sodium exchange was performed in aqueous NaCl, instead of $NaNO_3$.

According to **Table 3-1**, ion exchange resins are the heterogeneous catalysts with the highest acid capacity, except for the MPA catalysts. When the Amberlyst 15^{TM} was subjected to cation exchange under 310 rpm stirring, modified catalysts were obtained in powder form. Whereas, a stirring rate of 50 rpm conserved the original bead size. Acid capacities of powder and bead form of the resin catalysts were similar. Sodium modification was previously performed in literature [15,189], wherein 51% cation exchange in meq H^+ basis resulted in 2.4 meq H^+/g cat for Amberlyst 15^{TM}. Consistently, the exchange ratio of protons was in the range of 23-71 mol% when using 0.2-1.0 M of metal solutions and the corresponding acid capacity was between 3.5-1.3 mmol H^+/g_{cat} (**Table 3-1**). Metal cation exchange on Amberlyst 15^{TM} reduced the acid capacity by i) increasing the concentration of metal salt solution (from 0.2 M to 1.0 M), ii) increasing the atomic size of the metal cation (from Li^+ to Cs^+), and iii) increasing the metal's oxidation state (from Li^+ to La^{+3}). Acid capacities of pristine ion exchange resins followed as Amberlyst 15^{TM} < Amberlyst 35^{TM} < Amberlyst 36^{TM}, consistent with the values reported by the producer. Acid capacities of zeolites were much lower than that of ion exchange resins, with zeolite Beta (Si/Al=150) having a higher acid capacity than zeolite Y (Si/Al=40). Zeolite modifications didn't have significant or reasonable effects on acid capacity. For pristine zeolites, acid capacity increased with decreasing SiO_2/Al_2O_3 ratio, as expected. Heteropolyacids in bulk forms had high acid capacities in the following order; TSA < TPA < MPA. However, supporting them on mesoporous silica leads to an almost two-fold decrease in their acid capacity.

SEM images of the pristine and 0.4 M Na^+-exchanged Amberlyst 15^{TM} samples indicated that the resin morphology did not change significantly upon cation exchange modification (**Figure 3-1 a-f**). Acid capacities of the used ion exchange resins were similar to the fresh catalysts in the 10% error range, so we do not anticipate leaching of the [$–SO_3^-H^+$]

groups from the structure. However, size reduction because of cracking during mixing was observed in the used catalyst (**Figure 3-1 g-i).**

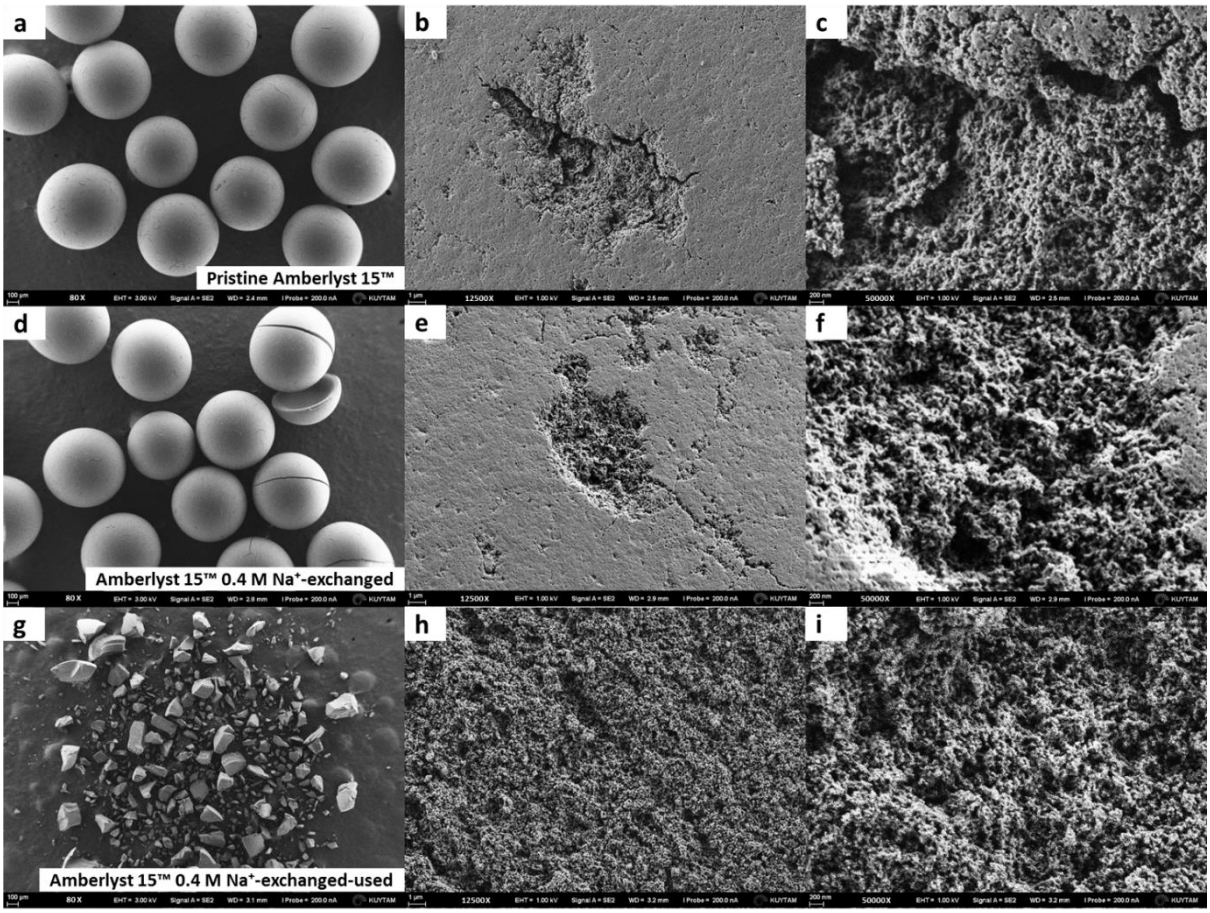

Figure 3-1. SEM images at 80X, 12500X and 50000X magnifications for **a to c:** pristine Amberlyst 15™; **d to f:** 0.4 M Na^+-exchanged Amberlyst 15™; **g to i:** 0.4 M Na^+-exchanged and used Amberlyst 15™ (reaction at 75 °C, 7.5 wt% of glycerol catalyst loading, IB:G=3:1 mol:mol, autogenic pressure, 1200 rpm, 6 h).

Acid capacities of zeolites were much lower than that of ion exchange resins, with H-Beta having higher acid capacity than H-Y. For pristine zeolites, acid capacity increased with decreasing Si/Al ratio, as expected (**Table 3-1**). Zeolite modifications did not indicate any

detectable effect on acid capacity determined by acid-base titration. Acid-base titration is manual thus more prone to errors especially for the low acid capacity zeolites. Moreover, it is an indirect method of counting the acid sites, as it counts the protons exchanged with sodium in the high molarity sodium chloride solution. Some protons might not leave the structure in the case of microporous materials. Thus, zeolite H-Y (CBV780) and H-Beta (CP811C-300) were further analyzed by NH_3-TPD for the number of desorbed ammonia molecules, related to the number of Brønsted acid sites, and by XRF to determine their Si/Al ratios.

The number of desorbed NH_3 molecules on pristine H-Y which was 0.185 mmol NH_3/g_{cat} dropped to 0.178 and 0.177 mmol NH_3/g cat upon 1 h and 3 h steaming, respectively. NH_3-TPD thus appears to be a better method for counting the number of Brønsted acid sites on zeolites. Besides, Si/Al ratios of steam treated zeolite H-Y, determined by XRF, were slightly higher than that of the pristine zeolite. For instance, Si/Al=50 of zeolite H-Y (CBV780) increased to 52 and to 58, upon 1 h and 3 h steam exposure, respectively, indicating slight dealumination. We also checked the crystal structure of H-Y by XRD before and after steaming. Crystallinity of the pristine and steam treated zeolite H-Y samples were almost identical (**Figure 3-2**), therefore the crystal structure was mostly preserved after the steam exposure.

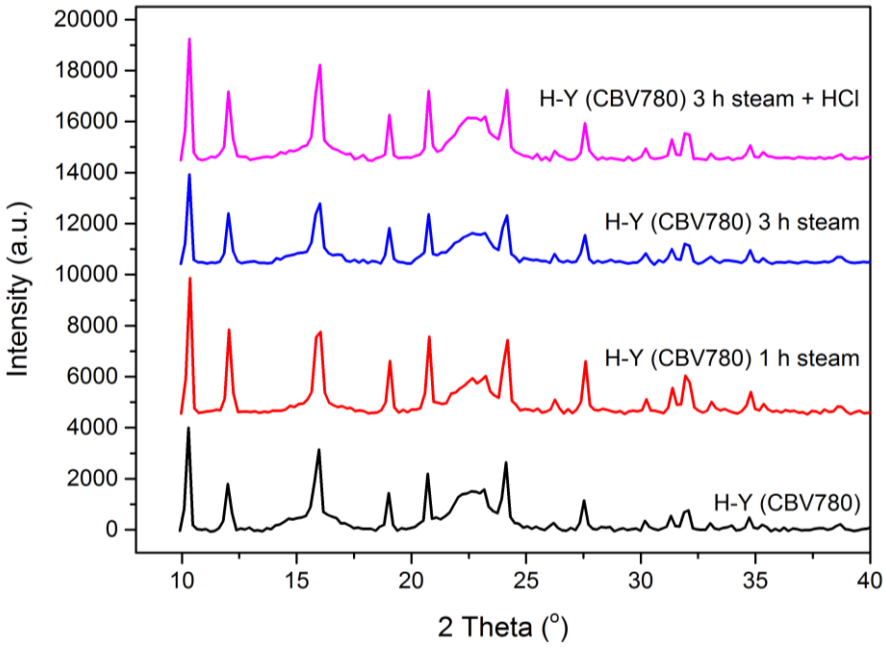

Figure 3-2 XRD patterns of zeolite H-Y (CBV780) before and after steam treatments.

Crystal structure of H-Beta, on the other hand, was altered following 1 h steam treatment (**Figure A-1**) (**Appendix A**). XRF analysis did not yield in any meaningful change in the Si/Al=121 of the pristine H-Beta, probably because it covered both framework and extra-framework aluminum species. Steam exposure creates extra framework aluminum species via framework dealumination, yet bulk Si/Al ratio may remain unchanged while NMR-determined framework Si/Al ratio increases [185]. However, the drop in the desorbed ammonia from 0.257 mmol NH_3/g_{cat} in the pristine zeolite to 0.215 mmol NH_3/g_{cat} in 1 h steamed zeolite upon steaming indirectly referred to the removal of some Brønsted acidity related Al_2O_3 species from the framework. In the case of 0.4 M La^{+3}-exchange, 0.404 mmol NH_3/g_{cat} implied the formation of new Brønsted acid site. This phenomena is thought to occur in the presence of water in the zeolite pores with $La(H_2O)_2^{+3} \rightleftharpoons La(OH)(H_2O)_2^{+2} + H^+ \leftrightarrow La(OH)_2 + 2H^+$ reaction [56]. Therefore 1 La is associated with the formation of 1.5 H^+s on average. XRF analysis suggested the La:Al ratio to be 0.35 mol:mol. Assuming that the framework Brønsted acid sites do not

change in number, we can convert the La:Al=0.35 mol:mol to the ratio of La and Al associated H^+s, giving 0.53 mol:mol. This number is similar to (0.404-0.257)/0.257=0.57 mol:mol, which explains the contribution of lanthanum in the formation of new Brønsted acid sites. Si/Al ratio upon La^{+3} and Ce^{+3}-exchange were similar to that of the pristine zeolite.

Figure 3-3 presents the NH_3-TPD signals of the zeolite and heteropolyacid samples associated with high catalytic performance, as will be explained in **Section 3.3.2**. Steam treatment improved the strength of the weak Brønsted acid sites of H-Y and H-Beta samples, recognized from the elevated peak temperatures between 168-355 °C (**Figure 3-3 a-b**). Framework dealumination was also deduced by our XRF analysis. The five or six coordinate extra framework Al species with Lewis acidity forms when four coordinate Al is removed from the framework. This Lewis acid sites might draw electrons from the O–H Brønsted acid sites, resulting in diminished O–H bond strength and associated stronger Brønsted acidity [190]. La^{+3}-exchange in H-Beta blue-shifted the high temperature NH_3 desorption peaks to more than 30 °C (**Figure 3-3 b**). The enlarged peaks prove the formation of new Brønsted acid sites upon lanthanum introduction. Zeolite treatments with lanthanum was claimed to improve the number, distribution, and strength of the Brønsted acid sites [56,191]. We consider La^{+3} cations as sources of Brønsted and Lewis acidity, wherein the Brønsted acid strength is enhanced by the existence of Lewis acidity.

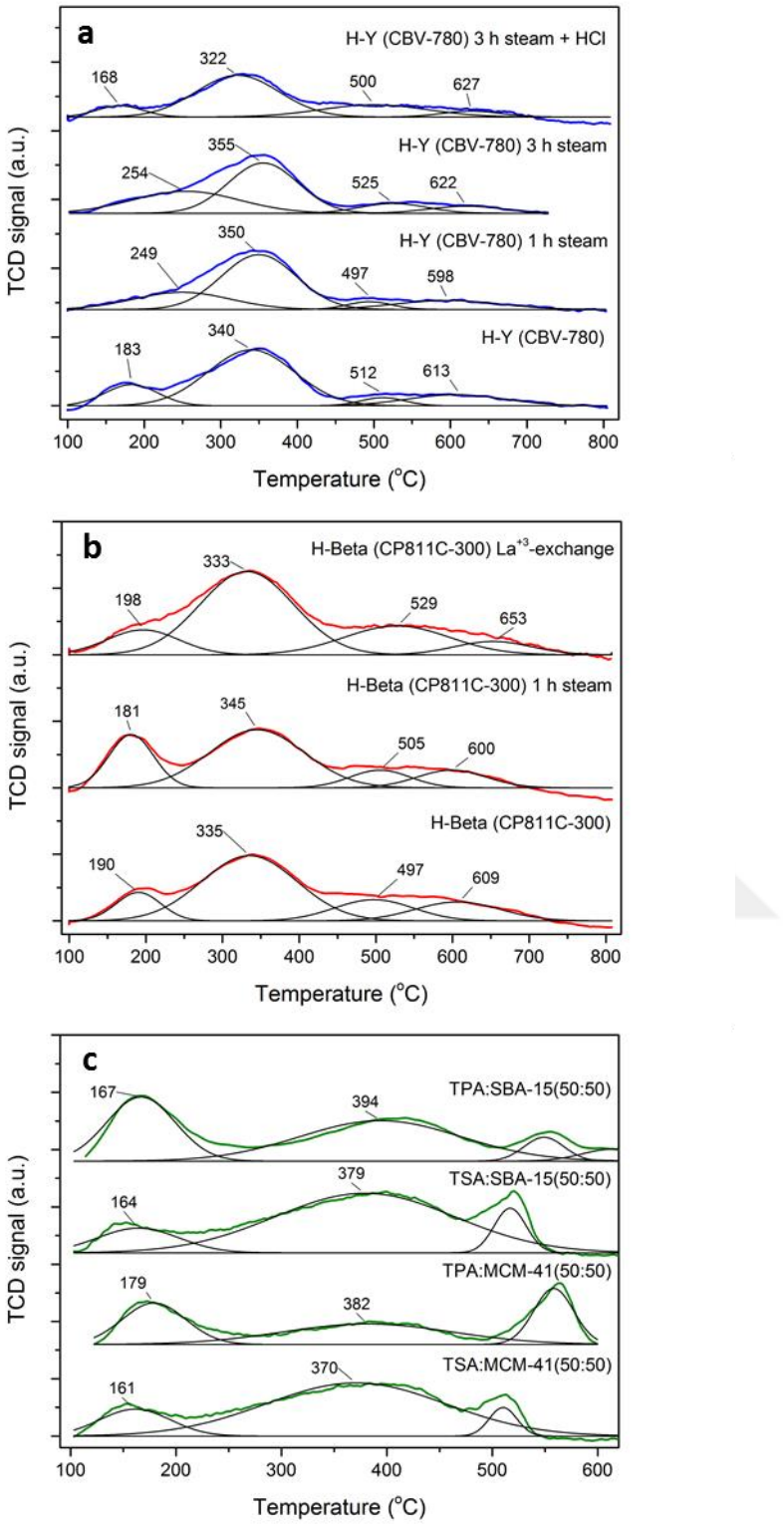

Figure 3-3. Ammonia desorption signals of the catalysts as a function of temperature; **a:** zeolite H-Y (CBV780, Si/Al=40); **b:** zeolite H-Beta (CP811C-300, Si/Al=150); **c:** Mesoporous silica supported heteropolyacids TSA and TPA.

Surface properties of zeolite samples determined by BET analysis are given in **Table 3-2**. Previously, H-Y was reported to have higher surface area than H-Beta (average of 700 m^2/g and 500 m^2/g, respectively) [15]. Consistently, the surface area and pore diameter of our H-Y samples were higher than H-Beta samples. BET analysis for untreated and 1 h steam treated H-Y samples indicated almost two-fold increase in average mesoporous pore diameter upon steam treatment (8 nm to 21 nm), while the surface area decreased. For H-Beta, no meaningful change in the mesoporous pore diameter upon steam exposure was observed. However, there could have been changes in the microporous region, which is not shown in our analysis. Synthesis of desilicated zeolite Beta could be suggested to achieve a higher mesopore volume and improved acid strength [192].

Table 3-2. Surface and acid properties of zeolites with high catalytic performance.

Catalyst	BET surface area (m^2/g)	Average pore diameter* (Å)
H-Y (CBV780)	728	79
H-Y (CBV780) 1 h steam	625	213
H-Beta (CP811C-300)	527	49
H-Beta (CP811C-300) 1 h steam	532	50
H-Beta (CP811C-300) 0.4 M La^+-exchange	516	50

* Average pore diameter for the mesoporous region.

Acid capacity of the bulk TSA was higher than TPA, however their 50 wt% impregnation on mesoporous silica supports yielded in similar acid capacities 0.5-0.8 mmol H^+/g cat, based on acid-base titration and NH_3-TPD data (**Table 3-1**). In a recent study, the total number of acid sites in 50 wt% TPA loaded on MCM-41 were determined as 0.54 mmol H^+/g cat experimentally, and 0.52 mmol H^+/g cat theoretically [193]. Therefore we assume that all HPA joined the porous structure. **Figure 3-3 c** presents the NH_3 desorption signals of TSA and TPA supported on mesoporous silica MCM-41 and SBA-15. We considered ammonia desorption in the low and medium temperature regions (first and second peaks < 400 °) for the

calculation of total number of acid sites, because the third peak was associated with TPA decomposition [193]. According to **Figure 3-3 c**, NH_3 desorbed at higher temperatures for TPA, compared to the TSA based catalysts, pointing out to higher acid strength of TPA. Indeed, the Brønsted acid strength of TPA is higher than TSA, with the corresponding DPE values of 1085 kJ/mol and 1105 kJ/mol, respectively [194-196]. The unmodified SiO_2, MCM-41 and SBA-15 supports were associated with significantly low acid capacities (< 0.1 mmol H^+/g cat) (**Table 3-1**). 50 wt% heteropolyacid loaded SiO_2 has support had comparable number of acid sites with the mesoporous silica supports. Increasing the heteropolyacid loading from 5 to 50 wt% increased the number of acid sites 5 to 10 fold. Cs salt of heteropolyacids had lower acid capacities compared to the bulk form. Impregnating the CsHPAs in mesoporous silica decreased the acid capacities further. Acid capacities of heteropolyacids dropped after the reaction to approximately half of the initial values, indicating the leaching from the support during the reaction under vigorous mixing of 1200 rpm. Therefore both heterogeneous and homogeneous forms of heteropolyacids might be acting in the reaction.

3.3.2. Comparison of the catalytic performance

All of the catalysts presented in **Table 3-1** were tested for glycerol etherification with isobutene in a batch reactor system under identical conditions: 75 °C temperature, 7.5 wt% of glycerol catalyst loading, an isobutene/glycerol ratio of 3 mol/mol, an initial pressure of 10.5 bar, 1200 rpm stirring rate, and 6 h reaction time. At the end of each performance measurement, the product mixture was analyzed visually; if a non-viscous ether phase of a high liquid level was observable, the sample was subjected to composition analysis. **Figure 3-4** demonstrates two different product mixtures obtained at the end of 6 h run period using two different catalysts. Product mixtures with high liquid level as shown in **Figure 3-4 a** were further subjected to GC/MS analysis. However, in the case of reactions with low glycerol conversion, similar to that in **Figure 3-4 b**, the final mixtures were viscous, liquid levels were low because of very low

conversion; and the catalyst was difficult to separate from the viscous phase. Such samples were not subjected to the gas chromatographic analysis. The products of the performance tests performed on 42 out of 71 of the catalysts considered were subjected to GC/MS analysis. Results (as presented in **Table 3-3**) indicated that these catalysts provided more than 65 wt% glycerol conversion.

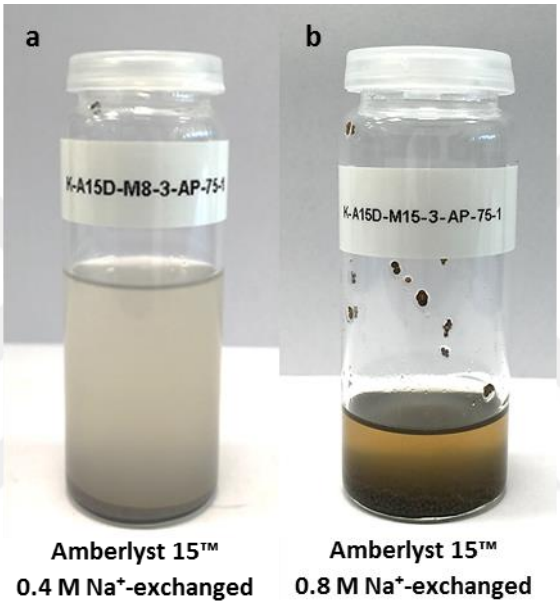

Figure 3-4. Appearance of reaction mixtures at the end of the batch run; **a:** high glycerol conversion by Amberlyst 15^{TM} 0.4 M Na^+-exchange (bead) catalyst; **b:** low glycerol conversion by Amberlyst 15^{TM} 0.8 M Na^+-exchange (bead) catalyst.

Table 3-3. Product selectivity of the catalysts with high glycerol conversion and high desired GTBE selectivity (75 °C, 7.5 wt% of glycerol catalyst loading, IB:G=3:1 mol:mol, autogenic pressure, 1200 rpm, 6 h).

Catalyst	Product selectivity[a] (wt%)				Glycerol conversion (wt%)	Desired ether selectivity[b] (mol%)
	MTBGE	DTBGE	TTBGE	DIB		
Ion exchange resins						
Amberlyst 15™	11.1	58.6	16.3	12.0	100	87.1
Amberlyst 15™ 0.4 M Na^+-exchange (powder)	6.7	63.0	23.1	2.0	100	89.7
Amberlyst 15™ 0.6 M Na^+-exchange (powder)	7.3	69.4	17.2	0.8	100	89.2
Amberlyst 15™ 0.2 M Na^+-exchange (bead)	8.7	59.4	23.5	6.6	100	90.5
Amberlyst 15™ 0.3 M Na^+-exchange (bead)	7.6	60.3	26.9	3.5	100	92.0
Amberlyst 15™ 0.4 M Na^+-exchange (bead)	9.3	64.7	21.9	2.1	100	90.3
Amberlyst 15™ 0.4 M Na^+-exchange (with NaCl) (bead)	7.2	63.5	23.0	1.4	100	89.1
Amberlyst 15™ 0.6 M Na^+-exchange (bead)	7.8	69.4	16.9	0.9	100	88.5
Amberlyst 15™ 0.4 M Li^+-exchange	10.7	56.2	24.0	2.5	100	93.5
Amberlyst 15™ 0.4 M K^+-exchange	19.8	64.6	7.1	0.6	100	72.0
Amberlyst 15™ 0.4 M Cs^+-exchange	34.6	57.4	1.7	0.4	91	55.2
Amberlyst 35™	9.2	57.9	16.9	8.9	100	84.8
Amberlyst 36™	12.8	58.9	13.6	9.2	100	85.0
Amberlyst 36™ 0.1 M Na^+-exchange (bead)	10.1	60.5	20.1	7.4	100	88.9
Amberlyst 36™ 0.3 M Na^+-exchange (bead)	9.0	67.3	19.9	2.4	100	90.6
Zeolites						
Zeolite Y (CBV 780) (SiO_2/Al_2O_3=80)	28.9	60.1	6.1	1.9	90	62.0
Zeolite Y (CBV 780) 1 h steam	9.1	62.2	22.3	2.8	100	86.4
Zeolite Y (CBV 780) 3 h steam	12.4	60.6	20.9	2.8	100	81.9
Zeolite Y (CBV 780) 3 h steam + HCl	22.5	57.8	12.8	2.3	100	68.7
Zeolite Y (CBV 780) HCl	20.4	61.2	12.2	2.4	92	71.5
Zeolite Y (CBV 780) 0.4 M La^+-exchange	26.2	67.0	1.6	1.6	90	65.4
Zeolite Y (CBV 780) 0.4 M Ce^+-exchange	26.0	65.7	3.3	1.8	92	65.6
Zeolite Beta (CP811C-300) (SiO_2/Al_2O_3=300)	11.3	73.8	0.8	7.7	100	82.7
Zeolite Beta (CP811C-300) 1 h steam	10.0	71.7	1.1	9.5	100	84.0
Zeolite Beta (CP811C-300) 3 h steam	11.1	72.0	0.8	8.9	100	82.6
Zeolite Beta (CP811C-300) 3 h steam + HCl	13.3	72.3	0.7	8.0	100	79.9
Zeolite Beta (CP811C-300) HCl	15.5	70.0	0.6	8.1	100	76.7
Zeolite Beta (CP811C-300) 0.4 M La^+-exchange	8.4	80.1	0.2	5.5	100	87.4
Zeolite Beta (CP811C-300) 0.4 M Ce^+-exchange	11.1	77.5	0.4	5.5	100	83.6
Zeolite Beta (CP814E) (SiO_2/Al_2O_3=25)	29.3	59.9	0.1	5.3	89	59.8
Heteropolyacids						
TSA	21.4	47.3	24.1	4.8	78	69.1
CsTSA	10.3	61.5	21.0	2.3	93	84.6
TPA	18.3	47.0	25.0	7.4	85	72.6
Supported Heteropolyacids						
TSA/SiO_2 (20:80)	16.6	52.5	22.7	4.0	87	75.5
TSA/SiO_2 (50:50)	12.0	51.6	24.6	8.9	90	81.1
TPA/SiO_2 (20:80)	40.4	39.0	1.9	7.5	83	42.1
TPA/SiO_2 (50:50)	16.6	51.5	21.5	5.4	86	74.9
TSA/MCM-41 (50:50)	15.3	48.7	13.5	14.2	90	73.8

TSA/SBA-15 (50:50)	23.9	45.2	19.3	9.3	76	64.7
CsTSA/SBA-15 (50:50)	73.4	21.6	0.4	0.6	78	17.9
TPA/MCM-41 (50:50)	11.2	49.1	21.1	6.4	91	82.3
TPA/SBA-15 (50:50)	28.3	54.3	9.0	5.1	67	61.2

[a]Products other than listed are TIB, TetraIB, and TBA, generally cover less than 10 wt% of total products. [b]Glycerol based selectivity towards desired ethers (DTBGE and TTBGE). Glycerol based selectivity is calculated as the moles of DTBGE and TTBGE formed per moles of glycerol reacted.

Previous literature studies using Amberlyst 15^{TM} in the bead form have yielded between 70-80 wt% desired ethers, representing the sum of the weight based DTBGE and TTBGE selectivity in the overall product mixture, and 10-15 wt% di-isobutene selectivity in the final product mixture at > 95% glycerol conversion under various reaction conditions, such as 60-90 °C, 5-7.5 wt% catalyst loading, IB:G=3:1-4:1, 4-50 h reaction time [39,42,181]. Our data indicated a selectivity of 75 and 12 wt% for desired ether and di-isobutene, respectively, consistent with the literature. Out of five separate batch reactor experiments with pristine Amberlyst 15^{TM}, the error associated with individual product selectivity were smaller than 3 wt%, while the error range in selectivity for the desired ethers was less than 2 wt%. Amberlyst 15^{TM} counterparts in the powder and bead forms had comparable performance. Desired ether selectivity (in mole basis) for ion exchange resins in our study are very similar to each other with slight variations: Amberlyst 15^{TM} ≥ Amberlyst 36^{TM} ~ Amberlyst 35^{TM} (87.1% ≥ 85.0% ~ 84.8%; noting that the difference between the selectivity on Amberlyst 15^{TM} and those on other Amberlyst catalysts is slightly higher than the error range of our measurements). Less isobutene dimers were formed over the latter two catalysts, which could be because of the higher acid strength favoring the etherification route instead of the oligomerization route. The sulfonic acid sites in Amberlyst 35^{TM} and 36^{TM} were previously shown by ammonia adsorption flow microcalorimetry to have higher acid strength than that of Amberlyst 15^{TM} [197,198].

Cation exchange treatments on the best performing ion exchange resin Amberlyst 15^{TM} with lithium nitrate, potassium nitrate, sodium nitrate, and cesium nitrate yielded in final reaction mixtures with no observable glycerol phase, thus the products obtained on these

catalysts were further analyzed by GC/MS. Results indicated a glycerol conversion of higher than 90%. According to **Table 3-3**, cation exchange treatments reduced the selectivity of isobutene dimers, which supports the previous literature studies on partial neutralization of Amberlyst 15^{TM} acid sites by cation exchange [15,189]. Selectivity of glycerol to its desired ethers improved with increasing the degree of sodium exchange up to 0.3 M Na^+ (92.0 wt% for Amberlyst 15^{TM}, 90.6 wt% for Amberlyst 36^{TM}). At Na^+ concentrations over 0.6 M, glycerol could not be converted after a reaction time of 6 h, possibly because of a very low acid capacity. For 0.4 M metal cation exchange, the smallest cation (Li^+) gave the best performance, 93.5 wt% desired ether selectivity. The largest cation (Cs^+) was associated with high selectivity to mono-ether, as well as low glycerol conversion, probably caused by steric hindrance. Double (Ca^{+2}) and triple (Ni^{+3}, La^{+3}, Ce^{+3}) charged cations led to low glycerol conversions (< 65 wt%) as their acid capacities are significantly lower, below 1.4 mmol H^+/g cat (**Table 3-1**). In order to compare the catalytic performance of pristine and Na^+-exchanged Amberlyst 15^{TM} samples at incomplete glycerol conversions, we performed batch reactor experiments for shorter durations between 0.5-5 hours. At glycerol conversions exceeding 75 mol%, the desired DTBGE + TTBGE selectivity of the 0.5 M Na^+-exchanged catalyst kept higher than the pristine catalyst (**Figure A-2**). In our recent study, we observed that when the H^+s of the Brønsted acid [$–SO_3^-H^+$] sites were partially exchanged with Na^+, the remaining Brønsted acid sites improved in strength [189]. Stronger interaction of the MTBGE reaction intermediate with the stronger acid [$–SO_3^-H^+$] sites is envisaged to produce higher molecular weight ethers, as long as isobutene is available in the reaction environment. This is enabled by a better mixing of glycerol and isobutene phases above 60 mol% glycerol conversion [40], triggering the formation of DTBGE and TTBGE at high acid strength. The pristine and treated resins had less than 7.5 wt% water content. In a study elaborating the drying behavior of polystyrene macroporous sulfonic acid resins, the final moisture content decreased to 13 wt% and 5 wt% with drying under airflow

for 1 h at 59 °C and 93 °C, respectively [191]. Although we performed the drying in a vacuum oven at 70 °C for 12 h, the final moisture content is within the expected limits. Considering the initial presence of 0.45 g catalyst with 10 wt% water (2.5 mmol) and 196 mmol (11 g) isobutene in the reactor, according to the IB + $H_2O \rightarrow$ TBA isobutene hydration reaction, only 2.5 mmol TBA would form, constituting approximately 1.3 wt% of the 15 g reaction mixture, which was observed with the metal treated resins.

Among the zeolites tested, zeolite H-Beta (Si/Al=150) yielded in comparable performance with pristine Amberlyst catalysts; however, TTBG production was very low in the former one. The desired ether selectivity of H-Beta (Si/Al=150) was 82.7 wt%, consistent with the literature value of 85 wt% [41]. The shape selectivity towards the di-ethers was also reported to be pronounced in the literature and has been linked to the steric hindrance [39]. The maximum diameter of a sphere that can diffuse along the H-Beta framework (BEA) is 5.95 Å, while this number is 7.35 Å for the FAU structure of H-Y [199]. Considering the molecular size of DTBGE as 9.4 Å, it possibly forms on the external surface of H-Beta, while it was forming on both the external surface and inside the pores of H-Y. H-Beta samples were associated with higher selectivity to isobutene oligomers. Similar behavior was observed for H-Beta in which higher DIB formation was linked to Lewis acidity, coke formation, and diffusion limitation through narrow pores [54,131]. The performance of zeolites treated with steam and/or HCl have not been previously elucidated for the glycerol etherification with isobutene. Our results show that hydrothermal steam treatment on H-Y (CBV780) considerably improved the desired ether selectivity from 66 wt% up to 85 wt%, reasoned by the increase in glycerol conversion (**Table 3-3**), improvement in acid strength (**Figure 3-3 a**) and the two-fold increase in average pore size (**Table 3-2**). HCl treatment on H-Y improved the desired GTBE selectivity to 75 wt%. The catalyst was not characterized in detail, but the reason might be dealumination and enlarged pore size upon acid wash [49]. Citric acid treated H-Y and H-Beta did not have

any detectable change in product selectivity, which might be because of the weak acid nature of the citric acid.

As presented above, we also performed BET surface analysis for zeolites to determine the surface area as well as the pore volumes and average pore diameters for > 1.7 nm region. BET surface areas of the wide pore zeolites in Y and Beta structures were reported many times in literature with Y having higher surface area than Beta (average of 700 m^2/g and 500 m^2/g, respectively) [15]. Consistently, the surface area, pore volume, and pore diameter of zeolite Y samples were higher than zeolite Beta samples (**Table 3-2**). The cage size of zeolite Y favors the formation of TTBGE, whereas the formation of this bulky ether is almost hindered (< 1 wt% in the product mixture) in the channels of zeolite Beta. Consequently, the zeolite Y (Si/Al=40) samples were associated with three times lower selectivity for isobutene oligomers and relatively high selectivity for TTBGE. Isobutene dimerization on zeolite Beta was more pronounced than that on zeolite Y. Similar behavior of zeolite Beta was observed in literature, possibly due to Lewis acidity, coke formation, and diffusion limitation through narrow pores [54,131].

The effect of hydrothermal steam and HCl acid treatment on zeolites have not been studied in the literature for the glycerol etherification with isobutene reaction. Our results exhibit that hydrothermal steam and HCl acid treatments on zeolite Y (CBV-780) considerably improved the desired ether selectivity in this reaction. Steam treated Zeolite Y had comparable desired ether selectivity (86.4 wt% for 1 h steam treatment) with commercial ion exchange resins (85-87 wt%). BET analysis for untreated and 1 h-steam-treated zeolite Y samples indicated almost two-fold increase in average mesoporous pore diameter upon steam treatment (8 nm to 21 nm), while surface area and pore volume decreased. Hydrothermal treatment did not have any significant effect on zeolite Beta (CP811C-300), no meaningful change in the average pore diameter of this zeolite upon steam exposure was observed (average 5 nm

mesoporous pore diameter in all cases). However, lanthanum and cerium cation exchange treatments on zeolite Beta had some effect in decreasing the di-isobutene selectivity and in enhancing the desired ether selectivity slightly from 83 to 87 wt%. To achieve a higher mesopore volume in zeolite Beta structure with improved acid strength, synthesis of its desilicated form could be suggested [192].

Besides the pore size, Si/Al ratio was also observed to have an influence on the product selectivity. For instance, the desired ether selectivity over zeolite Beta with Si/Al=11.5 was lower that than of its counterpart with Si/Al=150, even though the acid capacity of the former one was four-fold higher. Remembering that the Brønsted acid strength is a significant parameter improving the selectivity to desired ethers [52,59,189,200], the higher Si/Al zeolite with higher acid strength might be producing the desired di-ethers at a higher selectivity.

The solid Brønsted acid catalysts in zeolite and heteropolyacid groups with improved desired ether selectivity were further analyzed for their acid strength using temperature programmed desorption of ammonia (NH_3-TPD) up to high temperatures (600-700 °C). Here, it is noted that the ion exchange resin catalysts could not be analyzed by NH_3-TPD because of the low thermal stability of these resin catalysts (their thermal decomposition starts below 200 °C). NH_3 desorption signals for good performing zeolite and supported heteropolyacid catalysts together with the NH_3 desorption temperature peaks are given in **Figure 3-3**.

As can be seen from **Figure 3-3 a**, steam treatment improved the strength of the weak Brønsted acid sites of zeolite Y samples, recognized from the elevated peak temperatures of these sites. Considering **Table 3-3** and **Figure 3-3 a** together, it can be interpreted that the acid strength is a critical parameter in determining the final product selectivity, because desired ether selectivity was substantially improved from 62 to 86 wt% over steam-treated zeolite Y catalyst having a lower surface area and a higher acid strength, probably having mesoporous molecule

ways allowing the transportation of desired ethers. In literature, hydrothermal steam treatment was observed to dealuminate the zeolites and form extra framework aluminum species [185]. Hydrochloric acid treatment was also applied as a way of dealumination; and if done by following steam treatment, it is known to remove the extra framework aluminum species, forming meso-sized pores [185]. However, the Brønsted acid strength in the 3 h-steam-treated plus HCl-acid-treated zeolite Y did not improve, revealing the possible role of extra framework aluminum species in glycerol etherification reaction.

For zeolite Beta samples, steam treatment did not have any significant effect in terms of enhancing the Brønsted acid strength; however, La^{+}-exchange had an obvious effect (**Figure 3-3 b**). Zeolite treatments with lanthanum and cerium ions are known to improve the Brønsted acid strength of zeolites [56]. Shifting of the ammonia desorption peaks to higher temperatures upon La^{+}-exchange for zeolite Beta supports this statement. According to our catalytic performance results, both La^{+} and Ce^{+}-exchange resulted in lower selectivity to di-isobutene (from 7.7 to 5.5 wt% upon cation exchange). The better performance of untreated zeolite Beta compared to zeolite Y in terms of higher glycerol conversion and selectivity to the desired ethers might arise from the presence of i) the higher number of acid sites and ii) the larger proportion of strong Brønsted acid sites over weaker Brønsted acid sites, namely the proportion of the areas larger than 400 °C to the areas smaller than 400 °C in TPD profiles (**Figure 3-3 a-b**). Besides, increasing the average pore size of zeolite Y by treatment results in comparable performance with zeolite Beta. It can be interpreted that the number of acid sites, acid strength, and pore size appear as the three crucial parameters controlling the glycerol etherification reaction towards the desired products over heterogeneous catalysts [15].

Heteropolyacids were used for glycerol etherification in a very limited number of studies in bulk and supported forms [15,38,184]. The reaction conditions employed were significantly different from each other; for instance, they varied between 60-90 °C, 2-7.5 wt% catalyst

loading, 5-20 h reaction time, 2:1-4:1 of isobutene/glycerol in moles and with/without emulsifier. TSA in homogeneous form provoked 47 wt% desired ether selectivity, while using 20 wt% TSA supported on clay significantly reduced this selectivity to 25 wt% [38]. We evaluated different heteropolyacid based catalysts under identical conditions considering that the product selectivity strongly depended on the reaction conditions. In our work, the desired ether selectivity of bulk heteropolyacids followed as CsTSA > TPA > TSA (**Table 3-1**). Partial exchange with cesium has been shown to create higher surface area and lower acid density, forming a heterogeneous heteropolyacid catalyst that is more active than its bulk form [201,202], which supports the higher performance of CsTSA compared to the bulk TSA. However, impregnation of CsTSA on SBA-15 yielded in lower desired ether selectivity, probably because of low acid capacity and pore blockage. For instance, high amount of MTBGE production indicates steric hindrance in the reaction environment. Glycerol could not be converted considerably in the case of bulk and supported forms of MPA. Inadequate activity of MPA might be linked to its low acid strength [203]. Desired ether selectivity increased from 42 to 75 wt% with an increase in TPA loading from 20 to 50 wt% over SiO_2-support (**Table 3-3**). When mesoporous silica MCM-41 and SBA-15 were used as the support, TPA with two-fold number of acid sites and also stronger Brønsted acidity when compared to TSA (lower deprotonation energy of TPA [196]) resulted in halved di-isobutene selectivity and improved yield of desired ethers. The MCM-41 supported TPA with 50 wt% loading yielded in over 21 wt% TTBGE selectivity, outperforming the commercial cation exchange resin and zeolite catalysts. High molecular weight ether production is linked to the super acidity of heteropolyacids. Nevertheless, considering the glycerol conversion and TTBGE selectivity together, the highest TTBGE yield (27 wt%) is obtainable with ion exchange resins. TTBGE content has recently been demonstrated by us to be crucial in terms of fuel additive properties

and gasoline compatibility [204]. Thus catalysts with high TTBGE yield will be promising for industrial utilization.

3.4.Conclusion

We performed a comprehensive catalyst screening study to test a large number of solid acid catalysts (more than 70 different) with Brønsted acid functionality (about more than half of them being reported for the first time), covering ion exchange resins, zeolites, and heteropolyacids, as well as their modified forms under identical reaction conditions. The relationships between the acidity and product selectivity of these catalysts were investigated. Selectivity to glycerol ethers, especially to the higher molecular weight ethers increased, while isobutene dimerization was suppressed with decreasing acid capacity for ion exchange resins. Moreover, strengthening in Brønsted acidity upon zeolite Y steam treatment, zeolite Beta La^{+}-exchange or switching from TSA to TPA for mesoporous silica functionalization yielded in higher selectivity to desired ethers.

3.5.Supplementary Material

Details on gas chromatographic analysis, characterizations and catalytic performance results of the unfocused catalysts are given in **Appendix A**.

Chapter 4

Assessment of Acid Strength in Sodium-Exchanged Resin Catalysts: Consequences on Glycerol Etherification with Isobutene in Batch and Flow Reactors

This chapter has been published in Molecular Catalysis 466 (2019) 1-12, by authors Ö.D. Bozkurt, N. Bağlar, S. Çelebi and A. Uzun. The original manuscript has been rearranged and reformatted to conform the format requirements of the dissertation.

4.1. Introduction

Ion exchange resins are crosslinked polystyrene materials with sulfonic acid [–SO_3H] functionalization. The catalytic reactivity involves proton donation from [–SO_3H] groups to the reactant, succeeded by the back-donation of proton from the intermediate species to the [–SO_3]$^-$ group [118]. Thus, the Brønsted acidity results from this exchangeable protonic sites of [–SO_3H] groups attached to the negatively charged polymer matrix [205]. Macroporous and highly crosslinked structure of ion exchange resins with acidic character have been applied in many different green applications, including etherification of olefins with alcohols to ethers, dehydration of alcohols to olefins, hydration of olefins to alcohols, alkylation of phenols to alkyl phenols, condensation reactions, and ester hydrolysis [118,206,207].

Among these applications, production of methyl tert-butyl ether (MTBE) as a gasoline additive constitutes the main utilization area of acidic ion exchange resins as catalysts. However, soil and ground water contamination associated with MTBE has triggered the need for other fuel additive alternatives [206,207]. Production of glycerol tertiary butyl ethers (GTBE) is one of these alternatives. GTBE production benefits from glycerol, a biomass platform molecule with an increasingly high level of oversupply, and isobutene, a relative low-valued product of crude-oil refining. It is a promising technology to i) provide environmentally friendly fuel additives, ii) sustain biodiesel industry, iii) reduce dependency on petroleum sources, and iv) meet future renewable targets [34-36]. Over catalysts with Brønsted acid function, etherification of the hydroxyl groups in glycerol with isobutene yields in three types of ethers with different degrees of isobutene addition to the glycerol: mono-tert-butyl glycerol ether (MTBGE), di-tert-butyl glycerol ether (DTBGE), and tri-tert-butyl glycerol ether (TTBGE) (**Scheme 4-1**). Among these products, di- and tri-ethers are classified as the desired ethers for fuel blends, because of their better solubility and lower polarity [101,208]. Besides these ethers, isobutene can also undergo oligomerization reaction to form mainly di-isobutene

(DIB) and tri-isobutene (TIB) as a side product consuming isobutene under the etherification conditions and hydrolysis reaction by reacting with water in the reaction medium to form low amounts of tertiary butyl alcohol (TBA).

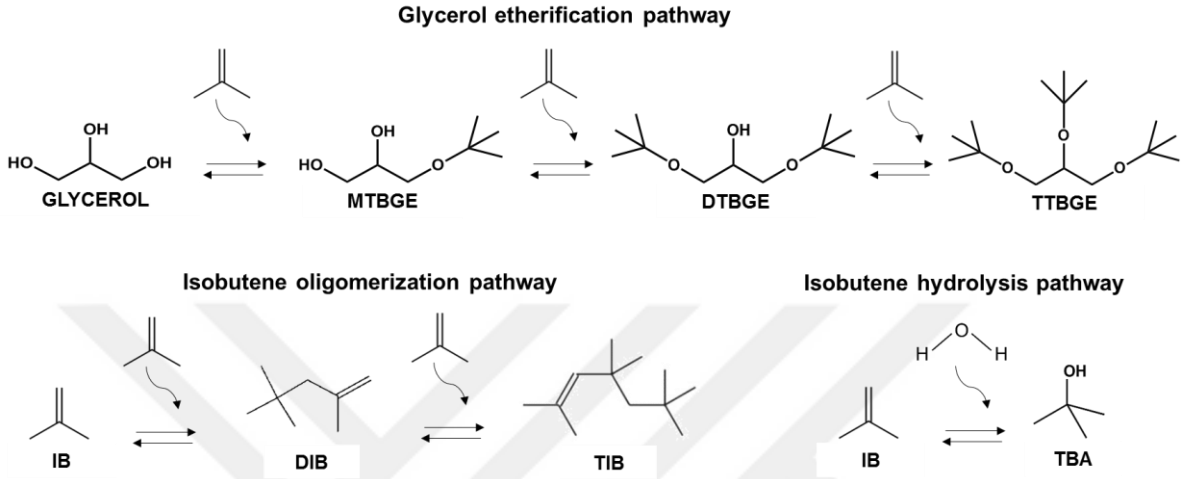

Scheme 4-1. Possible reactions taking place under glycerol etherification with isobutene conditions over a Brønsted acid catalyst.

Catalytic performance of several ion exchange resins has been reported for glycerol etherification with isobutene [38-41,54,181]. Comparing different types of ion exchange resins including Amberlyst 15^{TM}, glycerol conversion and desired ether yield have been found to depend on water content, pore-size, degree of crosslinking, and acid capacity [39,41]. In addition, partial exchange of protonic sites with cations, such as sodium, magnesium, aluminum, and silver found to have considerable effects on the performance of Amberlyst 15^{TM} [15,209]. The effect of cation exchange on the performance of ion exchange resins can be two-fold: First, and the obvious one, is a decrease in the number of acid sites because of the partial saturation of Brønsted sites by the cation exchange. And the second effect would be the modification of acid strength of the active sites. This latter effect is very challenging to assess. Because, the traditional approaches to measure the acid strength, such as temperature

programmed desorption (TPD) of a basic adsorbate (ammonia or pyridine), is not a suitable technique for ion exchange resins as these materials cannot withstand the elevated temperatures required for these measurements. Ammonia adsorption calorimetry was previously utilized to quantify the acid strength of ion exchange resins of different families, wherein acidic strength was defined as the average enthalpy of adsorption per mol of adsorbed ammonia, $\Delta H_{ads(NH_3)}$ [197,210-212]. However, the similarity of $\Delta H_{ads(NH_3)}$ values in the error range for cation exchange resins with different acid capacities obstructs the comparison in the case of slight structural changes.

Here, we first aimed at developing a spectroscopy-based methodology to assess the acid strength of Amberlyst 15^{TM} and its cation-exchanged counterparts. Then, we focused on elucidating the influence of acid strength on the catalytic performance on a test reaction, glycerol etherification with isobutene, an important green reaction to produce alternative fuel additives in batch reactors. Moreover, we also performed performance tests in once-through flow reactors, for the first time in literature, focusing on very low glycerol conversions to understand the consequences of the changes in acid strength on the fate of very first glycerol molecules interacting with the active sites. The results presented here offer a significant advance in the way of understanding the structure-performance relationships in these resin catalysts.

4.2. Material and Methods

4.2.1. Materials and synthesis

Amberlyst 15^{TM} (dry) ion exchange resin beads (Dow Chemical Co.) were used as catalyst in pristine and Na^+-exchanged form. Approximately 2.5 g of as-received Amberlyst 15^{TM} (dry) was treated in 15 ml aqueous sodium nitrate (≥ 99.5%, Merck) solutions of 0.1, 0.2, 0.3, 0.4, and 0.5 mol/L for 12 h under 50 rpm at room temperature for Na^+ exchange. After the treatment, the liquid portion was removed using a Pasteur pipette, the solid was washed twice with 15 ml

deionized water, and finally it was dried under vacuum at 70 °C for 12 h. Sodium nitrate (≥ 99.5%, Merck), sodium chloride (≥ 99.5%, Merck), and sodium hydroxide (1.0 M, Merck) were used for sodium exchange and titration. Glycerol (≥ 99.5%, DB Agricultural Energy) and isobutene (99.9%, Messer) were used as reactants in the test reaction. Ethanol (≥ 99.8%, Sigma Aldrich), 1-octanol (≥ 99.0%, Merck), (±)-3-tert-butoxy-1,2-propanediol (≥ 97.0%, Sigma Aldrich) and 2,4,4-trimethylpentene (≥ 90.0%, Merck) were used in gas chromatograph (GC) calibration and sample preparation. Heteropolyacids (HPAs), tungstosilicic acid (TSA) and tungstophosphoric acid (TPA), were purchased from Sigma Aldrich and used for preparing supported Brønsted acid catalysts. HPAs were first dried at 100 °C for 12 h to remove water. 0.5 g dried HPA was then dissolved in 10 ml water and the solution was added dropwise on 0.5 g SiO_2 and MCM-41 silica supports (Sigma Aldrich), which were already calcined at 550 °C in air. The mixture was stirred at room temperature under 100 rpm for 24 h. The white precipitate was dried at 110 °C under vacuum for 12 h and then calcined at 300 °C for 3 h.

4.2.2. Characterization

4.2.2.1. Acid-base titration

Acid capacities (number of acid sites) of pristine and Na^+-exchanged Amberlyst 15^{TM} samples were determined by acid-base titration. Approximately 55±5 mg of catalyst was treated in 10 ml of 2.0 M NaCl solution under 100 rpm for 24 h. After stirring, the liquid portion was transferred into a beaker under stirring and titrated with 0.01 M NaOH solution using a syringe pump (Aladdin, World Precision Instruments) and monitoring the pH with a pH-meter (WTW Inolab, pH electrode WTW Sentix 41) until the pH increased to neutral (pH=7.0±0.1), while the volume of NaOH solution added was recorded. Brønsted acid capacity per gram of catalyst in mmol H^+/g_{cat} was calculated using the volume and molarity of NaOH solution consumed and the corresponding catalyst amount.

4.2.2.2. Ammonia adsorption

Ammonia pulse chemisorption measurements on pristine and Na^+-exchanged Amberlyst 15^{TM} samples were performed to chemisorb NH_3 on [$–SO_3H$] Brønsted acid sites until reaching saturation. A Micrometrics AutoChem II 2920 instrument with a TCD detector was used for these measurements. Catalysts were crushed and sieved into 75-125 μm particle size fractions prior to measurements. Then they were dried in a vacuum oven for 1 h at 110 °C. 25±3 mg catalyst was then loaded into the quartz sample holder of the instrument. Sample was flushed with helium (50 ml/min) for 1 h at 110 °C and then cooled to 30 °C. Then the TCD recording was started, and the sample was pulsed with NH_3/He (10/90 vol%) mixture from a 5-ml loop with a total of 15 pulses by using helium as carrier gas at a rate of 75 ml/min. The TCD signal baseline stabilization was achieved between each pulse injections. The sample was then flushed with 75 ml/min helium at 110 °C to remove any physisorbed ammonia, until the TCD signal baseline was stabilized. The resulting treated catalyst was removed from the sample holder and spectroscopy measurements were performed. For Na^+-exchanged Amberlyst 15^{TM} samples MS signals were also collected with MKS Cirrus II mass spectrometer connected to the exhaust stream of AutoChem to detect mass output during adsorption and removal of physisorbed ammonia. For comparison, bulk heteropolyacids, TSA and TPA, were also considered for ammonia adsorption. For this purpose, the heteropolyacids in hydrate forms were first dried overnight at 100 °C to remove water. In a quartz reactor, 150 mg dried heteropolyacids were treated in flowing He (30 ml/min) at 100 °C for 1 h. The reactor was cooled to ambient conditions and the catalysts were treated with 50 ml/min 10 vol% NH3-He at room temperature, while the outlet gas was analyzed by an online mass spectrometer (Hiden QGA). Ammonia treatment continued until the ammonia signal stabilizes indicated that all the surface sites were saturated with ammonia. Then the catalysts were treated in He for 2 h at 100 °C to remove any

physisorbed ammonia. We then stopped the helium flow when no ammonia signal was visible anymore, indicating that only chemisorbed ammonia retained on the sample.

4.2.2.3. Scanning electron microscopy coupled with energy-dispersive X-ray spectroscopy (SEM/EDX)

SEM images were retrieved by using a Zeiss Ultra Plus field emission scanning electron microscope. Na^+-exchanged samples were analyzed under ultra-high vacuum with 10 kV accelerating voltage and at 5.0 mm working distance. A secondary electron detector was used for imaging and XFlash 5010 detector with 123 eV resolution was used for EDX mapping.

4.2.2.4. X-ray fluorescence (XRF)

Sodium loading on Na^+-exchanged Amberlyst 15^{TM} samples were determined by X-ray fluorescence measurements. A Bruker S8 Tiger XRF spectrometer in standardless mode under helium atmosphere with an 18 mm mask was used for these measurements. Catalysts were crushed and sieved into 75-125 μm particle size fractions prior to analysis. The crushed samples were loaded into an XRF sample cup (Chemplex Industries Inc., Cat. No: 1430) with a thin-film support (Prolene film with 4μm thickness, Chemplex Industries, Inc., Cat. No: 426). The loose powder method was selected for the measurement together with "Best analysis" and the matrix was assumed to be "C_8H_9". SpectraPlus Eval2 V2.2.454 was used for data interpretation. Concentrations of sulfur and sodium were calculated in wt%, which were then converted into moles to obtain the ratio of sodium to sulfur, corresponding to the sodium loading on the catalyst. The amount of sodium determined by XRF in mmol Na^+/g_{cat} was based on the assumption that the molecular formula of a unit structure was $(CHCH_2)_n$-(C_6H_4)-SO_3H with a molecular weight of 222 g/mol. The molecular weight was calculated regarding the acid capacity of pristine Amberlyst 15^{TM} determined by titration (4.5 mmol H^+/g_{cat}). For instance as there is 4.5 mmol H^+ in 1 g catalyst, there should be 1 mol of H^+ in 222 g catalyst, therefore there is also 1 mol of sulfur in 222 g catalyst. As the XRF analysis enables the moles of sodium

per mole sulfur, mole of sodium per g of catalyst was calculated. XRF analysis of Na^+-exchanged Amberlyst 15^{TM} samples were also performed following ammonia pulse chemisorption to confirm retaining of the exchanged sodium.

4.2.2.5. Thermogravimetric analysis (TGA)

Thermal stabilities of pristine and Na^+-exchanged Amberlyst 15^{TM} samples were determined by TGA. Measurement was performed on a TA Instruments TGA Q500 model instrument. Approximately 12 mg catalyst grinded into powder form was used for each measurement. Measurements were performed at a temperature ramp rate of 5 °C/min from room temperature to 110 °C, followed by an isothermal treatment for 1 h at 110 °C, and then a temperature ramp from 110 to 700 °C in flowing nitrogen (60 ml N_2/min) at a heating rate of 3 °C/min. Decomposition onset temperatures (T'_{onset}) were attained from the temperature vs. derivative weight graph using TA Universal Analysis software [213,214].

4.2.2.6. Temperature programmed decomposition of Amberlyst 15™ (TPD)

TPD of pristine Amberlyst 15^{TM} was studied to determine the first leaving groups during thermal decomposition. A Micrometrics AutoChem II 2920 instrument with a thermal conductivity detector (TCD) coupled with an MKS Cirrus II mass spectrometer was used for these measurements. 12 mg catalyst in bead form was loaded into the sample holder of the instrument. Helium (50 ml/min) was passed through the sample with a temperature ramp rate of 5 °C/min from room temperature to 110 °C, isothermal for 1 h at 110 °C and then temperature ramp rate of 3 °C/min from 110 to 250 °C. Signals from TCD and MS detectors were retrieved.

4.2.2.7. Fourier transform infrared (FTIR) spectroscopy

A Bruker Vertex 80v spectrometer with a capability to evacuate the sample chamber was used in transmission mode at a resolution of 2 cm^{-1}. Pristine and Na^+-exchanged Amberlyst 15^{TM} samples were crushed and sieved into 75-125 μm particle size fractions to obtain a powder form because their bead form was not suitable for analysis. Pristine and Na^+-exchanged Amberlyst

15^{TM} samples both before and after ammonia pulse chemisorption were subjected to IR analysis. Prior to IR measurements, the catalysts were dried in a separate vacuum oven at 110 °C for 1 h to remove moisture. Before each measurement 128 background scans were collected under vacuum and averaged. Then a few milligrams of the catalyst sample were placed between two potassium bromide windows. The windows were settled into the sample vacuum chamber of the spectrometer. A series of spectra were collected in a repeated scan mode with 8 repetitions. Each repetition consisted of 128 scans in a frequency range of 4000-400 cm^{-1} and there were 300 sec waiting time between each repetition. Water related peaks were observed to diminish after the 4th repetition under vacuum. Spectra at 8th repetition were used as the final spectra for each sample wherein the moisture content was minimized by keeping the samples the vacuum chamber (< 3 milibars) for more than 1 h at room temperature. The final spectra were further processed. The final spectra both before and after ammonia pulse chemisorption were baseline corrected using Rubberband method with 21 baseline points and normalized with respect to the sharp peak at 1598 cm^{-1} of benzene ring stretching vibration [215]. For each sample, difference spectra were calculated by subtracting the "before" spectra from the "after ammonia pulse chemisorption spectra". Peak deconvolution were performed in Fityk (version 0.9.8) software [186] assuming Voigt distribution. Prior to the peak deconvolution, the difference spectra of pristine and Na^+-exchanged Amberlyst 15^{TM} samples were cut into stretching and fingerprint regions, baselines corrected again and curves smoothed by averaging 21 points. In Fityk, the best fit is obtained by minimizing the weighted sum of squared residuals (WSSR), between the measured and modeled points:

$$\boldsymbol{WSSR = \sum_{i=1}^{n} \frac{1}{SD_i^2} (Y_{obs,i} - Y_{calculated,i})} \qquad \textbf{(Equation 4-1)}$$

The calculated WSSR values were ≤ 0.07, indicating strong fit. Alternative deconvolution trials with different initial guesses did not alter the resulting peak positions within the spectral resolution of 2 cm^{-1}.

4.2.3. Computational methods

Density functional theory (DFT) calculations were performed using the Spartan'14 Parallel Suite (Wavefunction Inc., version 1.1.4) software on a PC equipped with an Intel Core i7-4960X CPU and 32 GB of RAM. Geometries were fully optimized at the Becke's three parameter hybrid exchange functional [216] and the Lee-Yang-Parr [217] correlation functional (B3LYP) with 6-31G** basis set. The self-consistent field (SCF) convergence criteria was set to 1×10^{-6} with the tolerance values for gradient and displacement of 5.5×10^{-5}. Three sulfonated styrene groups were considered as a representative geometry of Amberlyst 15^{TM} (denoted as Amb15-HHH). As a starting geometry, the protons were first located at the center of $[-SO_3]^-$ groups and the geometries were fully optimized to let the protons to locate themselves on the most preferable oxygen atom in the $[-SO_3]^-$ group. The Na^+-exchanged counterparts were considered by replacing the protons located on the side sulfonated styrene groups with Na^+ followed by full geometry optimization (Amb15-HHNa and Amb15-NaHNa for one and two Na^+ exchanged, respectively). The deprotonation energies (DPE) were calculated as the energy difference between the total energy of the neutral systems (Amb15-*x*H*y*, representing the corresponding Amberlyst 15^{TM} geometry, where *x* and *y* can be either H^+ or Na^+, depending on the geometry considered) and the total energies of the negatively charged systems, [Amb15-*x*_*y*]$^-$, considering the energy of the removed proton itself as zero with no electrons present. The calculations on the deprotonated geometries were calculated at a total charge of -1, while other geometries were optimized considering the geometries neutral. The adsorption energy of ammonia was calculated by:

$$\Delta E_{NH_3} = E_{Amb15-xHy+NH_3} - (E_{Amb15-xHy} + E_{NH_3}) \quad \textbf{(Equation 4-2)}$$

where, ΔE_{NH_3} is the adsorption energy of ammonia on a geometry representing the structure of the corresponding Amberlyst 15^{TM} (either pristine or cation-exchanged). $E_{Amb15-xHy+NH_3}$ is the calculated energy of a given geometry containing the adsorbing molecule and the

corresponding Amberlyst 15^{TM} geometry. $E_{Amb15-xHy}$ and E_{NH_3} are the energies of the corresponding Amberlyst 15^{TM} geometry and the gas phase ammonia, respectively. The corresponding Cartesian coordinates of the geometries are provided in **Appendix B**.

4.2.4. Catalytic performance measurements

4.2.4.1. Measurements using batch reactors

Catalytic performance tests of pristine and Na^+-exchanged Amberlyst 15^{TM} samples (in bead forms) were performed in a Parr Series 5000 Multiple Reactor System consisting of six parallel stainless steel autoclave reactors of 75 ml each with magnetic stirring. Each run was performed by loading 0.45 g catalyst and 6.0 g glycerol into the reactor and followed by purging and pressurizing the reactor to 8 bar with nitrogen. 18 ml (11 g) isobutene (IB) was then delivered into the reactor at this pressure in liquid form with the nitrogen as carrier gas, using a dosing system where the liquid isobutylene volume is measured with a graduated translucent Teflon piping. The reactor was then heated to 75 °C, resulting in 15±1 bar total pressure. The reaction was run at autogenous pressure at a stirring rate of 1200 rpm. The reaction was carried out for 6 h until complete glycerol conversion was reached.

4.2.4.2. Measurements using a flow reactor

A once-through 1/4”-stainless steel reactor was used in a flow reactor system, illustrated in **Figure 6-1** (**Appendix B**), for these measurements focusing primarily on very low glycerol conversions to identify the primary and secondary products. Pristine and 0.5 M Na^+-exchanged Amberlyst 15^{TM} samples (in bead forms) were crushed and sieved to obtain 250-425 μm size fractions. This particle size was determined by applying the Weisz Rule so that the operation was free of any mass transfer limitations. The fractioned catalyst was dried at 110 °C for 2 h under vacuum and then loaded into a stainless steel tubular reactor (4.35 mm I.D.) located in a 3-zone furnace (Thermocraft) with three independent temperature controllers. The reactor was heated to 75 °C and pressurized to 15 bar with nitrogen. Reactor pressure was controlled with

a back pressure regulator (Equilibar) at the exit. Isobutene and glycerol were fed into the reactor in liquid phase at 15 bar at an isobutene/glycerol mol:mol ratio of 3:1 by using two separate high pressure syringe pumps (Iscopump 500D). For differential glycerol conversions (< 3 wt%), glycerol based space velocity was kept between 2-20 $mol_{glycerol}$ x $(mol_{H^+}$ x min$)^{-1}$, corresponding to the glycerol residence times of 0.05 to 0.5 min. Several liquid samples (each 15±5 ml) were collected, kept at room temperature for a few hours to evaporate unconverted isobutene and then weighed to calculate the mass-based glycerol conversion based on gas chromatographic sample analysis.

4.2.4.3. Gas chromatographic (GC) analysis

An Agilent 7890B GC equipped and a 5977A Series GC/MSD gas chromatograph-mass spectrometer (GC-MS) system with an HP Innowax column (30 m x 0.25 mm x 0.25 µm) was used for analyzing the product mixture. Sample was collected at the end of reaction, homogenized by vortexing and filtered. Quantification of products was done by using octanol as internal standard and ethanol as solvent. In a typical analysis, 165.0±0.5 mg octanol was mixed with 510±1 mg reactor sample and diluted to 10 ml with ethanol. Calibration equations for glycerol, glycerol mono-tertiary butyl ether, and di-isobutene were constructed by using commercially available standards. Calibration equations for di-ether, tri-ether, tri-isobutene, tetra-isobutene, and tertiary butyl alcohol were obtained by using GC-FID response factor method [188]. The weight-based response factors (R_{wt}) were calculated with respect to octanol as:

$$\boldsymbol{R_{wt} = \frac{MW_{compound}}{MW_{octanol}} \, x \, \frac{ECN_{octanol}}{ECN_{compound}}} \qquad \textbf{(Equation 4-3)}$$

where, MW is molecular weight in g/mol and *ECN* is the effective carbon number [192]. The amount of each compound was calculated using its R_{wt} as:

$$\boldsymbol{m_{compound} = R_{wt} \, x \, m_{octanol} \, x \, \frac{A_{compound}}{A_{octanol}}} \qquad \textbf{(Equation 4-4)}$$

where, A is the flame ionization detection (FID) signal peak area in Pa.s. Peak assignments of all products were confirmed by GC-MS. 1 µl mixture sample was injected into the column with a split ratio of 100:1. Oven temperature raised from 40 to 240 °C with 10 °C/min increments. Product concentrations in the sample were determined by a FID following chromatographic separation.

4.3. Results and Discussion

4.3.1. Change in acid capacity upon sodium exchange

Distribution of Na^+ in Amberlyst 15^{TM} matrix in the cation-exchanged samples was examined by SEM/EDX imaging. A representative SEM/EDX image on a representative Na^+-exchanged sample (0.4 M $NaNO_3$) is given in **Figure 4-1**. The images illustrate a uniform distribution of sodium atoms on each of Na^+-exchanged sample, confirming that Na^+-exchange was successful throughout the samples. After confirming the uniform distribution of Na^+ sites, the pristine and Na^+-exchanged (at six different levels) Amberlyst 15^{TM} samples were characterized by acid-base titration to measure the number of protonic sites in mole basis per gram of catalyst. These results were further evaluated on the basis of number of Na^+ atoms determined by XRF measurements (**Table 4-1**) and calculated from the maximum possible number of Na^+ exchanged with the catalyst from the $NaNO_3$ solutions at saturation (**Table B-1).** Ammonia pulse chemisorption enabled the total saturation of Brønsted acid sites with ammonia without any physisorbed ammonia (**Figure B-2**).

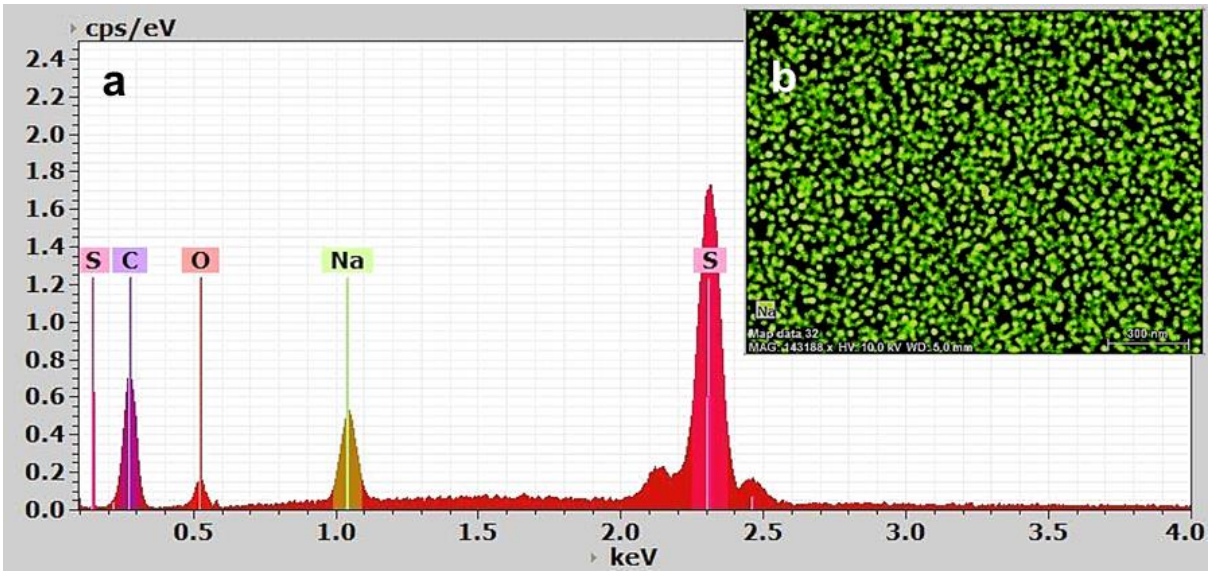

Figure 4-1. SEM-EDX data of a representative Na^+-exchanged sample (cation-exchanged in 0.4 M $NaNO_3$); **a:** detected elements; **b:** distribution of sodium in the matrix.

Table 4-1.Results of titration and XRF analysis of Amberlyst 15^{TM} samples.

Na^+-exchange treatment	**Acid capacity by titration (mmol H^+/g_{cat})**	**Na^+ loading by XRF (mol Na^+/mol S)**	**Na^+ loading by XRF (mmol Na^+/g_{cat})**
No exchange	4.5	0	0
0.1 M	3.9	0.17	0.8
0.2 M	3.5	0.29	1.3
0.3 M	2.9	0.41	1.9
0.4 M	2.7	0.45	2.0
0.5 M	2.3	0.60	2.7

According to **Table 4-1**, increasing the sodium concentration of the treatment solution from 0 to 0.5 mol/L, partial neutralization of acid sites by Na^+-exchange yielded in different Amberlyst 15^{TM} samples with a sodium loading ranging from 0 to 2.7 mmol Na^+/g_{cat}. Acid capacity was observed to be inversely correlated with sodium loading. Acid capacity of pristine Amberlyst 15^{TM} was determined to be 4.5 mmol H^+/g_{cat} by our titration method, which is close to the commercial value (4.7 mmol H^+/g_{cat}). The sum of acid capacity and sodium loading

yielded in total cation capacity, which is closer to the acid capacity of pristine Amberlyst 15^{TM} within 10% error. Sodium loadings calculated by using XRF results were close to the maximum theoretical sodium loading. Besides, the catalysts before and after ammonia pulse chemisorption treatments had similar sodium loading values (**Table B-1**).

4.3.2. Spectroscopic quantification of acid strength

In general, the acid strength of solid acids is assessed by means of temperature programmed desorption (NH_3-TPD) measurements using a basic adsorbate, such as ammonia and/or pyridine. However, results of TGA measurements on the pristine and Na^+-exchanged Amberlyst 15^{TM} samples provided in **Figure B-3** and **Table B-2** illustrate that the samples start to decompose at approximately 220 °C. Data further indicate that this decomposition temperature shifts to higher temperatures with an increase in the Na^+-exchange degree. For instance, for a Na^+-exchange degree of 2.7 mmol Na^+/g_{cat}, the corresponding decomposition temperature was 264 °C. Such poor thermal stability limits of the samples indicate the inappropriateness of these resin catalysts for TPD measurements to quantify the acid strength. Thus, we focused on employing an infrared (IR) spectroscopy-based technique to quantify the acid strength of Amberlyst 15^{TM} samples prepared at different Na^+-exchange levels.

Interaction of a Brønsted acid site (AH) with a base in gas phase (B) is known to follow the following mechanism $\mathbf{AH + B \leftrightarrow AH\cdots B}$ to form a hydrogen bonded neutral complex. When the base has high proton affinity, such as that in ammonia or pyridine, proton transfer occurs as in $\mathbf{AH\cdots B \leftrightarrow A^{-}\cdots{}^{+}HB}$, forming an ionic pair. The IR spectra of the acid-base adduct differ from that of the free base, because new bands emerge resulting from hydrogen bonding. Subsequently, evaluation of the IR bands associated with a base adsorbed on acid sites can potentially provide a correlation between IR features and the acid strength for solid Brønsted acid catalysts. For instance, when

pyridine interacted with the acid sites in silica, pyridine ring vibration frequency at 1440-1465 cm-l region increased with increasing hydrogen bond strength [218]. Although there is no study investigating the ν(N–H) as an indicator of Brønsted acid strength, we envisaged that ν(N–H) of ammonia would change when it forms a hydrogen bond or gets protonated by a Brønsted acid site. Accordingly, if the acid strength of a Brønsted acid site is high, then the ν(N–H) of ammonia interacting with the Brønsted acid site will be higher and closer to that of a free ammonium ion. With this approach, we decided to use the shifts in N–H vibrational frequencies of ammonium ion as an indicator of acid strength in Amberlyst 15™ solid acid catalyst.

Free ammonium species with high symmetry has two IR active vibration modes: N–H stretching at 3340 cm^{-1} and deformation at 1440 cm^{-1}. However, ammonium ions interacting with Brønsted acid sites lose their symmetry and acquire several IR active modes including i) stretching and bending vibrations of hydrogen bonded N–H [219-221], ii) combinations of bending vibrations, and iii) mixing of bending vibration overtones with the stretching vibrations of hydrogen bonded N–H, called the Fermi resonance. The N–H bonds perturbed by hydrogen bonding, tend to have a lower ν(N–H) and larger bandwidth compared to free N–H bonds that are far away from hydrogen bond [222]. The number of modes further increases with the effect of combinations, overtones, and Fermi resonance, yielding in complex absorption features. As a result, N–H vibration features of adsorbed ammonia (forming an ammonium ion) tend to appear as broad bands thus, it is required to deconvolute them into distinct bands. Here, we speculate that high Brønsted acid strength is represented by N–H bands at high energy, namely those are closest to free ammonium ion.

FTIR spectrum of the pristine Amberlyst 15^{TM} given in **Figure B-4** indicates O–H stretching vibrations of [–SO_3H] groups constituting a broad band in 3500-3200 cm^{-1} region as

well as a distinct band at 2399 cm^{-1} specific to the polymer, an asymmetric C–H stretching vibration at 2921 cm^{-1}, benzene ring skeleton vibrations at 1598, 1493, 1448, and 1413 cm^{-1}, stretching vibrations of S=O groups at 1338, 1160, 1095, 1006, 887, and 832 cm^{-1}, and stretching vibrations of C–S groups at 654 cm^{-1}, consistent with the literature [223-225].

IR spectra of pristine and Na^+-exchanged Amberlyst 15^{TM} samples before and after NH_3 pulse chemisorption are given in **Figure B-5**, showing that ammonia chemisorption yielded in new high intensity peaks of N–H vibrations in 3400-2400 cm^{-1} and 1500-1350 cm^{-1} regions. Construction of their difference spectra enabled the elimination of C–H vibrations associated with the Amberlyst 15^{TM} back bone that can otherwise interfere with the N–H vibrations in the same region. The spectra were normalized with respect to the benzene C=C stretching vibration at 1598 cm^{-1}. The C=C stretching peak positions were almost identical within ±0.3 cm^{-1} (with the peak shape remaining the same) as the degree of Na^+-exchange varied (**Figure B-6**). Thus, as the presence of Na^+ did not influence the benzene ring vibrations, we infer that our normalization procedure does not deliver any artifacts in the subtracted spectra of the samples with different degrees of Na^+-exchange. The difference spectra represent the ammonium ions interacting with Brønsted acid sites via hydrogen bonding. Deconvolution of the difference spectra of Amberlyst 15^{TM} samples was performed to reveal the individual peaks in the stretching region as given in **Figure 4-2** and **Table 4-2** (the scatter plots of **Table 4-2** are given in **Figure B-8**, while the lower wavenumber region is provided in **Figure B-7** and **Table B-3**). For this purpose we considered fitting the data using seven, eight, nine, and ten peaks in a region where we expect to have ν(N−H) bands, from 2400 to 3400 cm^{-1}. Among them, the fits obtained using nine peaks were considered for the rest of the study, as these fits are the ones with the lowest number of peaks providing an acceptable level of absolute residuals (almost in the range of noise level). However, we also note that considering seven and eight peaks provides very

similar results as represented in **Table 4-2** and does not change the main conclusions of this study as illustrated in **Table B-4** to **Table B-7** and in **Figure B-9**.

Results presented in **Figure 4-2** and **Table 4-2** indicate the presence of ammonium ions in 3328-2627 cm^{-1}**.** The N–H stretching vibrations associated with the N–H groups of adsorbed ammonia interacting with the acid sites (forming an ammonium ion stabilized by hydrogen bonding), namely the lower energy ν(N–H) bands, were located at 3050, 2985, 2830, 2763, and 2639 cm^{-1} on pristine Amberlyst 15^{TM}, whereas the stretching bands at 3324 and 3206 cm^{-1} were associated with the N–H groups of the ammonium ion that are not involved in hydrogen bonding. To eliminate the effect of any remaining hydration on our peak analysis, we deconvoluted the difference spectra collected at the end of 1st, 2nd, 3rd, and 4th hours in the IR chamber. The peak positions did not change upon prolonged dehydration, as the peak values were almost the same within an error range of 2 cm^{-1}. In summary, the existence of any adsorbed water which might left even after drying did not induce any significant effect on the vibrations of adsorbed NH_4^+ ions.

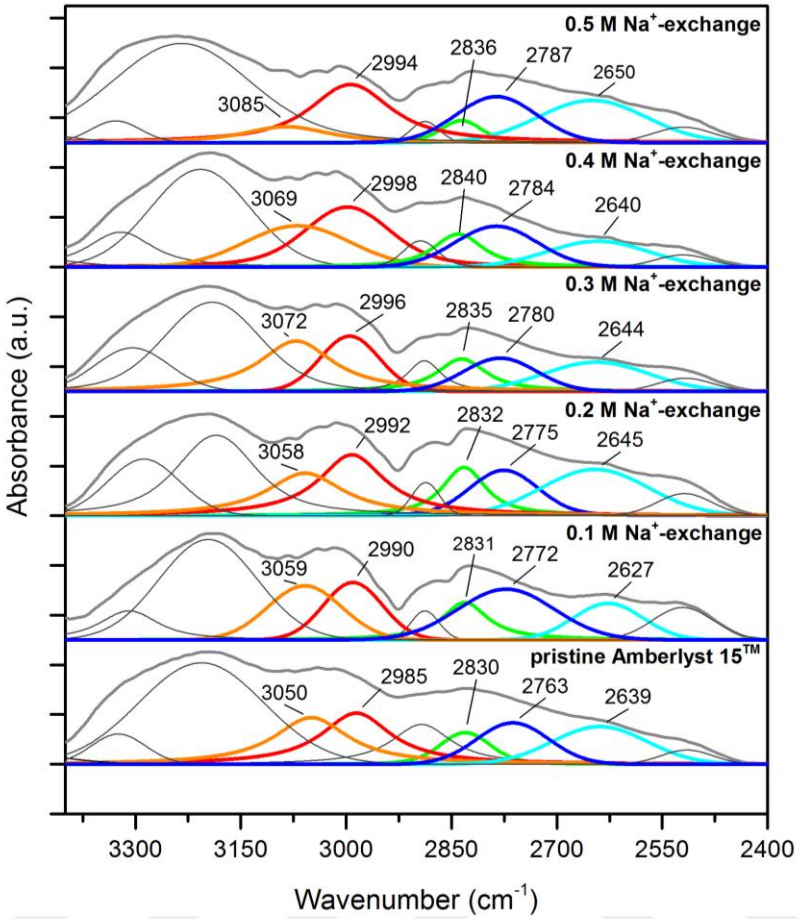

Figure 4-2. Difference FTIR spectra obtained by subtracting the spectra of samples before NH_3 chemisorption from their corresponding counterparts after chemisorption in the stretching region.

Table 4-2. Brønsted acidity related vibrational frequencies of Amberlyst 15^{TM} samples in deconvoluted difference spectra.

Acid capacity (mmol H^+/g_{cat})	**ν(N–H)**				
4.5	3050	2985	2830	2763	2639
3.9	3059	2990	2831	2772	2627
3.5	3058	2992	2832	2775	2645
2.9	3072	2996	2835	2780	2644
2.7	3069	2998	2840	2784	2640
2.3	3085	2994	2836	2787	2650
R^2*	0.894	0.769	0.703	0.985	0.386

* Correlation coefficients with respect to changes in acid capacity.

The lower energy ν(N–H) bands shift to higher frequencies upon Na^+-exchange. For instance, the band at 3050 cm^{-1} presents a blue shift of approximately 35 cm^{-1}, while that on 2763 cm^{-1} shifts to 2787 cm^{-1} upon Na^+-exchange in 0.5 M $NaNO_3$ solution. We infer that the degree of blue shift on these ν(N–H) band positions correlates with the acid strength. We especially considered the variation of the ν(N–H) band in 2763-2787 cm^{-1} region with the degree of Na^+-exchange as illustrated in **Figure 4-3**. This band was assigned to the stretching frequency of ammonia directly interacting with the Brønsted acid site. Among the other possibilities listed in **Table 4-2**, this band was considered because i) the change in peak position was significantly higher than the spectral resolution of 2 cm^{-1}, ii) its correlation coefficient (R^2) with the number of acid sites was the highest, and iii) its peak area was high compared to the other bands given in **Table 4-2**. Moreover, we would like to note that the corresponding correlations on the other peaks listed in **Table 4-2** are also fairly high; for instance, the R^2 for the peak at 3050 cm^{-1} on pristine Amberlyst 15^{TM} is 0.898. We also note that for the peaks which have an R^2 lower than 0.8, the variation of band positions is within ±5 cm^{-1} of the average value, so there might not be any significant change in the peak position. We speculate that these peaks might be associated with the ammonia molecules which are adsorbed on surface sites, where Na^+ could not be transported, thus they are not influenced significantly from the increase in Na^+ concentration. We also speculate that the peak positions of the N–H stretching of the groups that are not directly interacting with the Brønsted sites can also be influenced indirectly by the interaction of other N–H groups with the acid sites.

According to **Figure 4-3**, ν(N–H) located at 2763 cm^{-1} on ammonia-saturated pristine Amberlyst 15^{TM} gradually shifts to higher energies presenting a strong correlation with a decrease in acid capacity from 4.5 to 2.3 mmol H^+/g_{cat}. This blue shift with increasing sodium loading indicates a stronger N–H bonding in the $A^{-}\cdots{}^{+}HB$ ion

pair with increasing Na^+-exchange degree. Thus, we infer that even though the cation exchange reduces the number of acid sites in Amberlyst 15™, it helps to increase the individual acid strength of these sites; and this increase in acid strength is strongly correlated with the degree of cation exchange.

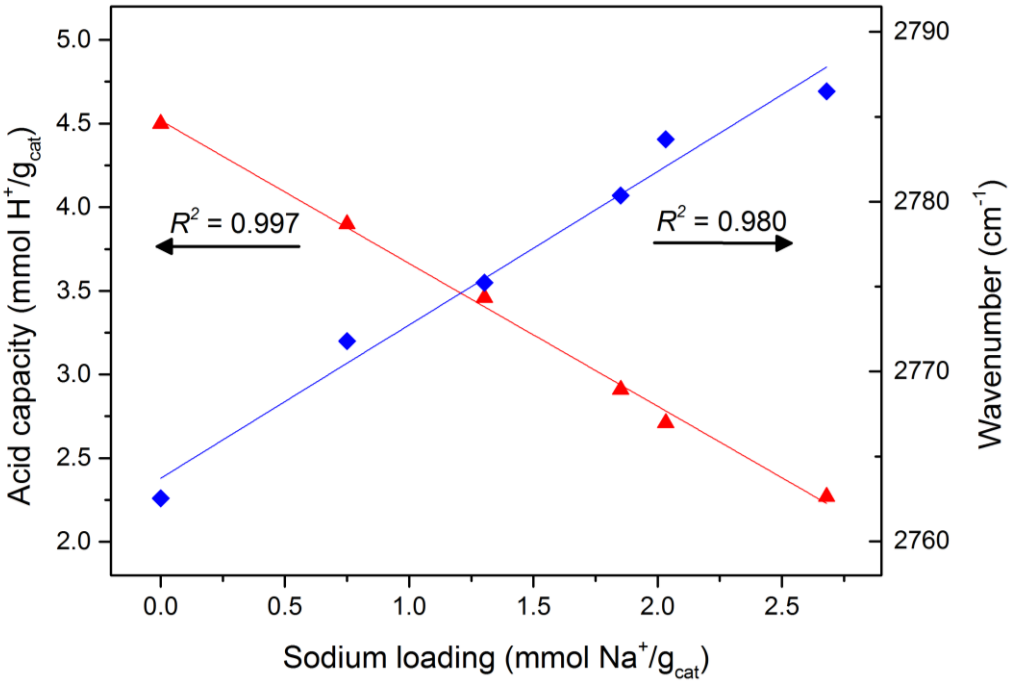

Figure 4-3. Relationship between sodium loading, acid capacity, and ν(N–H) bands for pristine and Na^+-exchanged Amberlyst 15™ samples (acid capacity (▲); ν(N–H) (♦)).

To confirm the validity of this approach on different solid acid catalysts, we extended our investigation to heteropolyacids, considering TSA and TPA, and performed the same analysis on their ammonia saturated counterparts. Similar to the case with Amberlyst 15™ samples, the difference IR spectra were cut in the 3800-2400 cm^{-1} region and deconvoluted (**Figure B-10**). Data showed that the peak positions of ν(N−H) on ammonia-saturated TSA (2777, 2810, 3000, and 3040 cm^{-1}) were lower than those on ammonia-saturated TPA (2787, 2820, 3008, and 3050

cm^{-1}), indicating that the TPA has a stronger acidity. Consistently, it was reported that the DPE of TPA is approximately 20 kJ/mol lower than that of TSA [196]. Thus, we infer that our IR-based methodology for comparing the acid strengths of resin catalysts that we present in this study can be extended to heteropolyacids as well.

4.3.3. Quantum chemical assessment of changes in acid strength with Na^+ exchange

DFT calculations were performed to understand the effect of Na^+ exchange on the DPE of sulfonic acid moieties in Amberlyst 15^{TM}. Our infrared spectroscopic analysis (**Figure B-4**) shows that intensity of the H_2O bending vibration at 1650 cm^{-1} significantly decreased upon drying in the IR chamber and the remaining water did not influence on the stretching vibrations of ammonia. Thus, we assumed the effect of water to be negligible for our DFT analysis.

Three sulfonated styrene rings were considered as a representative model for Amberlyst 15^{TM} as shown in **Figure 4-4 a**. This model is denoted as Amb15-HHH, where HHH represents the Brønsted acid sites on each of sulfonated styrene rings. Only one sulfonyl-benzene ring was previously used to represent an ion exchange resin catalysts [226,227], thus we infer that our three-sulfonated styrene ring model can sufficiently represent at least two different Na^+-exchange degrees for Amberlyst 15^{TM}. To represent the Na^+-exchanged counterparts, the model was modified by exchanging the protons located on the side sulfonated styrene rings with Na^+. **Figure 4-4 b** represents the geometry of a model when one of the protons was exchanged (Amb15-HHNa, corresponding to 1.5 mmol Na^+/g_{cat} with a cation exchange degree of 33.3%), while **Figure 4-4 c** illustrating the Amb15-NaHNa with both protons located on the side [$-SO_3H$] groups were exchanged with Na^+, corresponding to a Na^+-exchange degree of 3 mmol Na^+/g_{cat} (with a cation exchange degree of 66.7%).

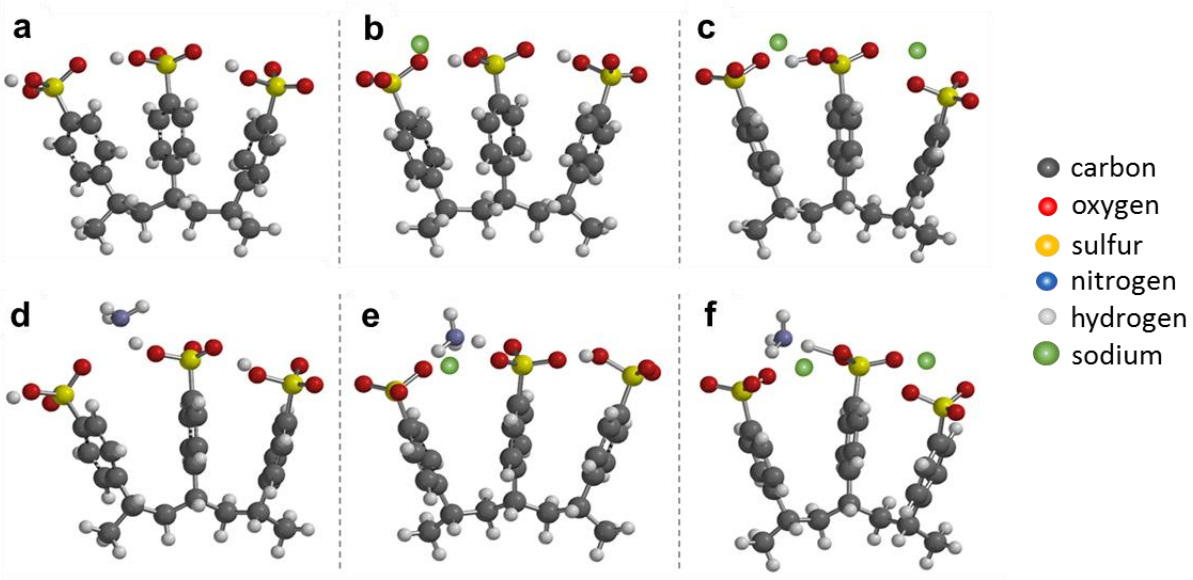

Figure 4-4. Optimized geometries of the model structures representing the pristine and Na^+-exchanged Amberlyst 15^{TM} catalysts and their NH_3 adsorbed counterparts; **a:** Amb15-HHH (representing pristine Amberlyst 15^{TM}); **b:** Amb15-NaHH (representing a Na^+-exchange degree of 33.3%); **c:** Amb15-NaHNa (representing a Na^+-exchange degree of 66.7%); and optimized geometries of structures representing NH_3 adsorbed on **d:** Amb15-HHH; **e:** Amb15-NaHH; and **f:** Amb15-NaHNa.

The DPE value for Amb15-HHH calculated at the B3LYP/6-31G** level was 1266 kJ/mol, whereas the corresponding value decreased to 1263 and 1246 kJ/mol, on Amb15-HHNa and Amb15-NaHNa, respectively. The optimized geometries illustrated in **Figure 4-4 b and 4 c** indicate that the Na^+ cation in Amb15-HHNa and Amb15-NaHNa was shared between the oxygen atoms located on two neighboring sulfonated styrene rings. This sharing leads to a decrease in electron density allocated for keeping the Brønsted acid proton as evidenced by the electrostatic potential maps presented in **Figure B-11**. Because of this effect, the DPE decreases, leading to an increase in acid strength. Thus, we infer that the acid strength increases as the neighboring protons located on the side sulfonated styrene rings were exchanged with

Na^+. Data further show that this increase in acid strength correlated well with the degree of Na^+ exchange as illustrated in **Figure B-12**, strongly complementing the experimental results presented in **Figure 4-3**.

This conclusion was further supported by the ammonia adsorption energies calculated on these model geometries. Accordingly, the adsorption energy of ammonia on the proton located in the middle-sulfonated styrene group was -89.2 kJ/mol on Amb-15-HHH (**Figure 4-4 d**). This value becomes more negative with Na^+ exchange: on Amb15-HHNa (**Figure 4-4 e**) and Amb15-NaHNa (**Figure 4-4 f**), the corresponding ammonia adsorption energy values were -92.9 and -121.5 kJ/mol, respectively. These results present a perfect correlation with the DPE energies as illustrated on **Figure B-13**. Thus, we infer that the acid strength of [$–SO_3H$] group increases with an increase in the Na^+ exchange degree. Besides, our DFT results indicated that the adsorbed NH_3 did not directly interact with Na^+. For this reason, any possible effects of the presence of sodium on the enthalpy of ammonia adsorption were ruled out.

Even though the difference between the DPE values calculated on the model geometries representing the pristine and 33% Na^+-exchange is close to the determination limit of DFT calculations, we emphasize that changes in the DPE data are self-consistent with the ammonia adsorption energies calculated on the same geometries. Hence, these DFT results complement the experimental results illustrating the consequences of cation exchange on the acid strength of Brønsted acid sites in resin catalysts. To the best of our knowledge, this effect has heretofore been neglected in evaluating the performance of cation-exchanged resin catalysts, although it might possibly have a strong influence on the catalytic performance.

4.3.4. Consequences of Na^+-exchange on catalytic performance

4.3.4.1. Batch reactor measurements at high glycerol conversions

As illustrated above, modification of Amberlyst 15^{TM} by Na^+-exchange strongly alters both the number and the strength of acid sites. Next, we investigated the consequences of this

modification on an industrially relevant test reaction: glycerol etherification with isobutene to produce green alternative fuel additives. For this purpose, catalysts were first loaded into batch reactors, and their catalytic performances were measured under identical conditions (75 °C, 10-15 bar, IB:G=3:1 mol:mol, 7.5 wt% of glycerol catalyst loading, 6 h run). Product mixture consisted of MTBGE, DTBGE, TTBGE, di-isobutene (DIB), tri-isobutene (TIB), tetra-isobutene (TetraIB), and trace amounts of tertiary butyl alcohol (TBA). The selectivity of each catalyst towards these products was determined after reaching complete glycerol conversion following a run period of six hours. Results of the product analysis are given in **Table 4-3**.

Table 4-3. Catalytic performance of Amberlyst 15^{TM} catalyst samples in batch reactor under identical conditions (75 °C, 10-15 bar, IB:G=3:1 mol:mol, 7.5 wt% of glycerol catalyst loading, 1200 rpm mixing, after 6 h run, complete glycerol conversion).

	Product selectivity* (wt%)			
Na^+-exchange treatment	**MTBGE**	**DTBGE**	**TTBGE**	**DIB**
No exchange	11.1	58.6	16.3	12.0
0.1 M	9.9	59.1	19.6	9.0
0.2 M	8.7	59.4	23.5	6.6
0.3 M	7.6	60.3	26.9	3.5
0.4 M	9.3	64.7	21.9	2.1
0.5 M	8.1	67.3	21.7	1.5

*Other products, TIB and TBA, together are less than 2.7 wt% of the total products. Thus, they are excluded in the table.

As reported previously in the literature, pristine Amberlyst 15^{TM} provides a desired ether selectivity in the range of 70-80 wt% accompanied by a selectivity for di-isobutene of 10-15 wt% at glycerol conversion values exceeding 95% (at various reaction conditions: temperature ranging from 60 to 90 °C, with a catalyst loading of 5 to 7.5 wt%, and at an IB:G ratio of 3:1 to 4:1 with a reaction time of 4 to 50 h) [15,39,42,181]. In **Table 4-3**, data for pristine Amberlyst 15^{TM} indicate a selectivity of 75 wt% towards desired ethers with approximately 12 wt% di-

isobutene in the product mixture at complete glycerol conversion in 6 hours. Thus, we infer that catalytic testing of dried Amberlyst 15^{TM} provided similar performance results to the literature under comparable conditions. Apart from that, we analyzed the product mixtures of Amberlyst 15^{TM} by stopping the batch runs at the end of 0.5, 1, 2, and 4 hour of run periods. Almost 99 wt% glycerol conversion was achieved in 4 hours. The product selectivity at the end of 4 and 6 hours were almost the same, with up to ±1 wt% differences (as presented in **Figure B-14**). Therefore, the effect of secondary reactions which might take place at complete glycerol conversion were neglected.

Data further showed that the selectivity of desired ethers increased from 75 to 89 wt% when the 0.5 M-Na^+-exchanged catalyst (corresponding to approximately 50% Na^+-exchange) was used. Among the ethers, Na^+-exchange modification reduced the MTBGE selectivity in general, while improving the DTBGE selectivity almost linearly. However, the case for TTBGE selectivity was different; it first increased up to a Na^+-exchange degree of 0.3 M and then decreased with a further increase in Na^+-exchange degree to 0.5 M. This decrease in TTBGE selectivity at high Na^+-exchange degrees can originate from an enhancement in acid strength at high Na^+-exchange, which might be playing a role in the cracking of newly formed TTBGE molecules back to DTBGE. We also note that the formation of TTBGE might also be hindered because of the higher polarity of the sites at higher acid strength. Because of this effect at high Na^+-exchange levels, the active sites become less selective for the formation of TTBGE with lower polarity compared to DTBGE. Furthermore, data also indicate that there is a substantial drop in the selectivity of isobutene oligomers by almost an order of magnitude with increasing sodium loading from 0 to 2.7 mmol Na^+/g_{cat} as the degree of Na^+-exchange reaches to 50%.

Aiming at understanding the consequences of structural differences on the catalytic performance, we investigated the reaction selectivity towards desired ethers or oligomerization products with respect to the acid strength assessed quantitatively by the positions of ν(N–H)

bands in 2787-2763 cm^{-1} region in **Figure 4-5**. Data show that improving the Brønsted acid strength upon partial neutralization of active sites by Na^{+}-exchange resulted in lower concentrations of isobutene oligomers while increasing the selectivity for desired ethers (also seen in **Table 4-3**). As illustrated in **Figure 4-5**, these changes in product selectivity present a strong correlation with the acid strength quantified by the corresponding ν(N–H) band positions.

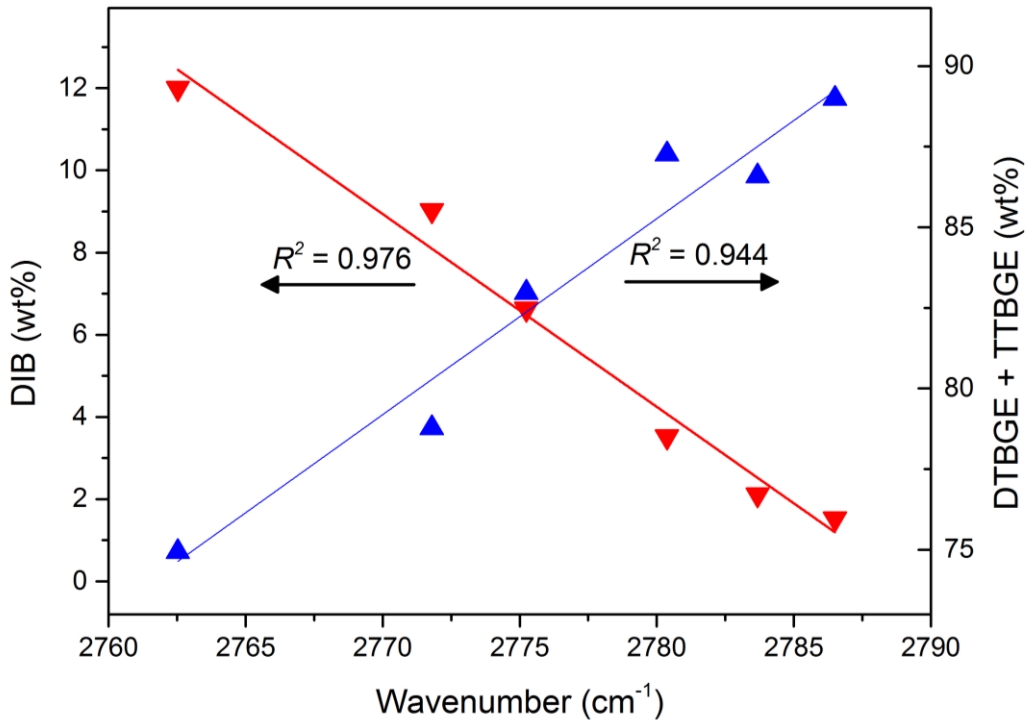

Figure 4-5. Variation of product selectivity of desired ethers and di-isobutene as a function of ν(N–H).

Catalytic performance depends on the amount, strength, and accessibility of the acid sites. Enhancement of desired ether selectivity in glycerol etherification over zeolites with improved acid strength was previously shown in literature [49,52,59,183]. However, to the best of our knowledge, these results are the first to support this concept on ion exchange resins. Our

data point out that the lower selectivity of isobutene to its oligomers might also be because of the synergistic effect of the strengthening of Brønsted acid sites and the decrease in acid site density. To further confirm the effect of acid strength, we tested two different heteropolyacids (HPAs), TSA and TPA, supported on SiO_2 and MCM-41 (50:50 wt% HPA loadings). TSA is known to have a lower acid strength than TPA with the corresponding DPE values of 1105 kJ/mol and 1085 kJ/mol, respectively [194-196]. Catalytic performance was tested under identical conditions to that of Amberlyst 15^{TM} samples. Product selectivity of supported HPA catalysts were found to remain in the same range with slightly higher selectivity to desired ethers, probably because of the higher acid strength of HPA protonic sites compared to sulfonic acid sites. Out of these two different HPAs, the one with higher acid strength (TPA) provided a lower di-isobutene and higher ether selectivity than TSA does (**Table B-8**). These results further validate the effect of acid strength on the etherification selectivity.

Reactions of reactants with different polarities over ion exchange resin catalysts (*e.g.* etherification) are known to follow Eley-Rideal type mechanism [118]. For instance, alcohol molecules with high dielectric constant are preferred to adsorb on the active sites of ion exchange resin catalysts in alcohol-olefin mixtures [228]. Etherification initiates with the protonation of alcohol, then the protonated alcohol reacts with the olefin [229]. Moreover, kinetic analysis of methanol etherification with C4 and C5 olefins pointed out the reaction between adsorbed alcohol with olefin from the reactant phase, forming an adsorbed ether intermediate [230,231]. Moreover, acid strength is also important for the stabilization of intermediates. For instance, in dehydration of methanol to dimethyl ether, protonated methanol dimers adsorbed on the Brønsted acid sites are stabilized by the electrostatic interactions with the deprotonated acid site. Lower deprotonation energy of the Brønsted acid site, the higher acid strength of the Brønsted acid sites, enhanced the stability of the protonated dimer intermediate [232]. Similarly, stronger acid sites stabilized the cationic transition state in which

protonated isobutanal interacted with isobutene in Prins condensation [233]. Although there is no study about glycerol adsorption on ion exchange resins, adsorption of glycerol on stronger Brønsted acid sites in amorphous aluminosilicate yielded in heavier carbon species in glycerol dehydration [234]. These results are consistent with our inference on the dependence of the Brønsted acid catalyzed etherification of glycerol with isobutene on the differences in acid strength. Accordingly, glycerol etherification with isobutene involves the adsorption of glycerol on the [–SO_3H] sites of Amberlyst 15^{TM} and the consequent interaction of protonated glycerol with isobutene to form the transition state for MTBGE formation. Hence, we envision the variations on the acid strength with Na^+-exchange to alter the reaction network for the etherification.

4.3.4.2. Flow reactor measurements at differential glycerol conversions

Elucidating the changes in the reaction network requires performance testing at very low glycerol conversions so that the variation of the primary and secondary products with acid strength can be monitored. However, the literature on glycerol etherification with isobutene presents studies using only batch reactors, which are not convenient for operating at very low conversions. Thus, they are not suitable for determining the fate of the very first glycerol and/or isobutene molecules upon their interactions with the acid sites. More information is required for identifying the primary and secondary products and their roles in the complex reaction network.

Aiming at identifying the changes in primary and secondary products upon changes in acid strength, we conducted performance tests using a once-through tubular flow reactor, to the best of our knowledge, for the first time in the literature [235]. Using a flow reactor at different space velocities allowed us to focus on very low glycerol conversion levels (< 3 wt%). The catalyst particle size fractions of 250-425 μm were applied as the optimum size, as the original bead size of 400-700 μm was observed to provoke internal mass transfer limitations, while the

smaller particle sizes of < 250 µm caused a substantial pressure drop along the reactor. For the 250-425 µm particle size, corresponding to an average of 338 microns, we applied Mears and Weisz Prater criteria to assess the possibility of the presence of any external and internal mass transfer limitations, respectively. MR, the Mears number uses the ratio of the reaction rate over the mass transfer coefficient. CWP, the Weisz Prater parameter, on the other hand, is the ratio of the reaction rate to diffusion rate. Accordingly, the external mass transfer limitations can be neglected if MR < 0.15; while the internal mass transfer limitations are insignificant when CWP is << 1 [236]. We considered the highest glycerol conversion rate, the lowest bulk concentration of glycerol, and the slowest glycerol and isobutene feed rates to calculate the maximum possible MR and CWP values under the conditions of our flow reactor experiments. Accordingly, the maximum values for MR and CWP were determined as 0.033 and 0.238, respectively, confirming that the whole operation range was free of any significant external and internal mass transfer limitations. Data presented in **Figure B-15** illustrate that the conversion remains nearly constant within less than ±0.2 wt% for almost 10 h during a run under constant space velocity.

Variation of the individual product selectivity (MTBGE, DTBGE, TTBGE, DIB and TIB) with respect to the corresponding residence time are represented in **Figure 4-6.** Differential glycerol conversions (< 3 wt%) were achievable at residence times lower than 0.6 min corresponding to a glycerol conversion rate of approximately 0.22±0.02 and 0.06±0.01 $mol_{glycerol\ converted}$ x $(mol_{H^+}$ x $min)^{-1}$ on pristine and 0.5 M Na^+-exchanged Amberlyst 15^{TM} catalysts, respectively. Individual product selectivity obtained at differential glycerol conversion were extrapolated to zero residence time (approaching to zero glycerol conversion) for both catalysts. By extrapolation, we aimed to determine what happens when a glycerol molecule interacts for the first time with an isobutene molecule.

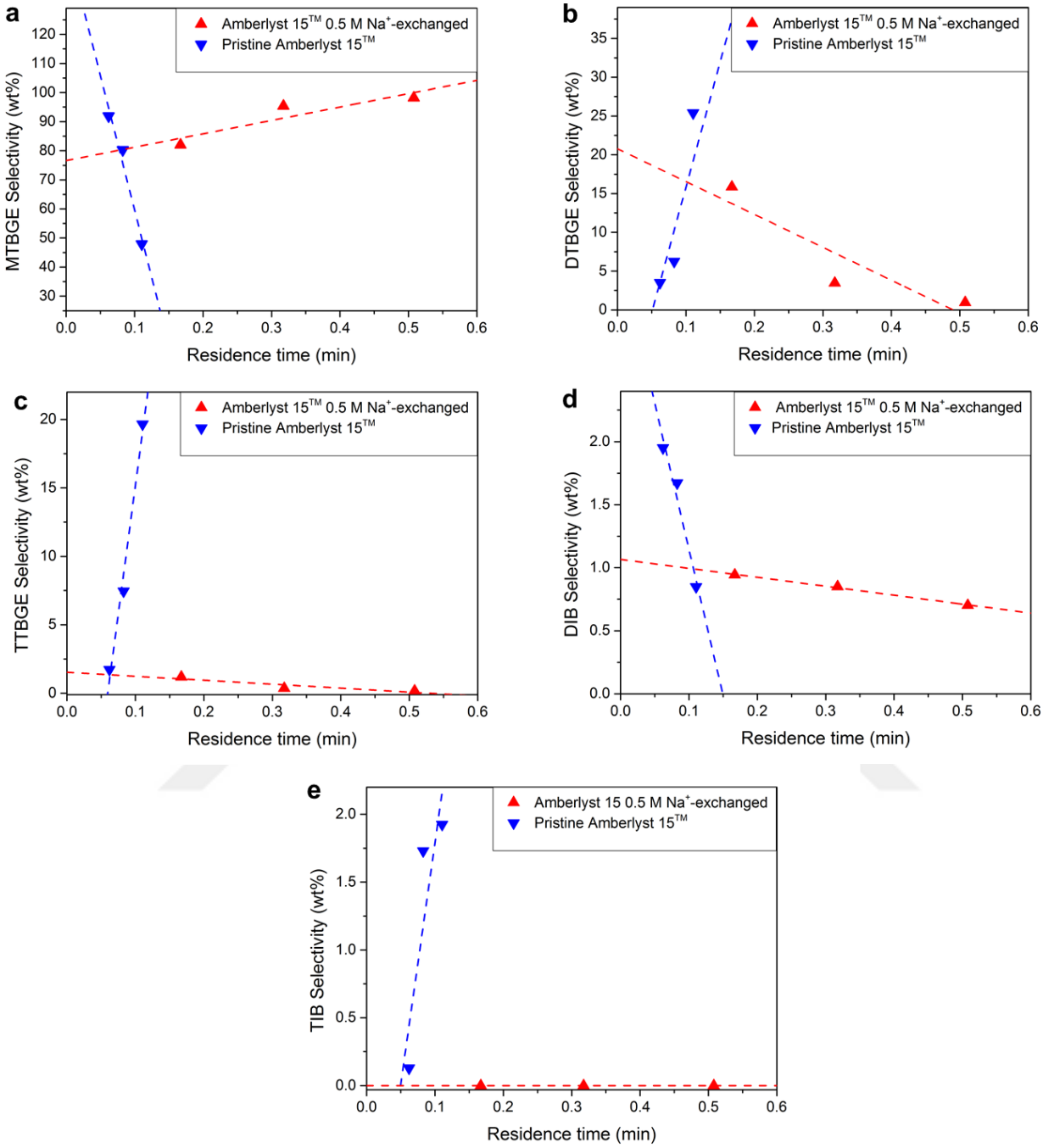

Figure 4-6. Catalytic performance of pristine and 0.5 M Na^+-exchanged Amberlyst 15™ in flow reactor under differential conversion conditions (at ≤3 wt% glycerol conversion, 250-425 μm catalyst size, 75 °C, 15±3 bar, IB:G=3:1 mol:mol, glycerol space velocity of 2-20 $mol_{glycerol} \times (mol_{H^+} \times min)^{-1}$.

According to the results presented in **Figure 4-6**, identities of the primary and secondary products were different on pristine and 0.5 M Na^+-exchanged Amberlyst 15^{TM}. For instance, on both of these catalysts, MTBGE was identified as a primary product (**Figure 4-6 a**). Data further indicated that while DTBGE and TTBGE form as secondary product on pristine Amberlyst 15^{TM}, these higher ethers could form simultaneously with MTBGE as primary products on 0.5 M Na^+-exchanged Amberlyst 15^{TM} (**Figure 4-6 b-c**). We also considered plotting product selectivity as a function of glycerol conversion. The assignment of primary and secondary products did not change **(Figure B-16).** However, the experimental error associated with the liquid product collection and quantification steps resulted in ±0.8 error in terms of wt% in the calculated glycerol conversion. Therefore, we preferred to report the selectivity vs. residence time plots rather than reporting the change in conversion and we noted that the glycerol conversion did not exceed 3 wt% even at the highest residence times that we considered in **Figure 4-6**.

The conversion range in **Figure 4-6** is considerably lower than the phase-merge conversion (approximately 60 wt% [38,40]), thus at these very low conversions the MTBGE is the main product. The data of the pristine catalyst indicate that the selectivity of this primary product decreases with increasing residence time (the conversion was in the differential conversion range). This decrease in MTBGE selectivity was accompanied by an increase in the selectivities of DTBGE, TTBGE, and a decrease in DIB selectivity. However, on the Na^+-exchanged catalysts, the protonated glycerol interacts with isobutene to form a stable adsorbed intermediate, which can have another chance for reacting to form DTBGE and TTBGE before being desorbed from the surface. This is why these higher molecular weight ethers are also primary products on Na^+-exchanged catalyst. At higher residence times on the same catalyst (still at differential conversions), on the other hand, the MTBGE selectivity increases with a corresponding decrease in DTBGE, TTBGE, and DIB selectivity. We speculate that when the

residence time increases, the newly formed primary products may re-adsorb and react to form secondary products at longer residence times. This possibility might be leading to a decrease in the amount of DTBGE or TTBGE through their interaction with the pre-adsorbed protonated glycerol to form more MTBGE as the amount of isobutene dissolved in glycerol is limited. Hence, the MTBGE is formed both as a primary and a secondary product on Na^+-exchanged catalysts as indicated by an increase in its selectivity accompanied by a decrease in the selectivity of higher ethers with an increase in the residence time. Data further indicated that DIB is also a primary product on both of the catalysts; however, the selectivity for this product was significantly lower on the catalyst with stronger acid sites (and with lower acid density) (**Figure 4-6 d**). TIB, on the other hand, was detected as a secondary product on pristine catalyst, while it was not detectable on the Na^+-exchanged catalyst (**Figure 4-6 e**).

Based on these flow reactor results, our understanding on the effect of acid strength on the reaction network is as follows: The catalytic Brønsted acid sites in Amberlyst 15^{TM} are –SO_3H groups. Sodium cations act as Lewis acids attracting electron density from nearby Brønsted acid groups, weakening the Brønsted acid O–H bonds (as shown by DFT-calculated electrostatic potential maps presented in **Figure B-11**. The effect of Na^+ ions' Lewis acidity in catalysis is neglected, as Lewis acid catalysts are much less active than Brønsted acid catalysts for the etherification reaction. To rule out the possibility of having an activity on Lewis acid sites, we saturated the catalyst with Na^+ using an ion-exchange solution with a much higher Na^+ concentration of 1.0 M. The catalytic performance test performed on this catalyst showed that the glycerol conversion was almost negligible. Thus, we infer that Na^+ interacts with the reacting species electrostatically, but not catalytically. We also assume the solvating environment to remain constant such that a nearby Na^+ cation or a nearby protonic site interacts with the adsorbed (and protonated) reactant to a similar degree. Strong interaction of the active [–SO_3H] site with glycerol and the relatively polar intermediate/product MTBGE in Na^+-

exchanged Amberlyst 15^{TM} might be favoring the reaction to cascade to produce bulkier ethers, provided that a sufficient number of isobutene molecules are available in the reaction environment. At the [–SO_3H] sites with higher acid strength, the higher molecular weight ether is protonated more easily, moreover the transition state of the protonated ether and isobutene is anticipated to have a higher stability resulting in preferred formation of DTBGE and TTBGE. In the meantime, the competitive adsorption of relatively less polar isobutene on the active sites to produce dimers and higher oligomers is inhibited. On the pristine catalyst, MTBGE cannot stay on the active site because of its weaker adsorption and it is desorbed before finding any chance for forming higher ethers. Here, we also note that apart from the acid strength effect, the proximity effect can also be influential. Isobutene concentration in the reaction medium is higher than glycerol concentration (IB:G=3:1 in mol basis). Partial neutralization of the active sites by Na^+-exchange might be isolating the active sites and preventing the accumulation of multiple isobutene molecules around the sites. According to our results, the occurrence of glycerol etherification in the case of isolated sites supports the Eley-Rideal mechanism. The Langmuir-Hinshelwood mechanism would require nearby sites for separate glycerol and isobutene adsorption to initiate glycerol etherification, which is much less possible because of the site isolation especially in catalysts with a high degree of Na^+-exchange.

Hence, we infer that elucidation of the variations in acid strength in resin catalysts with different degrees of cation exchange provides a crucial understanding on the structural-performance relationships of these industrially important class of catalysts. We emphasize that these results obtained using flow reactors also set the basis for an ongoing study focusing solely on the kinetics of the complex reaction network.

4.4.Conclusion

An IR spectroscopy-based methodology for assessing the Brønsted acid strength of partially sodium exchanged Amberlyst 15^{TM} is presented. The ν(N–H) band positions in ammonia chemisorbed Amberlyst 15^{TM} samples reveal that the acid strength increases with decreasing acid capacity upon sodium exchange. DFT calculations confirmed these results and indicated that the DPE of a sulfonated styrene group decreases upon Na^+ exchange on its neighboring counterparts. Consequences of the variation in acid strength upon cation exchange were investigated on glycerol etherification with isobutene to produce green alternative fuel additives. Product selectivity at high glycerol conversion (> 99 wt%) illustrates a strong correlation with the acid strength probed by ν(N–H) bands on the corresponding Amberlyst 15^{TM} samples with different Na^+-exchange degrees. Accordingly, the product selectivity towards higher ethers is improved by limiting the isobutene oligomerization with an increase in acid strength. Flow reactor measurements were also performed, for the first time, focusing on very low glycerol conversions to provide a better understanding on the consequences of changes in acid strength on the fate of very first glycerol molecules interacting with the active sites. Data indicated the formation of higher glycerol ethers as the primary products on Na^+-exchanged catalyst, while they were the secondary products on the pristine catalyst. These results provide opportunities for the assessment of the variations in acid strength in resin catalysts and for the determination of their consequent effects on the product selectivities.

4.5.Supplementary Material

Additional data on ammonia pulse chemisorption, TGA analysis and FTIR spectra of Amberlyst 15^{TM} samples, DFT model of Amberlyst 15^{TM} including the Cartesian coordinates, a simplified scheme of the flow reactor system and the catalytic performance of heteropolyacid catalysts in the batch reactor are provided in the **Appendix B**.

Chapter 5

Etherification of Glycerol with Isobutene in a Once-Through Fixed Bed Tubular Flow Reactor

5.1.Introduction

Glycerol (G) market is currently exploited by the food & beverage, pharma, personal care and healthcare industries [237]. The global glycerol consumption is expected to reach 4.1 million tons by 2022. Global biodiesel production, on the other hand, is projected to exceed 35 million tons in 2021 [238,239]. More than 65% of the global glycerol market is fed by the biodiesel industry, where each 10 kg of biodiesel is associated with the production of one kg of crude glycerol [36]. Increasing demand to the bio-based and renewable chemicals is forecasted to trigger the transformation of glycerol to biolubricants, biopolymers, and biofuels [240].

Etherification of glycerol with isobutene is a route for the conversion of glycerol into fuel additives, called glycerol tertiary butyl ethers (GTBE). Mono-, di-, and tri-GTBE are formed in the consecutive reaction system: G → MTBGE → DTBGE → TTBGE depending on how many isobutene molecules are incorporated into the glycerol backbone. DTBGE and TTBGE are the desired ether products because of their relatively lower polarity compared to that of MTBG, thus they offer a better miscibility with hydrocarbon fuels [38,39,181]. GTBE can directly be blended with diesel, biodiesel and gasoline and it can be used in the existing internal-combustion engine configurations without any need for any significant modifications [34,36,204]. GTBE blended with diesel fuel improves the cetane number, reduces viscosity, and diminished emissions of particulates and NO_x [14,87,88,241]. Gasoline blends with GTBE, however, have not been widely studied. Improvement in gasoline octane number upon GTBE blending was reported in a few patents [242,243]. GTBE is claimed to have a potential to replace the conventional gasoline additive methyl *tert*-butyl-ether (MTBE), which is classified as an environmental pollutant contaminating the groundwater sources in several countries in EU together with US and Japan [204,244-246].

Glycerol etherification with isobutene has been performed in batch reactors, which are quite limited in terms of capacity, and the literature lacks any investigation on this reaction carried out in a flow reactor system. Several patents have embodied GTBE production in continuous stirred tank reactors (CSTR) using homogeneous or heterogeneous catalysts [241,247-250]. Fixed bed reactor systems, on the other hand, enable working with heterogeneous catalysts without any need for separation of the catalyst particles from the product. A patent, in this regard, has implicitly demonstrated that the etherification of glycerol with isobutene could be performed in a fixed-bed reactor [248].

Here, we aim at unlocking the full potential of operation in a tubular flow reactor for the glycerol etherification with isobutene. We present the results of our investigation on a lab-scale once-through fixed-bed flow reactor system using Amberlyst 15™ ion exchange resin as catalyst with strong emphasis on the operational parameters determined by the transport limitations. We report the effect of catalyst particle size, space velocity, temperature, and isobutene: glycerol molar ratio on the catalytic performance and on the desired ether production rate, to the best of our knowledge, for the first time in literature. The assessment of external and internal mass transfer limitations at different space velocities were done by applying Mears and Weisz-Prater criteria. We also compared the rates of desired ether production of the flow reactor with those of a batch reactor. Results demonstrate that the flow reactor operation offers a broad potential for the large-scale conversion of bio-glycerol to liquid fuel additives that could potentially replace environmentally unfriendly MTBE.

5.2.Material and Methods

5.2.1. Chemicals

Amberlyst 15^{TM} (dry) ion exchange resin (Dow Chemical Co.) was used as the catalyst in glycerol etherification with isobutene. The resin beads of 400-700 μm diameter were crushed and sieved into smaller particle sizes of 53-75 μm, 75-125 μm, 125-250 μm and 250-425 μm to study particle size effect in the reactor. The catalysts were dried in a vacuum oven for 2 h at 110 °C prior to use. Ethanol (≥ 99.8%, Sigma Aldrich), 1-octanol (≥ 99.0%, Merck), (±)-3-*tert*-butoxy-1,2-propanediol (≥ 97.0%, Sigma Aldrich) and 2,4,4-trimethylpentene (≥ 90.0%, Merck) were used in gas chromatograph (GC) calibration and sample preparation.

5.2.2. Flow reactor operation

Reactions were carried in a once through 1/4" stainless steel tube located in a three-zone furnace (Thermocraft) with three independent temperature controllers. The reactor system is illustrated in **Scheme 5-1**. The reactor was heated to the desired reaction temperature and pressurized with nitrogen. Reactor temperatures of 65, 75, 85 and 95 °C were applied. Reactor pressure was controlled by a back pressure regulator (Equilibar) whose diaphragm was adjusted by high pressure nitrogen. The pressure was kept at 15 bar. Feeding of the isobutene and glycerol reactants in liquid phase to the reactor was done by two separate high pressure syringe pumps (Iscopump 500D). Flow rates varied between 0.03-0.16 ml glycerol/min and 0.129-0.776 ml isobutene/min, and the catalyst loading changed from 40-450 mg to achieve glycerol based space velocities from 5 to 500 $g_{glycerol} \times (g_{cat} \times h)^{-1}$, corresponding to to the residence times from 12 to 0.12 min. Tested molar feed ratios of isobutene to glycerol were 2:1, 3:1 and 4:1 mol:mol. Glycerol based space velocity was calculated as:

$$\boldsymbol{Space\ velocity}\ \left[\frac{g\ Gly}{g\ cat.h}\right] = \frac{\boldsymbol{Glycerol\ mass\ flow\ rate}\ [\frac{g\ Gly}{min}]}{\boldsymbol{Catalyst\ loading}\ [g\ cat]}\ \boldsymbol{x}\ \mathbf{60}\ \frac{min}{h} \qquad \textbf{(Equation 5-1)}$$

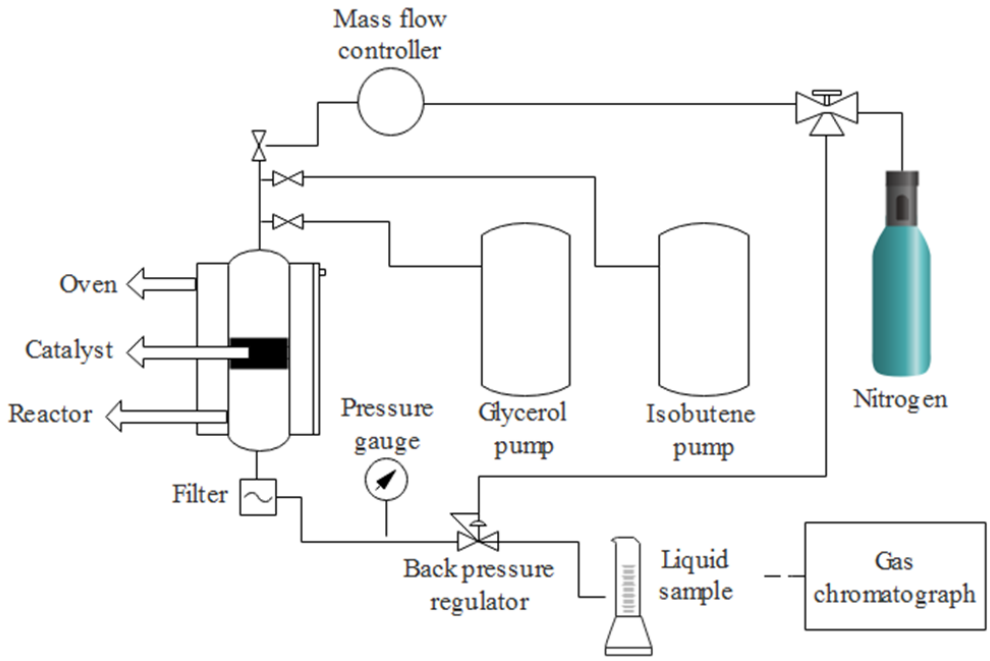

Scheme 5-1. The once-through fixed-bed tubular flow reactor set-up used for the glycerol etherification with isobutene [235].

5.2.3. Product collection and analysis

Liquid samples from the outlet of the back pressure regulator connected to the exit of the flow reactor were collected at different time-on-stream values to determine if the reaction reached the steady-state. At least three liquid samples were collected at steady-state for each different condition considered. The sample volume collected in each time was 15±5 ml. We kept the liquid samples at room temperature for a few hours to remove any unconverted isobutene dissolved in the liquid product. Depending on the extent of glycerol conversion, the liquid samples were present in either a single-phase or two-phase. For instance, conversions smaller than 9 wt% yielded in a single glycerol-rich phase, whereas above 85 wt% resulted in a single ether- (and oligomer-) rich phase. Reaction samples with two phases corresponded to a glycerol conversion in between these two limits. Mass of each phase was measured to calculate the overall product selectivity in each sample.

Composition of each phase was analyzed by an offline gas chromatography (GC, Agilent 7820 GC with flame ionization detector (FID) with HP Innowax column (30 m × 0.25 mm × 0.25 µm)). Octanol was used as the internal standard. 0.5±0.1 g sample from the phase was mixed with 0.165±0.005 g octanol and diluted to 10 ml with ethanol. Sample injection volume was 1 µl and the split ratio was 100:1. Oven temperature was increased from 40 to 240 °C at a ramp rate of 10 °C/min and kept at 240 °C for 6 min. To quantify the amounts of glycerol, mono-*tert*-butyl glycerol ether (MTBGE), and di-isobutene (DIB), we used calibration equations retrieved by us using the commercially available standards. Quantification of di-*tert*-butyl glycerol ether (DTBGE), tri-*tert*-butyl glycerol ether (TTBGE), tri-isobutene (TIB), tetra-isobutene (TetraIB), and *tert*-butyl alcohol (TBA) were done by their carbon-number based response factors [188]. Glycerol conversion was calculated by subtracting the total mass of unconverted glycerol distributed in the upper and lower phases (mainly in the lower phase) from the mass of the inlet glycerol fed to the reactor from the syringe pump during that corresponding liquid sample interval. Glycerol conversion rates were obtained by considering the glycerol conversion and space velocity together:

$$\textbf{Glycerol conversion rate}\left[\frac{g\ Gly\ converted}{g\ cat.h}\right] = \textbf{Space velocity}\left[\frac{g\ Gly}{g\ cat.h}\right] x\ \frac{\%\ Glycerol\ conversion}{100} \qquad \textbf{(Equation 5-2)}$$

Yield of desired ethers in weight basis were calculated by multiplying the weight percentages of individual ethers in the ether mixture with the weight based glycerol conversion. Rate of formation of the individual ethers were calculated using the mol based glycerol space velocity in mol glycerol/g cat.h, wherein *i* is the individual ether MTBGE, DTBGE or TTBGE:

$$\textbf{Rate}_i\left[\frac{mol\ ether}{g\ cat.h}\right] = \frac{n_i}{(n_{MTBGE} + n_{DTBGE} + n_{TTBGE})}\ x\ \frac{\%\ Glycerol\ conversion}{100}\ x\ \textbf{Space velocity}\left[\frac{mol\ Gly}{g\ cat.h}\right] \qquad \textbf{(Equation 5-3)}$$

Number of moles of individual ethers (n_i) were calculated by considering 100 g ether mixture. Rate of ether formation were converted from mole basis to gram basis by multiplying the individual rate with the molecular weights of MTBGE, DTBGE and TTBGE (148, 204 and 260 g/mol, respectively).

5.2.4. Analysis of external and internal mass transfer limitations

External mass transfer of glycerol from the liquid phase (glycerol + isobutene) and to the solid phase (Amberlyst 15^{TM} catalyst particles) was assessed by estimation of Mears parameter (C_M):

$$\boldsymbol{C_M = \frac{reaction\ rate}{mass\ transfer\ rate} = \frac{-r_{Gly,obs}\,\rho_b\,R\,n}{k_c\,C_{Gly,b}}} \qquad \textbf{(Equation 5-4)}$$

Accordingly, the external mass transfer limitations can be neglected if $C_M < 0.15$. The observed glycerol conversion rate $-r_{Gly,obs}$ in $mol_{glycerol\ converted} \times (g_{cat} \times s)^{-1}$ was obtained by multiplying the glycerol based space velocity in $mol_{glycerol} \times (g_{cat} \times s)^{-1}$ with glycerol conversion (in mol%). Bulk catalyst density, ρ_b was taken as 0.61 g/cm^3 [251]. Bulk catalyst density is related to porosity; however, we assumed the porosity to remain unchanged for the average particle diameters of 53 to 700 μm, wherein the ratio of the tube diameter to catalyst sphere diameter remained larger than 5 [252,253]. Radius of the catalyst particle, *R* was varied between 3.2 x 10^{-5} to 2.75 x 10^{-4} m from 53-75 to 400-700 μm catalyst size fractions, respectively. Reaction order with respect to glycerol was considered as first order. $C_{Gly,b}$ was the bulk concentration of glycerol in mol/ml, calculated from unconverted glycerol. Mass transfer coefficient k_c (in m/s) was calculated using the diffusivity of glycerol in the reaction mixture (in m^2/s), the corresponding Sherwood number calculated based on the flow conditions, and the catalyst diameter d_p (in m), with the formula: $\boldsymbol{k_c = \frac{D_{Gly,mix}\,Sh}{d_p}}$. The diffusivity of glycerol in the reaction mixture, $D_{Gly,mix}$, was estimated from the Wilke-Chang equation [254]: $\boldsymbol{D_{Gly,mix} = \frac{1.173x10^{-16}\,(\phi\,MA_{avg,mix})^{0.5}\,T}{\mu_{mix}\,V_{Gly}^{0.6}}}$ wherein the association parameter for glycerol (ϕ) was taken as 1.5 [236], $MA_{avg,mix}$ is the average molecular weight of the reaction mixture (between 58-66 g/mol), μ_{mix} is the average dynamic viscosity of the mixture (between 2.7-8.4 × 10^{-4} Pa.s), *T* is the reaction temperature in K, V_{Gly} is the molar volume of glycerol as 0.0962 m^3/mol. Sherwood number was calculated by: $\boldsymbol{Sh = 2 + 0.6Re^{1/2}Sc^{1/3}}$, with $\boldsymbol{Re = \frac{\rho_{mix}\,d_p\,U}{\mu_{mix}}}$ and $\boldsymbol{Sc = \frac{\upsilon_{mix}}{D_{Gly,IB}}}$. The calculated average density of the reaction mixture, ρ_{mix}, was varied between 670-790 kg/m^3.

Superficial liquid velocity, *U*, calculated from the total liquid outflow rate and 1.5×10^{-5} m^2 pipe cross-sectional area, varied between 7×10^{-5} and 2×10^{-3} m/s. Average dynamic viscosity of the reaction mixture, μ_{avg}, was estimated from the individual dynamic viscosities of the components assuming ideal solution [255]: $\boldsymbol{ln(\mu_{ideal}) = \sum x_i\, ln(\mu_i)}$. Dynamic viscosities of glycerol, isobutene, ethers, and oligomers were taken as 3.6×10^{-2} Pa.s (75 °C, 1 bar) [256], 9.1×10^{-5} Pa.s (taken as isobutane, 75 °C, 15 bar) [257], 5.5×10^{-3} Pa.s (40 °C, 1 bar, our data), 3.5×10^{-4} Pa.s (taken as isooctane, 75 °C, 15 bar) [258]. Average kinematic viscosity of the mixture, υ_{mix} (in m^2/s), was then calculated with the formula: $\boldsymbol{\upsilon_{mix} = \frac{\mu_{mix}}{\rho_{mix}}}$. The calculated average dynamic and kinematic viscosities of the reaction mixture were between 8.7×10^{-4} and 1.5×10^{-3} Pa.s and 1.2×10^{-6} and 1.9×10^{-6} m^2/s, respectively.

Another method to assess the adequacy of the external mass transport is to evaluate the change in reaction rate with the superficial flow velocity. If the velocity is high enough to reduce the external resistance across the catalyst pellet, the mass transfer coefficient k_c becomes large to make the external mass transport limitations negligible. Thus, we also plotted the glycerol conversion rate as a function of superficial flow velocity to double check the presence of any significant external mass transfer limitations.

Internal mass transfer of glycerol from the catalyst surface to the inner pores is limited if the diffusion rate is small compared to the reaction rate. Weisz-Prater parameter (C_{WP}) indicates whether internal mass transfer limitations can be neglected or not [259]:

$$\boldsymbol{C_{WP} = \frac{reaction\ rate}{diffusion\ rate} = \frac{-r_{Gly,obs}\,\rho_b\,R^2}{D_e\,C_{Gly,s}}} \qquad \textbf{(Equation 5-5)}$$

Accordingly, when $C_{WP} << 1$, internal mass transfer limitations are negligible. The effective diffusivity was calculated with the formula $\boldsymbol{D_e = \frac{D_{Gly,mix}\,\phi_p\,\sigma_c}{\tau}}$ by taking ϕ_p (pellet porosity) = 0.36, τ (tortuosity) = 1.3, σ_c (constriction factor) = 1 [251]. The surface concentration of glycerol, $C_{Gly,s}$, was taken as equal to bulk glycerol concentration, as in most cases our system was free from external mass transfer limitations ($C_M < 0.15$).

5.3.Results and Discussion

5.3.1. Assessment of transport limitations

Pressure drop can be a significant issue when operating with viscous liquids, such as glycerol, in a flow reactor. Thus, we first worked on determining the smallest particle size, which does not impose any significant pressure drop. For this purpose, we tested different Amberlyst 15™ catalyst size fractions of 53-75, 75-125, 125-250, and 250-425 μm along with the original bead size of 400-700 μm at a low (25 $g_{glycerol} \times (g_{cat} \times h)^{-1}$) and a high (150 $g_{glycerol} \times (g_{cat} \times h)^{-1}$) glycerol space velocities. Reaction conditions were set to 75 °C, IB:G=3 (isobutene:glycerol molar feed ratio), and 15 bar. The pressure drop was considered as the difference between the set pressure of the glycerol syringe pump and that at the reactor outlet. Accordingly, for the 53-75 μm particle size fraction, a pressure drop of up to 50 bar was experienced, whereas the corresponding pressure drop values were up to 24 bar and 7 bar, for the catalyst particle size fractions of 75-125 and 125-250 μm, respectively. The largest particle size fractions, 250-425 and 400-700 μm, did not give any significant pressure drop (less than 0.1 bar). Thus, we infer that the size fractions of 53-75, 75-125, and 125-250 μm were not suitable for continuous operation.

The calculated Mears parameters for the 250-425 μm and 400-700 μm particle sizes were lower than 0.15 at both of the low and high space velocities indicating that the operation was free of any significant external mass transfer limitations on these particle size fractions. The corresponding Weisz-Prater parameters for the 250-425 μm size fraction at the low and high space velocities were 0.29 and 0.21, respectively. However, the corresponding values were 0.95 and 0.56, respectively, on the 400-700 μm size fraction, indicating that the original bead size was vulnerable to internal mass transfer limitations especially at low space velocities.

Next, we considered varying the glycerol space velocity from 5.5 to 500 $g_{glycerol} \times (g_{cat} \times h)^{-1}$ at 75 °C and 15±2 bar to determine the lowest space velocity above which the mass transfer limitations remain insignificant. **Figure 5-1** illustrates the variation of the Mears and Weisz-Prater parameter for the 250-425 μm particle size fraction. It shows that both of these paramters are below their corresponding limiting values for a significant transport limitation. Thus, we infer that both external and internal mass transport resistance can be neglected in the tested space velocity range. Moreover, glycerol conversion rate remained almost constant with varying superficial flow velocity for this catalyst fraction (**Figure C-1**). The rates of glycerol conversion were calculated by multiplying the glycerol conversion with the space velocity. The reaction system does not have significant external mass transfer limitations, as the glycerol conversion rate was stable around 7.0±1.5 $g_{glycerol\ converted} \times (g_{cat} \times h)^{-1}$ for the applied superficial velocities between $2x10^{-4}$-$1.1x10^{-3}$ m/s corresponding to the nine tested space velocities.

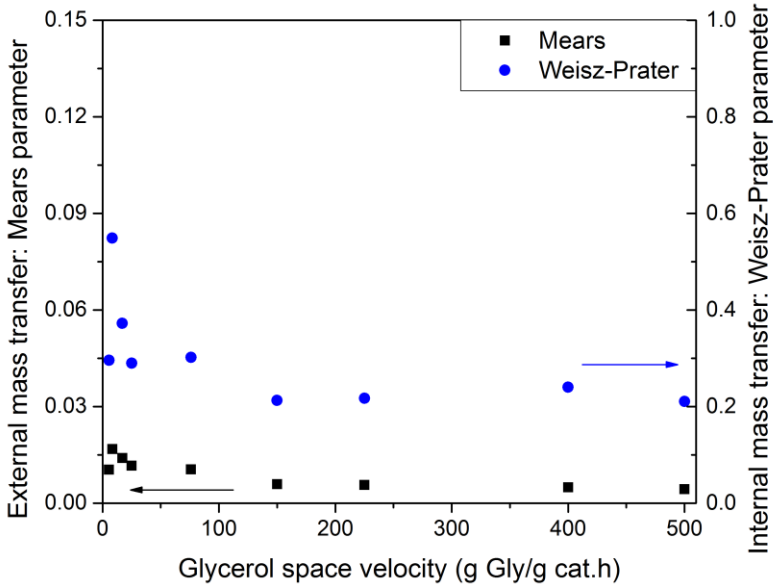

Figure 5-1. Calculated Mears and Weisz-Prater parameters as a function of space velocity at 5.5, 8.4, 17, 25, 76, 150, 225, 400 and 500 $g_{glycerol} \times (g_{cat} \times h)^{-1}$ glycerol space velocity for 250-425 μm particle size at 75 °C, IB:G=3:1 mol:mol, 15±2 bar.

For the original bead size of 400-700 μm fraction, external transfer limitations can be neglected between 8.4-294 $g_{glycerol} \times (g_{cat} \times h)^{-1}$ space velocity (**Figure C-2**). **Figure C-2** supports this statement as glycerol conversion rate remained constant at around 6.2 ±0.5 $g_{glycerol\ converted} \times (g_{cat} \times h)^{-1}$ between $2x10^{-4}$-$1.7x10^{-3}$ m/s superficial space velocity interval corresponding to ≥ 8.4 $g_{glycerol} \times (g_{cat} \times h)^{-1}$. However at lower tested space velocities of 0.3, 3.0 and 7.5 $g_{glycerol} \times (g_{cat} \times h)^{-1}$, reaction rate significantly dropped indicating external mass transfer limitation. **Figure C-3** indicated that the 400-700 μm particle size may have internal mass transfer limitation at 8.4 and 25 $g_{glycerol} \times (g_{cat} \times h)^{-1}$ because the estimated Weisz-Prater number were 0.96 and 0.95, respectively, which should normally be much smaller than one to neglect internal mass transfer resistance. Thus, we infer that only the size fraction of 250-425 μm was completely free of external mass transfer limitations within the operating flow conditions.

5.3.2. Evaluation of catalytic performance

Once we determined the size fraction free of any mass transfer limitations, the glycerol conversion was varied from 1 to 100 wt% by varying the space velocity from 5.5 to 500 $g_{glycerol} \times (g_{cat} \times h)^{-1}$ (**Figure 5-2**) on this size fraction (250-425 μm). While a space velocity of 5.5 $g_{glycerol} \times (g_{cat} \times h)^{-1}$ yielded in complete glycerol conversion, a near complete (> 99 wt% but not 100%) glycerol conversion was achieved at a space velocity of 8.4 $g_{glycerol} \times (g_{cat} \times h)^{-1}$. **Figure 5-3** presents the variation of weight percent selectivity of the products, MTBGE, DTBGE, TTBGE, DIB, and TIB, with the glycerol space velocity.

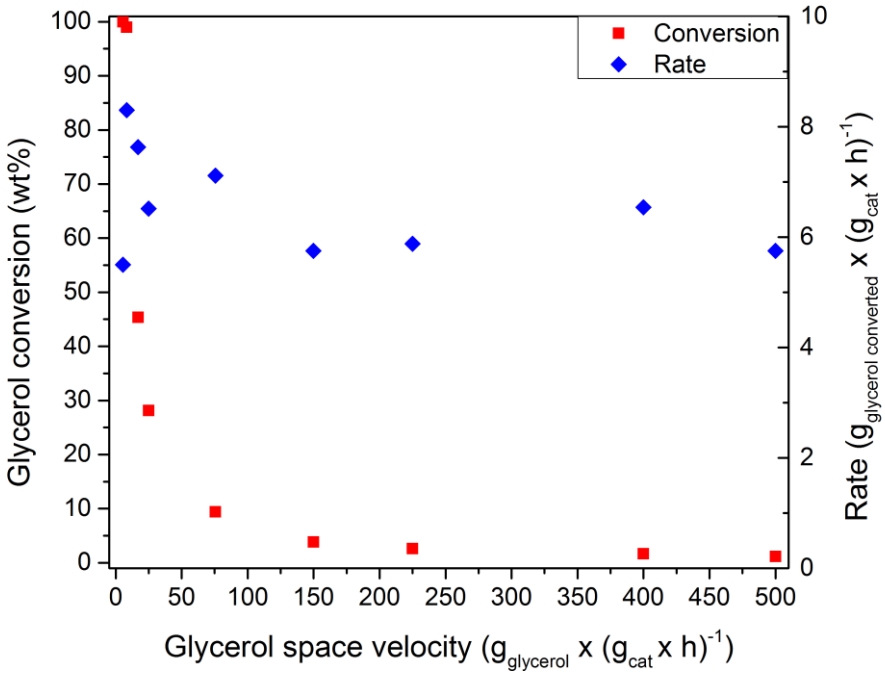

Figure 5-2. Glycerol conversion and reaction rate as a function of space velocity at from 5.5 to 500 $g_{glycerol} \times (g_{cat} \times h)^{-1}$ for Amberlyst 15™ particle size fraction of 250-425 µm at 75 °C, IB:G=3:1 mol:mol, and 15 bar.

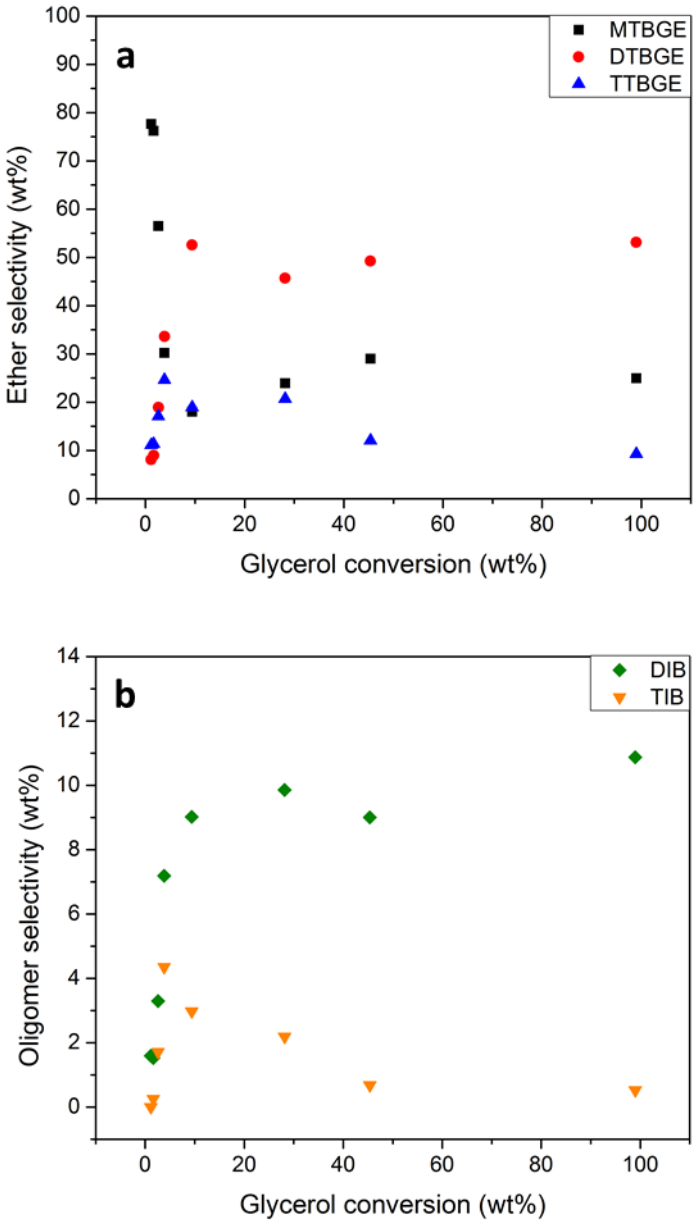

Figure 5-3. Selectivity of; **a:** ethers and **b:** oligomers in the final product mixture as a function of glycerol conversion for an Amberlyst 15™ particle size fraction of 250-425 μm in a space velocity range of from 8.4 to 500 $g_{glycerol} \times (g_{cat} \times h)^{-1}$ at 75 °C, IB:G=3:1 mol:mol, and 15 bar conditions.

As can be seen in **Figure 5-3**, MTBGE is the primary ether product formed at low (< 2 wt%) glycerol conversions. DTBGE and TTBGE formation is triggered with increasing glycerol conversion from 2 to 9 wt% at the expense of MTBGE. Therefore DTBGE and TTBGE are the secondary products of the reaction system which require MTBGE to form primarily. Product selectivities at infinitesimal glycerol conversion were studied in more detail in a recent study [189]. While MTBGE is being converted to the higher ethers, we observe increasing DIB and TIB selectivity, but still low compared to ethers. From 9 wt% to 45 wt% glycerol conversion, we observed an increase in MTBGE production with a slight decrease in TTBGE formation. The active sites would be favoring glycerol to form MTBGE, instead of favoring MTBGE to form the higher ethers In a previous study, we illustrated that the selectivity of the desired ethers can be strongly influenced by the acid strength and deprotonation energy of the individual sulfonic acid active sites [189]. For instance, the total DTBGE and TTBGE selectivity at a complete glycerol conversion was lower for the regular (pristine) Amberlyst 15^{TM} compared to its partial Na^+-exchanged of with higher strength of the sulfonic acid sites, because the formation of DTBGE and TTBGE on regular Amberlyst 15^{TM} depended on the desorption of MTBGE, and re-adsorption on the available active sites to react with isobutene further. At these mild glycerol conversion conditions (9-45 wt%) in which there are considerable amounts of glycerol and MTBGE in the reaction medium, the acid sites of Amberlyst 15^{TM} would prefer the adsorption and reaction of free glycerol molecules. Isobutene dimerization slightly increases with glycerol conversion, possibly because of diminishing glycerol coverage of the active sites (**Figure 5-3 b**). Besides, isobutene trimerization forming TIB and TTBGE formation indicated a similar pattern. Both TIB and TTBGE appear as the secondary products of the reaction system (as their selectivity approach to zero at zero glycerol conversion), forming from adsorbed DIB and DTBGE, respectively.

To determine the long term activity of the catalyst at the high (99 wt%) and mild (28 wt%) glycerol conversions, we plotted product selectivity and glycerol conversion as a function of time on stream (**Figure 5-4 a and b**). The similarity between several consecutive samples indicate that the catalyst can retain its activity for more than two days.

Yields of the desired di- and tri-ethers, as well as their production rate in gram catalyst per hour basis were plotted as a function of glycerol conversion for 8.4-500 $g_{glycerol} \times (g_{cat} \times h)^{-1}$ as shown in **Figure 5-5**. The yield of the desired ethers, namely the amount of DTBGE and TTBGE in a 100 g ether mixture multiplied by the glycerol conversion, linearly increased with glycerol conversion (**Figure 5-5 a**). Thus, the data suggest that one should work at high glycerol conversions to reach high yields of the desired products. At complete glycerol conversion, 71 wt% yield means that it is possible to obtain 71 g desired ethers (and 29 g MTBGE) from an initial of 49 g glycerol. The rate of desired ether formation increases with glycerol conversion of up to 9 wt%, then almost stabilizes at 11.4±0.8 $g_{DTBGE+TTBGE} \times (g_{cat} \times h)^{-1}$ (**Figure 5-5 b**). The volumetric productivity of the flow reactor increases with glycerol conversion and reaches to 7400 $g_{DTBGE+TTBGE} \times (L_{cat} \times h)^{-1}$ at near complete glycerol conversion (**Figure 5-5 c**).

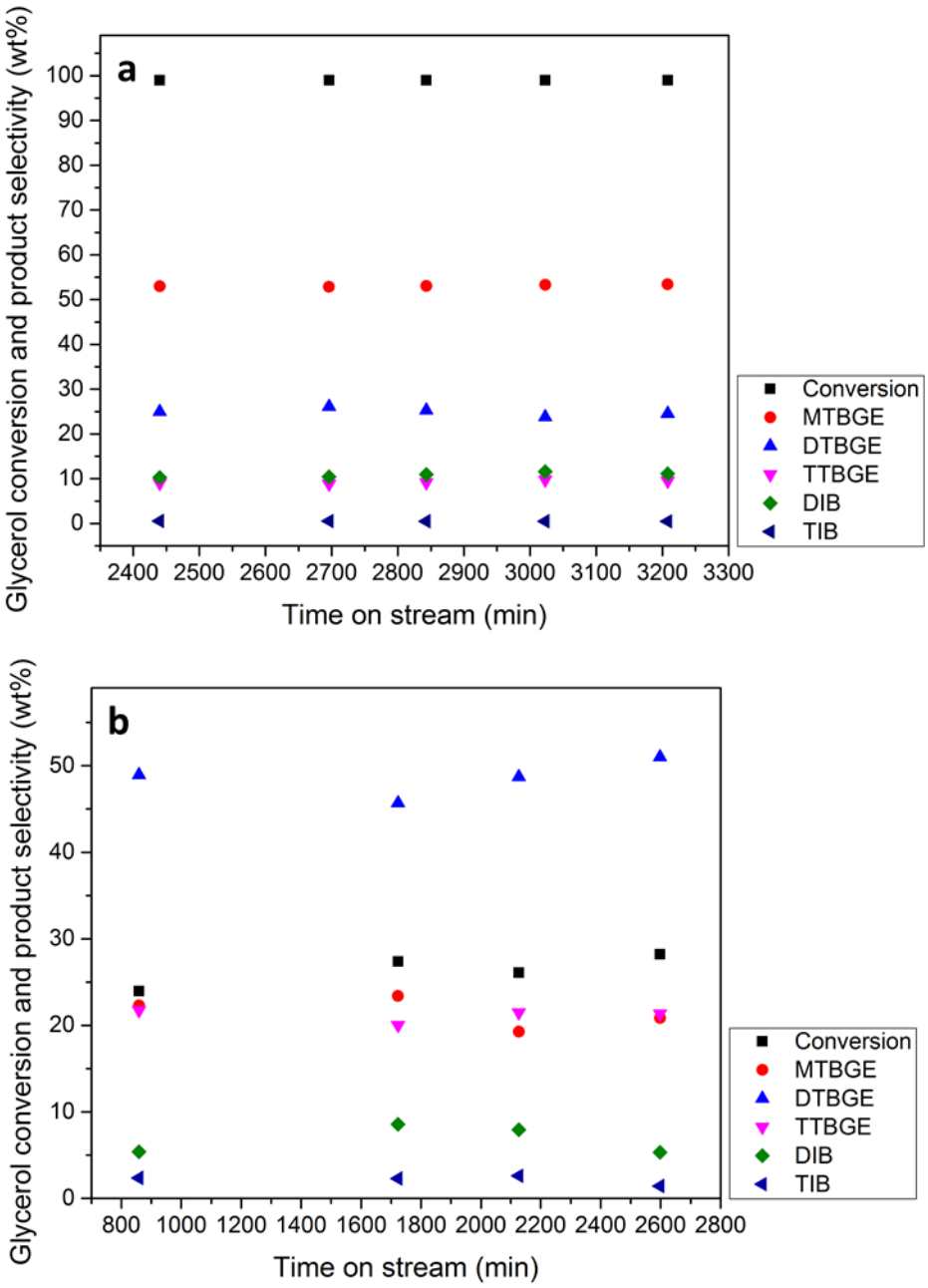

Figure 5-4. Catalytic performance of the Amberlyst 15™ in a size fraction of 250-425 μm for an extended time-on-stream of up to 2 days at; **a:** 8.4 $g_{glycerol} \times (g_{cat} \times h)^{-1}$ (note that the glycerol conversion was near complete, > 99 wt% but not 100%) and **b:** 25 $g_{glycerol} \times (g_{cat} \times h)^{-1}$ at 75 °C, IB:G=3:1 mol:mol, 15 bar.

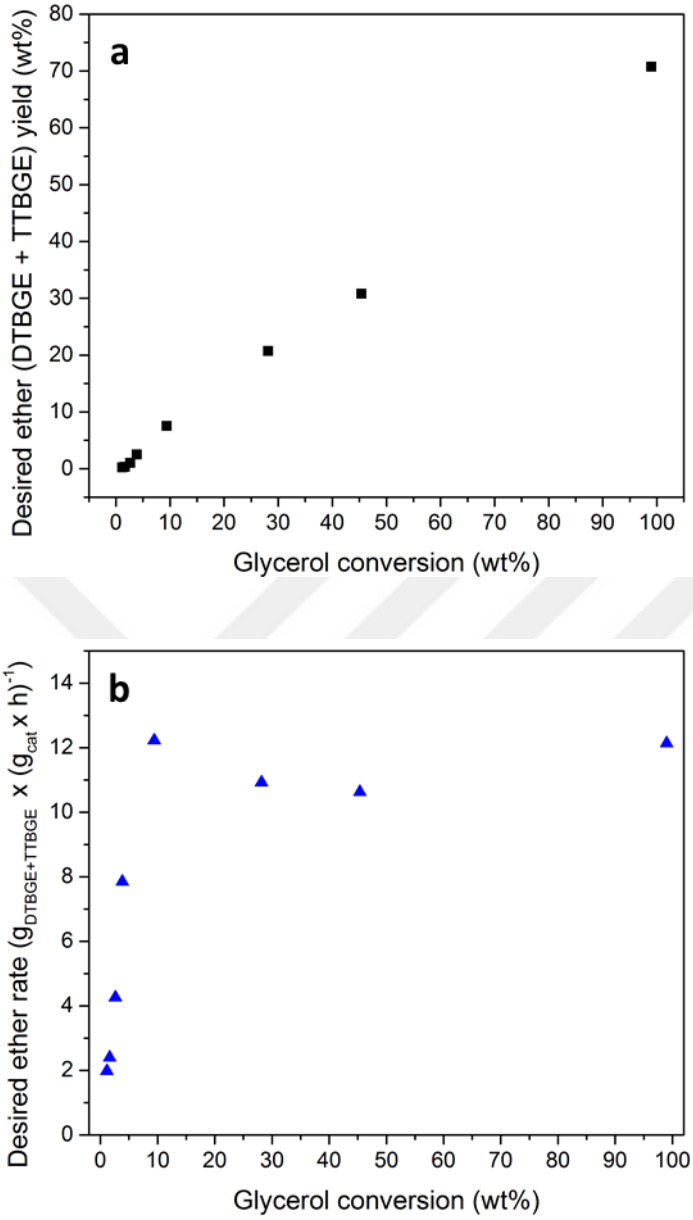
a
Desired ether (DTBGE + TTBGE) yield (wt%)
Glycerol conversion (wt%)
b
Desired ether rate ($g_{DTBGE+TTBGE}$ x (g_{cat} x h)$^{-1}$)
Glycerol conversion (wt%)

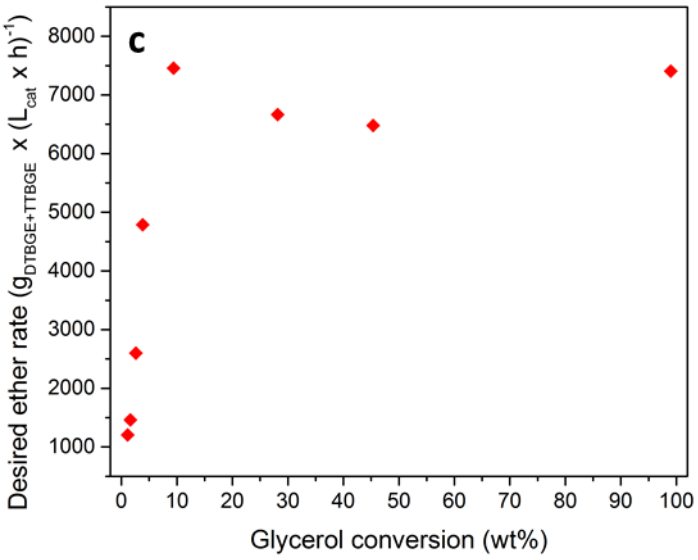

Figure 5-5. Change in **a:** desired ether (DTBGE + TTBGE) yield among all three ether products; **b:** desired ether formation rate in gram catalyst basis and c) desired ether formation rate in liter catalyst with glycerol conversion on an Amberlyst 15™ particle size fraction of 250-425 µm at a space velocity range of 8.4 to 500 $g_{glycerol} \times (g_{cat} \times h)^{-1}$ and at IB:G=3:1 mol:mol, T=75 °C, and 15 bar.

The relationship between glycerol conversion and space velocity for the 400-700 µm size fraction suggests a similar network with the 250-425 µm size fraction (**Figure C-5**). MTBGE and DIB emanate as the primary products, while DTBGE, TTBGE and TIB are the secondary products. However, isobutene oligomerization is much more pronounced in the 400-700 µm size fraction, with DIB selectivity among the other products changing between 20-40 wt% (**Figure C-5 b**). Selectivity of DIB was always lower than 11 wt% for the 250-425 µm particle fraction. We interpret the enhanced oligomerization rates in the larger particle size as slower mass transfer of isobutene in the catalyst pores so that the slowly travelling isobutene molecules find more chance on the active sites for the IB + IB → DIB reaction. Moreover, it

might be also because of the fact that some of the sites were not saturated with glycerol as it has stronger mass transfer limitations; instead, they were saturated with IB, which can undergo dimerization to form DIB in the absence of any pre-adsorbed glycerol. Desired ether yield for the original bead size linearly improved with glycerol conversion (**Figure C-6 a**), similar to that obtained with the 250-425 μm particle size. However, the highest obtained yield of desired ethers for the 400-700 fraction, 52 wt%, was much lower compared to the 250-425 μm fraction (71 wt%). The trends in the rate of desired ether formation indicate better performance of the 250-425 μm size at higher glycerol conversions (**Figure C-6 b**). Besides, the 400-700 μm particle size was associated with almost triple di-isobutene formation rates (**Figure C-6 c**) consistent with the higher isobutene conversions observed on this large particle size fraction. Consumption of more isobutene might be desirable in terms of making use of the isobutene as long as the presence of DIB and TIB molecules along with the ethers are accepted in the fuel additive formulation. We also plotted the activity of the Amberlyst 15^{TM} 400-700 μm particle size fraction during for up to 67 h time-on-stream. Stable product selectivity and glycerol conversion for the four consecutive samples taken between the 1172-4059 minutes of the experiment indicate the lack of any catalyst deactivation as in the case observed on a size fraction of 250-425 μm (**Figure C-7**).

We also tested the effect of temperature (65, 75, 85, and 95 °C) and IB:G molar feed ratio (2, 3, and 4) at 25 $g_{glycerol} \times (g_{cat} \times h)^{-1}$ to see if we can further optimize the desired ether production rate using Amberlyst 15^{TM} beads (**Figure C-8**). Desired ether rates decreased in the other tested temperatures mainly because of lower glycerol conversion, lower DTBGE selectivity and elevated DIB selectivity. IB:G ratio of 2:1 halved the glycerol conversion, while the IB:G ratio of 4 had promising results with 11.8 $g_{DTBGE+TTBGE} \times (g_{cat} \times h)^{-1}$, similar to that of IB:G=3. However, an IB:G ratio of 4 was associated with a slightly higher DIB selectivity.

Therefore, we may suggest to operate at IB:G of 3 to have still high conversion and to produce less DIB, utilizing isobutene in a more efficient way for etherification.

We have compared the performance of our flow reactor with the batch reactor systems investigated in literature with Amberlyst 15^{TM} at the comparable conditions. The details on the batch reactor experiments conducted by us was reported in a previous study [189]. Stirring rates higher than 1000 rpm were previously determined in other studies to eliminate any external mass transfer limitations for the Amberlyst beads [39,40]. We applied 1200 rpm stirring with a magnetic bar. Complete glycerol conversion was achieved within 6 h. We plotted the desired ether formation rate as a function of glycerol conversion (**Figure C-9 a** and **b**). Rates from previous literature are also included in **Figure C-9**. The maximum rate of desired ether formation in our batch system was **3.7** $g_{DTBGE+TTBGE} \times (g_{cat} \times h)^{-1}$, considering the 6 h operation with 1 h of product collection, reactor cleaning and refilling period. It should be noted that at large scale batch production, the total duration excluding the reaction may vary between 3-6 hours therefore batch productivity drops significantly [236]. Previous studies with the similar sized batch reactors (50-150 ml autoclaves) did not exceed this rate [39,52,260]. The volumetric productivity of our batch reactor at complete glycerol conversion was **66** $g_{DTBGE+TTBGE} \times (L_{reactor} \times h)^{-1}$. **7400** $g_{DTBGE+TTBGE} \times (L_{cat} \times h)^{-1}$ volumetric productivity in the flow reactor at near compete glycerol conversion was achieved using the 250-425 μm particle size fraction (**Figure 5-5 c**), Thus, the data that we present here illustrate that more than two orders of magnitude higher desired ether productivity per reactor volume could be achieved by using flow systems. Moreover, operation in flow reactors also offer a broad flexibility for the detailed analysis of the reaction kinetics for the glycerol etherification with isobutene, for which pretty much all of the studies to date use batch reactors, and thus, lack the flexibility of controllably varying the conversion to identify the consequences on the product pool.

5.4.Conclusion

Glycerol etherification with isobutene in a fixed bed tubular flow reactor system without any pressure drop and external/internal mass transfer limitations was possible by using a catalyst particle size fraction of 250-425 μm for the Amberlyst 15^{TM} cation exchange resin. A near complete glycerol conversion was achieved with this particle size at 8.4 $g_{glycerol} \times (g_{cat} \times h)^{-1}$, 75 °C, 3:1 isobutene:glycerol molar feed ratio and 15 bar conditions. Desired ether yield improved at elevated glycerol conversions. The formation rate of the desired ethers was 12 $g_{DTBGE+TTBGE} \times (g_{cat} \times h)^{-1}$, corresponding to 7400 $g_{DTBGE+TTBGE} \times (L_{cat} \times h)^{-1}$ volumetric productivity, which was significantly larger than those obtainable from the batch reactors. Thus, the results presented here demonstrate that etherification of glycerol with isobutene in a once-through fixed-bed flow reactor system offers a broad potential and flexibility both for the fundamental understanding of the reaction mechanisms on different catalysts and for scaling-up to meet the needs of industrial scale production.

5.5.Supplementary Information

Assessment of external and internal mass transfer in original Amberlyst 15^{TM} beads as well as the catalytic performance, and the productivity of the batch reactor system using Amberlyst 15^{TM} beads are presented in **Appendix C**.

Chapter 6

Compatibility of di- and tri-*tert*-butyl Glycerol Ethers with Gasoline

6.1.Introduction

Production of glycerol tertiary butyl ethers (GTBE) as alternative fuel oxygenates is a proposed route for glycerol valorization in which glycerol reacts with isobutene or tertiary butyl alcohol under mild conditions over solid Brønsted acid catalysts [71,180,192,261]. Out of three main ether products with varying degrees of isobutene incorporation, di- and tri-*tert*-butyl glycerol ethers, notated as DTBGE and TTBGE, respectively, are the desired ethers because of their better fuel mixing properties and lower water solubility compared to their mono- counterpart (**Scheme 6-1**) [13,34-36,189]. Isobutene oligomerization on the same sites produce di- and tri-isobutene (DIB and TIB) as the side products. GTBE can be obtained by employing commercial catalysts, such as Amberlyst ion exchange resins or wide pore zeolites and under reaction conditions similar to the production of well-established methyl tertiary butyl ether (MTBE) [7,8,38-40,54]. Preferred formation of DTBGE over zeolites has been claimed to be advantageous in terms of process economics because less isobutene is consumed per mol of glycerol [44,54]. However, the effect of DTBGE concentration in the downstream process as well as the fuel compatibility of the purified products have not been elaborated in literature. In this study, we first investigated the effect of GTBE content on physical properties of the GTBE mixtures. The GTBE mixtures mainly consisted of DTBGE and TTBGE (62-86 wt% DTBGE and 1-34 wt% TTBGE) and low amounts (< 12 wt%) of MTBGE. MTBGE is fully miscible at low concentrations in DTBGE and TTBGE mixtures [38,103].

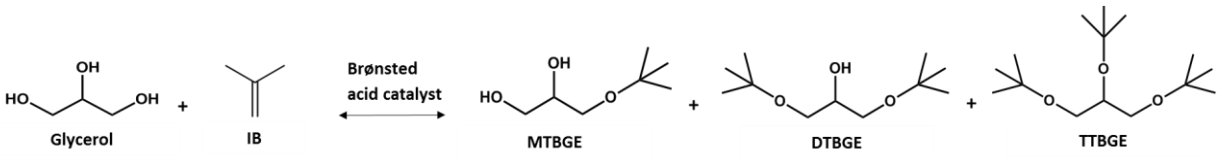

Scheme 6-1. Etherification of glycerol with isobutene to produce glycerol tertiary butyl ethers.

GTBE was previously shown to deliver similar octane boosting properties of MTBE when blended with gasoline. Adding 10 vol% GTBE with 7 wt% MTBGE, 68 wt% DTBGE and 25 wt% TTBGE content to gasoline improved the research octane number (RON) from 97.1 to 99.3 [242]. In a recent patent, blending pure MTBGE or pure DTBGE with gasoline from 1:99 to 10:90 volumetric proportions resulted in octane number improvement from RON of 94.1 up to 97.4, while the vapor pressure of blend decreased with increasing GTBE content [243]. GTBE was also anticipated to lower the viscosity of gasoline and reduce the particulate and NO_X emissions [14,88]. To our knowledge, no study has covered the power and emission performance of GTBE-gasoline blends in a gasoline engine. With this study, besides the physical properties of GTBE mixtures, we also examined the fuel characteristics of these mixtures blended at a ratio of 3.45 vol% with gasoline. Findings indicate improved octane number and reduced vapor pressure upon GTBE blending. The engine power-torque and exhaust emission tests demonstrated the applicability of GTBE as an alternative gasoline additive to MTBE. According to our experimental results, GTBE decreases the carbon dioxide and carbon monoxide emissions of gasoline under urban driving conditions.

6.2.Material and Methods

6.2.1. Production of GTBE

Amberlyst 15^{TM} (dry, Dow Chemicals) and Zeolite H-Beta (CP811C-300, Si/Al=150, Zeolyst International) were used as the catalysts for glycerol etherification. Amberlyst 15^{TM} was kept in a desiccator and used without any pretreatment. Zeolite H-Beta was calcined at 500 °C for 5 h in static air prior to use. Glycerol etherification with isobutene was performed in a multiple batch reactor system (Parr Series 5000). The aim was to produce high amount of liquid products, up to 500 ml from each catalyst using several batches. Each reactor of 75 ml coupled with a magnetic stirring system was first filled with 6.0 g glycerol (≥ 99.5%, Sigma Aldrich),

then 0.45 g Amberlyst 15^{TM} or H-Beta was added on glycerol, corresponding to 7.5 wt% catalyst loading. After the lid was sealed, the reactor was pressurized to 8.0 bar with N_2 and then 18 ml (11 g) of liquefied isobutene (99.9%, Messer) was transferred into the reactor. The reactor was heated to 75 °C, resulting an initial reaction pressure of 10.5±1 bar. The reaction was conducted at a stirring speed of 1200 rpm, for 6 hours. At the end of the batch runs, liquid products were separated from the solid catalyst particles first by means of a centrifuge and then by using syringe filters. Each reactor yielded approximately 15 ml product. Liquid products collected from the Amberlyst 15^{TM} experiments were mixed together and stored. The same procedure was applied to the products obtained using H-Beta as the catalyst.

Content of the product mixtures was determined by an Agilent 7890B gas chromatograph (GC) equipped with an FID detector. Retention times of the compounds were validated by a 5977A Series GC/mass spectrometer. An HP Innowax column (30 m x 0.25 mm x 0.25 µm) was used for chromatographic separations. Octanol was used as the internal standard. Calibration line equations for glycerol, mono-ether ((±)-3-*tert*-butoxy-1,2-propanediol, ≥ 97.0%, Aldrich), and di-isobutene (2,4,4-trimethylpentene, ≥ 90.0%, Merck) were experimentally obtained using the commercially available compounds. Calibration equations for commercially unavailable di-ether, tri-ether, tri-isobutene, tetra-isobutene, and tertiary butyl alcohol were calculated by using GC-FID response factor method [188]. The GC samples to be injected were prepared by mixing 165.0±0.5 mg octanol (≥ 99.0%, Merck) with 510±1 mg homogenized product, diluting to 10 ml with ethanol (≥ 99.8%, Sigma Aldrich) and vortexing vigorously. 1 µl sample was injected in split mode (100:1 split ratio). The initial oven temperature of 40 °C was ramped to 240 °C with 10 °C/min increment. Amounts of each compound in the product mixture were determined from the FID area data.

The GTBE products (either produced by using Amberlyst 15^{TM} or zeolite H-Beta as catalyst for the batch runs) were subjected to a purification step to remove the MTBGE and

DIB, yielding in a mixture consisting mainly of DTBGE and TTBGE. First, 500 ml product was mixed with 1 L deionized water in a 2 L separatory funnel with a tap at the bottom, shaked for 5 minutes vigorously and set to decantation for 2 h. The lower phase consisted of water with dissolved MTBGE, while the upper phase contained di-isobutene (DIB), tri-isobutene (TIB), DTBGE, TTBGE, and trace amounts of MTBGE. Using the tap, most of the lower phase was discharged. This procedure was repeated two more times. Finally, the upper phase was transferred to a round bottom evaporation flask (500 ml) and distilled to separate residual DIB and water for 2 hours at 100 mbar and 4 hours at 5 mbar at 55 °C in a rotary evaporator (Rotavap). The liquid phase remained in the evaporation flask containing GTBE mixture was subjected to GC analysis. Approximately 300 ml final liquid phase was obtained from each catalyst. The purified GTBE mixtures obtained from Amberlyst 15^{TM} and H-Beta were considered as the two stock mixtures for the preparation of four more GTBE mixtures. Following the GC analysis, the volumes of stock mixtures to be mixed were calculated by envisaging equal increments in product weight percentages for MTBGE, DTBGE, and TTBGE between each sample. In overall, six different ether surrogates with varying ether concentrations were formulated.

6.2.2. Analysis of the GTBE mixtures

Approximately 20 ml from each ether surrogate was allocated for the tests. Standard methods ASTM D4052 density (KYOTO-KEM DA-645), ASTM D6304 Karl Fischer water content (Kyoto MKC-610DT), ASTM D445 kinematic viscosity (PAC-Herzog HVM 472), ASTM D4809 gross heat of combustion (Parr 6400), ASTM D6079 lubricity (PCS Instruments HFRR), ASTM D1218 refractive index (Kem RA 600) and ASTM D7334 contact angle (Theta Lite Optical Densitometers TL 100) were applied to each mixture. Solubility of water in GTBE mixtures was determined by volumetric titration in which 1±0.03 g sample was mixed with 3±0.02 g of water, the solutions were kept at room temperature for 24 h for phase separation,

and finally the GTBE mixture containing upper phases were analyzed with ASTM D6304 Karl Fischer method. Infrared spectroscopic measurements of the GTBE mixtures were performed using a FTIR-ATR (Perkin Elmer-Frontier) in absorbance mode at 4 cm^{-1} resolution and the spectra were atmospherically corrected. Mass fractions of individual components in GTBE mixtures were analyzed by GC-FID. These mass fractions and mixture densities were inserted in equation $\boldsymbol{\rho_{mix}} = \sum \boldsymbol{x_i}\, \boldsymbol{\rho_i}$ in Matlab to calculate the individual densities of MTBGE, DTBGE, and TTBGE (notated as *i*). This equation assumes density of pure components to be close to the mixture densities. Therefore, mass fractions were taken equal to the volume fractions. Indeed, the differences between the mass and calculated volume fractions of MTBGE, DTBGE, and TTBGE were smaller than 2%.

6.2.3. Analysis of the GTBE mixtures-reference gasoline blends

Blends were prepared corresponding to 3.45 vol% GTBE mixture and 96.55 vol% reference gasoline. The refinery-based reference gasoline originates from the outlets of the continuous catalytic reforming (CCR) and C5-C6 isomerization units. The octane number of the reference gasoline was 95.0, and had no fuel additive (MTBE, etc.). Fuel properties and hydrocarbon content of the reference gasoline are given in **Table D-1** and **Figure D-1**, in **Appendix D**. Boiling point distribution of the reference gasoline was obtained by ASTM D86 atmospheric distillation (PAC OptiDist). Properties of fuel blends were determined by the following methods: ASTM D2699 octane number (Waukesha CFR), ASTM D4052 density (Kem DA 625), ASTM D5191 dry vapor pressure equivalent (PAC-Herzog HVP 972), ASTM D381 gum content (Seta Existent Gum Solid Block Bath - Steam or Air), ASTM D4809 gross heat of combustion (Parr 6400) and ASTM D525 induction period (Seta 15400).

6.2.4. Fuel performance tests

Reference gasoline, 3.45 vol% GTBE-blended reference gasoline, and 3.45 vol% MTBE-blended reference gasoline each 120 L were used for the fuel performance tests. An internal combustion engine of 1.0 L volume, 125 PS (93 kW) power, with three cylinders and with a turbocharged gasoline direct injection (GTDI) system integrated to 380 kW low inertia AVL Spirit engine dynamometer was used. The experimental setup is illustrated in **Scheme 6-2**. Engine test points were selected as the Engine Performance Curve (Full Load Curve) between 1000-6500 rpm (13 points) and an additional 5-part load data were selected within the emission cycle of New European Driving Cycle (NEDC) (points 14-18). In the full load curve, the accelerator pedal was 100% depressed so that maximum torque was obtained from the engine. However, the NEDC conditions fix the torque at a given engine speed at low pedal depression values (between 13-36%) adjusted during the experiment to provide the desired torque and engine speed. In all tests performed on the reference gasoline, MTBE blended gasoline and GTBE blended gasoline, the engine oil temperature was kept at 92±4 °C, while the differences in air suction temperature were less than 1 °C.

The data was collected after at least 5 minutes of waiting period for the stabilization of each measurement point. After stabilization, data was stored at a frequency of 10 Hz by the engine dynamometer automation system for 30 seconds. The emissions of CO_2, CO, NO_x and total hydrocarbon emissions (THC) were retrieved with AVL AMA i60 Exhaust Measurement System. For emissions, the average of 300 measurements were taken during the 30-second data recording. The emission values reported are the engine-out results. The power output of the engine dynamometer was calculated using **Equation 6-1**.

$$Power\ [W] = \frac{Torque\ [Nm]\ x\ Speed\ [rpm]}{9.5488} \qquad \textbf{(Equation 6-1)}$$

Fuel consumption was measured in kg/h and then converted into specific fuel consumption in g/kWh using the corresponding power value. Mean values for the specific fuel consumption and emissions were calculated by taking the arithmetic average of 13 points in the full load curve or the 5 points within the NEDC (n=13 or 5). The standard error (SE) was calculated using the standard deviation (SD) and the number of measurement points as in **Equation 6-2**.

$$SE = \frac{SD}{\sqrt{n}} \qquad \textbf{(Equation 6-2)}$$

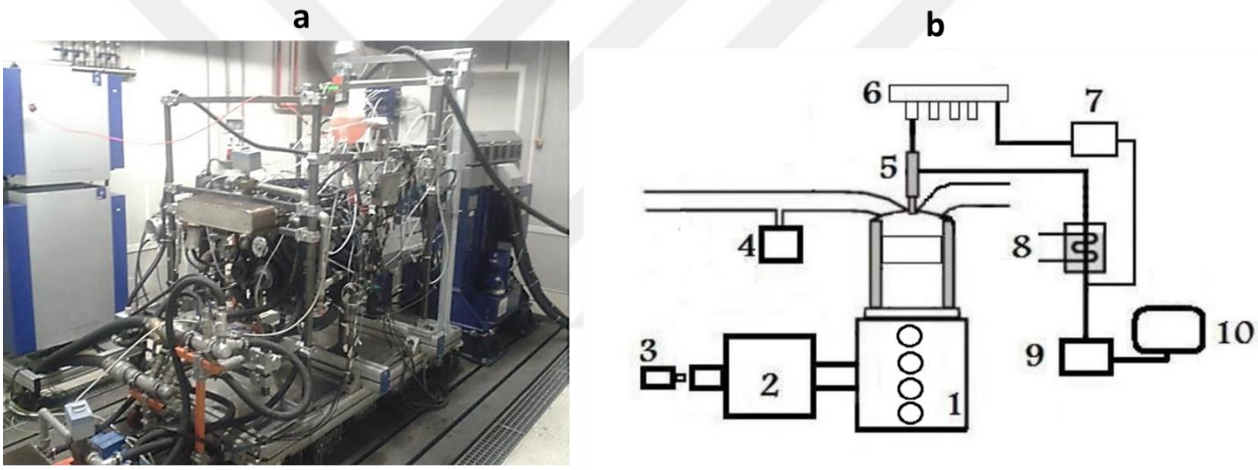

Scheme 6-2. Engine dynamometer setup; a: photo of the system; and b: schematic diagram, 1 - Engine, 2 - Dynamometer, 3 - Encoder, 4-AVL i60 Emission Bench (NOx, THC, CO, CO_2, O_2), 5 - Injector, 6 - Common-rail, 7 - High pressure pump, 8 - Fuel conditioner, 9 - Fuel consumption meter, 10 - Fuel tank.

6.3.Results and Discussion

The catalytic production of GTBE was realized over commercially available catalysts. K1 represented the GTBE mixture obtained by Amberlyst 15^{TM} catalyst with the highest TTBGE

concentration, whereas zeolite H-Beta catalyst was used for the production of K6, in which DTBGE concentration was the highest with a negligible amount of TTBGE. The rest of the GTBE mixtures (K2, K3, K4, and K5) were prepared by mixing K1 and K6 at different proportions so that DTBGE and TTBGE concentrations can be represented at equal increments. Composition of all GTBE mixtures are presented in **Table 6-1**. Linearity of the DTBGE and TTBGE concentrations in these mixtures are illustrated in **Figure D-2**.

Table 6-1. Composition analysis of the GTBE mixtures by GC-FID.

GTBE mixture	Concentration (wt%)					Total OH (moles)[c]
	MTBGE	DTBGE	TTBGE	DIB	TIB	
K1[a]	1.19	61.88	34.13	1.08	1.71	0.32
K2	1.39	67.48	29.26	0.69	1.18	0.35
K3	2.58	73.35	22.88	0.39	0.79	0.39
K4	5.12	77.91	15.95	0.28	0.73	0.45
K5	8.41	81.75	8.80	0.24	0.79	0.51
K6[b]	11.86	85.60	1.51	0.20	0.83	0.58

[a]Purified GTBE mixture obtained from Amberlyst 15^{TM}; [b]Purified GTBE mixture obtained from zeolite H-Beta CP811C-300 (Si/Al=150); [c]Total moles of OH groups of GTBE mixtures in 100 g mixture.

According to **Table 6-1**, Amberlyst 15^{TM} was associated with a significant degree of TTBGE production (K1), while the TTBGE produced over H-Beta (Si/Al=150) was below 2 wt% (K6). GC-FID analysis was performed three times for each sample, the corresponding error associated with the reported MTBGE, DTBGE, and TTBGE concentrations were less than 0.07 wt%. In a recent study, the reaction products at complete glycerol conversion contained 11 wt% MTBGE, 59 wt% DTBGE, 16 wt% TTBGE, 12 wt% DIB, 1 wt% TIB, and 1 wt% TBA for Amberlyst 15^{TM} and 11 wt% MTBGE, 74 wt% DTBGE, 1 wt% TTBGE, 8 wt% DIB, 1 wt% TIB and 5 wt% TBA for H-Beta (rest of the products were tetra-isobutene and tertiary butyl alcohol) [209]. The same study demonstrated the similarity of other cation exchange resins Amberlyst 35^{TM} and 36^{TM} with Amberlyst 15^{TM} in terms of product selectivity. In

addition, H-Beta yielded in the highest DTBGE concentration among several different zeolites considered. The steric hindrance in H-Beta seems to result in DTBGE as the main ether product since the kinetic diameter of TTBGE is larger than its pores [41,54]. Thus, we infer that Amberlyst 15^{TM} and H-Beta are the two potential commercial catalysts with complete glycerol conversion in the etherification of glycerol with isobutene. Hence, the product selectivity and the corresponding purified GTBE selectivity are expected to situate in the range of these two catalysts.

MTBGE and DIB contents reduced after the purification of the GTBE mixtures by washing, decantation and evaporation. MTBGE removal from the Amberlyst 15^{TM} product was much more efficient compared to the H-Beta product, probably because of the high concentration of TTBGE in the former mixture (**Table 6-1**, column 2). It seems that TTBGE content facilitates the separation of MTBGE in the washing-decantation stage. In contrast, DIB removal has an opposite trend, indicating the possible effect of high TTBGE content in keeping higher amounts of DIB in the evaporation step. Higher TIB content compared to DIB in the purified GTBE mixtures in **Table 6-1** exhibits the difficulty in removing the TIB with higher boiling point (177 °C) in vacuum distillation. *Tert*-butyl alcohol (TBA) content in the GTBE mixtures were below 0.5 wt%, thus neglected. Probably TBA was successfully removed in the washing/decantation step as a consequence of its high solubility in water [262]. With the help of these GTBE mixtures, it would be more convenient to explain the changes in physical and chemical properties with altering concentrations. Fuel related properties of the GTBE mixtures are given in **Table 6-2**.

.

Table 6-2. Properties of the GTBE mixtures determined according to standard tests.

	GTBE mixture → increasing MTBGE and DTBGE, decreasing TTBGE content					
Property	**K1**	**K2**	**K3**	**K4**	**K5**	**K6**
Density (g/cm^3, 15 °C)	0.886	0.890	0.896	0.904	0.911	0.919
Solubility of water (wt%)	2.658	3.122	3.732	4.672	5.444	7.391
Kinematic viscosity (cSt, 40 °C)	4.481	4.742	5.253	5.988	6.903	7.978
Gross heat of combustion (cal/gr)	8385	8316	8191	8078	8046	7924
Lubricity (microns, 60 °C)	233	181	215	218	252	271
Refractive index	1.423	1.424	1.424	1.425	1.427	1.428
Contact angle On Steel 316 (°) Mean	10.0	12.7	12.9	10.6	13.1	12.1
Glass (°) Mean	11.5	10.5	9.9	11.3	10.8	15.9

Table 6-2 points out to a well-correlated increment in density and kinematic viscosity of the GTBE mixtures as well as the solubility of water in GTBE mixtures with increasing MTBGE and DTBGE contents. Similar results for density and viscosity were obtained in a recent patent, where the presence of high TTBGE was associated with the lowest density and dynamic viscosity [243]. MTBGE and DTBGE have two and one hydroxyl groups, respectively, whereas TTBGE does not have any hydroxyl groups. Total number of hydroxyl groups is a good representative of any GTBE mixture, especially when di- and tri-isobutene concentrations are low, as in our case. We plotted density, solubility of water and kinematic viscosity as a function of total number of hydroxyl groups in all GTBE mixtures in **Figure 6-1**.

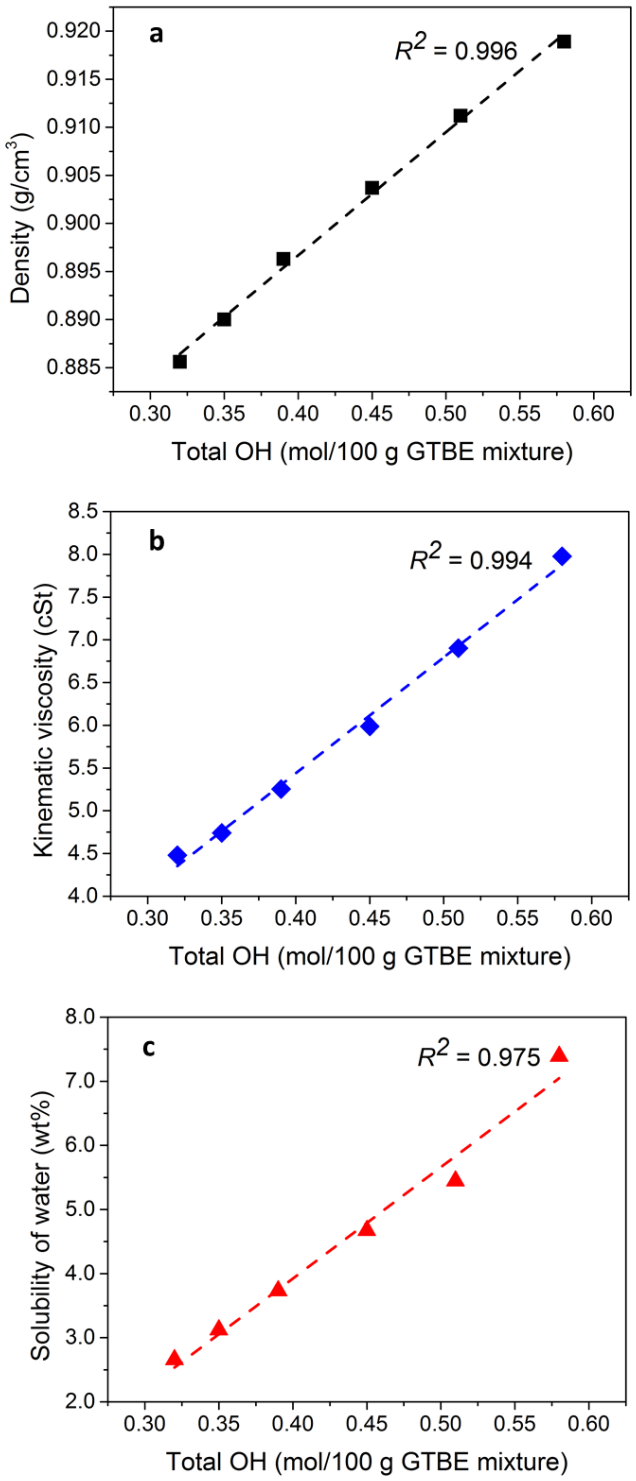

Figure 6-1. Relationship between the physical properties and total number of moles of OH in 100 grams of GTBE mixtures K1-K6; **a:** density; **b:** kinematic viscosity; **c:** solubility of water.

According to **Figure 6-1 a** and **b**, increasing number of total hydroxyl groups resulted in elevated density from 0.89 to 0.92 g/cm^3 and viscosity from 4.48 to 7.98 cSt, pointing out to the importance of having TTBGE in gasoline blends for maintaining the standards, as the TTBGE molecule is associated with lower number of hydroxyl groups. Water contents in each GTBE mixture following the washing and evaporation steps were measured to be approximately 700 ppm. Values up to 1000 ppm were observed upon sample contacting with air for 24 hours depending on the humidification level. The solubility of water in GTBE mixtures were determined after saturating the samples with water. The correlation of these solubility values with the hydroxyl content, as given in **Figure 6-1 c**, demonstrates that higher hydroxyl content prompted higher solubility of water in GTBE mixtures, as expected. This strong interaction of water with a GTBE mixture is more pronounced in the case of polar MTBGE molecule. It can be inferred that MTBGE interacts with water strongly, but not with the non-polar hydrocarbon fuels, which might cause fuel incompatibility problems. Indeed, DTBGE and TTBGE were mentioned to have better fuel blending properties [15]. Strong correlations in **Figure 6-1** enable the estimation of density, viscosity and solubility of water in different GTBE mixtures by simple GC-FID analysis, if the total number of hydroxyl groups range between 0.3-0.6 mol OH/100 g mixture.

Densities of MTBGE, DTBGE, and TTBGE ($\boldsymbol{\rho_i}$) were calculated with a simple model in Matlab using the equation $\boldsymbol{\rho_{mix}} = \sum \boldsymbol{x_i}\, \boldsymbol{\rho_i}$ wherein x_i is the mass fraction and ρ_{mix} is the mixture density measured at 15 °C (**Table 6-2**). The mixture consisted of six components MTBGE, DTBGE, TTBGE, DIB, TIB, and trace amount of water. The densities of DIB, TIB, and water were known (0.716 g/cm^3 for DIB [263], 0.77 g/cm^3 for TIB [264], and 1.00 g/cm^3 for water). The densities of MTBGE, DTBGE, and TTBGE were the three unknowns. Six equations with three unknowns were solved, yielding in 20 results for each ether density (**Figure D-3**). We then took the average and standard deviation of each ether densities. The

corresponding densities obtained are 1.003 g/cm^3 for MTBGE, 0.911 g/cm^3 for DTBGE, and 0.845 g/cm^3 for TTBGE (with a standard deviation of 0.030, 0.004, and 0.008, respectively). MTBGE density reported by the GC-FID calibration sample supplier is 1.0 g/cm^3 at 20 °C, consistent with our results [265]. The successful density match for MTBGE between the reported and calculated values indicate the validity of our model.

Gross heat of combustion indicates the amount of energy obtainable from a hydrocarbon fuel [266]. The ASTM D4809 test results pointed out to the highest energy release from K1, wherein both DTBGE and MTBGE concentrations were the lowest. For instance, the gross heat of combustion of GTBE mixture (K1) decreases by 5.5% by decreasing the TTBGE concentration from 34.1 wt% to 1.5 wt%. This outcome presents the positive effect of the TTBGE content in terms of the calorific value of the fuel additive.

In high frequency reciprocating rig (HFRR) tests, higher wear scar diameter in microns demonstrates poorer lubricity [267]. In our study, lubricity of the tested GTBE mixtures did not show any meaningful trend. Thus, we infer that changing the MTBGE, DTBE, and TTBGE concentrations does not have any measurable effect on the lubricity of the fuel additive. A maximum of 520 microns in ASTM diesel standard, and a maximum of 460 microns in the EU standard are the allowed for wear scare diameters [268]. In our study, wear scare diameters of 181-271 microns were obtained for all GTBE mixtures. Therefore, if used in diesel blends, GTBE can be applicable in terms of lubricity. Refractive index is a physical property which could be correlated with the density of fuel mixtures [269]. As presented in **Table 6-2**, refractive index has a slight increase at enhanced density from K1 to K6. Contact angle values ranging from 10° to 16° from K1 to K6 are indicative of excellent surface wetting on glass and steel surfaces. Moreover, wettability is more pronounced for GTBE mixtures with high TTBGE content.

The GTBE mixtures K1 to K6 were analyzed with ATR (Attenuated Total Reflectance) FTIR spectroscopy (**Figure 6-2**). Based on a molecular spectroscopic study of a GTBE mixture, the bands were assigned as follows: 3500-3400 cm^{-1} O–H stretch; 3000-2800 cm^{-1} C–H stretch, 1500-1150 cm^{-1} C–H bend; 1082 cm^{-1} asymmetric C–O stretch plus C–C stretch of glycerol backbone; 1062 cm^{-1} asymmetric C–O stretch contributing to hydrogen bonding between molecules; 1021 cm^{-1} CH_3 rocking; 982 and 943 cm^{-1} CH_2 rocking; 883 cm^{-1} C–O stretch plus C–C stretch of isobutene backbone; 855 cm^{-1} C–C stretch plus C–O symmetric stretch [270]. **Figure 6-2** demonstrates the alteration of peak absorbance values with changing concentrations of MTBGE, DTBGE and TTBGE in the GTBE mixtures.

According to **Figure 6-2 a**, the intensity of the O–H stretch at 3443 cm^{-1} grows from K1 to K6, confirming the presence of a higher number of hydroxyl groups with increasing DTBGE and MTBGE content. K1 has the highest intensity for the C–H stretching frequency at 2974 cm^{-1}, because of the high number of methyl groups at TTBGE. The intensities at 2934 cm^{-1} are comparable. In contrast, the magnitude of the C–H stretching signal at 2873 cm^{-1} is higher for K6 with the highest MTBGE content because MTBGE has abundant unsubstituted carbon bound to a hydroxyl group, two carbons and one hydrogen. Evaluating the vibrational spectra in the fingerprint region, **Figure 6-2 b** reveals the considerably high intensity of 1062, 1021, and 943 cm^{-1} bands for K6 sample with a high MTBGE content. The first one could be the indicative of the higher number of hydrogen bonds, while the latter two might be related to the number of $–CH_2$ groups existing in the presence of MTBGE.

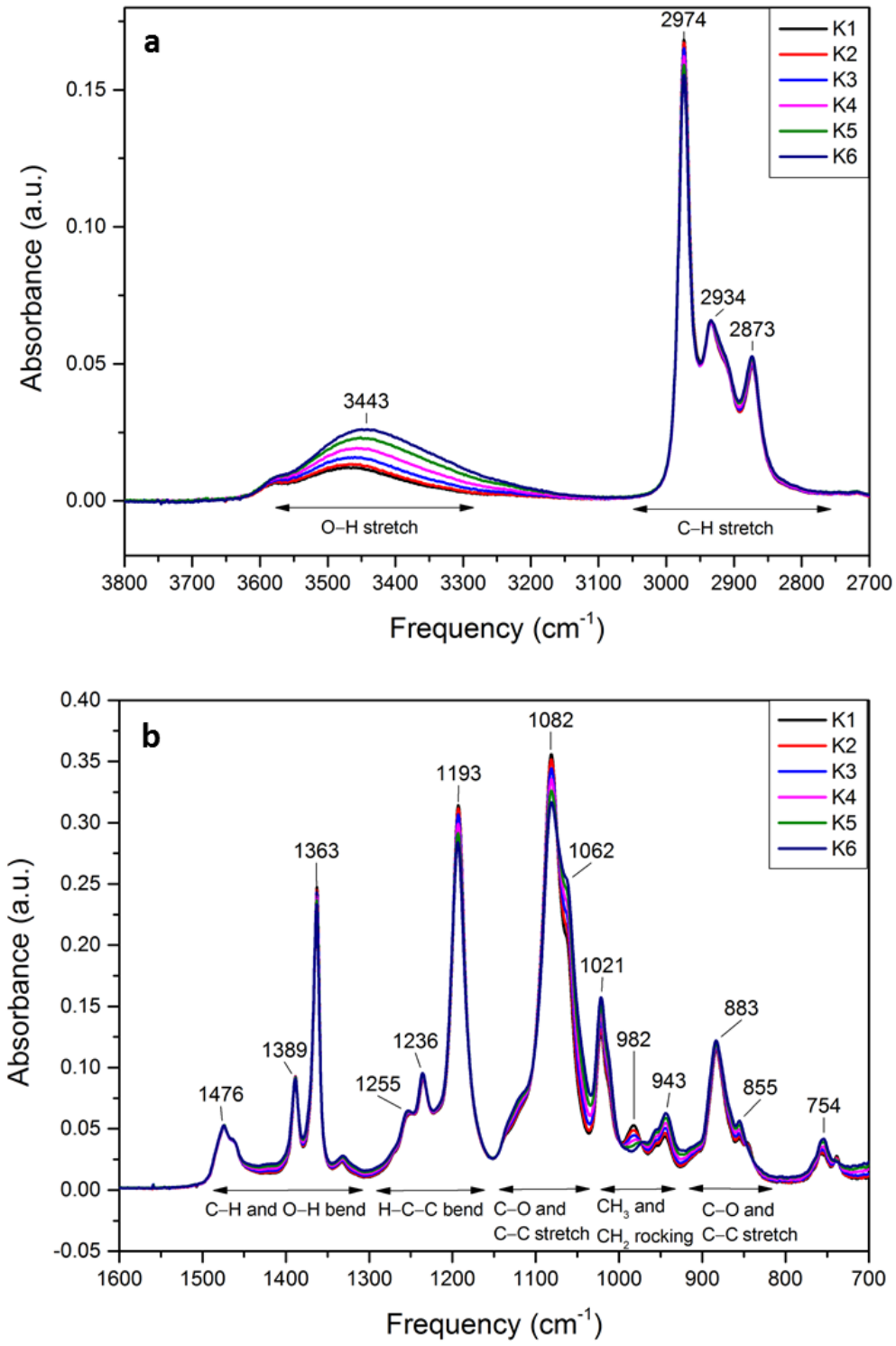

Figure 6-2. Infrared spectra of the GTBE mixtures K1 to K6; **a:** high energy region; **b:** low energy region.

In order to determine the fuel compatibility of GTBE mixtures, K1-K6 were mixed with a reference gasoline at a mixing ratio of 3.45 vol%. The reference gasoline does not contain any methyl-*tert*-butyl ether (MTBE) additive and has 44 vol% aromatic content. The appearance of the fuel blends is presented in **Figure 6-3.**

Figure 6-3. Appearance of **a:** the pure reference gasoline and **b to g**: its 3.45 vol% blends with the GTBE mixtures K1 to K6.

It is demonstrated in **Figure 6-3** that turbidity rises from K1 to K6, with increasing concentrations of MTBGE and DTBGE. The final solution (**Figure 6-3 g**) with the lowest fraction of the least polar TTBGE displays a mixing incompatibility. GTBE mixtures with greater number of hydroxyl groups is associated with blurred blends. We anticipate the elevated amounts of non-polar ethers as fuel additives to provoke higher solubility, thus higher compatibility in hydrocarbon fuels. Fuel related properties of the reference gasoline blends are given in **Table 6-3**.

Table 6-3. Properties of the GTBE mixtures-reference gasoline blends according to standard tests.

	3.45 vol% reference gasoline blends → increasing MTBGE and DTBGE, decreasing TTBGE content						
Property	**Pure**	**K1**	**K2**	**K3**	**K4**	**K5**	**K6**
Octane number (RON)	95.0	96.0	96.0	96.0	96.1	96.1	96.1
Density (g/cm^3, 15 °C)	0.7579	0.7631	0.7632	0.7633	0.7634	0.7636	0.7637
Vapor pressure, DVPE (kPa, 37.8 °C)	57.3	56.0	55.8	55.6	55.6	54.9	53.7
Gum formation (mg/100 ml)	0.4	1.4	1.6	2	3.4	2.6	0.4
Gross heat of combustion (cal/g)	8659	8514	7734	8973	8906	8522	9095
Induction period (min)	>1440	>1440	>1440	>1440	>1440	>1440	>1440

Table 6-3 indicates the enhancement in octane number, along with the reduction of vapor pressure, signifying the fuel property improvement of GTBE. The concentrations of MTBGE, DTBGE, and TTBGE did not have any significant effect in octane number. A volume based approach can be employed to calculate the octane number (ON) of gasoline-alcohol or ether blends using the formula $\boldsymbol{ON_{blend} = (1 - C_i)ON_{gasoline} + C_i\, ON_{alcohol}}$, in which C_i is the volumetric alcohol fraction in the blend [271]. Our GTBE mixtures-reference gasoline blends had almost constant RON of 96.05±0.5. Using this formula, research octane number of our GTBE mixtures were calculated as 125.4±1.4. In a recent patent, RON of pure gasoline was improved from 94.1 to 95.3 and 95.8 by blending with 5 vol% DTBGE and MTBGE, respectively [243]. Based on that data, pure MTBGE has a RON of 128, and pure DTBG had 118. Based on these reported RON values, RON of TTBGE was calculated to be 145±2, considering the most compatible gasoline blends with K1 to K3. Increasing DTBGE and decreasing TTBGE concentrations from K1 to K3 seems to yield in similar blend octane values.

Initial density of the reference gasoline increased from 0.758 to 0.764 g/cm^3 upon 3.45 vol% GTBE mixture blending, however density up to 0.775 g/cm^3 is allowed according to the

EN 228 standard [272]. Based on a simple density calculation, this density requirement will be agreed for up to 13 vol% GTBE mixture-reference gasoline blends. Besides, higher TTBGE content is recommended to keep the density as low as possible.

According to **Table 6-3**, vapor pressure of the reference gasoline of 57.3 kPa decreased more than 1.3 kPa upon blending. Considering that the maximum allowed vapor pressure in summer period is 60 kPa [273], GTBE blending suffices the EN 228 gasoline standard.

Gum formation has been noticed to boost with increasing DTBGE and MTBGE, except in samples K5 and K6 possibly because of the fuel incompatibility. Nevertheless, gumming was less than the allowed limit of 5 mg in 100 ml stated in EN 228 standard [272].

Gross heat of combustion of the GTBE mixtures ranging between 7924-8385 cal/g was slightly higher in the case of GTBE-gasoline blends (in the range of 7734-9095 cal/g), probably because of the higher gross heat of combustion of gasoline itself. The induction period of GTBE-gasoline blends were over 1440 min in all blends. Induction period refers to the long term oxidation stability and should be higher than 360 min [272].

GTBE mixture "K1" with the highest TTBGE content was prepared in high amounts for the fuel performance tests. An internal combustion engine dynamometer was operated for the fuel performance tests using the reference gasoline, 3.45 vol% MTBE-blended reference gasoline, and 3.45 vol% GTBE-blended reference gasoline. The reason for using an engine dynamometer instead of a chassis roll was to ensure data reliability and to focus on directly analyzing the effect of different fuel types on combustion and engine emissions, because the performance and emission values must be collected under steady-state conditions. There were no catalyst, silencer or any after treatment component connected to exhaust setup. To sum up, emission results present engine-out results. The emission bench sampling probe was connected to dyno exhaust pipe (single straight pipe specific for dyno test) which is beyond engine turbine

outlet. The engine speeds employed within the NEDC conditions between 1960-2800 rpm are the common values for an urban driving cycle. Power and torque curves of the three blends for the engine performance test are given in **Figure 6-4.** The specific fuel consumption and the mean emission profiles are presented in **Figure 6-5** and **Figure 6-6**, respectively. The inlet air flowrates and the exhaust gas flows were mostly similar for the tested blends, indicating comparability of the retrieved data (**Figure D-4**).

Figure 6-4 indicates that gasoline blended with the K1 GTBE mixture generates equal or slightly higher torque and power than the MTBE blended. The notable difference at 3000 rpm in the full load curve (**Figure 6-4 a**) might arise from the high air inflow rate for the GTBE blend (**Figure D-4**). The specific fuel consumption of the tested fuels, especially in the urban driving conditions are comparable (**Figure 6-5**). The average specific fuel consumption of the tested blends for measurement points 14-18 within the NEDC follow as 266.5 g/kWh for reference gasoline, 267.3 g/kWh for 3.45 vol% GTBE-gasoline blend and 266.7 g/kWh for 3.45 vol% MTBE-gasoline blend. This 0.24 wt% increase in fuel consumption upon switching from MTBE to GTBE might remain insignificant.

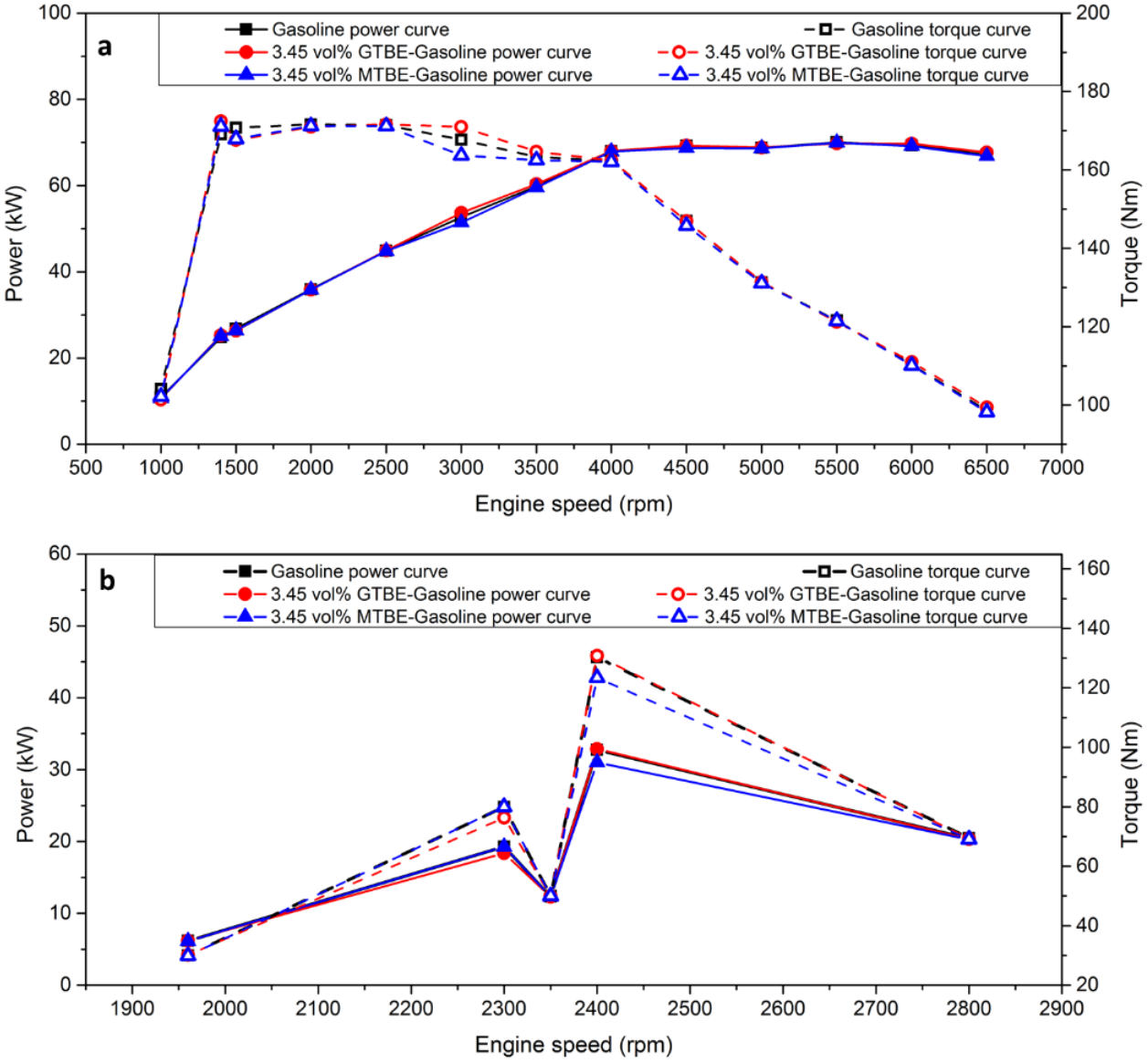

Figure 6-4. Comparison of the power and torque curves for the reference gasoline, GTBE (K1) blended gasoline and MTBE blended gasoline as a function of the engine speed; **a:** in the engine full load curve; **b:** points within the NEDC.

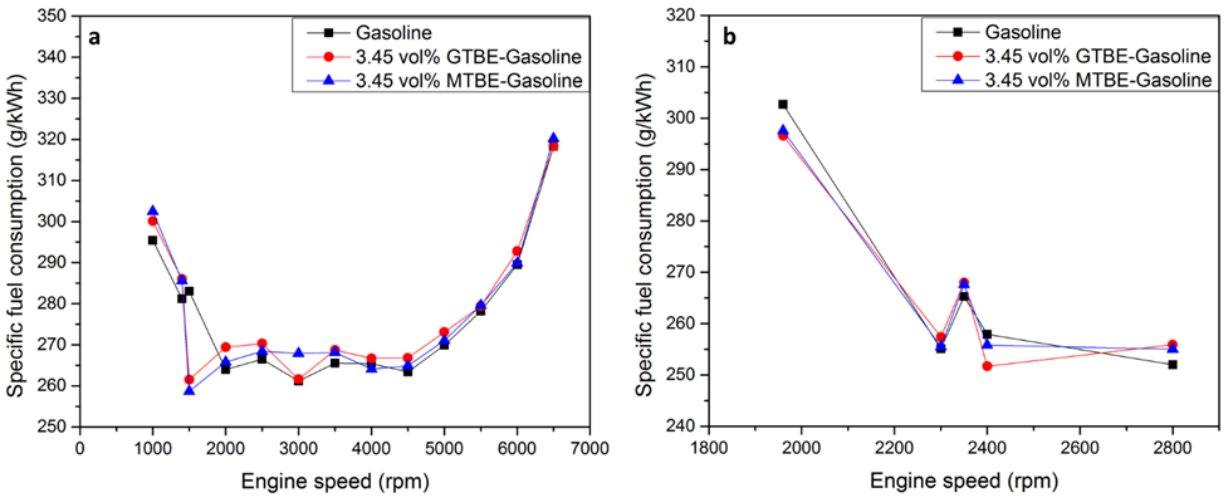

Figure 6-5. Comparison of the specific fuel consumption for the reference gasoline, GTBE (K1) blended gasoline and MTBE blended gasoline as a function of the engine speed; **a:** in the engine full load curve; **b:** points within the NEDC.

Mean emissions of CO_2, CO, NOx, and THC in g/kWh are presented in **Figure 6-6** for the NEDC range. The emissions represent pre-catalyst conditions. We have considered the NEDC part in our interpretations for better representation of the urban driving conditions. Using GTBE (K1) and MTBE as fuel oxygenates in gasoline in general reduced the CO_2 and CO emissions, while NOx and THC presented a slight increase. We also plotted the emissions both in the full load curve and in the NEDC range at each measurement point (**Figure D-5).**

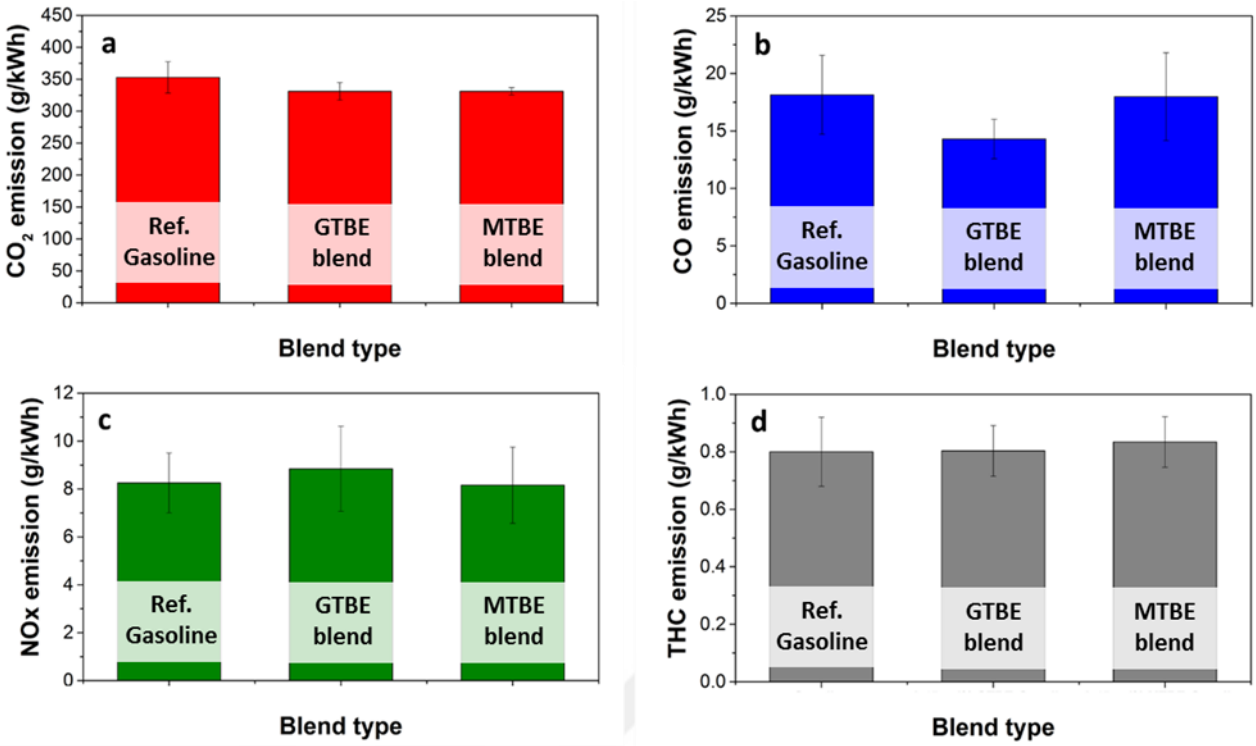

Figure 6-6. Comparison of the mean emissions with the corresponding standard errors; **a:** CO_2; **b:** CO; **c:** NOx; **d:** Total hydrocarbons for the reference gasoline, GTBE (K1) blended gasoline and MTBE blended gasoline. Mean emissions refer to the average of the measurement points 14-18 in the NEDC range.

In the NEDC range, the average CO_2 emission decreased from 353 to 331 g/kWh, while the CO emission dropped from 18 g/h to 14 g/kWh upon blending the gasoline with GTBE **(Figure 6-6 a and b)**. CO_2 emissions from the combustion of GTBE containing gasoline was the lowest between the measurement points 7-14 at high engine speed (**Figure D-5 a**). At different measurement points, CO emissions from the GTBE added gasoline were lower or equal to that of MTBE blend (**Figure D-5 b**). According to **Figure 6-6 c**, mean NOx emissions did not change upon MTBE blending. GTBE blending was observed to increase the NOx emissions of gasoline (from 8.2 to 8.8 g/kWh), yet this change is still in the standard error range. NOx emissions diminished only in the 2000-2500 rpm engine speed range for GTBE

(measurement points 4 and 5, **Figure D-5 c**). The initial mean THC emission of gasoline of 0.80 g/kWh, was almost similar for the GTBE blend and but slightly increased to 0.83 g/kWh upon MTBE blending (**Figure 6-6 d**). In the NEDC range (measurement points 11-13), the THC emissions from the GTBE blend were lower compared to the MTBE blend (**Figure D-5 d**).

6.4.Conclusion

Although glycerol *tert*-butyl ethers (GTBE) have been claimed in literature to replace the conventional gasoline oxygenate methyl *tert*-butyl ether (MTBE), no experimental study has demonstrated the effect of individual GTBE components in fuel additive mixture, in addition to the performance of GTBE in a gasoline engine. In this study, glycerol *tert*-butyl ethers (GTBE) were produced by the etherification of glycerol with isobutene. The desired ethers, namely the di- and tri-*tert*-butyl glycerol ether were separated from most of the mono-tert-butyl glycerol ether and isobutene oligomers with our unique purification method. Six GTBE mixtures with changing individual ether concentrations were prepared to test their fuel compatibility with gasoline. Density, viscosity and water solubility decreased with increasing tri-*tert*-butyl glycerol ether content. The GTBE mixture with the highest (34 wt%) tri-*tert*-butyl glycerol concentration formed the most homogenous and non-turbid solution as a 3.45 vol% blend in gasoline, with improved octane number and reduced vapor pressure of gasoline. Therefore the tri-*tert*-butyl glycerol ether was proven to be a significant gasoline additive molecule. An internal combustion engine dynamometer was used for the first time in literature to test the power output and emissions from the 34 wt% tri-*tert*-butyl glycerol containing GTBE blend. For comparison, a 3.45 vol% MTBE blend was also tested. At urban driving conditions, the power output of the GTBE blend was similar to that of the MTBE blend. The GTBE blend emitted lower CO_2 and CO compared to gasoline. Our results confirmed that GTBE is an

alternative gasoline additive to MTBE as their blends provide similar torque values, specific fuel consumption and emission profiles. Emission values and performance results can be improved if automotive companies and original equipment manufacturers use GTBE and MTBE in engine control unit calibration tests during the engine development phase

6.5.Supplementary Material

The properties of the reference gasoline, linearity of the GTBE concentrations in GTBE mixtures K1-K6, Matlab results for the estimation of the MTBGE, DTBGE, and TTBGE densities, the air flowrates and emission values at employed measurement points in the engine dynamometer are given in **Appendix D**.

Conclusion and Outlook

We have conducted a comprehensive review covering the published papers and patents on glycerol etherification with isobutene between years 1990-2018. Our review **revealed the need** of comparing different catalysts under identical conditions to perceive structure-performance relationship, using a flow reactor system to understand the glycerol conversion-product selectivity relationship and testing glycerol ethers in fuel blends to realize the commercial potential of this half-renewable alternative fuel additives.

In our extensive catalyst screening study, **by screening the largest number of catalysts in literature**, we demonstrated that high selectivity to the desired glycerol *tert*-butyl ethers (DTBGE + TTBGE) could be obtained at high acid strength. Zeolites and ion exchange resins were associated with high desired ether yields. A **patent application** was submitted to the Turkish Patent Institute on the **precise dosing of isobutene** in liquid phase into a multiple batch reactor system. We presented another **patent application** to the Turkish Patent Institute on conducting glycerol etherification with isobutene in a **tubular flow reactor system**.

Tubular flow reactor operation was investigated deeply **for the first time in literature** by or group. The catalyst particle size and flow conditions, as well as the collection and analysis of the liquid products were optimized. With the flow reactor, the **production rate** of the desired glycerol ethers per reactor volume were about **100 fold** that of a batch reactor.

Fuel additive properties of the glycerol ethers was demonstrated **primarily** by our group. Higher TTBGE content resulted in better **gasoline compatibility**. Thus, Amberlyst 15™ ion exchange resin with high TTBGE selectivity was a successful candidate for commercial ether production. We suggested a novel method for the separation of the desired DTBGE and TTBGE from most of the lower molecular weight ether MTBGE and isobutene oligomers (DIB and TIB). The **engine dynamometer** tests with GTBE blended gasoline was also conducted **for the first time in literature**. To achieve this, we prepared over four liters of DTBGE and

TTBGE rich ether mixtures, which was not done in any previous study. Similar power and emission from the gasoline engine justified that GTBE can be used as an **alternative** to the conventional gasoline oxygenate MTBE.

The future recommendations for this research mainly include the **experiments and calculations for the scale-up**. Crude glycerol and C4 olefin streams are indeed cost-effective raw materials. However, the laboratory scale trials so far have exploited their purified forms which are not only expensive but also infeasible for large scale applications. Besides, as the aim of this project is the production of GTBE from local sources, we should focus on the supply of glycerol and isobutene from Turkey's biodiesel and refining facilities.

The glycerol used in this study was **purified glycerol** ($\geq$ 99.5 wt% purity) supplied from a Turkish biodiesel producer in Izmir. This company produces over 100,000 ton/year biodiesel together with 10,500 ton/year crude glycerol. The crude glycerol is then purified in their plant to "purified glycerol", with approximately 9000 ton annual production. The price of this purified glycerol is $800/ton, with customers belonging to the pharmaceutical, food (chocolate, biscuits and cakes), cigarette and paint industries. Currently, no customer demand for crude glycerol exists. Previous literature studies on glycerol etherification revealed the deactivation of the catalysts with sodium hydroxide and methanol impurities emanating from the crude glycerol. However, experimental studies on the maximum allowable level of the impurities will be beneficial to decide whether a lower purity glycerol with a lower price could be utilized or not.

We have handled **pure isobutene** in this study with of 99.9 wt% purity purchased from a German gas producer. The source of isobutene in the Tüpraş refinery is the **C4 stream**, sourcing from the fluid catalytic cracking (FCC unit), which also contains 1-butene, trans-2-butene, cis-2-butene, n-butane, isobutane and 1,3-butadiene. In the conventional MTBE

production, methanol reacts with the C4 stream on ion exchange resin catalysts. The butenes in the C4 stream does not react with methanol under the concerned reaction conditions, thus remain unconverted. It is apparent that the hydrocarbons in the C4 stream other than isobutene do not harm or deactivate the catalyst. Trials with butenes and pure glycerol should be performed to determine if any **butyl glycerols** form during the reaction. If butyl glycerols form, their gasoline compatibility should further be tested. If the butenes remain unconverted, the alternative pathways to utilize these light olefins, such as oligomerization, should be addressed.

The **cost and activity of the catalyst** is crucial for the scale-up. Turkey imports 100,000 tons of MTBE each year. MTBE price in 2017 was approximately $700/ton. The annual import cost thus corresponded to **70 million dollars**. MTBE is blended with gasoline in volume basis. The density of MTBE (at 20 °C) is 0.74 kg/m^3, while the average GTBE density is 0.89 kg/m^3. Therefore 100,000 tons of MTBE will correspond to **120,000** tons of (desired) GTBE if their blending volumes are equal. We achieved 17 $g_{GTBE} \times (g_{catalyst} \times h)^{-1}$ ether production rate with Amberlyst 15^{TM} 250-425 um particle size at 8.4 $g_{glycerol} \times (g_{catalyst} \times h)^{-1}$ space velocity at 75 °C, 15 bar, isobutene:glycerol=3:1 mol:mol conditions. The corresponding rate of desired ether production was 12 $g_{DTBGE + TTBGE} \times (g_{catalyst} \times h)^{-1}$. In one year, assuming **330** operating days at continuous operation, or 7920 h production, 95 ton DTBGE + TTBGE per kg catalyst could be produced. If the same catalyst can remain active for **10 days**, then the catalyst should be replaced **33** times per year. Therefore, there will be **2.88 tons** of desired ether production per kg of catalyst each cycle. In every cycle, we should be producing 120000/33=**3636** tons of DTBGE + TTBGE. Thus in each cycle (each 10 days), 23636/2.88=**1263** kg, or 1.26 tons of catalyst should be used. The price of Amberlyst 15 (dry) is around $6000/ton, therefore the annual cost may exceed $249,500. However, this annual cost is 1/280 fold of the annual MTBE import.

We did not study the **change in the temperature** in the catalyst bed, as we used small amounts of catalyst and also the reaction is **mildly exothermic**. The estimated heat release at 75 °C during the formation of MTBGE is 30 kJ/mol. In our reactor, 99 wt% glycerol conversion occurs when Amberlyst 15^{TM} 250-425 um particle size fraction is used at 0.033 ml/min glycerol flowrate corresponding to $4x10^{-7}$ mmol/min flowing glycerol. Considering all glycerol is converted into MTBGE, the heat release would only be $1.3x10^{-5}$ J/min. Assuming that Amberlyst 15^{TM} is made of polystyrene with a specific heat capacity of 1220 J/kg°K [274], and considering that 300 mg catalyst is used in the reaction, the temperature increase would be $3.6x10^{-5}$ °C/min. Thus, in 10 days, the increase in temperature would be less than 0.5 °C. However, in a large scale application with one ton of catalyst, the temperature increase will be consequential. For this reason, the need for **reactor cooling** will arise. We observed accelerated formation of isobutene oligomers and trimers with an increase in temperature from 75 to 95 °C. In the case of hot spots, olefins will most probably be utilized to form oligomers, rather than glycerol ethers. Oligomers above a certain level are not demanded in fuel formulations. An additional **hydrogenation unit** might be required to saturate the double bonds and thus convert the oligomers to the suitable gasoline components.

MTBE and ethyl *tert*-butyl ether (**ETBE**) are the gasoline oxygenates in the market. The **profit margin** of the possible GTBE production should be considered together with these existing products. 2018 prices for methanol, ethanol, MTBE, and ETBE per ton was $400, $700, $800 and $1000, respectively [275]. The price of the isobutene in the olefinic C4 fraction is estimated to be $470/ton (inner reference). Glycerol price is considered as $800/ton (supplier information for purified glycerol). However crude glycerol of 80 wt% purity has much lower price of $300-400/ton [275].

1 ton Methanol + 1.75 ton Isobutene → 2.75 ton MTBE

1 x $400 + 1.75 x $470 → 2.75 x $800

Profit margin for one ton of MTBE production= $355

1 ton Ethanol + 1.2 ton Isobutene → 2.2 ton ETBE

1 x $700 + 1.2 x $470 → 2.2 x $1000

Profit margin for one ton of ETBE production= $425

1 ton Glycerol + 1 ton Isobutene → 2 ton GTBE

1 x $800 + 1 x $470 → 2 x $GTBE

In order to have a similar profit margin for GTBE and ETBE production, the approximate selling price of GTBE is supposed to be $1060/ton. Any rise in glycerol price will in this case make GTBE production less profitable. However, if a cheaper glycerol with lower purity could be used instead of purified glycerol, then the profit margin of GTBE production may overcome that of ETBE production. Apart from that, an ether production facility with elastic feeding of ethanol and glycerol would be another option, in which the co-production of glycerol ethers together with ethanol ethers can be realized.

Finally, a **conceptual process design** is recommended for further studies, consisting of equipment design, techno-economical assessment and sensitivity analysis. That study can help to calculate the net present value and payback time for different scenarios by changing the most significant process parameters. For example, the effect of catalyst lifetime, isobutene concentration in the C4 stream or glycerol price fluctuations can be investigated in silico.

References

[1] A. Corma, E. Corresa, Y. Mathieu, L. Sauvanaud, S. Al-Bogami, M.S. Al-Ghrami, A. Bourane, Crude oil to chemicals: light olefins from crude oil, Catalysis Science & Technology (2016).

[2] A. Corma, V. González-Alfaro, A.V. Orchillés, The role of pore topology on the behaviour of FCC zeolite additives, Applied Catalysis A: General 187 (1999) 245-254.

[3] S.A. Tabak, F.J. Krambeck, W.E. Garwood, Conversion of propylene and butylene over ZSM-5 catalyst, AIChE Journal 32 (1986) 1526-1531.

[4] M.L. Sarazen, E. Doskocil, E. Iglesia, Catalysis on solid acids: Mechanism and catalyst descriptors in oligomerization reactions of light alkenes, Journal of Catalysis 344 (2016) 553-569.

[5] Market Research Future, Light Olefins Market Research Report – Forecast to 2023 (2018).

[6] M. Quiroga, N. Fígoli, U. Sedran, Alternative catalysts for MTBE production, , React. Kinet. Catal. Lett. 63 (1998).

[7] J.G. Goodwin, S. Natesakhawat, A.A. Nikolopoulos, S.Y. Kim, Etherification on Zeolites: MTBE synthesis, Catalysis Reviews 44 (2002) 287-320.

[8] H. Hamid, M.A. Ali, Handbook of MTBE and Other Gasoline Oxygenates, CRC Press (2004) pp. 203-220.

[9] C.A.G. Quispe, C.J.R. Coronado, J.A.C. Jr., Glycerol: production, consumption, prices, characterization and new trends in combustion, Renewable and Sustainable Energy Reviews 27 (2013) 475-493.

[10] W. Kiatkittipong, S. Suwanmanee, N. Laosiripojana, P. Praserthdam, S. Assabumrungrat, Cleaner gasoline production by using glycerol as fuel extender, Fuel Processing Technology 91 (2010) 456-460.

[11] A.B. Leoneti, V. Aragão-Leoneti, S.V.W.B. de Oliveira, Glycerol as a by-product of biodiesel production in Brazil: Alternatives for the use of unrefined glycerol, Renewable Energy 45 (2012) 138-145.

[12] J.F. Izquierdo, M. Montiel, I. Palés, P.R. Outón, M. Galán, L. Jutglar, M. Villarrubia, M. Izquierdo, M.P. Hermo, X. Ariza, Fuel additives from glycerol etherification with light olefins: State of the art, Renewable and Sustainable Energy Reviews 16 (2012) 6717-6724.

[13] C.-H. Zhou, J.N. Beltramini, Y.-X. Fan, G.Q. Lu, Chemoselective catalytic conversion of glycerol as a biorenewable source to valuable commodity chemicals, Chemical Society Reviews 37 (2008) 527-549.

[14] D. Bradin, G.L. Grune, M. Trivette, 'US 20090013591 A1', Alternative fuel and fuel additive compositions (2009).

[15] Ö.D. Bozkurt, F.M. Tunç, N. Bağlar, S. Çelebi, İ.D. Günbaş, A. Uzun, Alternative fuel additives from glycerol by etherification with isobutene: Structure–performance relationships in solid catalysts, Fuel Processing Technology 138 (2015) 780-804.

[16] A. Jaecker-Voirol, I. Durand, G. Hillion, B. Delfort, X. Montagne, Glycerin for new biodiesel formulation, Oil & Gas Science and Technology - Rev. IFP 63 (2008) 395-404.

[17] R.R. Soares, D.A. Simonetti, J.A. Dumesic, Glycerol as a source for fuels and chemicals by low-temperature catalytic processing, Angewandte Chemie International Edition 45 (2006) 3982-3985.

[18] J. Dufour, D. Iribarren, Life cycle assessment of biodiesel production from free fatty acid-rich wastes, Renewable Energy 38 (2012) 155-162.

[19] I.M. Atadashi, M.K. Aroua, A.R.A. Aziz, N.M.N. Sulaiman, Refining technologies for the purification of crude biodiesel, Applied Energy 88 (2011) 4239-4251.

[20] K.G. Harding, J.S. Dennis, H. von Blottnitz, S.T.L. Harrison, A life-cycle comparison between inorganic and biological catalysis for the production of biodiesel, Journal of Cleaner Production 16 (2008) 1368-1378.

[21] M.J. Montefrio, T. Xinwen, J.P. Obbard, Recovery and pre-treatment of fats, oil and grease from grease interceptors for biodiesel production, Applied Energy 87 (2010) 3155-3161.

[22] Q. Shu, B. Yang, H. Yuan, S. Qing, G. Zhu, Synthesis of biodiesel from soybean oil and methanol catalyzed by zeolite beta modified with La3+, Catalysis Communications 8 (2007) 2159-2165.

[23] M.G. Kulkarni, R. Gopinath, L.C. Meher, A.K. Dalai, Solid acid catalyzed biodiesel production by simultaneous esterification and transesterification, Green Chemistry 8 (2006) 1056-1062.

[24] A. Kawashima, K. Matsubara, K. Honda, Development of heterogeneous base catalysts for biodiesel production, Bioresource Technology 99 (2008) 3439-3443.

[25] W. Xie, H. Peng, L. Chen, Transesterification of soybean oil catalyzed by potassium loaded on alumina as a solid-base catalyst, Applied Catalysis A: General 300 (2006) 67-74.

[26] H. Fukuda, A. Kondo, H. Noda, Biodiesel fuel production by transesterification of oils, Journal of Bioscience and Bioengineering 92 (2001) 405-416.

[27] Grand View Research, Glycerol market from biodiesel, fatty acids, fatty alcohols for personal care, alkyd resins, polyether polyols applications, downstream opportunities and segment forecasts to 2020 (2014).

[28] OECD/FAO, OECD-FAO Agricultural Outlook 2011, OECD Publishing (2011) p. 79.

[29] M. Gupta, N. Kumar, Scope and opportunities of using glycerol as an energy source, Renewable and Sustainable Energy Reviews 16 (2012) 4551-4556.

[30] C.A.G. Quispe, C.J.R. Coronado, J.A. Carvalho Jr, Glycerol:production, consumption, prices, characterization and new trends in combustion, Renewable and Sustainable Energy Reviews 27 (2013) 475-493.

[31] C. Beatrice, G. Di Blasio, C. Guido, C. Cannilla, G. Bonura, F. Frusteri, Mixture of glycerol ethers as diesel bio-derivable oxy-fuel: Impact on combustion and emissions of an automotive engine combustion system, Applied Energy 132 (2014) 236-247.

[32] European Parliament, Directive 2009/28/EC of the European Parliament and of the Council on 23 April 2009 (2009).

[33] IEA, Technology Roadmap Biofuels for Transport, International Energy Agency (2011).

[34] A. Behr, J. Eilting, K. Irawadi, J. Leschinski, F. Lindner, Improved utilisation of renewable resources: New important derivatives of glycerol, Green Chemistry 10 (2008) 13-30.

[35] M. Martín, I.E. Grossmann, Simultaneous Optimization and Heat Integration for the Coproduction of Diesel Substitutes: Biodiesel (FAME and FAEE) and Glycerol Ethers from Algae Oil, Industrial & Engineering Chemistry Research 53 (2014) 11371-11383.

[36] N. Rahmat, A.Z. Abdullah, A.R. Mohamed, Recent progress on innovative and potential technologies for glycerol transformation into fuel additives: A critical review, Renewable and Sustainable Energy Reviews 14 (2010) 987-1000.

[37] H. Noureddini, W.R. Dailey, B.A. Hunt, Production of ethers of glycerol from crude glycerol - the by-product of biodiesel production, Advances in Environmental Research 2 (1998) 232-243.

[38] A. Behr, L. Obendorf, Development of a Process for the Acid-Catalyzed Etherification of Glycerine and Isobutene Forming Glycerine Tertiary Butyl Ethers, Engineering in Life Sciences 2 (2002) 185-189.

[39] K. Klepáčová, D. Mravec, M. Bajus, tert-Butylation of glycerol catalysed by ion-exchange resins, Applied Catalysis A: General 294 (2005) 141-147.

[40] R.S. Karinen, A.O.I. Krause, New biocomponents from glycerol, Applied Catalysis A: General 306 (2006) 128-133.

[41] K. Klepáčová, D. Mravec, A. Kaszonyi, M. Bajus, Etherification of glycerol and ethylene glycol by isobutylene, Applied Catalysis A: General 328 (2007) 1-13.

[42] J.A. Melero, G. Vicente, G. Morales, M. Paniagua, J.M. Moreno, R. Roldán, A. Ezquerro, C. Pérez, Acid-catalyzed etherification of bio-glycerol and isobutylene over sulfonic mesostructured silicas, Applied Catalysis A: General 346 (2008) 44-51.

[43] V. Mangourilos, D. Bombos, T. Juganaru, I. Bolocan, M. Bombos, D. Ciuparu, Etherification of glycerol with isobutene on Amberlyst 35 ion exchange resin catalyst in presence of a cationic emulsifier, Revista de Chimie 60 (2009) 1338-1342.

[44] M. Di Serio, L. Casale, R. Tesser, E. Santacesaria, New Process for the Production of Glycerol tert-Butyl Ethers, Energy & Fuels 24 (2010) 4668-4672.

[45] H.J. Lee, D. Seung, K.S. Jung, H. Kim, I.N. Filimonov, Etherification of glycerol by isobutylene:tuning the product composition, Applied Catalysis A: General 390 (2010) 235-244.

[46] J.A. Melero, G. Vicente, G. Morales, M. Paniagua, J. Bustamante, Oxygenated compounds derived from glycerol for biodiesel formulation: Influence on EN 14214 quality parameters, Fuel 89 (2010) 2011-2018.

[47] W. Zhao, B. Yang, C. Yi, Z. Lei, J. Xu, Etherification of Glycerol with Isobutylene to Produce Oxygenate Additive Using Sulfonated Peanut Shell Catalyst, Industrial & Engineering Chemistry Research 49 (2010) 12399-12404.

[48] H.J. Lee, D. Seung, I.N. Filimonov, H. Kim, Etherification of glycerol by isobutylene. Effects of the density of acidic sites in ion-exchange resin on the distribution of products, Korean Journal of Chemical Engineering 28 (2011) 756-762.

[49] L. Xiao, J. Mao, J. Zhou, X. Guo, S. Zhang, Enhanced performance of HY zeolites by acid wash for glycerol etherification with isobutene, Applied Catalysis A: General 393 (2011) 88-95.

[50] V. Voicu, I. Bolocan, D. Ciuparu, Synthesis and characterization of sulfonic acid catalysts supported on mesoporous molecular sieves, Revista de Chimie 62 (2011) 1206-1212.

[51] F. Frusteri, L. Frusteri, C. Cannilla, G. Bonura, Catalytic etherification of glycerol to produce biofuels over novel spherical silica supported Hyflon(R) catalysts, Bioresource Technology 118 (2012) 350-358.

[52] M.D. González, Y. Cesteros, J. Llorca, P. Salagre, Boosted selectivity toward high glycerol tertiary butyl ethers by microwave-assisted sulfonic acid-functionalization of SBA-15 and beta zeolite, Journal of Catalysis 290 (2012) 202-209.

[53] V. Voicu, D. Bombos, I. Bolocan, C.R. Jang, D. Ciuparu, The influence of the character of emulsifiers on the performance of H(4)SiW(12)O40.30H(2)O heteropolyacid catalyst in glycerol etherification with isobutene, Revista de Chimie 63 (2012) 200-204.

[54] A. Turan, M. Hrivnák, K. Klepáčová, A. Kaszonyi, D. Mravec, Catalytic etherification of bioglycerol with C4 fraction, Applied Catalysis A: General 468 (2013) 313-321.

[55] M.D. Gonzalez, P. Salagre, E. Taboada, J. Llorca, Y. Cesteros, Microwave-assisted synthesis of sulfonic acid-functionalized microporous materials for the catalytic etherification of glycerol with isobutene, Green Chemistry 15 (2013) 2230-2239.

[56] W. Zhao, C. Yi, B. Yang, J. Hu, X. Huang, Etherification of glycerol and isobutylene catalyzed over rare earth modified Hβ-zeolite, Fuel Processing Technology 112 (2013) 70-75.

[57] M.D. González, P. Salagre, E. Taboada, J. Llorca, E. Molins, Y. Cesteros, Sulfonic acid-functionalized aerogels as high resistant to deactivation catalysts for the etherification of glycerol with isobutene, Applied Catalysis B: Environmental 136–137 (2013) 287-293.

[58] M.D. González, P. Salagre, M. Linares, R. García, D. Serrano, Y. Cesteros, Effect of hierarchical porosity and fluorination on the catalytic properties of zeolite beta for glycerol etherification, Applied Catalysis A: General 473 (2014) 75-82.

[59] M.D. González, P. Salagre, R. Mokaya, Y. Cesteros, Tuning the acidic and textural properties of ordered mesoporous silicas for their application as catalysts in the etherification of glycerol with isobutene, Catalysis Today 227 (2014) 171-178.

[60] V. Mangourilos, D. Bombos, M. Bombos, R. Ganea, I. Bolocan, Influence of catalyst porosity on the etherification of glycerol with isobutene, Revista de Chimie 65 (2014) 612-615.

[61] J. Zhou, Y. Wang, X. Guo, J. Mao, S. Zhang, Etherification of glycerol with isobutene on sulfonated graphene: reaction and separation, Green Chemistry 16 (2014) 4669-4679.

[62] V. Mangourilos, D. Bombos, M. Bombos, R. Ganea, I. Bolocan, Etherification of glycerol with isobutene on triflic acid/γAl2O3 catalyst, Revista de Chimie 65 (2014) 481-484.

[63] F. Frusteri, F. Arena, G. Bonura, C. Cannilla, L. Spadaro, O. Di Blasi, Catalytic etherification of glycerol by tert-butyl alcohol to produce oxygenated additives for diesel fuel, Applied Catalysis A: General 367 (2009) 77-83.

[64] N. Ozbay, N. Oktar, G. Dogu, T. Dogu, Conversion of biodiesel by-product glycerol to fuel ethers over different solid acid catalysts, International Journal of Chemical Reactor Engineering 8 (2010).

[65] W. Kiatkittipong, P. Intaracharoen, N. Laosiripojana, C. Chaisuk, P. Praserthdam, S. Assabumrungrat, Glycerol ethers synthesis from glycerol etherification with tert-butyl alcohol in reactive distillation, Computers & Chemical Engineering 35 (2011) 2034-2043.

[66] J.S. Chang, D.H. Chen, Optimization on the etherification of glycerol with tert-butyl alcohol, Journal of the Taiwan Institute of Chemical Engineers 42 (2011) 760-767.

[67] N. Ozbay, N. Oktar, G. Dogu, T. Dogu, Effects of sorption enhancement and isobutene formation on etherification of glycerol with tert-butyl alcohol in a flow reactor, Industrial & Engineering Chemistry Research 51 (2011) 8788-8795.

[68] M.P. Pico, A. Romero, S. Rodríguez, A. Santos, Etherification of glycerol by tert-butyl alcohol: kinetic model, Industrial & Engineering Chemistry Research 51 (2012) 9500-9509.

[69] V. E., C.S. Bildea, G. Bozga, Design and control of glycerol-tert-butyl alcohol etherification process, The Scientific World Journal 2012 (2012) 1-11.

[70] M.D. González, Y. Cesteros, P. Salagre, Establishing the role of Brønsted acidity and porosity for the catalytic etherification of glycerol with tert-butanol by modifying zeolites, Applied Catalysis A: General 450 (2013) 178-188.

[71] N. Viswanadham, S.K. Saxena, Etherification of glycerol for improved production of oxygenates, Fuel 103 (2013) 980-986.

[72] N. Ozbay, N. Oktar, G. Dogu, T. Dogu, Activity comparison of different solid acid catalysts in etherification of glycerol with tert-butyl alcohol in flow and batch reactors, Topics in Catalysis 56 (2013) 1790-1803.

[73] M.P. Pico, J.M. Rosas, S. Rodríguez, A. Santos, A. Romero, Glycerol etherification over acid ion exchange resins:effect of catalyst concentration and reusability, Journal of Chemical Technology & Biotechnology 88 (2013) 2027-2038.

[74] T.S. Galhardo, N. Simone, M. Gonçalves, F.C.A. Figueiredo, D. Mandelli, W.A. Carvalho, Preparation of sulfonated carbons from rice husk and their application in catalytic conversion of glycerol, ACS Sustainable Chemistry & Engineering 1 (2013) 1381-1389.

[75] M. Gonçalves, V.C. Souza, T.S. Galhardo, M. Mantovani, F.C.A. Figueiredo, D. Mandelli, W.A. Carvalho, Glycerol conversion catalyzed by carbons prepared from agroindustrial wastes, Industrial & Engineering Chemistry Research 52 (2013) 2832-2839.

[76] C. Beatrice, G. Di Blasio, M. Lazzaro, C. Cannilla, G. Bonura, F. Frusteri, F. Asdrubali, G. Baldinelli, A. Presciutti, F. Fantozzi, G. Bidini, P. Bartocci, Technologies for energetic exploitation of biodiesel chain derived glycerol:oxy-fuels production by catalytic conversion, Applied Energy 102 (2013) 63-71.

[77] C. Cannilla, G. Bonura, L. Frusteri, F. Frusteri, Glycerol etherification with TBA:high yield to poly-ethers using a membrane assisted batch reactor, Environmental Science & Technology 48 (2014) 6019-6026.

[78] P.A. Celdeira, M. Gonçalves, F.C.A. Figueiredo, S.M.D. Bosco, D. Mandelli, W.A. Carvalho, Sulfonated niobia and pillared clay as catalysts in etherification reaction of glycerol, Applied Catalysis A: General 478 (2014) 98-106.

[79] J.S. Chang, Y.C. Zhang, C.C. Chen, T.R. Ling, Y.J. Chiou, G.B. Wang, K.T. Chang, T.C. Chou, One-step synthesis of gasoline octane booster and diesel fuel from glycerol and tert-butyl alcohol, Industrial & Engineering Chemistry Research 53 (2014) 5398-5405.

[80] C. García-Sancho, R. Moreno-Tost, J.M. Mérida-Robles, J. Santamaría-González, A. Jiménez-López, P.M. Torres, Etherification of glycerol to polyglycerols over MgAl mixed oxides, Catalysis Today 167 (2011) 84-90.

[81] M. Ayoub, M.S. Khayoon, A.Z. Abdullah, Synthesis of oxygenated fuel additives via the solventless etherification of glycerol, Bioresource Technology 112 (2012) 308-312.

[82] M.V. Sivaiah, S. Robles-Manuel, S. Valange, J. Barrault, Recent developments in acid and base-catalyzed etherification of glycerol to polyglycerols, Catalysis Today 198 (2012) 305-313.

[83] Z. Gholami, A.Z. Abdullah, K.T. Lee, Selective etherification of glycerol over heterogeneous mixed oxide catalyst: optimization of reaction parameters, Chemical Engineering and Science 1 (2013) 79-86.

[84] M. Quiroga, N. Fígoli, U. Sedran, Alternative catalysts for MTBE production, Reaction Kinetics and Catalysis Letters 63 (1998) 75-80.

[85] J.G. Goodwin, S. Natesakhawat, A.A. Nikolopoulos, S.Y. Kim, Etherification on Zeolites: MTBE synthesis, LCTR 44 (2002) 287-320.

[86] J.A. Kent, Kent and Riegel's Handbook of Industrial Chemistry and Biotechnology: Vol. 1, Springer (2010) pp. 350, 388.

[87] H.S. Kesling, L.J. Karas, F.J. Liotta, 'US 5308365 A', Diesel fuel (1994).

[88] D.S. Bradin, 'US 5578090 A', Biodiesel fuel (1996).

[89] H. Noureddini, 'US 6174501 B1', A multicompartment chemical reactor comprising a transesterification unit, a transesterified triglycerides/crude glycerol separator unit, etherification unit, to form soluble etherified glycerol (2001).

[90] H. Noureddini, 'US6015440 A', Process for producing biodiesel fuel with reduced viscosity and a cloud point below thirty-two (32) degrees fahrenheit (2000).

[91] A. Demirbas, Glycerol-based fuel oxygenates for biodiesel and diesel fuel blends, Energy Sources, Part A: Recovery, Utilization, and Environmental Effects 31 (2009) 1770-1776.

[92] M.O. Guerrero-Pérez, J.M. Rosas, J. Bedia, J. Rodríguez-Mirasol, T. Cordero, Recent inventions in glycerol transformations and processing Recent Patents on Chemical Engineering 2 (2009) 11-21.

[93] M. Ayoub, A.Z. Abdullah, Critical review on the current scenario and significance of crude glycerol resulting from biodiesel industry towards more sustainable renewable energy industry, Renewable and Sustainable Energy Reviews 16 (2012) 2671-2686.

[94] A.B. Leoneti, V. Aragão-Leoneti, S.V.W.B. de Oliveira, Glycerol as a by-product of biodiesel production in Brazil:alternatives for the use of unrefined glycerol, Renewable Energy 45 (2012) 138-145.

[95] J.F. Izquierdo, M. Montiel, I. Palés, P.R. Outón, M. Galán, L. Jutglar, M. Villarrubia, M. Izquierdo, M.P. Hermo, X. Ariza, Fuel additives from glycerol etherification with light olefins:state of the art, Renewable and Sustainable Energy Reviews 16 (2012) 6717-6724.

[96] C.H. Zhou, J.N. Beltramini, Y.X. Fan, G.Q. Lu, Chemoselective catalytic conversion of glycerol as a biorenewable source to valuable commodity chemicals, Chemical Society Reviews 37 (2008) 527-549.

[97] C.H. Zhou, H. Zhao, D.S. Tong, L.M. Wu, W.H. Yu, Recent advances in catalytic conversion of glycerol, Catalysis Reviews 55 (2013) 369-453.

[98] S. Bagheri, N.M. Julkapli, W.A. Yehye, Catalytic conversion of biodiesel derived raw glycerol to value added products, Renewable and Sustainable Energy Reviews 41 (2015) 113-127.

[99] M.S. Ardi, M.K. Aroua, N.A. Hashim, Progress, prospect and challenges in glycerol purification process: A review, Renewable and Sustainable Energy Reviews 42 (2015) 1164-1173.

[100] T.M. Lovestead, T.J. Bruno, Comparison of diesel fuel oxygenate additives with composition-explicit distillation curve method Part 3: t-butyl glycerols, Energy & Fuels 25 (2011) 2518 - 2525.

[101] G.F. Versteeg, P. Ijben, W.N. Wermink, K. Klepacova, S. Van Loo, W. Kesber, 'EP 2294043 A2', Method of Preparing Glycerol Alkyl Ethers (2011).

[102] J. Liu, B. Yang, Liquid–liquid–solid mass transfer and phase behavior of heterogeneous etherification of glycerol with isobutene, AIChE Journal 64 (2018) 2526-2535.

[103] J. Liu, Y. Yuan, Y. Pan, Z. Huang, B. Yang, Liquid–liquid equilibrium for systems of glycerol and glycerol tert-butyl ethers, Fluid Phase Equilibria 365 (2014) 50-57.

[104] J. Liu, B. Yang, C. Yi, Kinetic Study of Glycerol Etherification with Isobutene, Industrial & Engineering Chemistry Research 52 (2013) 3742-3751.

[105] V.P. Gupta, 'US 5476971 A', Etherification; reacting liquid phase isobutylene and glycerine in two phase reaction system (1995).

[106] J.K. Cheng, C.-L. Lee, Y.-T. Jhuang, J.D. Ward, I.L. Chien, Design and control of the glycerol tertiary butyl ethers process for the utilization of a renewable resource, Industrial & Engineering Chemistry Research 50 (2011) 12706-12716.

[107] E. Vlad, C.S. Bildea, Reactive distillation-a viable solution for etherification of glycerol with tert-butyl alcohol Chemical Engineering Transactions 29 (2012) 589-594.

[108] E. Vlad, C.S. Bildea, G. Bozga, Robust optimal design of an glycerol etherification process, Chemical Engineering & Technology 36 (2013) 251-258.

[109] L. Simasatitkul, P. Kaewwisetkul, W. Wiyaratn, S. Assabumrungrat, A. Arpornwichanop, Optimal design and performance analyses of the glycerol ether production process using a reactive distillation column, Journal of Industrial and Engineering Chemistry 43 (2016) 93-105.

[110] N. Oktar, K. Mürtezaoğlu, G. Doğu, İ. Gönderten, T. Doğu, Etherification rates of 2-methyl-2-butene and 2-methyl-1-butene with ethanol for environmentally clean gasoline production, Journal of Chemical Technology & Biotechnology 74 (1999) 155-161.

[111] C.O.T. Lemos, L.L. Rade, M.A.d.S. Barrozo, L. Cardozo-Filho, C.E. Hori, Study of glycerol etherification with ethanol in fixed bed reactor under high pressure, Fuel Processing Technology 178 (2018) 1-6.

[112] M.R. Nanda, Z. Yuan, W. Qin, H.S. Ghaziaskar, M.-A. Poirier, C. Xu, A new continuous-flow process for catalytic conversion of glycerol to oxygenated fuel additive:catalyst screening, Applied Energy 123 (2014) 75-81.

[113] Dow Chemical, DOWEX Ion Exchange Resins (2000) http://msdssearch.dow.com/PublishedLiteratureDOWCOM/dh_0032/0901b803800326ca.pdf?filepath=liquidseps/pdfs/noreg/177-01837.pdf&fromPage=GetDoc (Last accessed 20.12.14)

[114] Y.d. Miguel, T. Rohr, D.C. Sherrington, in: M.R. Buchmeiser (Ed.), Polymeric Materials in Organic Synthesis and Catalysis, WILEY-VCH Verlag GmbH & Co. KGaA, Weinheim (2006) pp. 1-6.

[115] N.M. Bortnick, 'US 3037052 A', Catalyzing reactions with cation exchange resin (1962).

[116] Aldrich, Nafion® resins:novel device applications https://www.sigmaaldrich.com/content/dam/sigma-aldrich/docs/Aldrich/Brochure/al_pp_nafion.pdf (Last accessed 20.12.14)

[117] D. Mravec, K. Klepáčová, E. Hájeková, M. Bajus, Oxygenates to diesel fuels by tert-butylation of glycerol, 13th International Congress on Catalysis, Book of Abstracts 2 (P4 005) (2004).

[118] B.C. Gates, Handbook of Heterogeneous Catalysis, Wiley-VCH Verlag GmbH & Co. KGaA (2008).

[119] M. Mazzotti, B. Neri, D. Gelosa, A. Kruglov, M. Morbidelli, Kinetics of liquid-phase esterification catalyzed by acidic resins, Industrial & Engineering Chemistry Research 36 (1997) 3-10.

[120] C. Saengarun, A. Petsom, D.N. Tungasmita, Etherification of Glycerol with Propylene or 1-Butene for Fuel Additives, The Scientific World Journal 2017 (2017) 11.

[121] Zeolyst International, FAQ's http://www.zeolyst.com/faqs.aspx (Last access 20.12.14)

[122] J.B. Uytterhoeven, L.G. Christner, W.K. Hall, Studies of the hydrogen held by solids. VIII. the decationated zeolites, The Journal of Physical Chemistry 69 (1965) 2117-2126.

[123] P.A. Jacobs, H.K. Beyer, Evidence for the nature of true Lewis sites in faujasite-type zeolites, The Journal of Physical Chemistry 83 (1979) 1174-1177.

[124] D. Coster, A.L. Blumenfeld, J.J. Fripiat, Lewis acid sites and surface aluminum in aluminas and zeolites:a high-resolution NMR study, The Journal of Physical Chemistry 98 (1994) 6201-6211.

[125] S. Li, A. Zheng, Y. Su, H. Zhang, L. Chen, J. Yang, C. Ye, F. Deng, Brønsted/Lewis acid synergy in dealuminated HY zeolite: a combined solid-state NMR and theoretical calculation study, Journal of the American Chemical Society 129 (2007) 11161-11171.

[126] J. Huang, Y. Jiang, V.R.R. Marthala, B. Thomas, E. Romanova, M. Hunger, Characterization and acidic properties of aluminum-exchanged zeolites X and Y, The Journal of Physical Chemistry C 112 (2008) 3811-3818.

[127] A.W. Peters, in: S.M. John, M.M. Maurice (Eds.), Studies in Surface Science and Catalysis, Elsevier (1993) pp. 183-221.

[128] W. Hölderich, M. Hesse, F. Näumann, Zeolites: Catalysts for Organic Syntheses, Angewandte Chemie International Edition in English 27 (1988) 226-246.

[129] A. Kogelbauer, A.A. Nikolopoulos, J.G. Goodwin, G. Marcelin, Reactant Adsorption and Its Impact upon MTBE Synthesis on Zeolites, Journal of Catalysis 152 (1995) 122-129.

[130] C. Dewattines, H. Hinnekens, 'EP 0649829 A1', Process for the production of glycerol ethers (1995).

[131] K. Hauge, E. Bergene, D. Chen, G.R. Fredriksen, A. Holmen, Oligomerization of isobutene over solid acid catalysts, Catalysis Today 100 (2005) 463-466.

[132] H.K. Beyer, Post-Synthesis Modification I, Springer Berlin Heidelberg (2002) pp. 203-255.

[133] A.W. O'Donovan, C.T. O'Connor, K.R. Koch, Effect of acid and steam treatment of Na- and H-mordenite on their structural, acidic and catalytic properties, Microporous Materials 5 (1995) 185-202.

[134] R. Srivastava, N. Iwasa, S.-i. Fujita, M. Arai, Dealumination of zeolite beta catalyst under controlled conditions for enhancing its activity in acylation and esterification, Catalysis Letters 130 (2009) 655-663.

[135] Z. Yu, S. Li, Q. Wang, A. Zheng, X. Jun, L. Chen, F. Deng, Brønsted/Lewis acid synergy in H-ZSM-5 and H-MOR zeolites studied by 1H and 27Al DQ-MAS solid-state NMR spectroscopy, The Journal of Physical Chemistry C 115 (2011) 22320-22327.

[136] D.P. Serrano, T.J. Pinnavaia, J. Aguado, J.M. Escola, A. Peral, L. Villalba, Hierarchical ZSM-5 zeolites synthesized by silanization of protozeolitic units: Mediating the mesoporosity contribution by changing the organosilane type, Catalysis Today 227 (2014) 15-25.

[137] R.B. Borade, A. Clearfield, Effect of fluoride ions on the acidic and catalytic properties of beta zeolite, Journal of the Chemical Society, Faraday Transactions 91 (1995) 539-547.

[138] R. Sadeghbeigi, in: R. Sadeghbeigi (Ed.), Fluid Catalytic Cracking Handbook (Second edition), Gulf Professional Publishing, Houston (2000) pp. 84-124.

[139] D. Mravec, A. Turan, A. Filková, N. Mikesková, E. Volkovicsová, G. Onyestyák, S. Harnos, F. Lónyi, J. Valyon, A. Kaszonyi, Catalytic etherification of bioglycerol with bioethanol over H-Beta, H-Y and H-MOR zeolites, Fuel Processing Technology 159 (2017) 111-117.

[140] P. Lanzafame, K. Barbera, G. Papanikolaou, S. Perathoner, G. Centi, M. Migliori, E. Catizzone, G. Giordano, Comparison of H+ and NH4+ forms of zeolites as acid catalysts for HMF etherification, Catalysis Today 304 (2018) 97-102.

[141] P. Lanzafame, G. Papanikolaou, S. Perathoner, G. Centi, M. Migliori, E. Catizzone, A. Aloise, G. Giordano, Direct versus acetalization routes in the reaction network of catalytic HMF etherification, Catalysis Science & Technology 8 (2018) 1304-1313.

[142] F. Jamil, S.K. Saxena, A.a.H. Al-Muhtaseb, M. Baawain, M. Al-Abri, N. Viswanadham, G. Kumar, A.M. Abu-Jrai, Valorization of waste “date seeds” bio-glycerol for synthesizing oxidative green fuel additive, Journal of Cleaner Production 165 (2017) 1090-1096.

[143] D.P. Serrano, J.A. Melero, G. Morales, J. Iglesias, P. Pizarro, Progress in the design of zeolite catalysts for biomass conversion into biofuels and bio-based chemicals, Catalysis Reviews 60 (2018) 1-70.

[144] C. Aquino, T. Maschmeyer, in: V. Valtchev, S. Mintova, M. Tsapatsis (Eds.), Ordered Porous Solids, Elsevier, Amsterdam (2009) pp. 3-30.

[145] W. Schmidt, in: V. Valtchev, S. Mintova, M. Tsapatsis (Eds.), Ordered Porous Solids, Elsevier, Amsterdam (2009) pp. 51-75.

[146] T.R. Pauly, T.J. Pinnavaia, Pore size modification of mesoporous HMS molecular sieve silicas with wormhole framework structures, Chemistry of Materials 13 (2001) 987-993.

[147] I.K. Mbaraka, D.R. Radu, V.S.Y. Lin, B.H. Shanks, Organosulfonic acid-functionalized mesoporous silicas for the esterification of fatty acid, Journal of Catalysis 219 (2003) 329-336.

[148] I.K. Mbaraka, B.H. Shanks, Design of multifunctionalized mesoporous silicas for esterification of fatty acid, Journal of Catalysis 229 (2005) 365-373.

[149] P. Dhepe, M. Ohashi, S. Inagaki, M. Ichikawa, A. Fukuoka, Hydrolysis of sugars catalyzed by water-tolerant sulfonated mesoporous silicas, Catalysis Letters 102 (2005) 163-169.

[150] J.A. Bootsma, B.H. Shanks, Cellobiose hydrolysis using organic-inorganic hybrid mesoporous silica catalysts, Applied Catalysis A: General 327 (2007) 44-51.

[151] D. Margolese, J.A. Melero, S.C. Christiansen, B.F. Chmelka, G.D. Stucky, Direct syntheses of ordered SBA-15 mesoporous silica containing sulfonic acid groups, Chemistry of Materials 12 (2000) 2448-2459.

[152] J.A. Melero, G.D. Stucky, R. van Grieken, G. Morales, Direct syntheses of ordered SBA-15 mesoporous materials containing arenesulfonic acid groups, Journal of Materials Chemistry 12 (2002) 1664-1670.

[153] J.A. Melero, L.F. Bautista, G. Morales, J. Iglesias, R. Sánchez-Vázquez, Biodiesel production from crude palm oil using sulfonic acid-modified mesostructured catalysts, Chemical Engineering Journal 161 (2010) 323-331.

[154] D. Ciuparu, Y. Chen, S. Lim, Y. Yang, G.L. Haller, L. Pfefferle, Mechanism of cobalt cluster size control in Co-MCM-41 during single-wall carbon nanotubes synthesis by CO disproportionation, The Journal of Physical Chemistry B 108 (2004) 15565-15571.

[155] H. Wan, L. Liu, C. Li, X. Xue, X. Liang, Facile synthesis of mesoporous SBA-15 silica spheres and its application for high-performance liquid chromatography, Journal of Colloid and Interface Science 337 (2009) 420-426.

[156] W. Zhao, P. Salame, F. Launay, A. Gédéon, Z. Hao, Sulfonic acid functionalised SBA-15 as catalysts for Beckmann rearrangement and esterification reaction, Journal of Porous Materials 15 (2008) 139-143.

[157] S. Sadjadi, M.M. Heravi, Current advances in the utility of functionalized SBA mesoporous silica for developing encapsulated nanocatalysts: state of the art, RSC Advances 7 (2017) 30815-30838.

[158] M. Śliwa, K. Samson, M. Ruggiero–Mikołajczyk, A. Żelazny, R. Grabowski, Influence of montmorillonite K10 modification with tungstophosphoric acid on hybrid catalyst activity in direct dimethyl ether synthesis from syngas, Catalysis Letters 144 (2014) 1884-1893.

[159] S. Storck, W.F. Maier, I.M. Miranda Salvado, J.M.F. Ferreira, D. Guhl, W. Souverijns, J.A. Martens, Amorphous Sn/Si mixed oxides, mild solid lewis acid catalysts for esterification and etherification reactions, Journal of Catalysis 172 (1997) 414-426.

[160] C. Beatrice, G. Di Blasio, M. Lazzaro, E. Mancaruso, R. Marialto, L. Sequino, B.M. Vaglieco, Investigation of the combustion in both metal and optical diesel engines using high-glycerol ethers/diesel blends, International Journal of Engine Research 16 (2015) 38-51.

[161] M.S. Sidhu, M.M. Roy, W. Wang, Glycerine emulsions of diesel-biodiesel blends and their performance and emissions in a diesel engine, Applied Energy 230 (2018) 148-159.

[162] A.-M. Al-Lal, J.-E. García-González, A. Llamas, A. Monjas, L. Canoira, A new route to synthesize tert-butyl ethers of bioglycerol, Fuel 93 (2012) 632-637.

[163] Y. Zheng, X. Chen, Y. Shen, Commodity chemicals derived from glycerol, an important biorefinery feedstock, Chem Rev 108 (2008) 5253-5277.

[164] R. Ciriminna, C.D. Pina, M. Rossi, M. Pagliaro, Understanding the glycerol market, European Journal of Lipid Science and Technology 116 (2014) 1432-1439.

[165] M. Pagliaro, R. Ciriminna, H. Kimura, M. Rossi, C. Della Pina, From glycerol to value-added products, Angewandte Chemie International Edition 46 (2007) 4434-4440.

[166] F. Yang, M. Hanna, R. Sun, Value-added uses for crude glycerol--a byproduct of biodiesel production, Biotechnology for Biofuels 5 (2012) 13.

[167] I. Wan, N.R. Wan, R. Che, A. Zatil, M. Ismail, J. Mohd Jahim, M.A. Yarmo, Recovery and purification of crude glycerol from vegetable oil transesterification, Separation & Purification Reviews 44 (2014) 250-267.

[168] ICIS, Asia glycerine market poised to firm on tight supply (2015) http://www.icis.com/resources/news/2015/01/22/9854502/asia-glycerine-market-poised-to-firm-on-tight-supply/ (Last access 08.05.15)

[169] J.A. Posada, Higuita, J. C., Cardona, C. A., , Optimization on the use of crude glycerol from the biodiesel to obtain poly-3-hydroxybutyrate World Renewable Energy Congress, Linkoping, Sweden (2011).

[170] A. Uzun, B.C. Gates, Dynamic Structural Changes in a Molecular Zeolite-Supported Iridium Catalyst for Ethene Hydrogenation, Journal of the American Chemical Society 131 (2009) 15887-15894.

[171] H. Fukuda, T. Fujii, T. Ogawa, Microbial production of C3 and C4 hydrocarbons under aerobic conditions, Agricultural and Biological Chemistry 48 (1984) 1679-1682.

[172] H. Fukuda, T. Fujii, T. Ogawa, Production of isobutene by Rhodotorula yeasts, Agricultural and Biological Chemistry 49 (1985) 1541-1543.

[173] T. Fujii, T. Ogawa, H. Fukuda, Isobutene production by Rhodotorula minuta, Applied Microbiology and Biotechnology 25 (1987) 430-433.

[174] T. Fujii, T. Ogawa, H. Fukuda, Preparation of a cell-free, isobutene-forming system from Rhodotorula minuta, Applied and Environmental Microbiology 54 (1988) 583-584.

[175] H. Fukuda, T. Fujii, E. Sukita, M. Tazaki, S. Nagahama, T. Ogawa, Reconstitution of the isobutene-forming reaction catalyzed by cytochrome P450 and P450 reductase from Rhodotorula minuta: decarboxylation with the formation of isobutene, Biochemical and Biophysical Research Communications 201 (1994) 516-522.

[176] J. Sun, K. Zhu, F. Gao, C. Wang, J. Liu, C.H.F. Peden, Y. Wang, Direct conversion of bio-ethanol to isobutene on nanosized ZnxZryOz mixed oxides with balanced acid–base sites, Journal of the American Chemical Society 133 (2011) 11096-11099.

[177] U.S. EPA, Methyl Tertiary Butyl Ether (2016) https://archive.epa.gov/mtbe/web/html/faq.html#concerns (Last access 16.01.18)

[178] J.H. Gibbons, Interagency Assessment of Oxygenated Fuels, National Science and Technology Council (1997).

[179] U.S. EPA, Regulatory Determinations Support Document for Selected Contaminants from the Second Drinking Water Contaminant Candidate List (CCL 2), Chapter 13: MTBE, (2008) pp. 13-11 to 13-76.

[180] B.P. Pinto, J.T. de Lyra, J.A.C. Nascimento, C.J.A. Mota, Ethers of glycerol and ethanol as bioadditives for biodiesel, Fuel 168 (2016) 76-80.

[181] H. Noureddini, W.R. Dailey, B.A. Hunt, Production of ethers of glycerol from crude glycerol the by-product of biodiesel production, Adv. Environ. Res. 2 (1998) 232–243.

[182] D.B. V. Mangourilos, T. Juganaru, I. Bolocan, M. Bombos, D. Ciuparu Etherification of glycerol with isobutene on Amberlyst 35 ion exchange resin catalyst in presence of a cationic emulsifier, Rev. Chim. 60 (2009) 1338-1342.

[183] M.D. González, Y. Cesteros, P. Salagre, Establishing the role of Brønsted acidity and porosity for the catalytic etherification of glycerol with tert-butanol by modifying zeolites, Applied Catalysis A: General 450 (2013) 178-188.

[184] V. Voicu, D. Bombos, I. Bolocan, C.R. Jang, D. Ciuparu, The influence of the character of emulsifiers on the performance of H 4SiW 12O 40.30H 2O heteropolyacid catalyst in glycerol etherification with isobutene, Revista de Chimie 63 (2012) 200-204.

[185] J.L. Agudelo, E.J.M. Hensen, S.A. Giraldo, L.J. Hoyos, Influence of steam-calcination and acid leaching treatment on the VGO hydrocracking performance of faujasite zeolite, Fuel Processing Technology 133 (2015) 89-96.

[186] W. M., Fityk : a general-purpose peak fitting program, Journal of Applied Crystallography 43 (2010) 1126-1128.

[187] F. Lónyi, J. Valyon, On the interpretation of the NH3-TPD patterns of H-ZSM-5 and H-mordenite, Microporous and Mesoporous Materials 47 (2001) 293-301.

[188] J.T. Scanlon, D.E. Willis, Calculation of Flame Ionization Detector Relative Response Factors Using the Effective Carbon Number Concept, Journal of Chromatographic Science 23 (1985) 333-340.

[189] Ö.D. Bozkurt, N. Bağlar, S. Çelebi, A. Uzun, Assessment of Acid Strength in Sodium-Exchanged Acid Resins: Consequences on Glycerol Etherification with Isobutene in Batch and Flow Reactors, Molecular Catalysis 466 (2019) 1-12.

[190] Z. Yu, S. Li, Q. Wang, A. Zheng, X. Jun, L. Chen, F. Deng, Brønsted/Lewis Acid Synergy in H–ZSM-5 and H–MOR Zeolites Studied by 1H and 27Al DQ-MAS Solid-State NMR Spectroscopy, The Journal of Physical Chemistry C 115 (2011) 22320-22327.

[191] W. Xiaoning, Z. Zhen, X. Chunming, D. Aijun, Z. Li, J. Guiyuan, Effects of Light Rare Earth on Acidity and Catalytic Performance of HZSM-5 Zeolite for Catalytic Cracking of Butane to Light Olefins, Journal of Rare Earths 25 (2007) 321-328.

[192] S.K. Saxena, A.a.H. Al-Muhtaseb, N. Viswanadham, Enhanced production of high octane oxygenates from glycerol etherification using the desilicated BEA zeolite, Fuel 159 (2015) 837-844.

[193] E. Kocaman, Ö. Akarçay, N. Bağlar, S. Çelebi, A. Uzun, Isobutene oligomerization on MCM-41-supported tungstophosphoric acid, Molecular Catalysis 457 (2018) 41-50.

[194] M.E. Chimienti, L.R. Pizzio, C.V. Cáceres, M.N. Blanco, Tungstophosphoric and tungstosilicic acids on carbon as acidic catalysts, Applied Catalysis A: General 208 (2001) 7-19.

[195] N. Narkhede, S. Singh, A. Patel, Recent progress on supported polyoxometalates for biodiesel synthesis via esterification and transesterification, Green Chemistry 17 (2015) 89-107.

[196] M.L. Sarazen, E. Doskocil, E. Iglesia, Effects of Void Environment and Acid Strength on Alkene Oligomerization Selectivity, ACS Catalysis 6 (2016) 7059-7070.

[197] S.P. Felix, C. Savill-Jowitt, D.R. Brown, Base adsorption calorimetry for characterising surface acidity: a comparison between pulse flow and conventional “static” techniques, Thermochimica Acta 433 (2005) 59-65.

[198] P.F. Siril, H.E. Cross, D.R. Brown, New polystyrene sulfonic acid resin catalysts with enhanced acidic and catalytic properties, Journal of Molecular Catalysis A: Chemical 279 (2008) 63-68.

[199] C. Baerlocher, L.B. McCusker, Database of Zeolite Structures, http://www.iza-structure.org/databases/ (Last access 28.09.18)

[200] L. Xiao, J. Mao, J. Zhou, X. Guo, S. Zhang, Enhanced performance of HY zeolites by acid wash for glycerol etherification with isobutene, Applied Catalysis A: General 393 (2011) 88-95.

[201] T. Okuhara, T. Nishimura, H. Watanabe, M. Misono, Insoluble heteropoly compounds as highly active catalysts for liquid-phase reactions, Journal of Molecular Catalysis 74 (1992) 247-256.

[202] K. Narasimharao, D.R. Brown, A.F. Lee, A.D. Newman, P.F. Siril, S.J. Tavener, K. Wilson, Structure–activity relations in Cs-doped heteropolyacid catalysts for biodiesel production, Journal of Catalysis 248 (2007) 226-234.

[203] L. Pizzio, P. Vázquez, C. Cáceres, M. Blanco, Tungstophosphoric and Molybdophosphoric Acids Supported on Zirconia as Esterification Catalysts, Catalysis Letters 77 (2001) 233-239.

[204] Ö.D. Bozkurt, N. Bağlar, F. Yılmaz, S. Çelebi, A. Uzun, Compatibility of di- and tri-tert-butyl glycerol ethers with gasoline, Fuel (2019) Under revision.

[205] R.M. Wheaton, L.J. Lefevre, Fundamentals of Ion Exchange, The Dow Chemical Company (2000).

[206] M.A. Harmer, Q. Sun, Solid acid catalysis using ion-exchange resins, Applied Catalysis A: General 221 (2001) 45-62.

[207] J.H. Clark, D.J. Macquarrie, Handbook of Green Chemistry and Technology, Wiley (2008) pp.

[208] T.M. Lovestead, T.J. Bruno, Comparison of Diesel Fuel Oxygenate Additives to the Composition-Explicit Distillation Curve Method. Part 3: t-Butyl Glycerols, Energy & Fuels 25 (2011) 2518-2525.

[209] Ö.D. Bozkurt, N. Bağlar, S. Çelebi, A. Uzun, Screening of Solid Acid Catalysts for Etherification of Glycerol with Isobutene under Identical Conditions, Catalysis Today (2019) Under review.

[210] M. Hart, G. Fuller, D.R. Brown, J.A. Dale, S. Plant, Sulfonated poly(styrene-co-divinylbenzene) ion-exchange resins: acidities and catalytic activities in aqueous reactions, Journal of Molecular Catalysis A: Chemical 182–183 (2002) 439-445.

[211] P.F. Siril, D.R. Brown, Acid site accessibility in sulfonated polystyrene acid catalysts: Calorimetric study of NH3 adsorption from flowing gas stream, Journal of Molecular Catalysis A: Chemical 252 (2006) 125-131.

[212] P.F. Siril, A.D. Davison, J.K. Randhawa, D.R. Brown, Acid strengths and catalytic activities of sulfonic acid on polymeric and silica supports, Journal of Molecular Catalysis A: Chemical 267 (2007) 72-78.

[213] M. Babucci, V. Balci, A. Akçay, A. Uzun, Interactions of [BMIM][BF4] with Metal Oxides and Their Consequences on Stability Limits, The Journal of Physical Chemistry C 120 (2016) 20089-20102.

[214] M. Babucci, A. Akçay, V. Balci, A. Uzun, Thermal Stability Limits of Imidazolium Ionic Liquids Immobilized on Metal-Oxides, Langmuir 31 (2015) 9163-9176.

[215] T. Shimanouchi, Tables of Molecular Vibrational Frequencies, National Bureau of Standards (1972) pp. 1-160.

[216] A.D. Becke, Density-functional thermochemistry. III. The role of exact exchange, The Journal of Chemical Physics 98 (1993) 5648-5652.

[217] C.T. Lee, W.T. Yang, R.G. Parr, Development of the Colle-Salvetti Correlation-Energy Formula into a Functional of the Electron-Density, Physical Review B 37 (1988) 785-789.

[218] E.P. Parry, An infrared study of pyridine adsorbed on acidic solids. Characterization of surface acidity, Journal of Catalysis 2 (1963) 371-379.

[219] E.A. Paukshtis, E.N. Yurchenko, Study of the Acid–Base Properties of Heterogeneous Catalysts by Infrared Spectroscopy, Russian Chemical Reviews 52 (1983) 242-258.

[220] H. Knozinger, S. Huber, IR spectroscopy of small and weakly interacting molecular probes for acidic and basic zeolites, Journal of the Chemical Society, Faraday Transactions 94 (1998) 2047-2059.

[221] S. Bordiga, C. Lamberti, F. Bonino, A. Travert, F. Thibault-Starzyk, Probing zeolites by vibrational spectroscopies, Chemical Society Reviews 44 (2015) 7262-7341.

[222] A. Zecchina, L. Marchese, S. Bordiga, C. Pazè, E. Gianotti, Vibrational Spectroscopy of NH4+ Ions in Zeolitic Materials: An IR Study, The Journal of Physical Chemistry B 101 (1997) 10128-10135.

[223] G. Fan, C. Liao, T. Fang, S. Luo, G. Song, Amberlyst 15 as a new and reusable catalyst for the conversion of cellulose into cellulose acetate, Carbohydrate Polymers 112 (2014) 203-209.

[224] P.U. Singare, R.S. Lokhande, R.S. Madyal, Thermal Degradation Studies of Some Strongly Acidic Cation Exchange Resins, Open Journal of Physical Chemistry Vol.01No.02 (2011) 10.

[225] C.N.R. Rao, R. Venkataraghavan, T.R. Kasturi, Contribution to the Infrared Spectra of Organosulphur Compounds, Canadian Journal of Chemistry 42 (1964) 36-42.

[226] Y. Liu, B. Yang, C. Yi, Density Functional Theory Investigation for Catalytic Mechanism of Gasoline Alkylation Desulfurization over NKC-9 Ion-Exchange Resin, Industrial & Engineering Chemistry Research 52 (2013) 6933-6940.

[227] Q. Ma, D. Chakraborty, F. Faglioni, R.P. Muller, W.A. Goddard, T. Harris, C. Campbell, Y. Tang, Alkylation of Phenol: A Mechanistic View, The Journal of Physical Chemistry A 110 (2006) 2246-2252.

[228] V.J. Cruz, J.F. Izquierdo, F. Cunill, J. Tejero, M. Iborra, C. Fité, Acid ion-exchange resins catalysts for the liquid-phase dimerization/etherification of isoamylenes in methanol or ethanol presence, Reactive and Functional Polymers 65 (2005) 149-160.

[229] R.S. Karinen, J.A. Linnekoski, A.O.I. Krause, Etherification of C5- and C8-Alkenes with C1- to C4-Alcohols, Catalysis Letters 76 (2001) 81-87.

[230] L.K. Rihko, P.K. Kiviranta-Pääkkönen, A.O.I. Krause, Kinetic Model for the Etherification of Isoamylenes with Methanol, Industrial & Engineering Chemistry Research 36 (1997) 614-621.

[231] D. Parra, J. Tejero, F. Cunill, M. Iborra, J.F. Izquierdo, Kinetic study of mtbe liquid-phase synthesis using C4 olefinic cut, Chemical Engineering Science 49 (1994) 4563-4578.

[232] R. Gounder, A.J. Jones, R.T. Carr, E. Iglesia, Solvation and acid strength effects on catalysis by faujasite zeolites, Journal of Catalysis 286 (2012) 214-223.

[233] S. Wang, E. Iglesia, Catalytic diversity conferred by confinement of protons within porous aluminosilicates in Prins condensation reactions, Journal of Catalysis 352 (2017) 415-435.

[234] D. Yun, Y.S. Yun, T.Y. Kim, H. Park, J.M. Lee, J.W. Han, J. Yi, Mechanistic study of glycerol dehydration on Brønsted acidic amorphous aluminosilicate, Journal of Catalysis 341 (2016) 33-43.

[235] S. Çelebi, N. Bağlar, E. Kocaman, A. Uzun, Ö.D. Bozkurt, Ö. Akarçay, 'Turkish Patent Institute Patent pending 2016/17804', Gliserinin eterifikasyonu için bir sistem ve yöntem-A system and method for glycerine etherification (2016).

[236] H.S. Fogler, Elements of Chemical Reaction Engineering, 4th ed., Pearson Education International (2006) pp. 757-851.

[237] I. Global Market Insights, Glycerol Market worth $3.04bn by 2022, (2016).

[238] OECD/FAO, OECD-FAO Agricultural Outlook 2017-2026 (2017) p. 121.

[239] OECD/FAO, OECD-FAO Agricultural Outlook 2018-2027 (2018) pp. 191-206.

[240] Techavio, Global Glycerol Market to Grow at Almost 9% CAGR Through 2021 (2017) https://www.businesswire.com/news/home/20170525006127/en/Global-Glycerol-Market-Grow-9-CAGR-2021 (Last access 04.11.18)

[241] H. Noureddini, 'US6174501B1', System and process for producing biodiesel fuel with reduced viscosity and a cloud point below thirty-two (32) degrees fahrenheit (2001).

[242] R.D. Wessendorf, W. Graf, 'EP 0718270 A2', Process for the preparation of polyol alkyl ethers (1996).

[243] G.F. Versteeg, W.N. Wermink, 'WO 2017/105246 A2', Gtbe compositions, methods and installations for enhanced octane boosting (2017).

[244] S.J. Kwang, H.K. Jae, G.K. Myung, C.C. Sang, N.F. Igor, 'WO2009066925A2', Method of manufacturing glycerol ether (2009).

[245] D. Sunil Shivajirao, N. Vinod Sankaran, M. Rekha, H. Umesh Krishna, 'WO2016120830A1', Methods for preparing glycerol tert-butyl ethers (2016).

[246] F. Frusteri, C. Cannilla, G. Bonura, L. Spadaro, A. Mezzapica, C. Beatrice, G. Di Blasio, C. Guido, Glycerol Ethers Production and Engine Performance with Diesel/Ethers Blend, Topics in Catalysis 56 (2013) 378-383.

[247] V.P. Gupta, 'US 5476971 A', Glycerine ditertiary butyl ether preparation (1995).

[248] H. Gerard, D. Bruno, D. Isabelle, 'US8419810B2', Method for producing biofuels, transforming triglycerides into at least two biofuel families: Fatty acid monoesters and ethers and/or soluble glycerol acetals (2013).

[249] A. Victor Manuel, J.B. Deborah, J.C. Patrick, P.K. David, C.C. Angella, 'US20070238905A1', Processes for converting glycerol to glycerol ethers (2007).

[250] S. Darbha, R. Paul, S. Lakshmi, 'WO2009113079A8', A process for the preparation of primary alkyl glycerol ethers useful as biofuel additive from glycerol (2009).

[251] Z. Ziyang, K. Hidajat, A.K. Ray, Determination of Adsorption and Kinetic Parameters for Methyl tert-Butyl Ether Synthesis from tert-Butyl Alcohol and Methanol, Journal of Catalysis 200 (2001) 209-221.

[252] A.B. Yu, Discrete element method: An effective way for particle scale research of particulate matter, Engineering Computations 21 (2004) 205-214.

[253] F. Benyahia, K.E. O'Neill, Enhanced Voidage Correlations for Packed Beds of Various Particle Shapes and Sizes, Particulate Science and Technology 23 (2005) 169-177.

[254] C.J. Geankoplis, Transport Processes and Separation Process Principles, 4th ed., Prentice Hall (2003) pp. 432.

[255] D. Papaioannou, T. Evangelou, C. Panayiotou, Dynamic viscosity of multicomponent liquid mixtures, Journal of Chemical & Engineering Data 36 (1991) 43-46.

[256] J.B. Secur, H.E. Oberstar, Viscosity of Glycerol and Its d J Aqueous Solutions, Industrial & Engineering Chemistry 43 (1951) 2118.

[257] N.A. Agayev, A.D. Yusibova, The Viscosity of Isobutane at High Pressures, US Air Force (1969).

[258] A.A.H. Pádua, J.M.N.A. Fareleira, J.C.G. Calado, W.A. Wakeham, Density and Viscosity Measurements of 2,2,4-Trimethylpentane (Isooctane) from 198 K to 348 K and up to 100 MPa, Journal of Chemical & Engineering Data 41 (1996) 1488-1494.

[259] P.B. Weisz, C.D. Prater, in: W.G. Frankenburg, V.I. Komarewsky, E.K. Rideal (Eds.), Advances in Catalysis, Academic Press (1954) pp. 143-196.

[260] F. Frusteri, L. Frusteri, C. Cannilla, G. Bonura, Catalytic etherification of glycerol to produce biofuels over novel spherical silica supported Hyflon® catalysts, Bioresource Technology 118 (2012) 350-358.

[261] V.O. Samoilov, D.N. Ramazanov, A.I. Nekhaev, A.L. Maximov, L.N. Bagdasarov, Heterogeneous catalytic conversion of glycerol to oxygenated fuel additives, Fuel 172 (2016) 310-319.

[262] C.M. Zhang, A.A. Adesina, M.S. Wainwright, Solubility Studies of Isobutene in Tertiary Butyl Alcohol + Water Mixtures, Journal of Chemical & Engineering Data 47 (2002) 1476-1480.

[263] Sigma Aldrich, Diisobutylene (2018) https://www.sigmaaldrich.com/catalog/product/sial/38180?lang=en&region=TR (Last access 09.05.18)

[264] Green Stone Swiss Co., Triisobutylene (2018) http://www.chemical-reagent.com/products/Triisobutylene_82dce539/ (Last access 08.05.18)

[265] Sigma Aldrich, (±)-3-tert-Butoxy-1,2-propanediol (2018) https://www.sigmaaldrich.com/catalog/product/aldrich/20444?lang=en&region=TR (Last access 09.05.18)

[266] ASTM International, ASTM D4809-13, Standard Test Method for Heat of Combustion of Liquid Hydrocarbon Fuels by Bomb Calorimeter (Precision Method), West Conshohocken, PA (2013).

[267] ASTM International, ASTM D6079-11(2016), Standard Test Method for Evaluating Lubricity of Diesel Fuels by the High-Frequency Reciprocating Rig (HFRR), West Conshohocken, PA (2016).

[268] Chevron, Diesel Fuels Technical Review (2007).

[269] H.W. Yarranton, J.C. Okafor, D.P. Ortiz, F.G.A. van den Berg, Density and Refractive Index of Petroleum, Cuts, and Mixtures, Energy & Fuels 29 (2015) 5723-5736.

[270] M.E. Jamróz, M. Jarosz, J. Witowska-Jarosz, E. Bednarek, W. Tęcza, M.H. Jamróz, J.C. Dobrowolski, J. Kijeński, Mono-, di-, and tri-tert-butyl ethers of glycerol: A molecular

spectroscopic study, Spectrochimica Acta Part A: Molecular and Biomolecular Spectroscopy 67 (2007) 980-988.

[271] J.E. Anderson, U. Kramer, S.A. Mueller, T.J. Wallington, Octane Numbers of Ethanol−and Methanol−Gasoline Blends Estimated from Molar Concentrations, Energy & Fuels 24 (2010) 6576-6585.

[272] ECS, EN 228:2012 + A1:2017 Automotive fuels - Unleaded petrol - Requirements and test methods (2017).

[273] EC, Directive 2009/30/EC of the European Parliament and of the Council, Official Journal of the European Union L 140/88 (2009).

[274] M.F. Couturier, K. George, M.H. Schneider, Thermophysical properties of wood-polymer composites, Wood Science and Technology 30 (1996) 179-196.

[275] ICIS, (2019) www.icis.com (Last access 26.03.19)

[276] G. Zundel, Hydration and Intermolecular Interaction, Academic Press (1969) pp. 116-231.

Appendices

Appendix A

Supplementary Material for Chapter 3

Screening of Solid Acid Catalysts for Etherification of Glycerol with Isobutene under Identical Conditions

Product analysis: Determination of component amounts and glycerol conversion

A general calibration line equation (**Equation A-1**) using octanol as the internal standard is expressed as, where *a* and *b* are constants and *A* refers to FID area in pA.s:

$$\frac{A_{compound}}{A_{octanol}} = a\frac{m_{compound}}{m_{octanol}} + b \qquad \textbf{(Equation A-1)}$$

Calibration equation constants are given in **Table A-1**.

Table A-1. Calibration equation constants for the commercially available compounds.

Component	a	b
Glycerol	0.2974	-0.0532
MTBGE	0.5841	-0.0056
DIB	1.2005	-0.0057

The amount of Glycerol, MTBGE and DIB in the GC sample was calculated by **Equation A-2**. Masses are in gram basis.

$$m_{compound} = \frac{\frac{A_{compound}}{A_{octanol}} - b}{a} x\, m_{octanol} \qquad \textbf{(Equation A-2)}$$

Calibration constants for commercially unavailable DTBGE, TTBGE, TIB, TetraIB and TBA were calculated by using GC-FID response factor method [188]. In this method, octanol was taken as the basis, and the weight-based response factors (R_{wt}) of products were calculated with **Equation A-3.**

$$R_{wt} = \frac{MW_{compound}}{MW_{octanol}}\, x\, \frac{ECN_{octanol}}{ECN_{compound}} \qquad \textbf{(Equation A-3)}$$

where, *MW* is molecular weight in g/mol and *ECN* is the effective carbon number. The results are shown in **Table A-2**.

.

Table A-2. Numbers used in the response factor method and the calculated R_{wt} values for the commercially unavailable compounds.

Component	MW (g/mol)	ECN	R_{wt}
Octanol	139.23	7.5	1.000
DTBGE	204.30	8.5	1.384
TTBGE	260.30	12.0	1.249
TIB	168.32	11.9	0.815
TetraIB	223.42	15.9	0.813
TBA	74.12	3.75	1.138

The amount of Octanol was known in the GC sample (internal standard). The amounts of DTBGE, TTBGE, TIB, TetraIB and TBA were calculated by **Equation A-4**.

$$m_{compound} = R_{wt}\ x\ m_{octanol}\ x\ \frac{A_{compound}}{A_{octanol}} \qquad \textbf{(Equation A-4)}$$

To determine the glycerol conversion, amounts of MTBGE, DTBGE and TTBGE in the GC sample were calculated in moles (**Equation A-5**).

$$n_{compound} = \frac{m_{compound}}{MW_{compound}} \qquad \textbf{(Equation A-5)}$$

Glycerol conversion was then calculated by considering each one mole of ether is formed from one mole of glycerol (**Equation A-6**).

$$Glycerol\ conversion\ (mol\%) = \frac{n_{MTBGE} + n_{DTBGE} + n_{TTBGE}}{n_{Gly} + n_{MTBGE} + n_{DTBGE} + n_{TTBGE}}\ x\ 100 \qquad \textbf{(Equation A-6)}$$

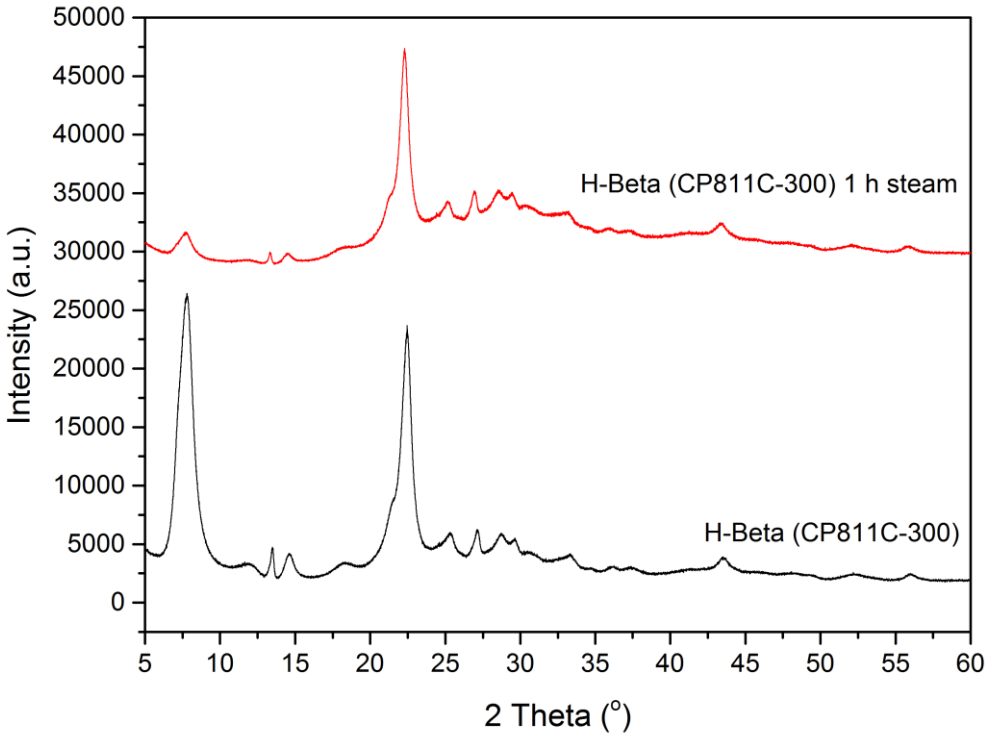

Figure A-1. XRD patterns of zeolite H-Beta (CP811C-300) before and after steam treatment.

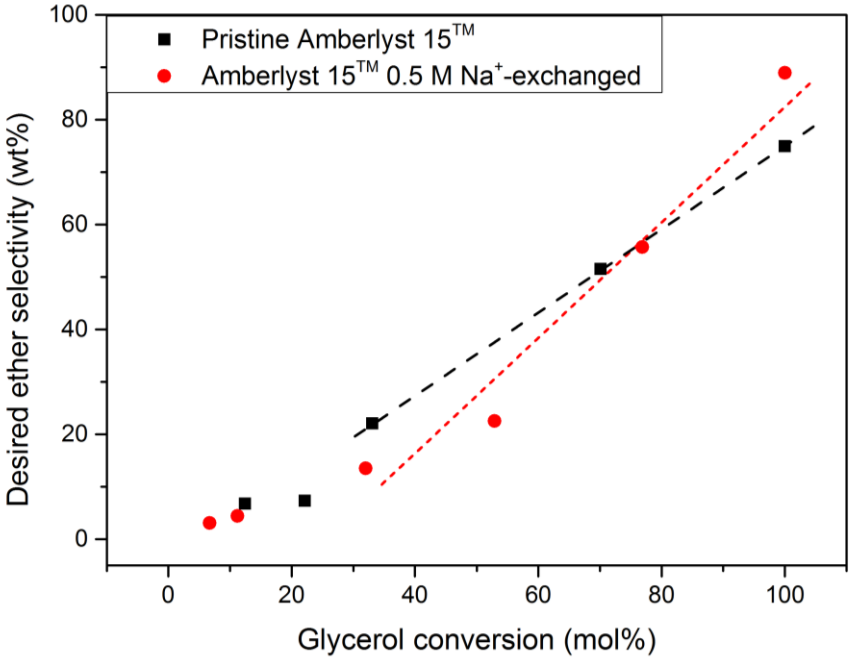

Figure A-2. Desired GTBE (DTBGE + TTBGE) selectivity of pristine and 0.5 M Na^+-exchanged Amberlyst 15™ catalysts with increasing glycerol conversion (75 °C, 7.5 wt% of glycerol catalyst loading, IB:G=3:1 mol:mol, autogenic pressure, 1200 rpm, 0.5-6 h).

Appendix B

Supplementary Material for Chapter 4

Assessment of Acid Strength in Sodium-Exchanged Resin Catalysts: Consequences on Glycerol Etherification with Isobutene in Batch and Flow Reactors

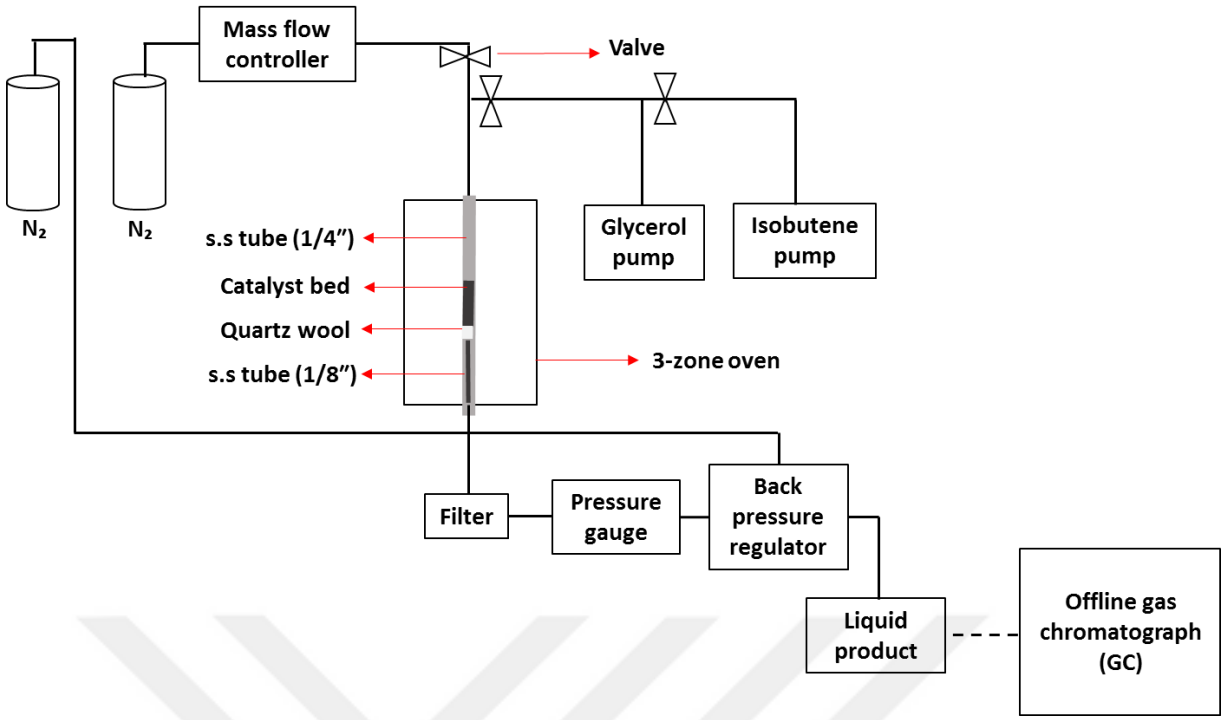

Figure B-1. Diagram of the liquid phase flow reactor system for glycerol etherification with isobutene [235]. The patent pending (Turkish Patent Institute - 2016/17804) with the title "Gliserinin Eterifikasyonu için Bir Sistem ve Yöntem-A System and Method for Glycerin Etherification".

Table B-1. Sodium loading on Amberlyst 15^{TM} samples.

Amberlyst 15^{TM} Na^+-exchange treatment	**Maximum sodium loading[a] (mmol Na^+/g_{cat})**	**Error[b] (mmol Na^+/g_{cat})**	**Sodium loading after NH_3 pulse chemisorption (mmol Na^+/g_{cat})**
No exchange	0	-	-
0.1 M	0.60	0.15	0.74
0.2 M	1.20	0.10	1.57
0.3 M	1.80	0.05	1.93
0.4 M	2.40	-0.37	2.39
0.5 M	3.00	-0.32	3.03

[a]Total amount of Na^+ in 15 ml $NaNO_3$ treatment solution divided by treated 2.5 g catalyst; [b]Difference between measured (by XRF) and calculated sodium loading.

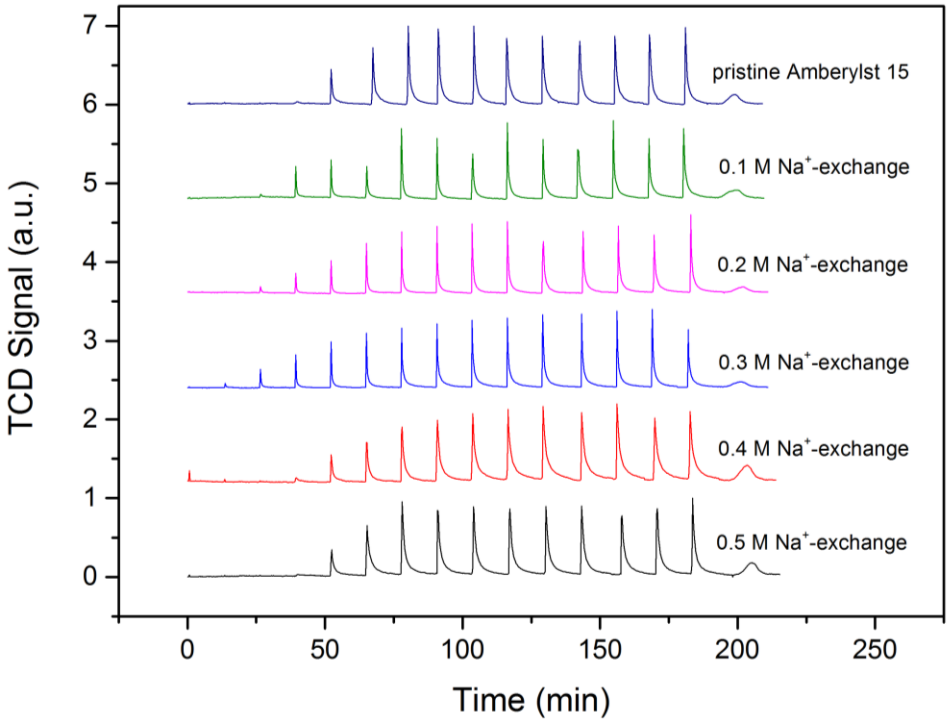

Figure B-2. Ammonia pulse chemisorption of pristine and Na^+-exchanged Amberlyst 15^{TM} samples.

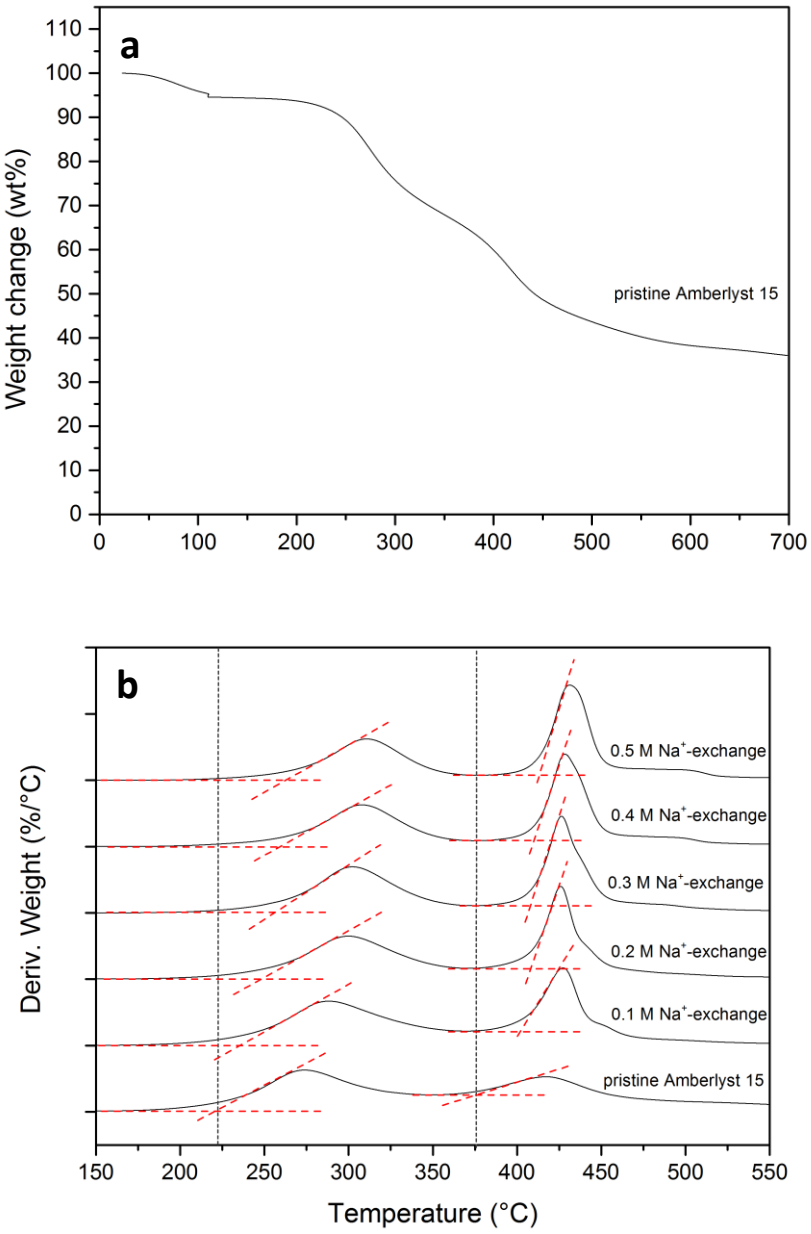

Figure B-3. Thermogravimetric analysis of Amberlyst 15^{TM} samples; **a:** weight change of pristine Amberlyst 15^{TM} with temperature; **b:** derivative weights and onset temperatures of pristine and Na^+-exchanged Amberlyst 15^{TM} samples.

Table B-2. Thermal decomposition onset temperatures of Amberlyst 15^{TM} samples.

Amberlyst 15^{TM} Na^+-exchange treatment	**T'_{onset} (°C)**
No exchange	224
0.1 M	236
0.2 M	249
0.3 M	256
0.4 M	261
0.5 M	264

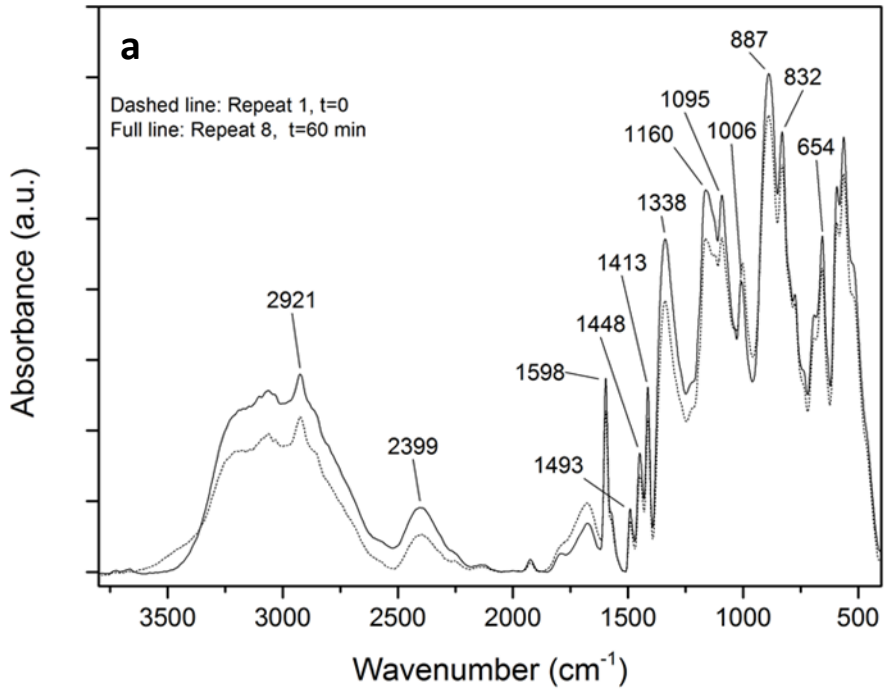
a
Dashed line: Repeat 1, t=0
Full line: Repeat 8, t=60 min
Absorbance (a.u.)
Wavenumber (cm-1)
3500
3000
2500
2000
1500
1000
500
2921
2399
1598
1493
1448
1413
1338
1160
1095
1006
887
832
654

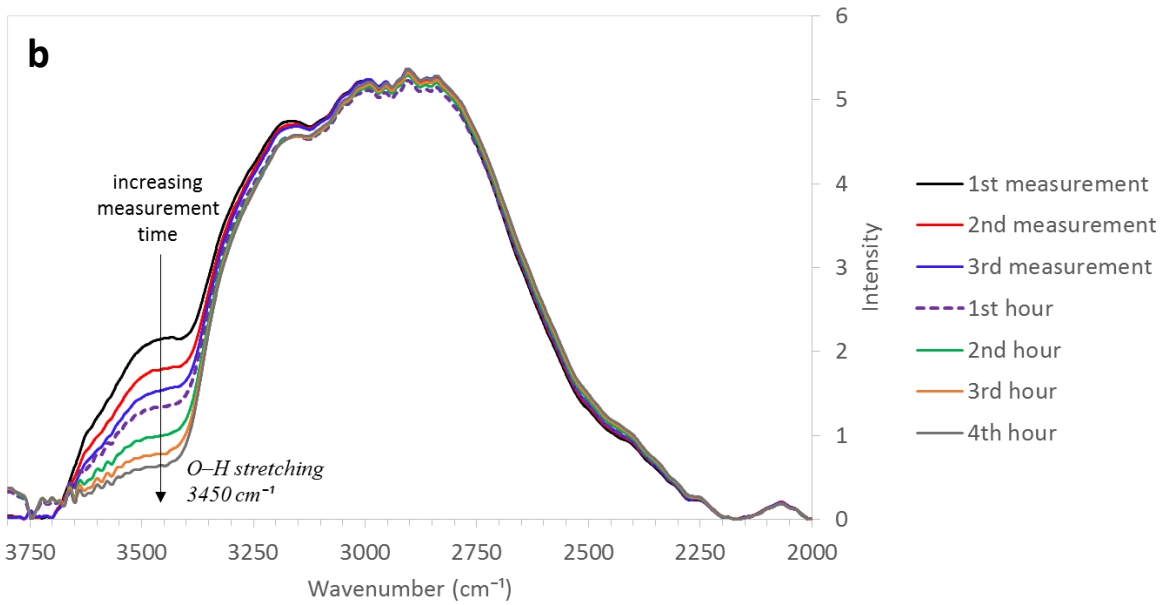
b
increasing measurement time
O–H stretching
3450 cm⁻¹
Wavenumber (cm⁻¹)
Intensity
3750
3500
3250
3000
2750
2500
2250
2000
0
1
2
3
4
5
6
1st measurement
2nd measurement
3rd measurement
1st hour
2nd hour
3rd hour
4th hour

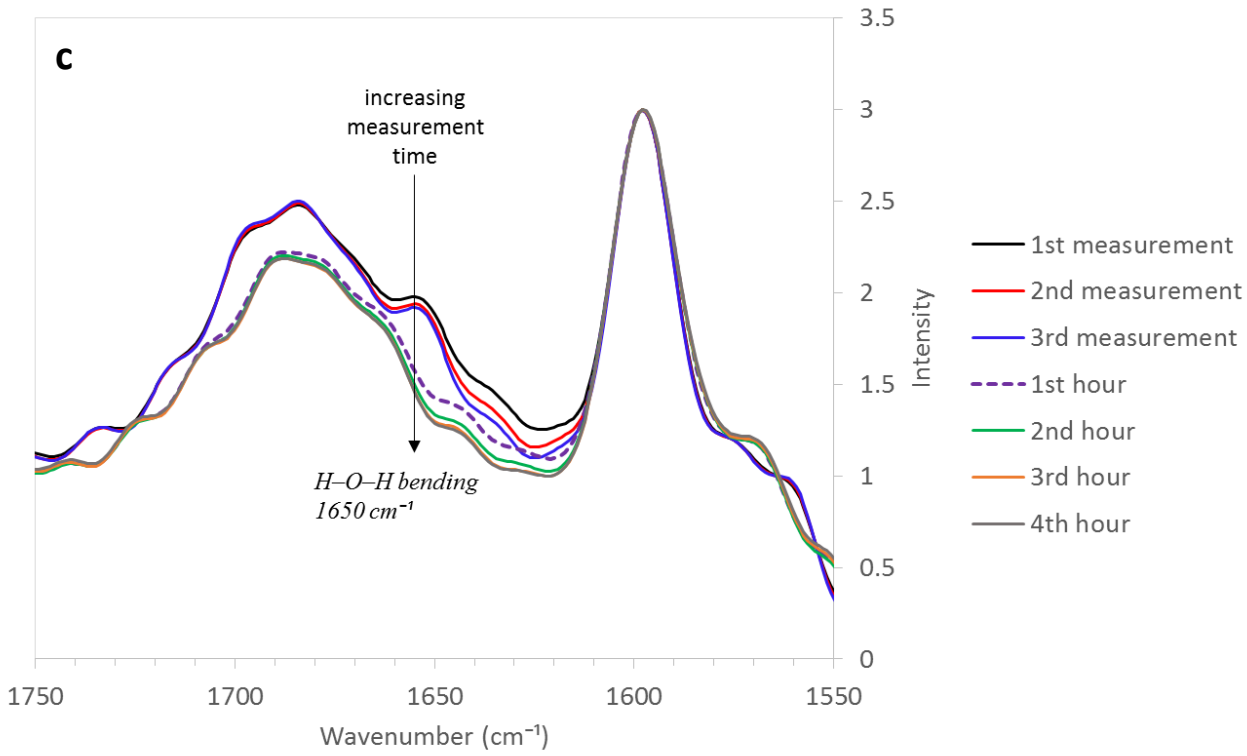

Figure B-4. FTIR spectra of pristine Amberlyst 15^{TM}; **a: i**nitial and final collected spectra; **b:** decreasing intensity of O–H stretching vibrations; **c:** decreasing intensity of H–O–H bending vibrations with time in the IR vacuum chamber. *Note: t=0 is the spectra of Amberlyst 15^{TM} dried for 1 h at 110 °C in a vacuum oven (< 10 mbar); t=60 min is its spectra of the dried* Amberlyst 15^{TM} *that is additionally kept in the IR chamber for 1 h at room temperature under high vacuum (2 mbar).*

3500-3200 cm^{-1} O–H stretching vibrations in sulfonic acid groups; 2399 cm^{-1} O–H stretching vibrations related to the polymer, 2921 cm^{-1} asymmetric C–H stretching vibrations in polystyrene/divinylbenzene chain –CH_2– units; 1676 cm^{-1} H–O–H bending; 1598, 1493, 1448, 1413 cm^{-1} skeleton vibrations in the aromatic ring; 1338 cm^{-1} –SO_2 asymmetric stretching of the double S=O bonds in –SO_3H; 1160 cm^{-1} –SO_3 symmetric stretching of the double S=O bonds in –SO_3H; 1095 cm^{-1} in plane skeleton vibrations of benzene ring in dried resin, 1006 cm^{-1} is in plane bending of the –CH groups of the benzene ring after thorough drying of the resin, 887 and 832 cm^{-1} are the stretching vibrations of the single S–O bond, again in dried form and 654 cm^{-1} C–S stretching vibrations in sulfonic acid groups attached to benzene rings [223-225,276]. Spectra indicate the active sites in the resin as in acid form.

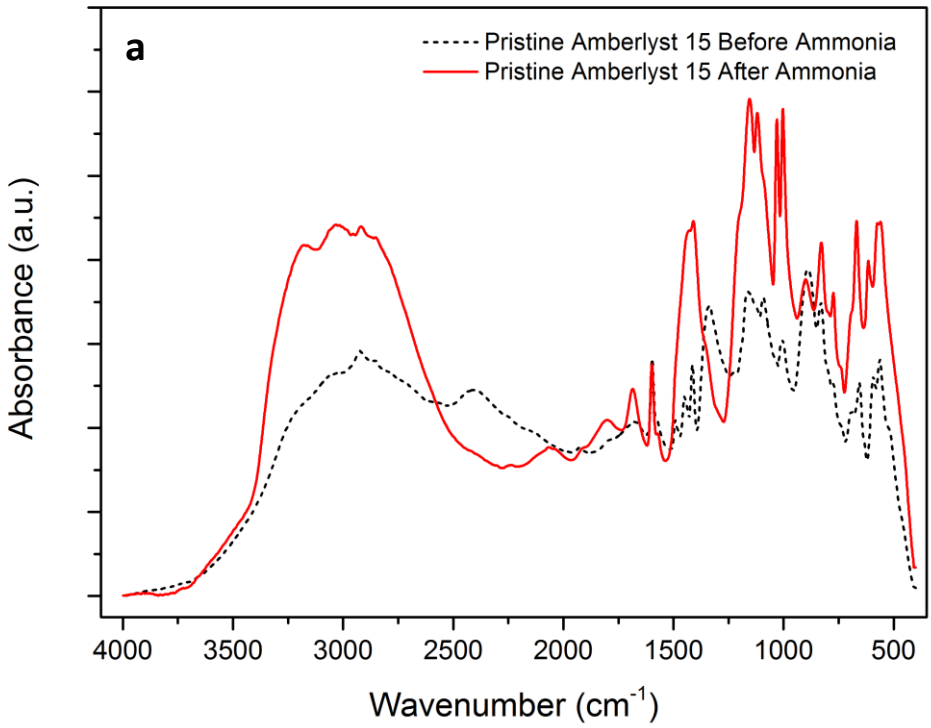
a
Pristine Amberlyst 15 Before Ammonia
Pristine Amberlyst 15 After Ammonia
Absorbance (a.u.)
4000
3500
3000
2500
2000
1500
1000
500
Wavenumber (cm-1)

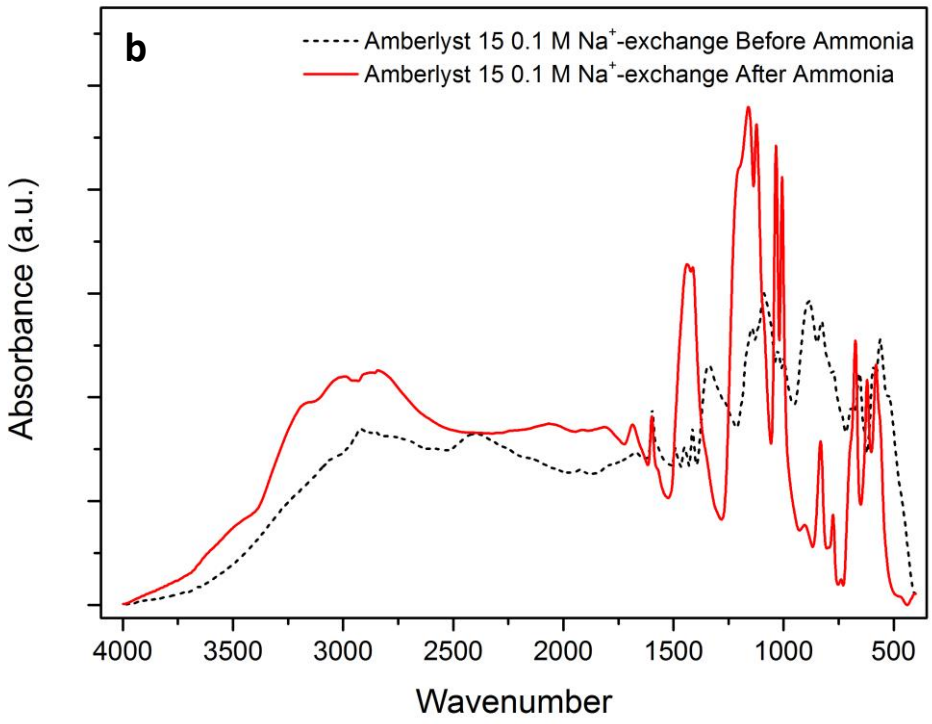
b
Amberlyst 15 0.1 M Na+-exchange Before Ammonia
Amberlyst 15 0.1 M Na+-exchange After Ammonia
Absorbance (a.u.)
4000
3500
3000
2500
2000
1500
1000
500
Wavenumber

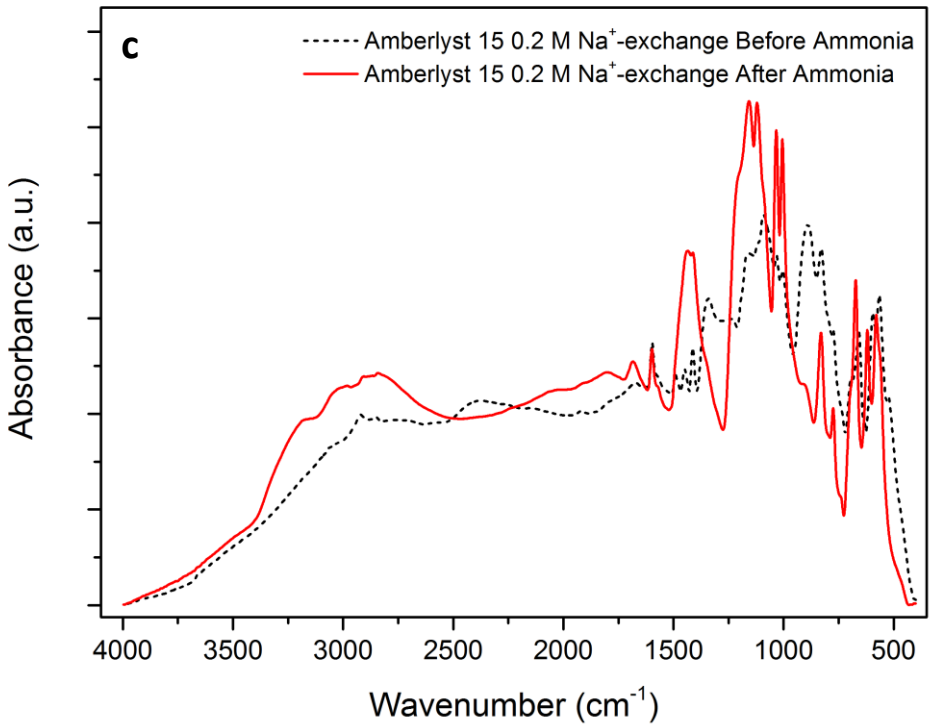
c
Amberlyst 15 0.2 M Na+-exchange Before Ammonia
Amberlyst 15 0.2 M Na+-exchange After Ammonia
Absorbance (a.u.)
4000
3500
3000
2500
2000
1500
1000
500
Wavenumber (cm-1)

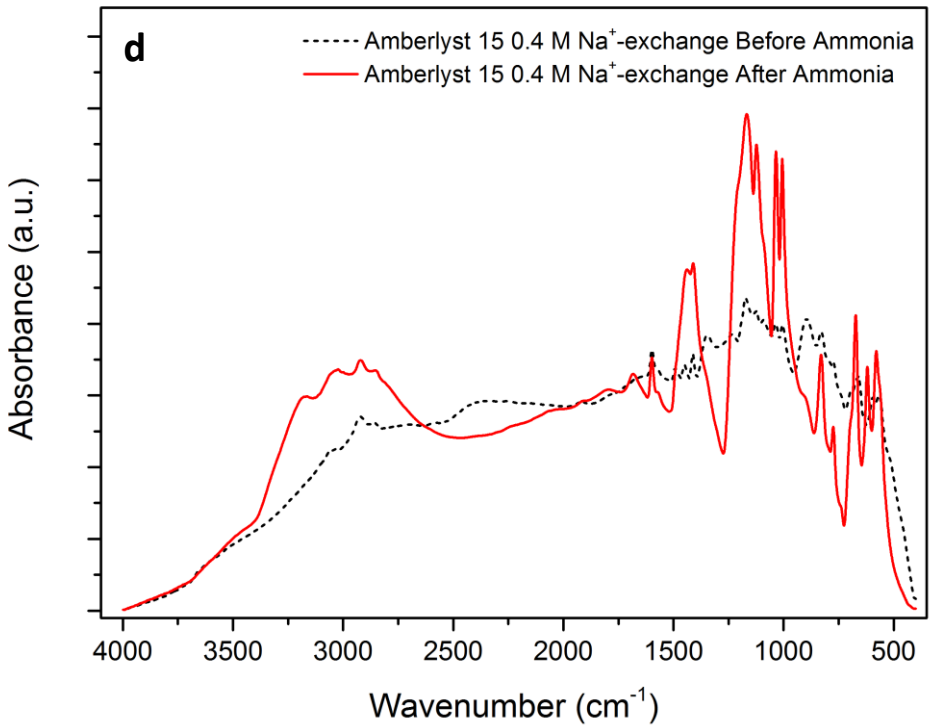
d
Amberlyst 15 0.4 M Na+-exchange Before Ammonia
Amberlyst 15 0.4 M Na+-exchange After Ammonia
Absorbance (a.u.)
4000
3500
3000
2500
2000
1500
1000
500
Wavenumber (cm-1)

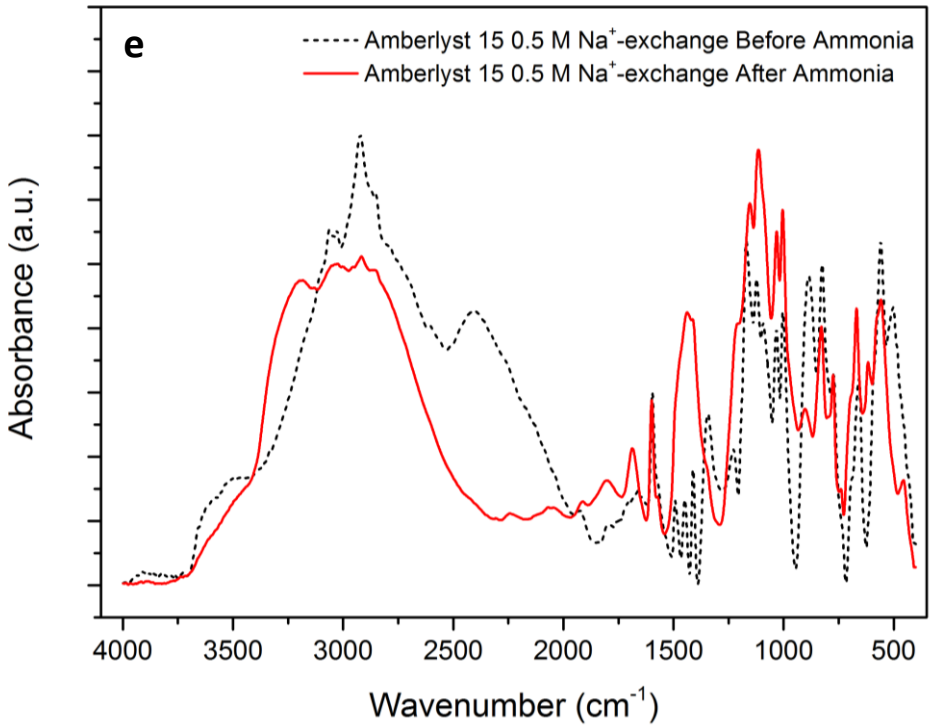

Figure B-5. FTIR spectra of **a:** pristine and **b to e:** Na^+-exchanged (b: 0.1 M; c: 0.2 M; d: 0.4 M; e: 0.5 M) Amberlyst 15^{TM} samples before and after NH_3 chemisorption. Curves are normalized with respect to 1598 cm^{-1}. Note: All spectra were collected after keeping the samples for 1 h at 110°C in a vacuum oven (< 10 mbar) and then for 1 h at room temperature under vacuum in the IR chamber (~ 2 mbar).

Table B-3. Peak values of the fit Voigt functions to the difference spectra of Amberlyst 15^{TM} and its Na^+-exchanged counterparts. Peaks 1-9 can be seen in **Figure 4-2** in the main text.

Peak No.	Na^+-exchange (M)					
	0	**0.1**	**0.2**	**0.3**	**0.4**	**0.5**
1	3324	3309	3288	3304	3321	3328
2	3206	3196	3185	3190	3207	3235
3	3050	3059	3058	3072	3069	3085
4	2985	2990	2992	2996	2998	2994
5	2893	2888	2887	2889	2894	2888
6	2830	2831	2832	2835	2840	2836
7	2763	2772	2775	2780	2784	2787
8	2639	2627	2645	2644	2640	2650
9	2514	2520	2518	2517	2520	2520
10	1464	1458	1465	1465	1464	1461
11	1430	1431	1430	1430	1430	1429
12	1398	1404	1397	1399	1401	1397

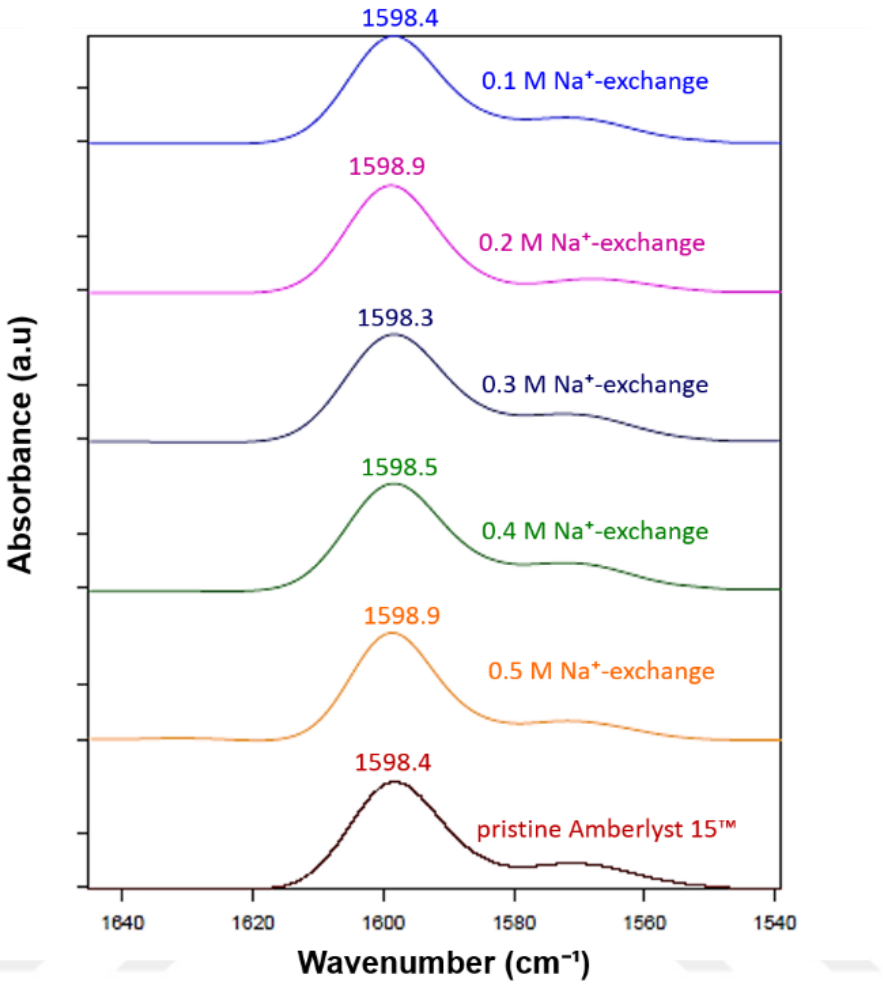

Figure B-6. Data presenting the position of aromatic C=C stretching vibrations, used for normalizing the data after ammonia adsorption. The corresponding peak position and shape remain the same upon Na^+-exchange at different degrees within the spectral resolution of the measurements. These results indicate that the presence of Na^+ does not influence this band position and its shape, confirming the validity of our normalization procedure.

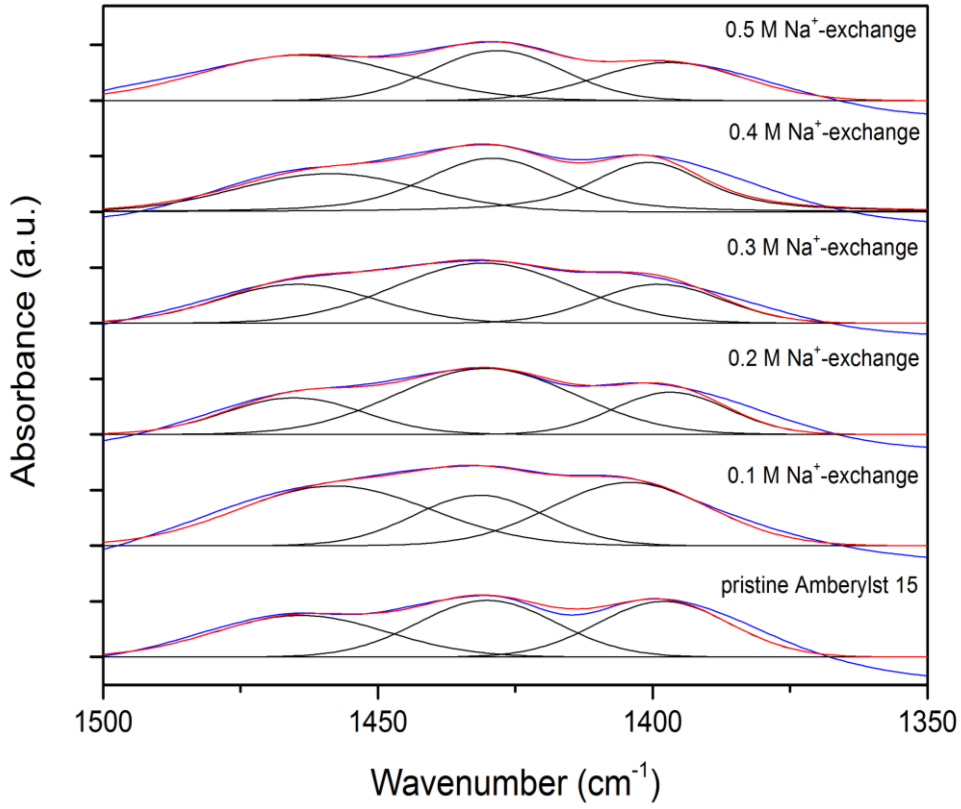

Figure B-7. Difference FTIR spectra obtained by subtracting the spectra of samples before NH_3 chemisorption from their corresponding counterparts after chemisorption for pristine and Na^+-exchanged Amberlyst 15™ samples in fingerprint region.

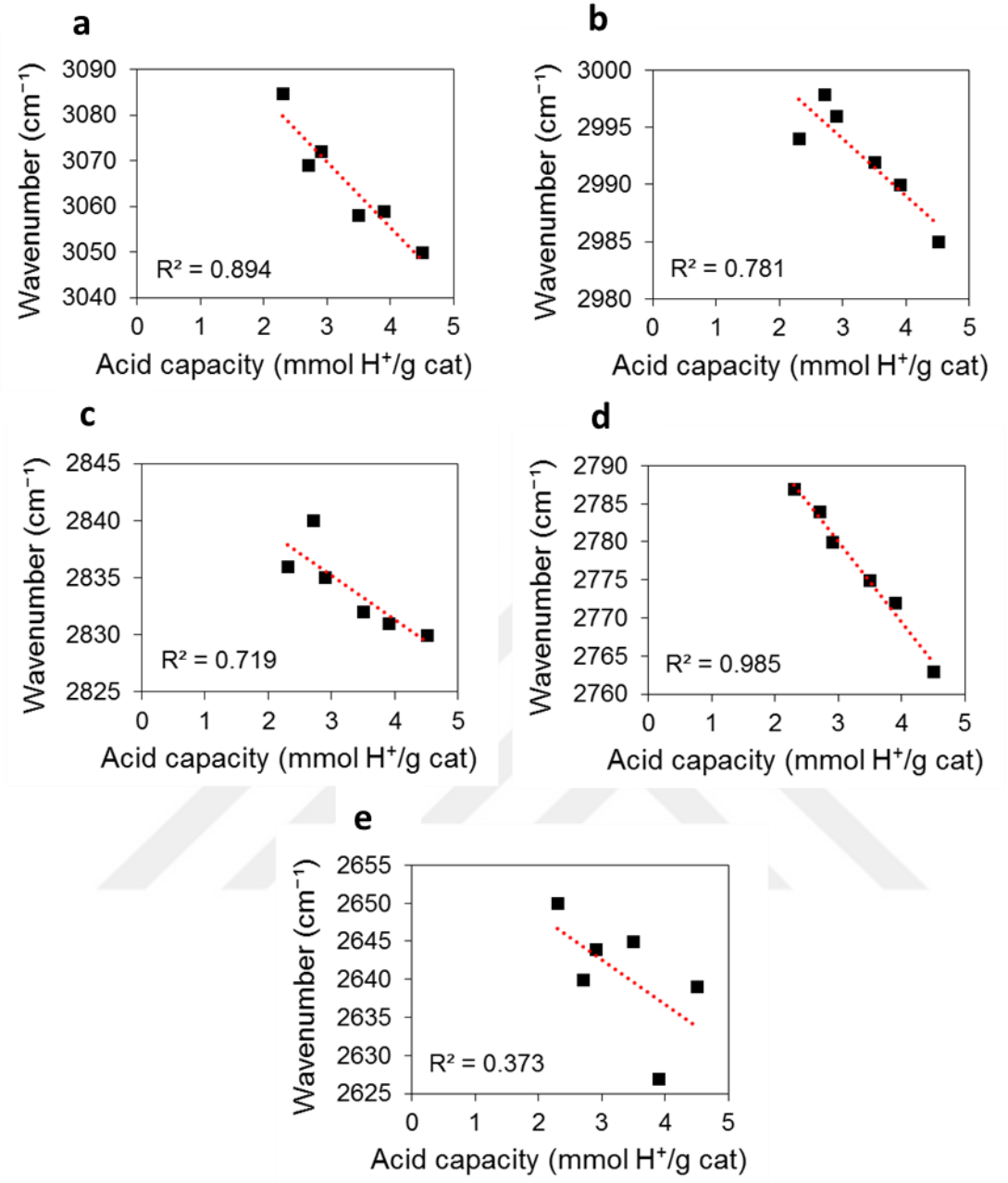

Figure B-8. Linear regression scatter plots of the data provided in **Table 4-2.**

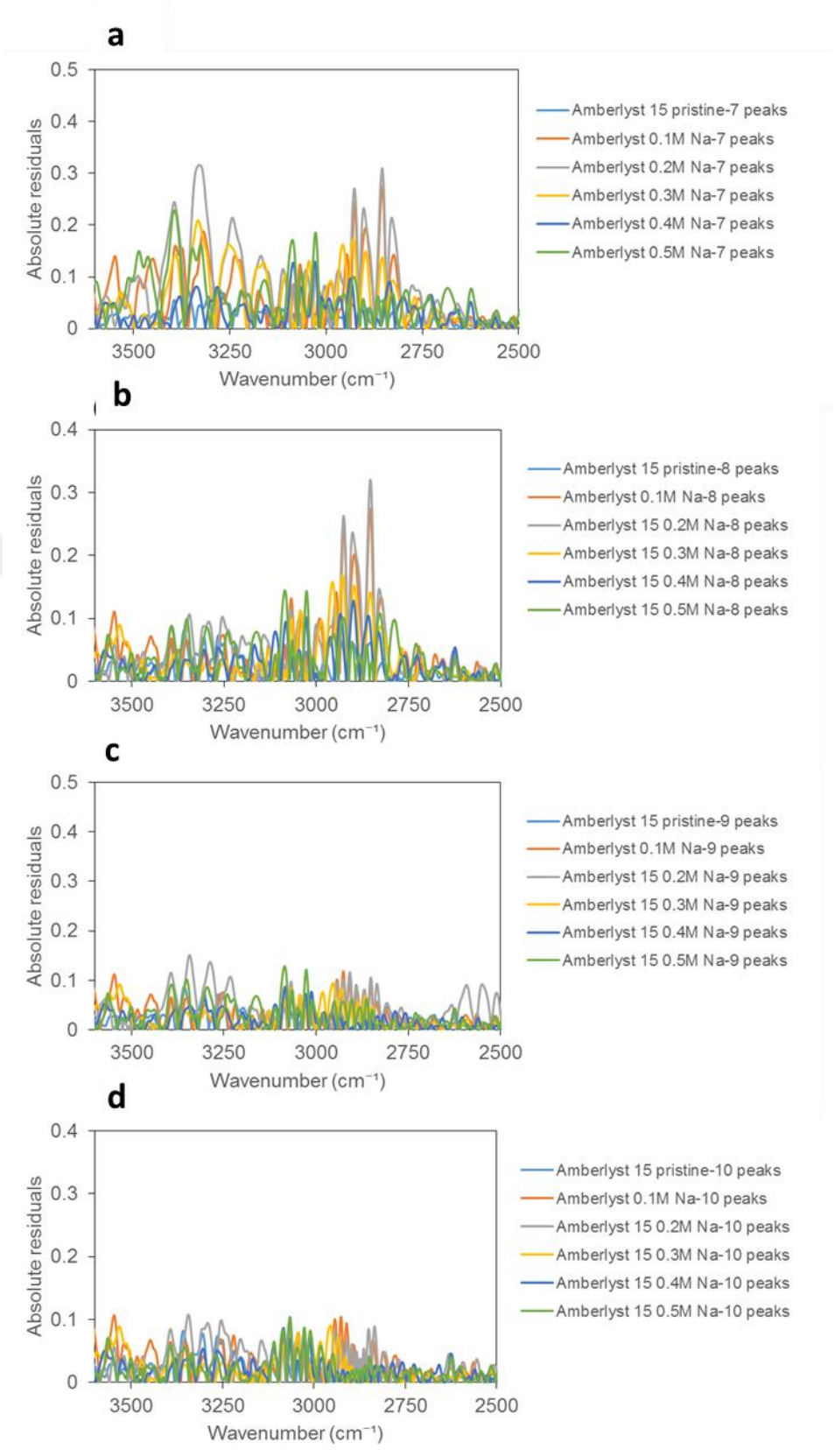

Figure B-9. Absolute residual plots in the case of fitting 7, 8, 9, and 10 peaks.

Table B-4. N−H vibrational frequencies of Amberlyst 15^{TM} samples in deconvoluted difference spectra with **seven peaks**.

Na^+-exchange treatment	**ν(N-H)**						
No exchange	3208	3028	2994	2869	2773	2621	2512
0.1 M	3196	3037	2983	2870	2781	2629	2512
0.2 M	3232	3046	2998	2875	2795	2642	2517
0.3 M	3224	3058	2990	2878	2795	2645	2517
0.4 M	3290	3179	3022	2894	2828	2659	2521
0.5 M	3282	3157	3005	2889	2823	2676	2528
R^2*	0.688	0.670	0.333	0.761	0.842	0.918	0.843

* Linear correlation coefficient with acid capacity

Table B-5. N−H vibrational frequencies of Amberlyst 15^{TM} samples in deconvoluted difference spectra with **eight peaks**.

Na^+-exchange treatment	**ν(N-H)**							
No exchange	3323	3205	3030	2988	2865	2777	2629	2511
0.1 M	3309	3191	3046	2987	2869	2780	2631	2514
0.2 M	3303	3193	3055	2990	2874	2785	2634	2515
0.3 M	3315	3197	3057	2988	2877	2791	2638	2517
0.4 M	3316	3205	3071	3000	2889	2793	2640	2524
0.5 M	3319	3212	3106	3000	2888	2813	2651	2518
R^2*	0.000	0.188	0.826	0.610	0.886	0.823	0.848	0.626

* Linear correlation coefficient with acid capacity

Table B-6. N−H vibrational frequencies of Amberlyst 15^{TM} samples in deconvoluted difference spectra with **nine peaks**.

Na^+-exchange treatment	**ν(N-H)**								
No exchange	3324	3206	3050	2985	2893	2830	2763	2639	2514
0.1 M	3309	3196	3059	2990	2888	2831	2772	2627	2520
0.2 M	3288	3185	3058	2992	2887	2832	2775	2645	2518
0.3 M	3304	3190	3072	2996	2889	2835	2780	2644	2517
0.4 M	3321	3207	3069	2998	2894	2840	2784	2640	2520
0.5 M	3328	3235	3085	2994	2888	2836	2787	2650	2520
R^2*	0.029	0.209	0.894	0.781	0.020	0.718	0.985	0.373	0.423

* Linear correlation coefficient with acid capacity

Table B-7. N−H vibrational frequencies of Amberlyst 15^{TM} samples in deconvoluted difference spectra with **ten peaks**.

Na^+-exchange treatment	**ν(N-H)**									
No exchange	3324	3204	3043	2969	2896	2859	2833	2760	2629	2511
0.1 M	3311	3196	3056	2987	2892	2869	2836	2772	2627	2513
0.2 M	3301	3195	3063	2986	2897	2874	2837	2775	2632	2513
0.3 M	3315	3200	3066	2991	2897	2871	2841	2779	2640	2516
0.4 M	3315	3206	3068	2994	2900	2875	2851	2782	2638	2523
0.5 M	3329	3241	3094	2989	2894	2870	2838	2790	2643	2518
R^2*	0.043	0.375	0.842	0.672	0.071	0.490	0.406	0.956	0.857	0.665

* Linear correlation coefficient with acid capacity

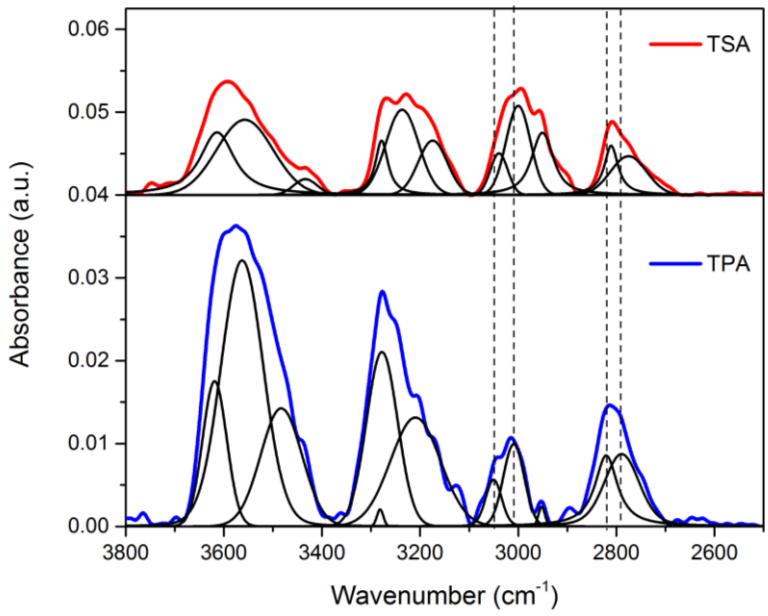

Figure B-10. Difference spectra for TSA and TPA heteropolyacids after ammonia chemisorption.

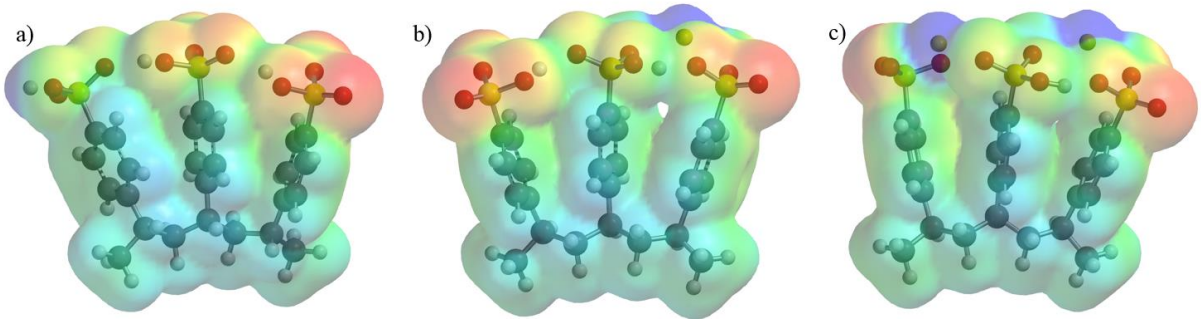

Figure B-11. Electrostatic potential maps calculated on optimized geometries representing the pristine and Na^+-exchanged Amberlyst 15^{TM} catalysts; **a:** Amb15-HHH (representing pristine Amberlyst 15^{TM}); **b:** Amb15-NaHH (representing a Na^+-exchange degree of 33.3%); and **c:** Amb15-NaHNa (representing a Na^+-exchange degree of 66.7%). Red and blue regions in electrostatic potential maps represent the electron rich and deficient regions, respectively. Color scale is to indicate approximate calculated value of potential in kJ/mol from a range of -200 (red) to 200 (blue).

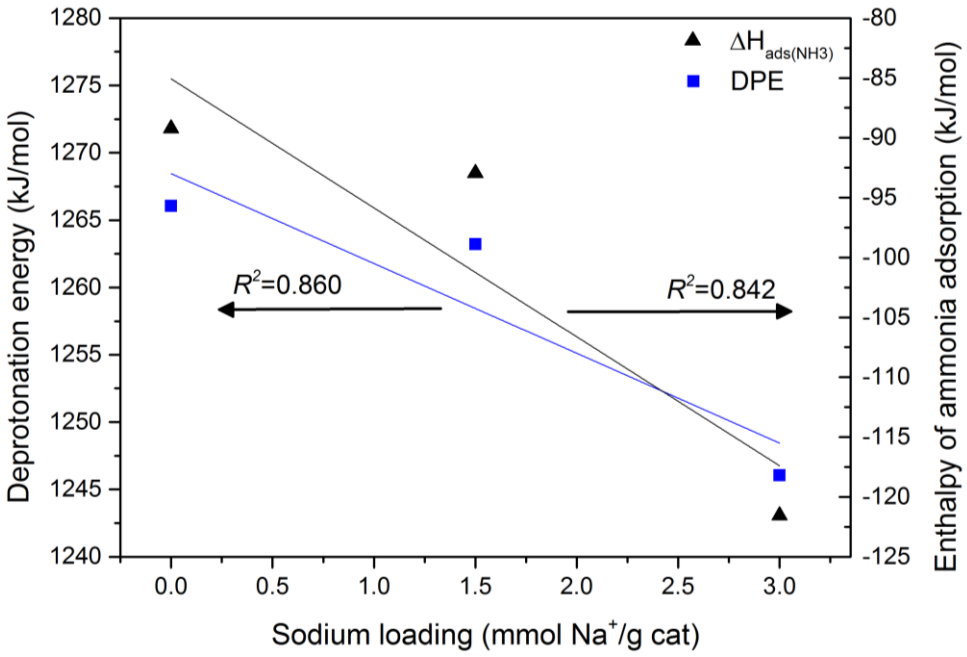

Figure B-12. Relationship between theoretical sodium loading and DFT calculated deprotonation energies and enthalpies of ammonia adsorption.

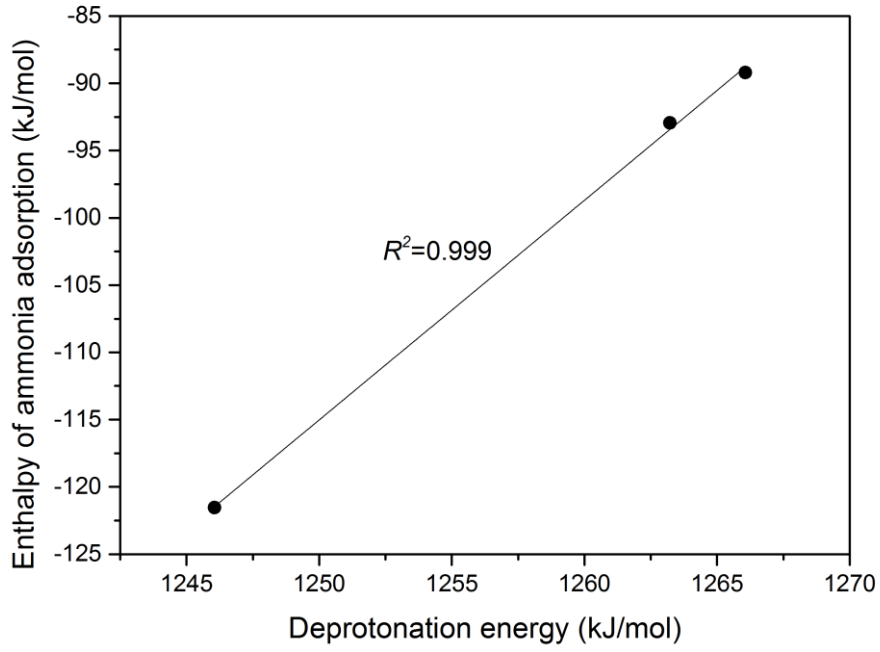

Figure B-13. Relationship between DFT calculated enthalpy of ammonia adsorption and deprotonation energies on geometries representing pristine Amberlyst 15^{TM} and its Na^+-exchanged counterparts.

Table B-8. Catalytic performance of supported heteropolyacid catalyst samples in batch reactor under identical conditions, at complete glycerol conversion (75 °C, 10-15 bar, IB:G=3:1 mol:mol, 7.5 wt% of glycerol catalyst loading, 1200 rpm mixing, 6 h run).

Supported HPA catalyst (wt%:wt%)	Acid capacity	Product selectivity* (wt%)			
	mmol H^+/g cat	MTBGE	DTBGE	TTBGE	DIB
TSA/SiO_2 (50:50)	0.5	12.0	51.6	24.6	8.9
TPA/SiO_2 (50:50)	2.0	16.6	51.5	21.5	5.4
TSA/MCM-41(50:50)	0.7	15.3	48.7	13.5	14.2
TPA/MCM-41(50:50)	1.4	11.2	53.6	23.1	6.4

*The sum of other products, tri-isobutene, tetra-isobutene and tertiary butyl alcohol are less than 6 wt% of the total products. They are excluded in the table.

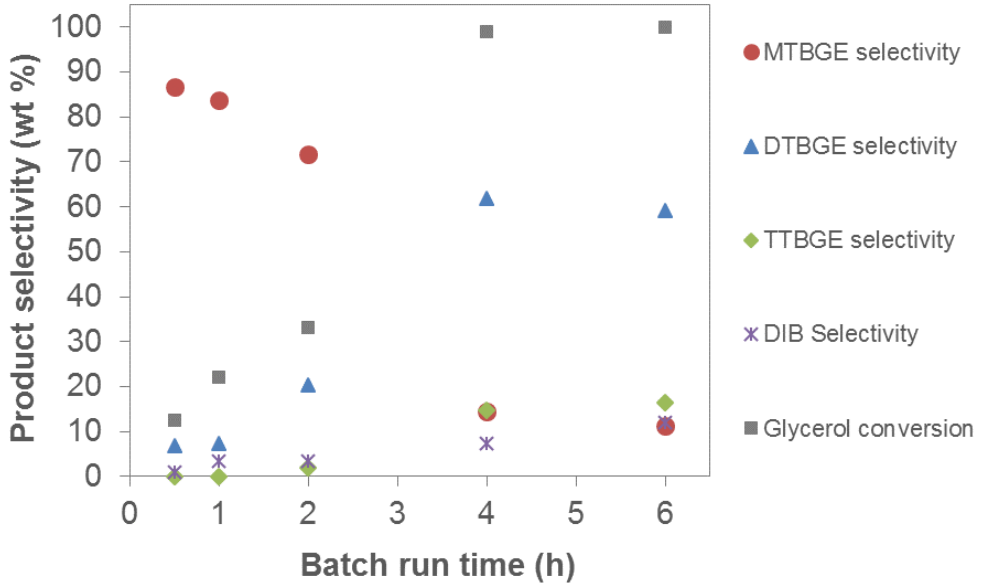

Figure B-14. Change in glycerol conversion and product selectivity as a function of batch run time for pristine Amberlyst 15™ catalyst at 75 °C, 10-15 bar, IB:G=3:1 mol:mol, 7.5 wt% of glycerol catalyst loading and 1200 rpm mixing.

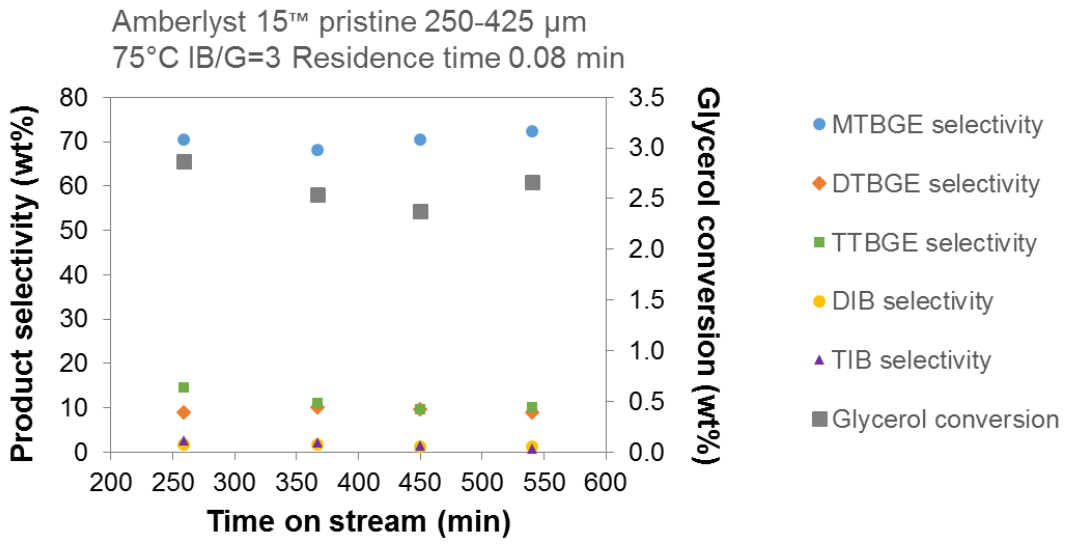

Figure B-15. Change in glycerol conversion and product selectivity as a function of time on stream for pristine Amberlyst 15^{TM} catalyst at ≤3 wt% glycerol conversion, 250-425 µm catalyst size, 75 °C, 15 bar, IB:G=3:1 mol:mol, space velocity 12 $mol_{glycerol}$ x $(mol_{H^+}$ x min$)^{-1}$, residence time 0.08 min.

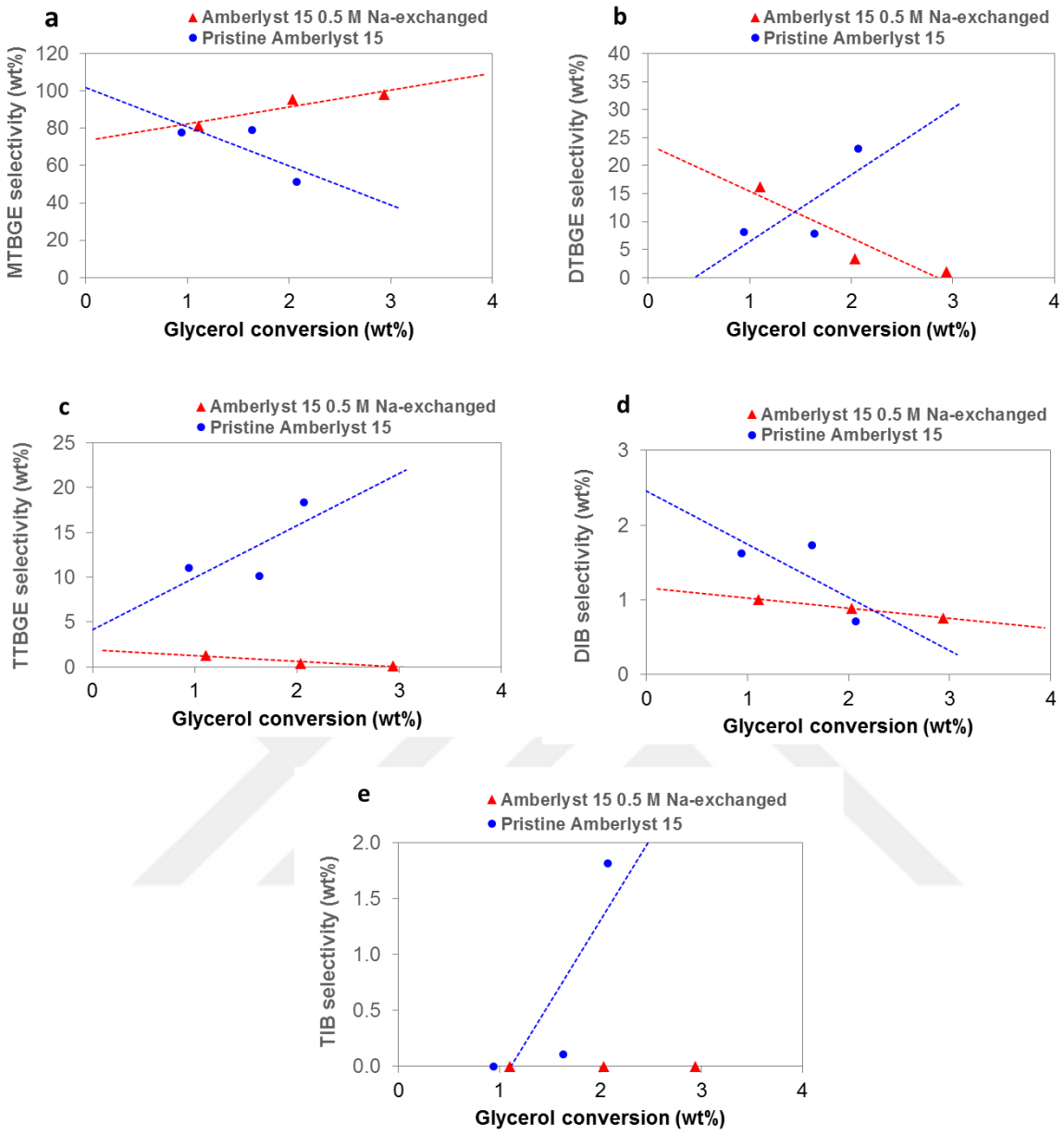

Figure B-16. Variation of product selectivity as a function of glycerol conversion conditions (at ≤3 wt% glycerol conversion, 250-425 µm catalyst size, 75 °C, 15±3 bar, IB:G=3:1 mol:mol, glycerol space velocity of 2-20 $mol_{glycerol}$ x $(mol_{H^+}$ x min$)^{-1}$.

Cartesian coordinates of optimized geometries presented in **Figure 4-4** in main text.

a. Amb15-HHH (representing pristine Amberlyst 15™)

S	-4.756551	2.072477	-0.533683
O	-5.682365	2.476125	0.768501
C	0.204279	-1.633272	-0.025905
C	0.171973	1.157824	-0.166661
C	-0.225242	-0.979543	-1.189965
C	0.625319	-0.851942	1.058888
C	0.621310	0.537826	0.999450
C	-0.250980	0.409278	-1.266884
H	-0.552236	-1.557482	-2.049243
H	0.981818	-1.341003	1.960170
H	0.976359	1.126865	1.837137
H	-0.579983	0.916281	-2.167185
S	0.101987	2.939582	-0.255754
C	3.290344	-2.512934	-0.307806
C	4.265233	0.060931	0.198792
C	3.795435	-2.169802	0.954605
C	3.360336	-1.559119	-1.332429
C	3.832342	-0.272081	-1.084917
C	4.281876	-0.890793	1.216749
H	3.786658	-2.909178	1.751590
H	3.011450	-1.808276	-2.330394
H	3.851438	0.480754	-1.865196
H	4.658227	-0.628420	2.199894
S	4.718632	1.761219	0.542947
O	4.675404	2.521435	-0.706122
O	1.225975	3.489818	0.512134
O	-3.671269	3.057823	-0.548319
O	-1.200397	3.294976	0.650730
O	5.905220	1.760497	1.389303
O	-5.646377	1.928148	-1.677553
C	3.462663	-4.698277	-1.577541
H	4.514867	-4.777137	-1.289993
H	3.422100	-4.232551	-2.567765
C	2.667063	-3.881648	-0.540875
H	2.718864	-4.423776	0.413327
C	1.171424	-3.826487	-0.943544
H	1.068719	-3.340917	-1.922365
H	0.845269	-4.863968	-1.089409
C	0.207113	-3.153361	0.072105
H	0.557963	-3.410330	1.081293
C	-1.215429	-3.761227	-0.065469
H	-1.109151	-4.847474	0.041351
C	-2.270962	-3.285582	0.971104
C	-3.340024	-4.375587	1.190778
H	-3.860720	-4.618882	0.258395
C	-2.928555	-1.957441	0.612782
C	-4.093744	0.495276	-0.046649
C	-2.769538	-0.836516	1.441727
C	-3.723445	-1.825231	-0.535753
C	-4.310415	-0.608300	-0.872712
C	-3.326038	0.394800	1.115084
H	-2.169629	-0.920426	2.342203
H	-3.883267	-2.678079	-1.188739
H	-4.916991	-0.505779	-1.765588
H	-3.151368	1.259855	1.745474
H	-2.879514	-5.296021	1.563266
H	-1.749199	-3.139557	1.926090
H	-1.591884	-3.595700	-1.082641
H	-4.091071	-4.051664	1.917235
H	3.056981	-5.711481	-1.669094
O	-0.139114	3.341019	-1.633098
O	3.488189	2.231867	1.487379
H	2.835528	2.797380	0.992858
H	-2.026174	3.313831	0.103610
H	-6.609156	2.481060	0.473663

b. Amb15-NaHH (representing one Na exchange out of three sites)

S	-4.481455	1.615627	0.883049

O	-5.820204	1.652945	0.297333
C	0.437707	-1.833322	0.330888
C	0.172015	0.942590	0.414299
C	0.518493	-1.069400	-0.843044
C	0.259556	-1.165876	1.547035
C	0.114399	0.218986	1.602271
C	0.399221	0.313035	-0.813998
H	0.680345	-1.560118	-1.797565
H	0.202127	-1.740368	2.465812
H	-0.059764	0.727917	2.543334
H	0.466081	0.893065	-1.730364
S	-0.084033	2.701924	0.436198
C	3.574538	-2.006560	-0.129985
C	4.188199	0.604339	-0.931784
C	3.761957	-0.990301	0.814927
C	3.771163	-1.697032	-1.485476
C	4.073761	-0.402343	-1.894069
C	4.057945	0.315699	0.425115
H	3.648146	-1.216056	1.871029
H	3.667647	-2.472272	-2.237974
H	4.218219	-0.166536	-2.943122
H	4.185683	1.104546	1.156449
S	4.456752	2.295645	-1.452570
O	5.282819	2.283758	-2.651617
O	1.127784	3.417656	0.031964
O	-4.377687	1.925490	2.349250
O	-0.666616	3.061146	1.752264
O	4.810631	3.086593	-0.274468
O	-3.496834	2.552161	0.161777
C	4.297299	-4.418680	-0.002268
H	5.246622	-4.089876	0.429926
H	4.445180	-4.531231	-1.081378
C	3.170878	-3.409980	0.305186
H	3.036565	-3.388987	1.394736
C	1.837758	-3.891950	-0.327160
H	1.852502	-3.689163	-1.405914
H	1.798894	-4.984188	-0.233839
C	0.517550	-3.351589	0.287343
H	0.479849	-3.705223	1.326442
C	-0.685212	-3.986992	-0.463792
H	-0.432359	-5.037864	-0.653080
C	-2.059815	-3.976242	0.251772
C	-3.025178	-4.948667	-0.456533
H	-3.184125	-4.660949	-1.501027
C	-2.697421	-2.599117	0.392419
C	-3.810784	-0.039973	0.687204
C	-3.028302	-2.098213	1.656532
C	-2.992892	-1.807316	-0.729311
C	-3.545006	-0.536980	-0.591985
C	-3.576503	-0.825535	1.814050
H	-2.836383	-2.705557	2.537792
H	-2.772809	-2.177470	-1.726003
H	-3.760224	0.065262	-1.469090
H	-3.811855	-0.431932	2.796196
H	-2.628107	-5.969550	-0.446865
H	-1.897645	-4.360308	1.267655
H	-0.781941	-3.520472	-1.451716
H	-4.000643	-4.956145	0.036469
H	4.058421	-5.405921	0.407621
O	-1.157758	2.936888	-0.702496
O	2.973524	2.737089	-1.953888
H	-2.103677	2.652627	-0.403270
Na	-2.810767	3.520059	2.165105
H	2.447532	3.084804	-1.196863

c. Amb15-NaHNa (representing two Na exchange out of three sites)

S	-4.812273	1.443242	-0.286380
O	-6.067940	1.264244	-1.012296
C	0.330313	-1.885548	-0.214255
C	-0.098524	0.838284	-0.643566
C	0.026210	-1.399206	-1.495565
C	0.463043	-0.962620	0.830285
C	0.262213	0.400633	0.631498

C	-0.200974	-0.047599	-1.720402
H	-0.067474	-2.088331	-2.329049
H	0.739009	-1.311122	1.819259
H	0.392653	1.104392	1.445016
H	-0.481124	0.311472	-2.703868
S	-0.447826	2.559857	-0.906300
C	3.475247	-2.410160	0.342467
C	4.023175	0.285341	0.900020
C	3.616408	-1.961995	1.662955
C	3.692344	-1.492393	-0.694658
C	3.959399	-0.152906	-0.423625
C	3.886161	-0.624075	1.948607
H	3.494381	-2.668361	2.481136
H	3.627242	-1.818601	-1.729311
H	4.118137	0.559301	-1.225653
H	3.985190	-0.281219	2.973276
S	4.163889	2.043701	1.268301
O	5.083180	2.178809	2.405082
O	0.729042	3.274838	-1.434697
O	-4.884266	2.070833	1.075951
O	-1.030695	3.118957	0.337560
O	2.741472	2.488392	1.547085
O	-3.784995	2.277782	-1.078841
C	4.183190	-4.602998	-0.712926
H	5.131758	-4.559444	-0.170268
H	4.347436	-4.167480	-1.704152
C	3.078528	-3.849768	0.052365
H	2.950170	-4.349530	1.022302
C	1.727976	-3.977207	-0.697603
H	1.819652	-3.533829	-1.696970
H	1.552786	-5.048162	-0.859440
C	0.486825	-3.381547	0.030921
H	0.642508	-3.521882	1.109241
C	-0.787308	-4.185808	-0.350464
H	-0.525309	-5.247160	-0.264037
C	-2.057398	-3.969922	0.513743
C	-3.041362	-5.139119	0.297117
H	-3.369360	-5.193937	-0.746399
C	-2.769906	-2.637937	0.306053
C	-4.058969	-0.169834	-0.046351
C	-2.967815	-1.767939	1.384047
C	-3.282237	-2.262968	-0.947340
C	-3.921263	-1.040124	-1.131572
C	-3.605010	-0.538777	1.218507
H	-2.607049	-2.049284	2.369786
H	-3.170895	-2.929891	-1.797881
H	-4.313697	-0.762349	-2.104476
H	-3.757605	0.129789	2.057932
H	-2.572403	-6.095399	0.551036
H	-1.739006	-4.003368	1.564639
H	-1.025401	-4.027085	-1.410300
H	-3.933491	-5.020600	0.918851
H	3.915391	-5.656172	-0.851020
O	-1.517501	2.564173	-2.062476
O	4.604640	2.686658	-0.025547
Na	2.634759	3.716683	-0.334471
H	-2.463567	2.310266	-1.702385
Na	-3.194235	3.526640	0.767819

d. NH_3 adsorbed on Amb15-HHH

S	-5.467009	-0.624980	0.464057
O	-6.434353	-0.721624	-0.897008
C	0.656911	1.675504	-0.038489
C	0.218588	-1.088355	0.139948
C	0.072523	1.108274	1.106088
C	1.004847	0.823278	-1.092479
C	0.804105	-0.552437	-1.009189
C	-0.155731	-0.264709	1.200290
H	-0.209578	1.743081	1.941745
H	1.471185	1.235964	-1.981777
H	1.113755	-1.203043	-1.819745
H	-0.603020	-0.701652	2.085902
S	-0.094327	-2.847861	0.223851

C	3.831472	2.045715	0.358192
C	4.424506	-0.641189	-0.107309
C	4.370757	1.632957	-0.867669
C	3.660641	1.089482	1.368838
C	3.943159	-0.252666	1.141926
C	4.669782	0.296057	-1.109560
H	4.540880	2.366540	-1.651461
H	3.268646	1.387022	2.336960
H	3.780378	-1.001069	1.909348
H	5.076120	-0.022755	-2.063587
S	4.644868	-2.378902	-0.449145
O	4.463294	-3.116137	0.801654
O	1.048349	-3.565420	-0.381748
O	-4.816113	-1.929362	0.575917
O	-1.307802	-3.022426	-0.704236
O	5.842488	-2.549785	-1.262818
O	-6.304379	-0.106425	1.547088
C	4.312449	4.157105	1.655694
H	5.373639	4.059863	1.408306
H	4.156086	3.690795	2.634150
C	3.434608	3.497775	0.575481
H	3.621078	4.028071	-0.368817
C	1.933879	3.691778	0.910819
H	1.713382	3.238032	1.884665
H	1.778528	4.770408	1.041635
C	0.918268	3.173068	-0.145600
H	1.360113	3.349774	-1.136460
C	-0.375141	4.026862	-0.087707
H	-0.067500	5.069671	-0.234344
C	-1.467252	3.702392	-1.144059
C	-2.252506	4.984323	-1.499927
H	-2.731431	5.415636	-0.614547
C	-2.433094	2.600302	-0.724885
C	-4.283305	0.621055	-0.015223
C	-2.541984	1.413281	-1.464595
C	-3.275440	2.767911	0.382697
C	-4.202021	1.790929	0.742839
C	-3.448074	0.415590	-1.113760
H	-1.895144	1.260658	-2.323034
H	-3.217452	3.678798	0.971276
H	-4.862746	1.928927	1.591142
H	-3.498401	-0.503243	-1.687721
H	-1.582201	5.742900	-1.917679
H	-0.962937	3.367821	-2.059878
H	-0.810722	3.985764	0.919176
H	-3.034659	4.778326	-2.236481
H	4.079806	5.222904	1.750901
O	-0.462132	-3.205292	1.602498
O	3.391748	-2.690859	-1.438682
H	2.619227	-3.029352	-0.905594
H	-2.363688	-3.328157	-0.252511
H	-7.274146	-0.341812	-0.587458
H	-3.939734	-4.215463	0.746757
N	-3.223761	-4.317399	0.036314
H	-3.582674	-4.738996	-0.811515
H	-2.450497	-4.910912	0.400045

e. NH_3 adsorbed on Amb15-NaHH

S	-4.847242	1.607075	-0.016226
O	-6.161967	1.610312	-0.658747
C	0.212826	-1.861662	0.279957
C	0.231222	0.940955	0.446991
C	0.597652	-1.077474	-0.818277
C	-0.153024	-1.206781	1.460852
C	-0.158084	0.184090	1.550227
C	0.631336	0.311752	-0.736663
H	0.916708	-1.559061	-1.737839
H	-0.447889	-1.793665	2.326061
H	-0.465589	0.683506	2.462155
H	0.990372	0.904871	-1.572134
S	0.242554	2.735348	0.558397
C	3.374194	-2.193282	0.487347
C	4.334034	0.385526	-0.026460

C	3.367196	-1.211271	1.485742
C	3.933141	-1.869382	-0.758880
C	4.408944	-0.587861	-1.023956
C	3.835025	0.077912	1.238287
H	2.966582	-1.451475	2.466566
H	3.987730	-2.622113	-1.540889
H	4.837922	-0.334782	-1.987465
H	3.811228	0.840688	2.008772
S	4.838141	2.066845	-0.387585
O	5.749275	2.033627	-1.525417
O	1.604596	3.170613	0.950403
O	-4.777791	2.008847	1.424174
O	-0.801387	3.064269	1.578100
O	5.208060	2.705142	0.873982
O	-3.807870	2.464838	-0.759160
C	3.910690	-4.652510	0.673398
H	4.751255	-4.398038	1.325140
H	4.297982	-4.746053	-0.346695
C	2.803881	-3.581013	0.758932
H	2.428322	-3.581731	1.790984
C	1.618248	-3.960603	-0.168321
H	1.864156	-3.698082	-1.205596
H	1.518660	-5.052890	-0.154346
C	0.226959	-3.381749	0.207149
H	-0.002972	-3.754327	1.215517
C	-0.848627	-3.964371	-0.750957
H	-0.576540	-5.008687	-0.949279
C	-2.313763	-3.977026	-0.239054
C	-3.153640	-4.971308	-1.067203
H	-3.177532	-4.691856	-2.125967
C	-2.981659	-2.608607	-0.196875
C	-4.174114	-0.062453	-0.092108
C	-3.353705	-2.032364	1.022214
C	-3.276044	-1.900141	-1.374384
C	-3.878724	-0.645594	-1.329552
C	-3.931308	-0.763978	1.085908
H	-3.170890	-2.574975	1.945898
H	-3.041634	-2.339324	-2.340380
H	-4.136681	-0.131022	-2.251135
H	-4.186796	-0.311332	2.037171
H	-2.735158	-5.980615	-1.000109
H	-2.288963	-4.354487	0.792301
H	-0.797709	-3.453201	-1.721518
H	-4.186563	-5.005071	-0.709075
H	3.526362	-5.632580	0.975460
O	-0.139420	3.214846	-0.819051
O	3.474088	2.732872	-0.944211
H	-1.100807	2.500504	-1.809215
Na	-2.936668	3.358603	1.210923
H	2.871327	2.995006	-0.193027
H	-1.612429	1.023679	-2.488909
N	-1.843053	2.013991	-2.416829
H	-1.890729	2.431159	-3.344514
H	-2.763286	2.125312	-1.882609

f. NH_3 adsorbed on Amb15-NaHNa

S	-4.457897	0.574650	1.176459
O	-5.906560	0.407124	1.037005
C	0.559342	-1.776673	-0.566410
C	-0.106813	0.892643	-1.158047
C	0.068494	-1.414364	-1.831253
C	0.692714	-0.765422	0.393883
C	0.388785	0.564697	0.106875
C	-0.272251	-0.096259	-2.130389
H	-0.041417	-2.169661	-2.604874
H	1.093772	-1.009520	1.371231
H	0.610739	1.333434	0.842563
H	-0.655909	0.172373	-3.108167
S	-0.469772	2.607224	-1.554669
C	3.893599	-1.897825	0.103006
C	4.074318	0.791971	0.890057
C	3.905718	-1.543278	1.459368
C	4.064593	-0.880978	-0.846764

C	4.147964	0.454974	-0.462765
C	3.992581	-0.208874	1.858028
H	3.821201	-2.322160	2.213817
H	4.095946	-1.128651	-1.904482
H	4.261976	1.240981	-1.200912
H	3.986797	0.061458	2.909010
S	3.921408	2.520677	1.384267
O	4.679918	2.691993	2.629585
O	0.818616	3.286789	-1.862489
O	-3.955285	1.242061	2.421026
O	-1.137049	3.200867	-0.347567
O	2.425272	2.737625	1.520607
O	-3.815562	1.307552	-0.010248
C	4.835511	-3.884971	-1.164830
H	5.784918	-3.769656	-0.634025
H	4.922391	-3.355826	-2.120010
C	3.664802	-3.340575	-0.325040
H	3.606111	-3.945633	0.590182
C	2.326302	-3.538205	-1.085842
H	2.349052	-2.950009	-2.010232
H	2.287139	-4.588945	-1.397401
C	1.030004	-3.201449	-0.272865
H	1.300307	-3.237472	0.790915
C	-0.057263	-4.290305	-0.493380
H	0.456135	-5.252402	-0.608079
C	-1.090000	-4.479729	0.646379
C	-1.876019	-5.789955	0.439173
H	-2.433846	-5.777989	-0.503512
C	-2.028045	-3.298106	0.828054
C	-3.633157	-1.019091	1.113881
C	-2.024679	-2.562259	2.017215
C	-2.916059	-2.911202	-0.188832
C	-3.714437	-1.782138	-0.054305
C	-2.813805	-1.421069	2.165927
H	-1.371118	-2.864435	2.831270
H	-2.958290	-3.480655	-1.113018
H	-4.371292	-1.476815	-0.862319
H	-2.779902	-0.830814	3.074533
H	-1.198142	-6.649443	0.413373
H	-0.518569	-4.583925	1.578971
H	-0.581896	-4.117805	-1.442030
H	-2.595021	-5.946119	1.248551
H	4.695637	-4.948437	-1.387328
O	-1.392965	2.568319	-2.739433
O	4.398353	3.314861	0.193708
Na	2.321173	3.958408	-0.391892
H	-2.925404	2.650234	-2.421035
Na	-2.245930	2.340732	1.340313
H	-4.529646	2.315414	-2.959966
N	-3.977640	2.710601	-2.200705
H	-4.129438	2.155726	-1.298398
H	-4.239715	3.685495	-2.064565

Appendix C

Supplementary Material for Chapter 5

Etherification of Glycerol with Isobutene Etherification of Glycerol with Isobutene in a Once-Through Fixed Bed Tubular Flow Reactor

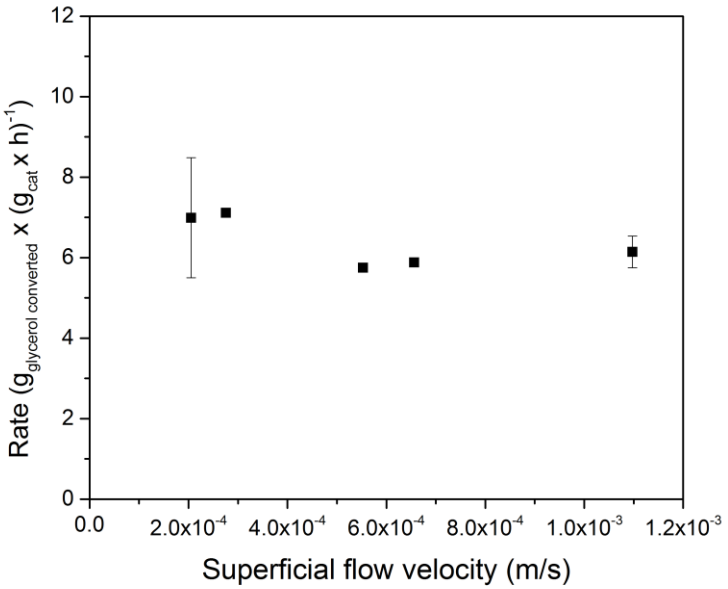

Figure C-1. Effect of superficial flow velocity on glycerol conversion rate for the 250-425 μm particle size at 5.5, 8.4, 17, 25, 76, 150, 225, 400 and 500 $g_{glycerol} \times (g_{cat} \times h)^{-1}$ at 75 °C, IB:G=3:1 mol:mol, 15±2 bar.

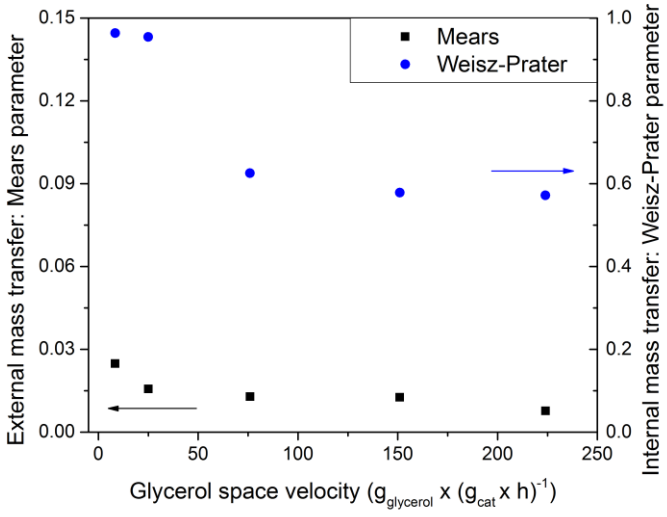

Figure C-2. Calculated Mears and Weisz-Prater parameters as a function of space velocity for 400-700 μm particle size at 8.4, 25, 76, 150 and 225 $g_{glycerol} \times (g_{cat} \times h)^{-1}$ at 75 °C, IB:G=3:1 mol:mol, 14±2 bar conditions.

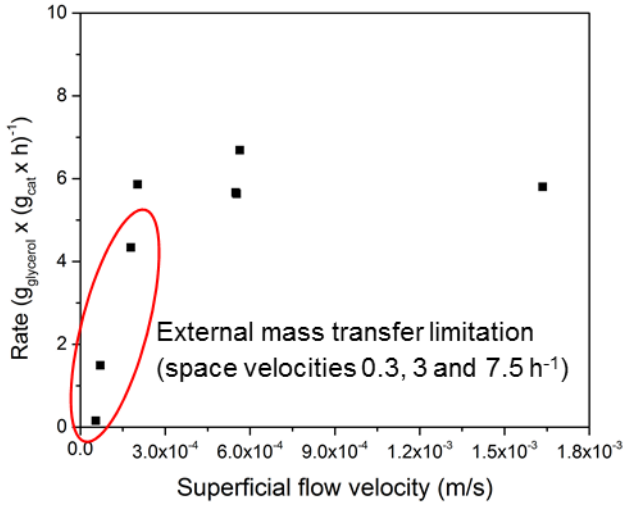

Figure C-3. Effect of superficial flow velocity on glycerol conversion rate for the 400-700 μm particle size at 0.3, 3.0, 7.5, 8.4, 25, 76, 150 and 225 $g_{glycerol} \times (g_{cat} \times h)^{-1}$ at 75 °C, IB:G=3:1 mol:mol, 14±2 bar conditions.

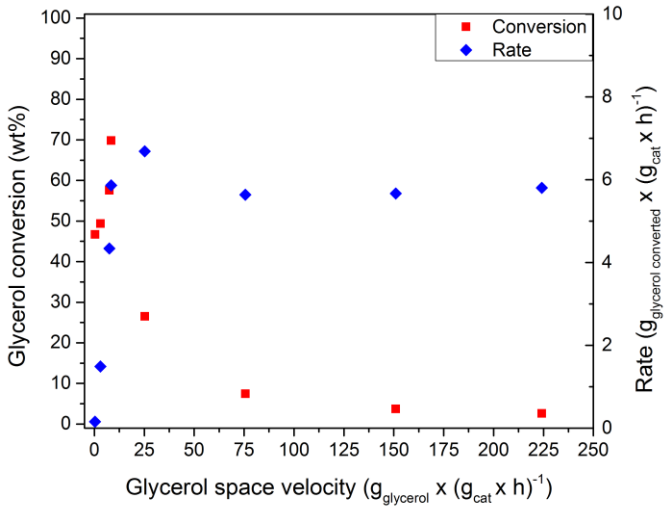

Figure C-4. Glycerol conversion and reaction rate as a function of space velocity for Amberlyst 15™ 400-700 µm original particle size at 0.3, 3.0, 7.5, 8.4, 25, 76, 150 and 225 $g_{glycerol}$ × (g_{cat} × h)$^{-1}$ at 75 °C, IB:G=3:1 mol:mol, 14±2 bar conditions.

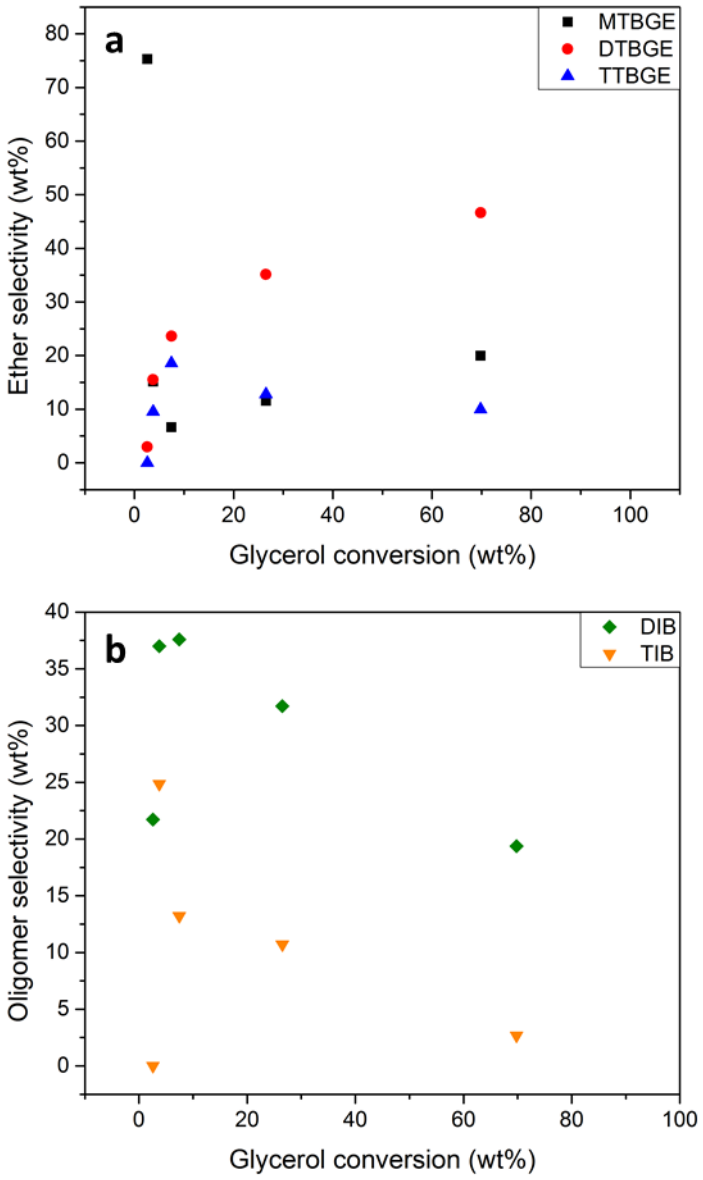

Figure C-5. Selectivity of **a:** ethers and **b:** oligomers in the final product mixture as a function of glycerol conversion for Amberlyst 15™ 400-700 μm particle size at 8.4, 25, 76, 150 and 225 $g_{glycerol} \times (g_{cat} \times h)^{-1}$ at 75 °C, IB:G=3:1 mol:mol, 14±2 bar conditions.

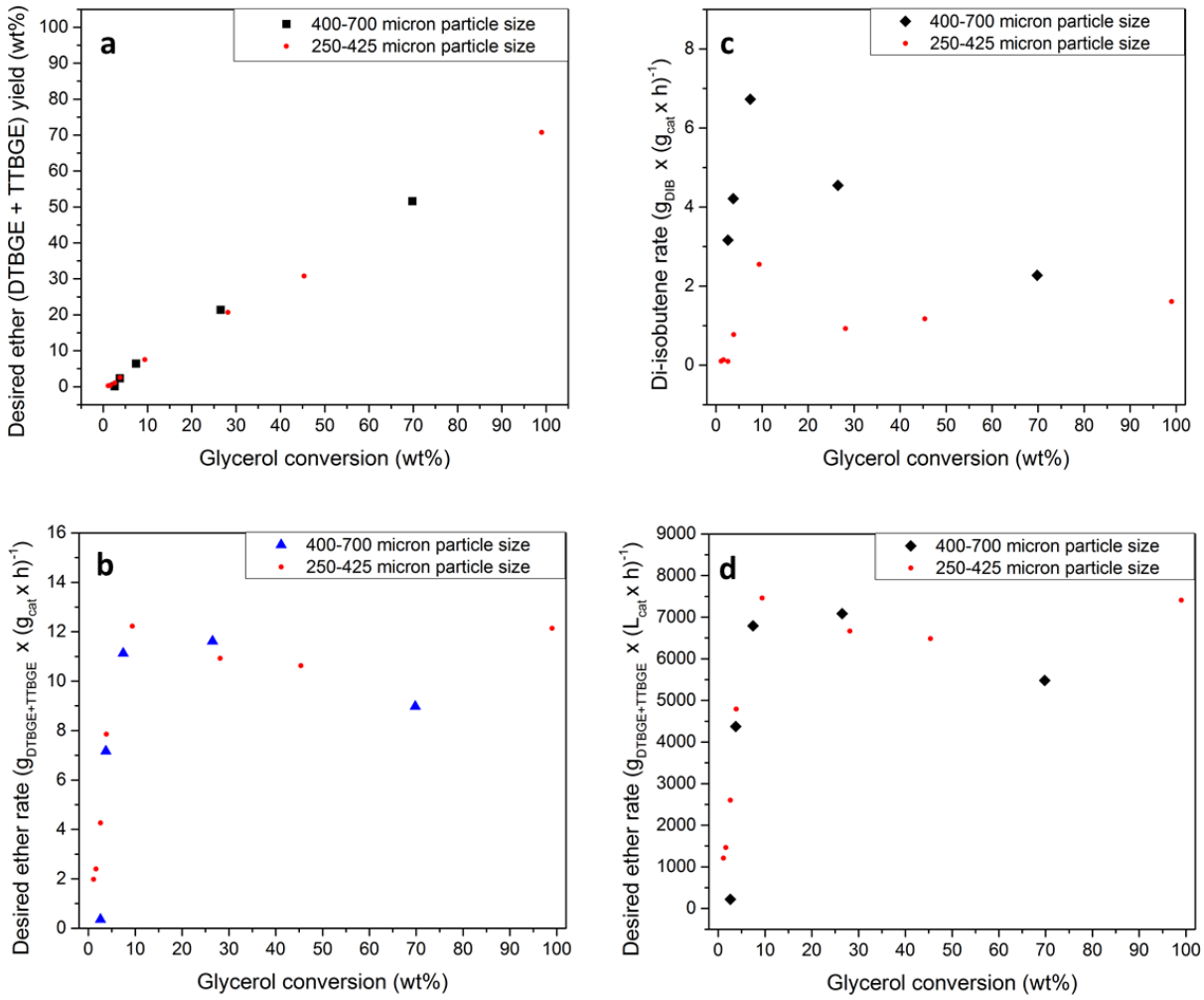

Figure C-6. a: Desired ether (DTBGE + TTBGE) yield; **b:** Desired ether formation rate in gram catalyst basis; **c:** di-isobutene (DIB) formation rate in gram catalyst basis; and **d:** desired ether formation rate in liter reactor basis as a function of glycerol conversion for Amberlyst 15™ 400-700 μm particle size at 8.4, 25, 76, 150 and 225 $g_{glycerol} \times (g_{cat} \times h)^{-1}$ (IB:G=3:1 mol:mol, T=75 °C, 14±3 bar). Note that the dots are added to compare the rates with the 250-425 μm particle size.

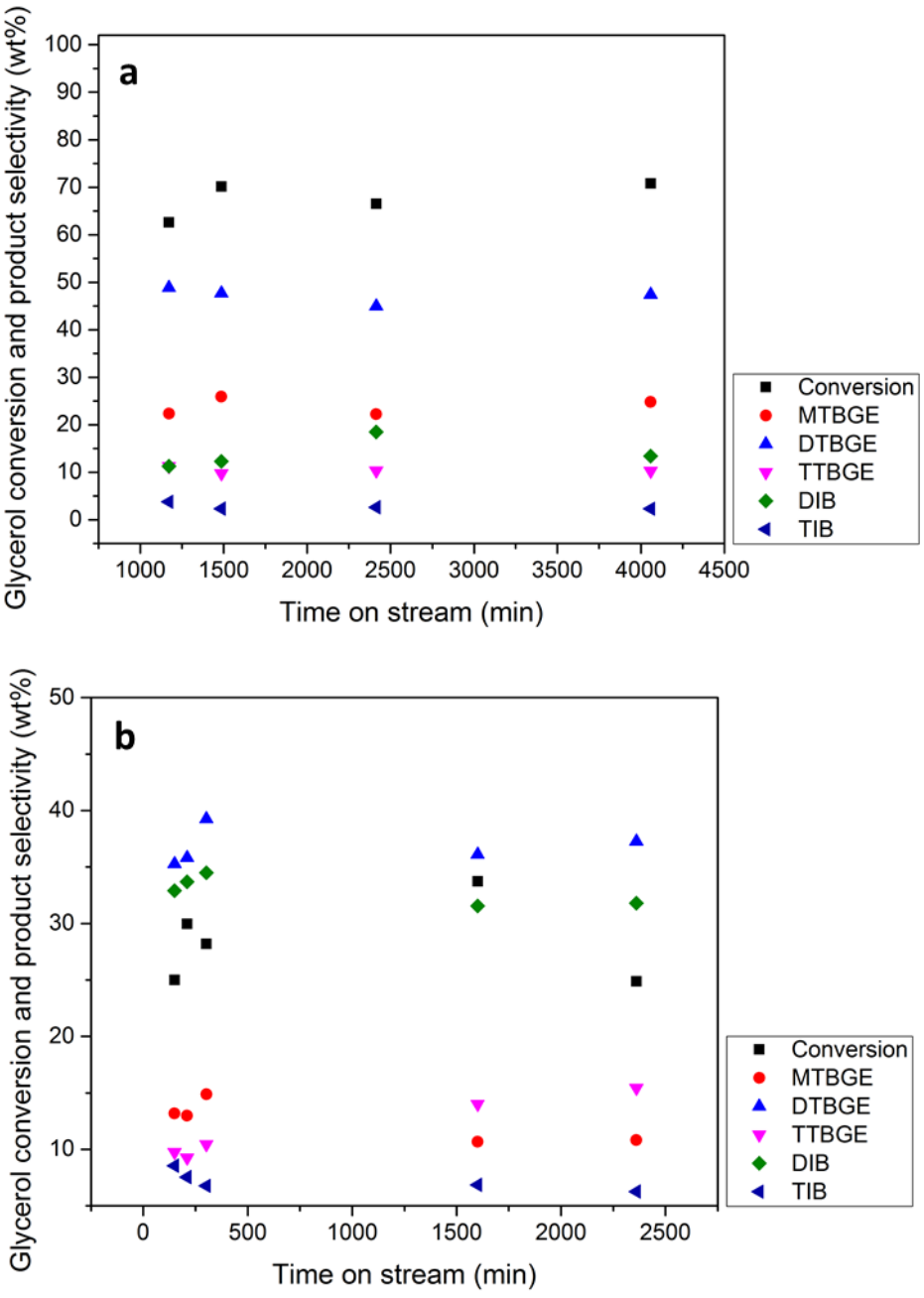

Figure C-7. Catalytic performance of Amberlyst 15™ 400-700 μm particle size at **a:** 8.4 $g_{glycerol}$ × (g_{cat} × h)$^{-1}$; and **b:** 25 $g_{glycerol}$ × (g_{cat} × h)$^{-1}$ at 75 °C, IB:G=3:1 mol:mol, 14±3 bar conditions.

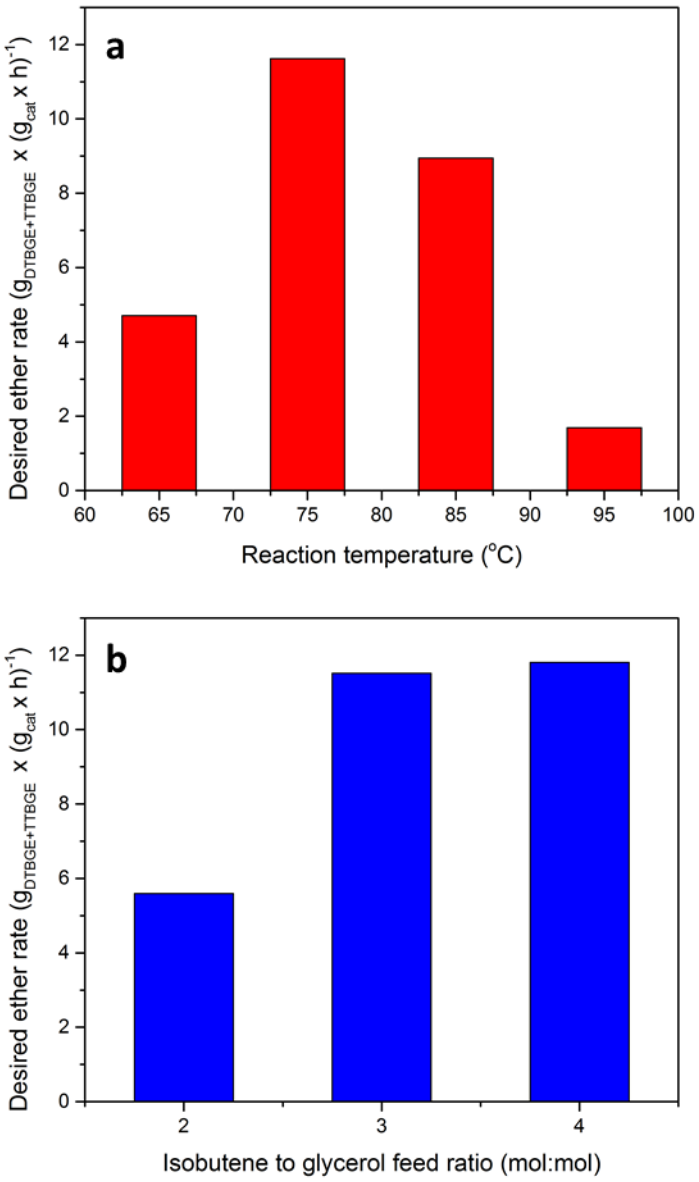

Figure C-8. Desired ether formation rate of Amberlyst 15™ 400-700 μm particle size at 25 $g_{glycerol} \times (g_{cat} \times h)^{-1}$ space velocity and at 14±3 bar at **a:** different temperatures; and **b:** different isobutene to glycerol molar feed ratios.

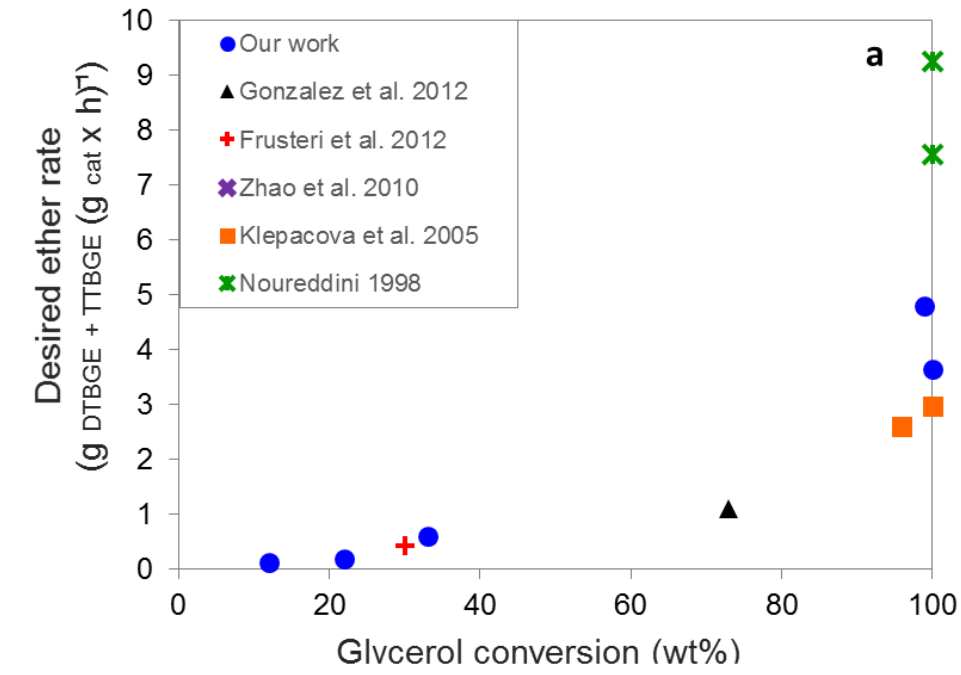
a
Our work
Gonzalez et al. 2012
Frusteri et al. 2012
Zhao et al. 2010
Klepacova et al. 2005
Noureddini 1998
Desired ether rate
(g DTBGE + TTBGE (g cat x h)-1)
Glycerol conversion (wt%)
0
1
2
3
4
5
6
7
8
9
10
0
20
40
60
80
100

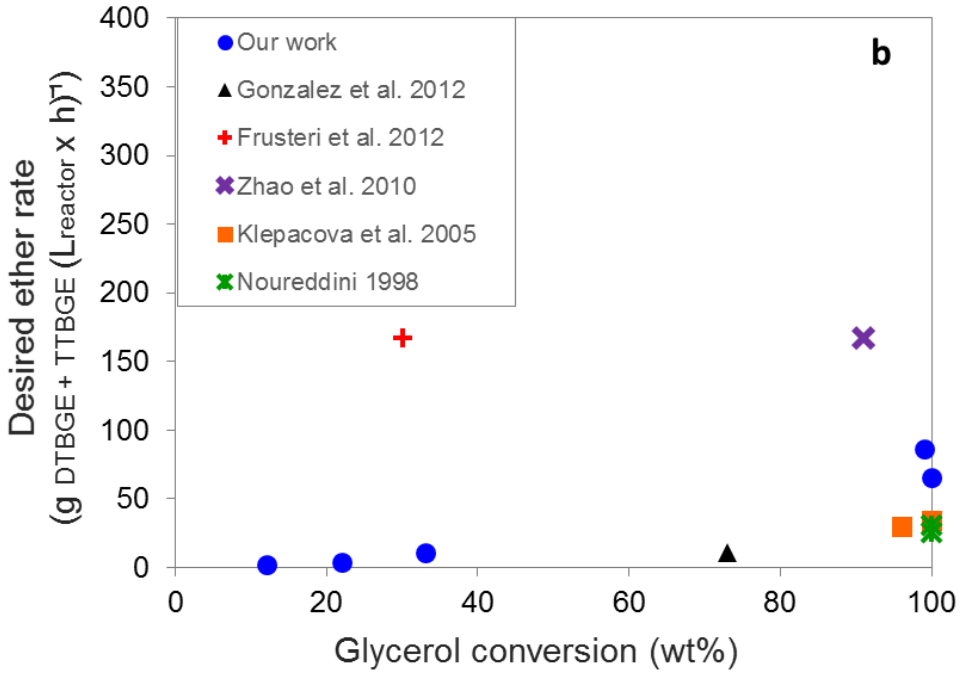
b
Our work
Gonzalez et al. 2012
Frusteri et al. 2012
Zhao et al. 2010
Klepacova et al. 2005
Noureddini 1998
Desired ether rate
(g DTBGE + TTBGE (Lreactor x h)-1)
Glycerol conversion (wt%)
0
50
100
150
200
250
300
350
400
0
20
40
60
80
100

	Temperature (°C)	IB:G ratio (mol:mol)	Reaction time (h)	Autoclave volume (ml)
Our work	75	3	0.5, 1, 2 and 6	75
Gonzalez et al. 2012 [52]	75	4	4	150
Frusteri et al. 2012 [260]	70	2.5	6	100
Zhao et al. 2010 [47]	70	4	2	1000
Klepáčová et al. 2005 [39]	60 and 90	4	8	100
Noureddini 1998 [181]	93	3	3 and 4	450

Figure C-9. Desired ether formation rates in batch reactor systems as a function of glycerol conversion in glycerol etherification with isobutene with Amberlyst 15^{TM} 400-700 μm regular bead size **a:** in gram catalyst basis; and **b:** in liter active reactor volume basis. Reaction conditions are presented in the table. Cleaning time for the batch reactor is assumed to be one hour. Active reactor volume (liquid volume) was assumed to be one third of the autoclave vessel volume.

Appendix D

Supplementary Material of Chapter 6

Compatibility of di- and tri-*tert*-butyl Glycerol Ethers with Gasoline

Table D-1. The results of model gasoline fuel analysis.

Test method	Property	Unit	Value
ASTM D 4052/1	Density (at 15 °C)	g/cm^3	0.7579
	API (at 15 °C)	API	55.1
ASTM D 5191	Vapor pressure (DVPE)	kPa	57.3
ASTM D 5453/1	Total sulfur content	mg/kg	7.5
ASTM D 6304/1	Water content	ppm	98
ASTM D 4809	Gross heat of combustion	cal/g	8659
ASTM D 86/1	Initial boiling point (IBP)	°C	33.8
	5%	°C	48.5
	10%	°C	55.1
	20%	°C	64.2
	30%	°C	73.5
	40%	°C	85.8
	50%	°C	100.7
	60%	°C	115.4
	70%	°C	127.1
	80%	°C	138.2
	90%	°C	151.7
	95%	°C	161.7
	Final boiling point (FBP)	°C	189.0
	Evaporation at 70 °C (E70)	%(v/v)	24.9
	Evaporation at 100 °C (E70)	%(v/v)	48.0
	Evaporation at 150 °C (E70)	%(v/v)	87.5

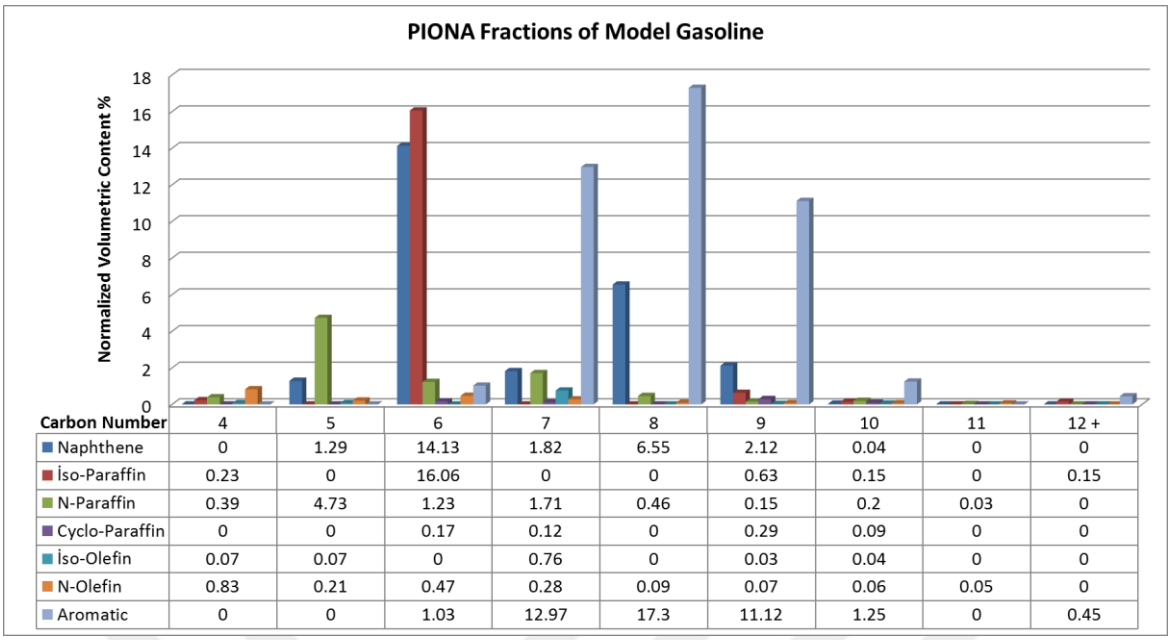

Carbon Number	4	5	6	7	8	9	10	11	12 +
Naphthene	0	1.29	14.13	1.82	6.55	2.12	0.04	0	0
İso-Paraffin	0.23	0	16.06	0	0	0.63	0.15	0	0.15
N-Paraffin	0.39	4.73	1.23	1.71	0.46	0.15	0.2	0.03	0
Cyclo-Paraffin	0	0	0.17	0.12	0	0.29	0.09	0	0
İso-Olefin	0.07	0.07	0	0.76	0	0.03	0.04	0	0
N-Olefin	0.83	0.21	0.47	0.28	0.09	0.07	0.06	0.05	0
Aromatic	0	0	1.03	12.97	17.3	11.12	1.25	0	0.45

Figure D-1. Normalized volumetric model gasoline content (PIONA analysis).

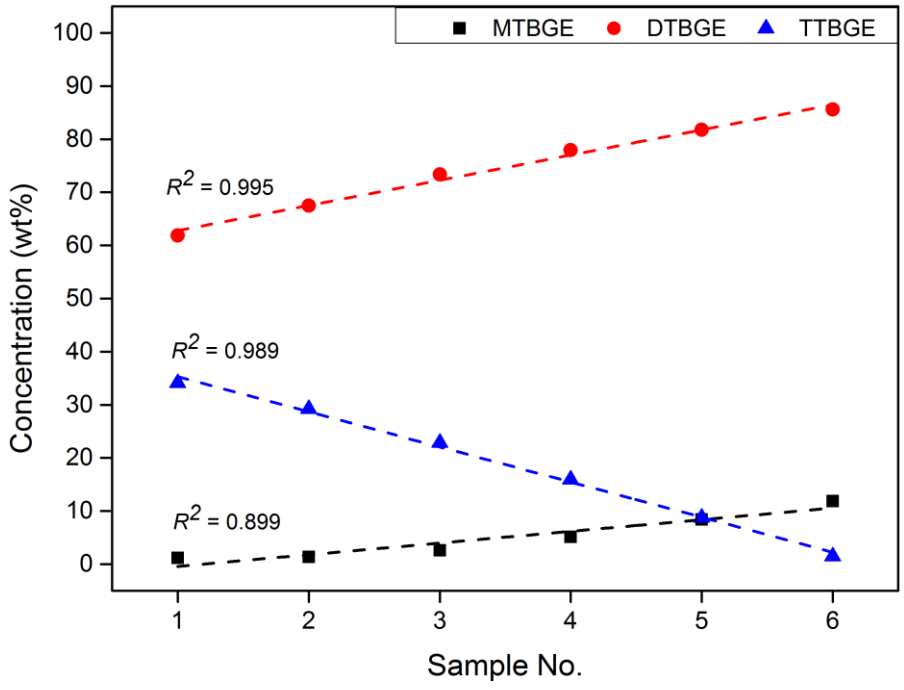

Figure D-2. Concentrations of MTBGE, DTBGE, and TTBGE in GTBE mixtures (K1-K6).

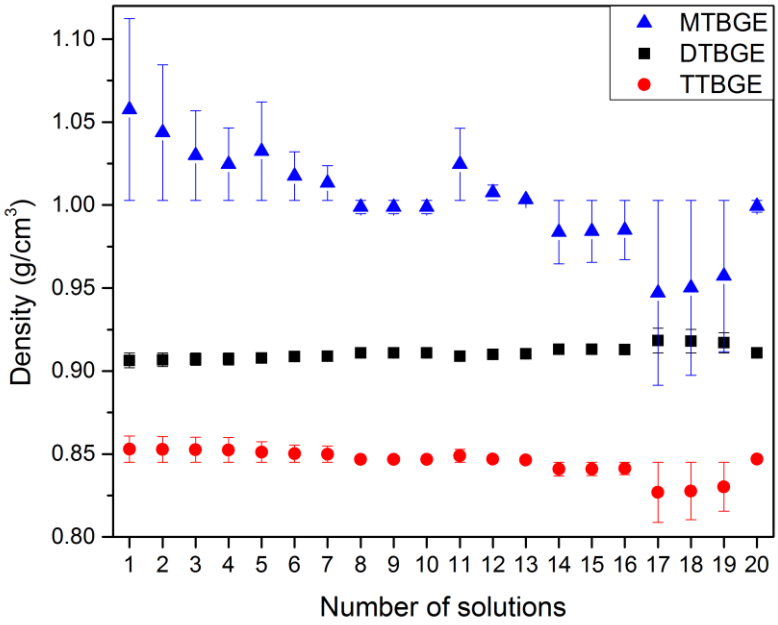

	Unit	DTBGE	TTBGE	MTBGE
Average density	g/cm^3	0.911	0.845	1.003
Standard deviation		0.004	0.008	0.030

Figure D-3. Matlab solutions for MTBGE, DTBGE, and TTBGE densities with error bars and statistics.

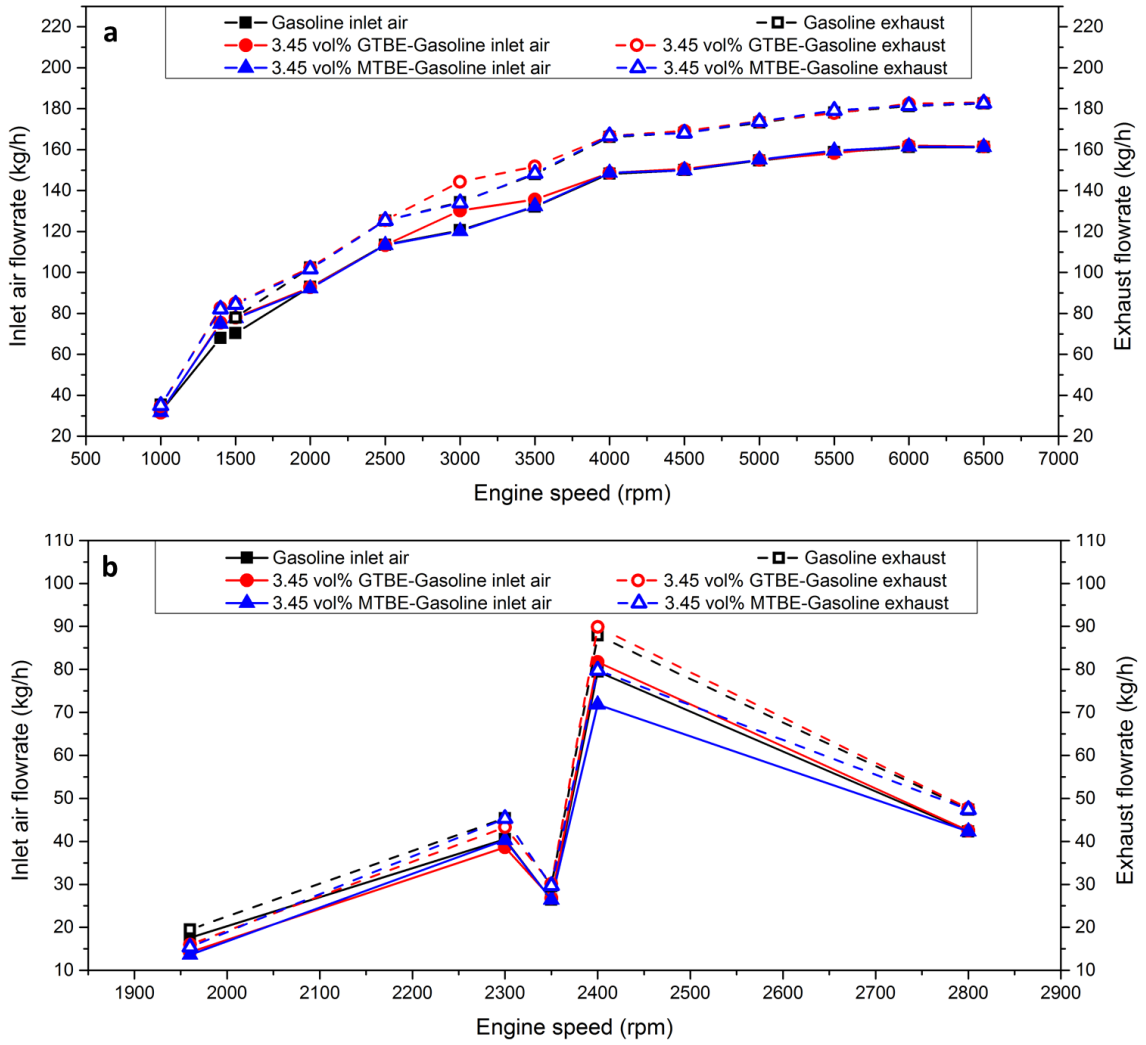

Figure D-4. Air inflow rates and exhaust outflow rates for the reference gasoline, GTBE (K1) blended gasoline and MTBE blended gasoline as a function of the engine speed **a:** in the engine full load curve; **b:** points within the NEDC. *Note: Exhaust outflow rate = Air inflow rate + Consumed fuel rate.*

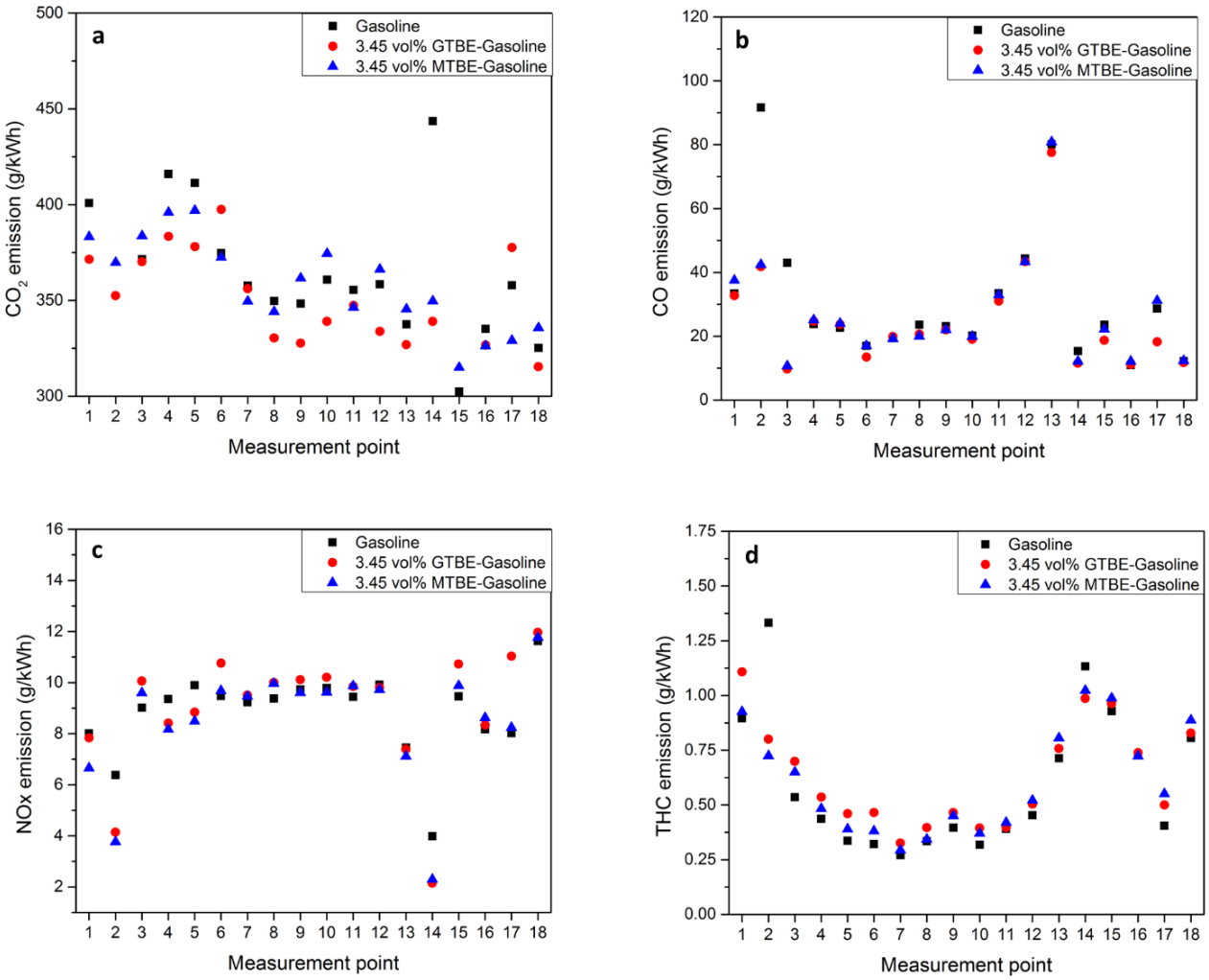

Figure D-5. Comparison of the emissions in the engine full load curve (points 1-13) and within the NEDC (points 14-18); **a:** CO_2; **b:** CO; **c:** NOx; and **d:** Total hydrocarbon content (THC) for the reference gasoline, GTBE (K1) blended gasoline, and MTBE-blended gasoline.